DTU

Technical University of Denmark

Estimation of Directional Wave Spectra from Measured Ship Responses

Ulrik Dam Nielsen

PhD thesis

May 2005

Department of Mechanical Engineering

MEK

Coastal, Maritime and Structural Engineering

Estimation of Directional Wave Spectra from Measured Ship Responses

Ulrik Dam Nielsen

TECHNICAL UNIVERSITY OF DENMARK
DEPARTMENT OF MECHANICAL ENGINEERING
SECTION OF COASTAL, STRUCTURAL AND MARITIME ENGINEERING
MAY 2005

Published in Denmark by
Technical University of Denmark

Copyright © U. D. Nielsen 2005
All rights reserved

Section of Coastal, Structural and Maritime Engineering
Department of Mechanical Engineering
Technical University of Denmark
Nils Koppels Alle, Building 403, DK-2800 Kgs. Lyngby, Denmark
Phone +45 4525 1360, Telefax +45 4588 4325
E-mail: info.skk@mek.dtu.dk
WWW: http://www.mek.dtu.dk/

Publication Reference Data
Nielsen, U. D.
Estimation of Directional Wave Spectra from Measured Ship Responses
PhD Thesis
Technical University of Denmark, Section of Coastal, Structural and Maritime Engineering.
May, 2005
ISBN 87-89502-51-5
Keywords: Sensor measurements,response spectra,directional wave spectra,cross specral analysis,in-service monitoring systems

Preface

This thesis is submitted as a partial fulfilment of the requirements for the Danish Ph.D. degree. The work has been carried out at the Section of Coastal, Maritime and Structural Engineering under the Department of Mechanical Engineering, the Technical University of Denmark (DTU). The work took place during the period of March 2002 to May 2005, including a three-month extension, and the project was supervised by Professor Jørgen Juncher Jensen, whom I wish to give special thanks for valuable guidance and help throughout the study.

The study has been financed by the Eureka project E!2097 MONITUS, and additional funding for a stay abroad has been provided by the Section of Coastal, Maritime and Structural Engineering, DTU.

Part of the work was performed during a five-month stay at the Tokyo University of Marine Science and Technology. Associate Professor Toshio Iseki made this stay possible, not to mention his great willingness to share knowledge of research subjects, much gratitude goes to him, Professor Kohei Ohtsu and Mrs. Michiko Oda for a very pleasant stay.

Validation of the work was made in collaboration with and during a stay at Det Norske Veritas (DNV). For this cooperation, many thanks go to Dr. Bo Cerup Simonsen and Dr. Øyvind Lund-Johansen, and, in particular, Mr. Andreas Aschim deserves posthumous thanks. The stay at DNV was financially supported by the European *Network of Excellence*, MARSTRUCT.

Preliminary work and validation were also conducted within the joint Danish project SeaSense. My thanks go to the partners and, especially, to IT Manager Jan Baatrup.

Moreover, a number of persons should be acknowledged for fruitful discussions, email correspondences, etc. These include: Dr. Rasmus Folsø, Registro Italiano Navale, Professor Noriaki Hashimoto, Port and Airport Research Institute, Japan, Dr. William D. Penny, Wellcome Department of Imaging Neuroscience, University College London, Dr. Eduardo A. Tannuri, University of São Paulo, and Dr. Philippe Corrignan, SIREHNA.

Finally, thanks to my colleagues in the Section, friends and family for help and support.

Copenhagen, May 31, 2005
Ulrik Dam Nielsen

This page is intentionally left blank.

Abstract

This thesis focuses on methodologies for estimation of directional wave spectra. The objective is to study and develop methods for estimating wave spectra on the basis of measured ship responses.

Traditionally, such methods, which are derived by use of linear spectral analysis, are based on either a parametric or a non-parametric procedure. In the parametric procedure the estimated wave spectrum is assumed to be composed of one parameterised spectrum or by the summation of several parameterised spectra, e.g. the generalised JONSWAP spectrum, so that it is the underlying wave parameters which are sought for. The non-parametric method, however, yields the directional wave spectrum in a number of discretised points of the wave field. In the thesis both procedures are dealt with, but with the very focus on the non-parametric method.

The non-parametric method, called the Bayesian estimation method, is based on Bayesian modelling, which introduces the use of prior information to make the directional wave spectrum smooth and to avoid an unrealistic solution.

The topic of on-site estimation of directional wave spectra from measured ship responses has its overall relevance in connection with decision support systems for safe navigation of ships. For this reason it is important that all the procedures used for estimation are fully automated. Thus, a cross spectral analysis of the measured responses is derived, so that the governing equations can be found automatically. Hence, so-called multivariate autoregressive (MAR) procedures are treated in detail. Moreover, general aspects in relation to decision support systems are treated in the thesis.

In order to verify the Bayesian estimation method, numerical simulations are carried out. Hence, from generated ship responses based on a theoretically known wave spectrum, the Bayesian estimation method is shown to predict the wave spectrum with good accuracy.

Following the numerical simulations, two different sets of full-scale data are analysed. In the first set, motion measurements from four test trials with a research and training ship form the basis of the estimated wave spectra. The wave parameters of the estimated spectra are compared with parameters from visual observations and, in general, the agreement is reasonable. The other set of full-scale data stems from a container ship and, in addition

to the motion measurements, knowledge of the on-site wave spectra from a wave radar system is at hand. These wave spectra are compared with the results from the Bayesian method and the underlying wave parameters are found with fair consistency between the two estimations. However, some discrepancies are observed for the data characterised by the severest sea states. Due to lack of redundancy in the data, it is not possible to settle which estimation is the most correct.

In general, the developed method is capable of estimating directional wave spectra on the basis of measured ship responses, and at the very end of the thesis, suggestions for improving the specific method are given.

Resume

Nærværende rapport omhandler metoder til bestemmelse af direktionale bølge- spektre på basis af målte skibsrespons.

Generelt skelnes der mellem parametriske og ikke-parametriske estimeringsmetoder, der i begge tilfælde baseres på en lineær spektralanalyse. I den parametriske metode antages det, at bølgespektret er sammensat af et eller flere parameteriseret spektre, således at der løses for de indgående bølgeparametre. Den ikke-parametriske metode tager udgangspunkt i et fuldstændig diskretiseret bølgefelt, hvilket betyder, at spektret bestemmes som løsningen til et stort antal ubekendte i en række bølgefrekvenser og -retninger. I nærværende rapport behandles begge metoder, men hovedvægten lægges i markant grad på en ikke-parametrisk metode.

Den ikke-parametriske metode er baseret på en Bayesisk modellering, hvilket indebærer introduktionen af a priori informationer, således at bølgespektret sikres delvist mod et ufysisk udseende. Som følge af det Bayesiske aspekt benævnes metoden som en Bayesisk estimeringsmetode.

Den primære interesse i estimering af bølgespektre på basis af målte skibsrespons skal findes indenfor beslutningsstøttesystemer til brug for skibes operationelle sikkerhed. I den sammenhæng er det derfor afgørende, at alle de i estimeringen involverede procedurer ikke behøver manuelle input. Af denne årsag foretages spektralanalysen derfor således, at de styrende ligninger findes automatisk. Specifikt sker dette ud fra brugen af såkaldte multivariable autoregressive (MAR) procedurer, hvorfor der gives en detaljeret udledning og behandling af disse. Ydermere indeholder rapporten generelt elementer af vigtighed for beslutningsstøttesystemer.

For at verificere den Bayesiske estimeringsmetode udføres analyser med numerisk simuleret data. Således genereres skibsrespons på basis af et teoretisk kendt bølge- spektrum, og det vises, at metoden ud fra de simulerede skibsrespons er i stand til at estimere et bølgespektrum i næsten fuld overensstemmelse med det teoretiske.

Efterfølgende de numeriske simuleringer analyseres to forskellige sæt af fuldskaladata. Det første sæt består af bevægelsesmålinger foretaget ombord på et japansk forskningsskib, og på basis af fire forsøgskørsler estimeres bølgespektret for hvert enkelt tilfælde. Under

forsøgskørslerne er foretaget visuelle observationer af bølge- parametre og disse sammenlignes med tilsvarende parametre fundet via den Baye- siske estimering. Generelt opnås en fornuftig overensstemmelse. Det andet sæt data stammer fra et containerskib, og i tillæg til de målte skibsrespons haves bølgeradar-baseret estimeringer af direktionale bølgespektre. Ud fra en sammenligning med de direktionale bølgespektre fundet via den Bayesiske metode ses en acceptabel overensstemmelse, hvilket også gælder for de indgående bølgeparametre. Dog noteres en mindre god overensstemmelse for de data sæt, som er karakteriseret ved den alvorligste søgang. Desværre haves der ikke redundans i bølgedataene, hvorfor det ikke kan afgøres, hvilken estimeringsmetode der er mest troværdig.

Sammenfattende ses den udviklede metode at være i stand til at bestemme direktionale bølgespektre. Slutningen af rapporten er tilegnet forslag til mulige forbedringer af metoden, og samtidig kommenteres på generelle muligheder indenfor estimering af bølgespektre på basis af målte skibsrespons.

Contents

Contents **vii**

1 Introduction **1**

1.1 Background and Motivation 1

1.2 The Wave Energy Spectrum 1

1.3 Analogy and General Assumptions 3

1.4 Existing Work and Literature 3

1.5 Limitations Due to Frequency Insensitivity 6

1.6 Estimations versus the True Wave Spectrum 7

1.7 Objectives and Scope of the Present Work 7

1.8 Structure of the Thesis 8

2 Decision Support Systems **11**

2.1 Introduction 11

2.2 Requirements and Properties 12

2.2.1 End Users 12

2.2.2 Ship Type 13

2.2.3 General Information 13

2.2.4 State-of-the-Art 14

2.3 Theoretical Procedures for Predictions 15

2.3.1 Sensors and Response Statistics 16

2.4 Example - SeaSense 18

2.4.1 Sea State and Sensors 18

2.4.2 User Interface 19

3 Bayesian Estimation **23**

3.1 Introduction 23

3.2 Basic Equations 25

3.3 Matrix Notation and Multivariate Expression 26

3.4 Numerical Considerations 29

3.4.1 Prespecified Wave Frequencies 29

3.4.2 Considering More Encounter Frequencies 32

3.4.3 Equivalence of Energy 34

3.5 Bayesian Modelling Procedure 34

3.5.1 Bayesian Statistics 35

3.5.2 Inverse Theory vs. Bayesian Modelling 35

3.5.3 Data Distribution 38

3.5.4 Prior Distribution 38

3.5.5 Posterior Distribution 41

3.6 Akaike's Bayesian Information Criterion 43

3.7 Solution Procedure 45

3.8 Calculation of the Directional Wave Spectra 47

3.8.1 Numerical Techniques 48

4 Parametric Estimation **51**

4.1 Introduction 51

4.2 Parameterised Wave Spectra 51

4.3 Frequency Dependent Spreading 52

4.4 Estimated Parameters 53

5 Cross Spectral Analysis **55**

5.1 Introduction 55

5.2 Basics of MAR Modelling 57

5.3 Spectral Estimation 57

5.4 Determination of the MAR Coefficients 61

5.5 Choice of the Optimal Order 62

5.6 Recursive Computational Procedure 63

5.7 Stepwise Least Squares Algorithm 65

5.7.1 LS Estimates for Fixed Order 65

5.7.2 Downdating the LS Estimates 67

5.8 Numerical Example 68

5.8.1 Time Series Generation 68

5.8.2 Behaviour of Order Criteria 69

5.9 The Recursive Procedure vs. the LS Algorithm 73

6 Response Signals **75**

6.1 Introduction 75

6.2 In-hand Time Series 75

6.3 Type of Responses 76

6.4 Basic Treatment of Response Signals 77

6.4.1 Time Synchronisation 77
6.4.2 Equidistant Time Steps and Filtering 78
6.4.3 Filtering 78
6.4.4 Cross Spectral Analysis 79
6.5 Estimation of the Wave Height 80
6.5.1 Integration of Acceleration Signal 80
6.5.2 Determination of Wave Height 81
6.6 Complex-valued Transfer Functions 83

7 Numerical Test Cases **87**
7.1 Introduction 87
7.2 Simulation of Time Series 87
7.3 One-dimensional Estimations 88
7.3.1 Quartering Sea 89
7.4 Directional Estimations 93
7.4.1 Frequency Insensitivity 95
7.5 Conclusions 97

8 Full-Scale Data - Comparisons with Visual Observations **99**
8.1 Introduction 99
8.2 Bayesian Estimation 101
8.2.1 Wave Parameters 102
8.2.2 Response Spectra 102
8.2.3 Following versus Head Waves 108
8.3 Conclusions 110

9 Full-Scale Data - Comparisons with WAVEX **113**

9.1 Introduction 113

9.2 Wave Parameters 116

9.2.1 Bayesian vs. WAVEX 116

9.2.2 Parametric Estimations 121

9.3 Comparative Plots 123

9.4 Response Spectra 132

9.5 Parameter Study 134

9.5.1 Hyperparameter 134

9.5.2 Discretisation 136

9.5.3 Normalisation 136

9.5.4 Sway versus Roll 140

9.6 Conclusions 141

10 Conclusions and Recommendations **143**

10.1 Conclusions 143

10.2 Recommendations for Future Work 146

10.2.1 The Bayesian Estimation Method 146

10.2.2 Estimations of Wave Spectra 147

References **149**

A Transfer Functions **157**

A.1 Introduction 157

A.2 The Shioji-Maru 158

A.3 The Container Ship 162

B Time Series **169**

B.1 Introduction 169

B.2 The Shioji-Maru 170

B.3 The Container Ship 173

C Preliminary Studies **179**

C.1 Introduction 179

C.2 Assumptions on the Wave Spectrum 179

C.3 Estimation by Use of Shape Functions 180

C.4 Optimisation of JONSWAP Spectra 182

C.5 Results 184

C.6 General Comments on the Estimations 194

C.7 Estimation Based on Optimisation 194

C.8 Estimation Based on Shape Functions 195

C.9 Conclusions 195

C.10 Transfer Functions 196

C.11 Response Spectra 197

C.12 Time History of Wave Height 202

D Numerical Simulations **205**

D.1 Introduction 205

D.2 One-peaked Spectrum 205

D.3 Double-Peaked Wave Spectrum 208

E Additional Results for the Shioji-Maru **211**

E.1 Introduction 211

E.2 Normalised Response Spectra 211

F Additional Results for the Container Ship **213**

F.1 Introduction 213

F.2 Comparative Plots - Sway in place of Roll 214

F.3 Directional Wave Spectra 223

F.4 Comparative Plots - Non-normalised Equation System 227

List of PhD Theses Available from the Department **237**

Chapter 1

Introduction

1.1 Background and Motivation

As regards the operational safety of ships, it is strongly believed that this can be increased by use of in-service monitoring systems where a set of sensors measures specific ship responses. From a measured set of ship responses, future risk events can be derived on the basis of trend analysis of the past recorded signals. However, to increase the operational safety, the effect of changing operational parameters (speed, course, draft, ...) must be included. Based on linear spectral analysis – which requires the directional wave spectrum as input – statistical predictions of future events can be carried out as function of the operational parameters. Therefore, it is paramount to have an estimate of the directional wave spectrum, when in-service monitoring systems applied to decision support are dealt with.

Today, means of obtaining estimations of the directional wave spectrum exist. Such means include moored wave rider buoys and current meters, satellite measurements and wave radar systems. The latter two of these means do not suffer from the problems related to the fixed position of a moored buoy and current meters, but do, on the other hand, require complex computational hardware and have a high initial cost, cf. Tannuri et al. (2003), not to mention calibration and maintenance. For this reason it is of interest to be able to estimate the wave spectrum from measured ship responses, which are easily accessible – and, as a matter of fact, already at hand – from the sensor measurements done in an in-service monitoring system.

1.2 The Wave Energy Spectrum

From standard textbooks on water waves and naval architecture, e.g. Dean and Dalrymple (1991), Jensen (2001) and Lloyd (1998), it is known that any irregular wave time history

can be comprised of an infinite sum of regular sine waves. Hence, to quantify the relative importance of the component sine waves making up the irregular ocean wave field, the directional wave energy density spectrum, or for short, the wave spectrum, is introduced.

Basically, a directional wave energy spectrum is a description of how the energy (per square metre of sea surface) of the waves is distributed with frequency and direction. By definition, the wave spectrum is given so that the area bounded by a frequency as well as a directional range is proportional to the total energy per square metre of sea surface of all the wave components within that area of frequencies and directions, cf. Lloyd (1998). Thus, it follows, by integration over all frequencies and directions, that the total area enclosed by the wave spectrum is proportional to the total energy (per square metre) held by the wave field.

In Figure 1.1 an example of a directional wave spectrum is seen with a) being the distribution of the energy in a 3-D visualisation, whereas b) indicates the contour lines of the wave spectrum in a polar plot. From an integration over all directions for each frequency, the integrated frequency spectrum, sometimes denoted the power spectrum, is found, see Figure 1.2.

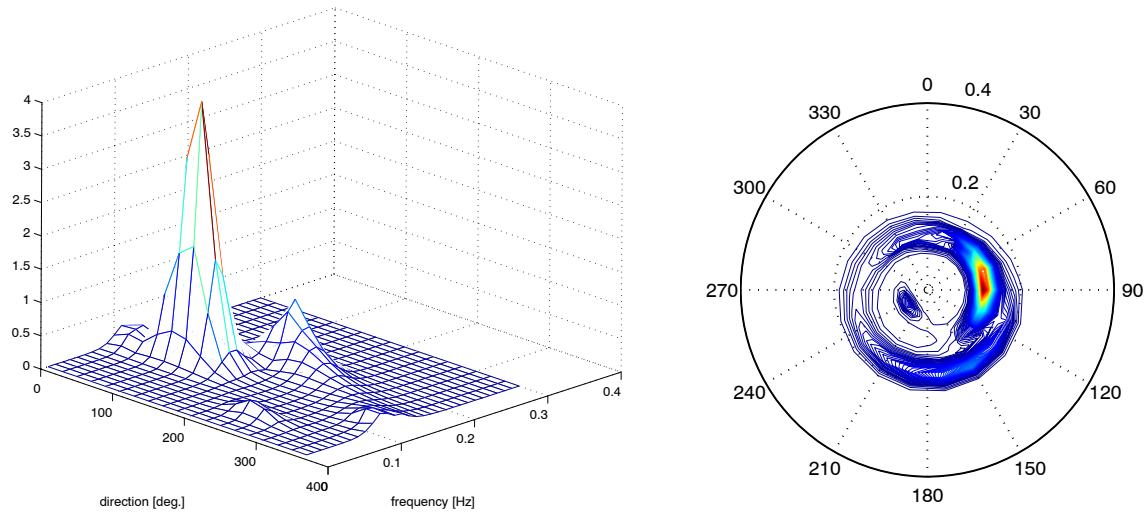

a) b)

Figure 1.1: a) *A directional wave spectrum.* b) *Polar plot of the directional wave spectrum.*

Not to mention the origin and the meteorological conditions prevailing over the outcome of the wave energy spectrum seen in Figures 1.1 and 1.2, it is worth to note how the spectrum has its energy distributed in three areas, most clearly seen from Figure 1.1 a). This seems to suggest the presence of (low-frequency) swells as well as the presence of wind waves from two directions. As the example is only studied for the purpose of visualisation, comments are left out on the origin and the meteorological conditions for which reason it is not to be said whether the spectrum is likely or not.

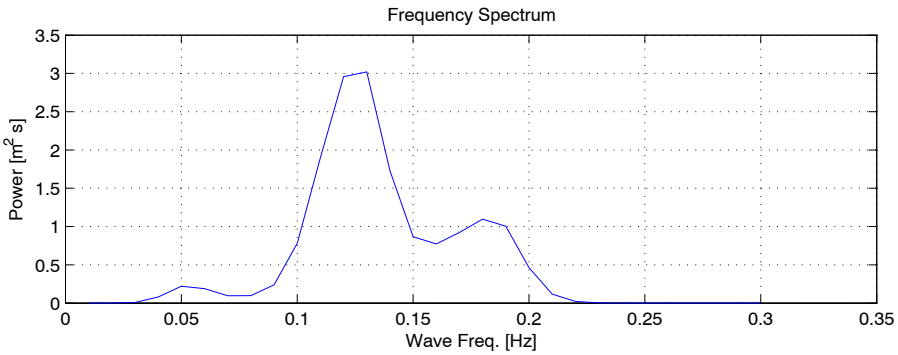

Figure 1.2: *Integrated frequency wave spectrum.*

1.3 Analogy and General Assumptions

A wave rider buoy is, in general, considered to be a reliable device for obtaining the directional wave energy spectrum of ocean waves because of the well known dynamical behaviour of the buoy, e.g. Longuet-Higgins et al. (1961), Ewans and van der Vlugt (1999) and Ewans (1998). The concept of a wave rider buoy may also be applied to ships. However, a ship sails at a speed in some arbitrary direction on the ocean. This fact adds complexity to the concept of the ship being a wave rider buoy, and it must be properly taken into account when the measured ship motions are used for estimation of the wave spectrum. On the other hand, for decision support, the wave spectrum is needed in the specific position of the ship, and thus it is an obvious advantage to use the ship itself and not rely on numerous wave buoys.

Ship responses are, in general, non-linearly related to the governing excitation forces, i.e. the waves. However, for light and moderate sea states, linearity is in many cases a good assumption to introduce between the ship motions and the waves. With a linear relationship the responses can be expressed by complex-valued transfer functions. In the present area of research, this assumed linearity combined with the assumption of the random seaway being a stationary stochastic process means that the ship motions do not have to be considered in their entirety as time series. Instead, by use of adequate transformation procedures, the responses can be studied in the frequency domain, facilitating a linear spectral analysis of the responses.

1.4 Existing Work and Literature

To the knowledge of the author, all methods, developed for the estimation of a wave energy spectrum – one-directional or multi-directional – on the basis of measured ship responses, have as the fundamental idea that linear spectral analysis is used to set up conditions/equations which relate the measured ship responses – the one hand side – with the wave energy spectrum through complex-valued transfer functions – the other hand side. Thus,

from this relation, the principle is to minimise, in the least squares sense, the difference between the two sides, see Figure 1.3.

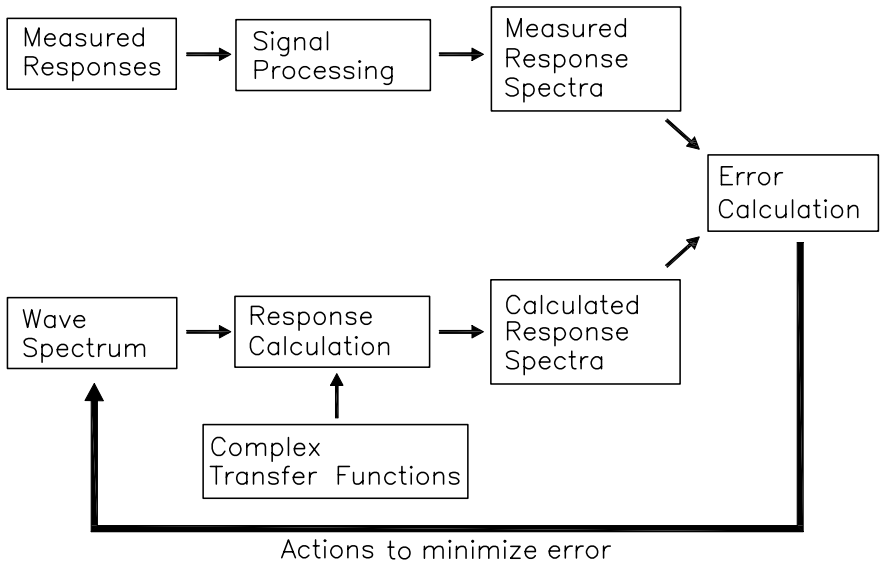

Figure 1.3: *The fundamental idea in the estimation of wave spectra based on measured ship responses.* Aschehoug (2003).

In the application of linear spectral analysis, there are basically two main concepts for estimation of the wave energy spectrum: 1) a parametric method where the wave spectrum is determined from an optimisation of one or several known parameterised wave spectra (e.g. generalised JONSWAP, Bretschneider, ...) resulting in certain wave parameters, or 2) a non-parametric method where the directional wave spectrum is found 'directly' as the values in a completely discretised frequency-directional domain, see Figure 1.4.

As regards 1), i.e. the optimisation of specific wave parameters, studies have among others been carried out by Nielsen (2003), Tannuri et al. (2003), in the EC project HullMon+ Aschehoug (2003) and by Hua and Palmquist (1994), of which works the former three are the most advanced. In general, all of the mentioned works are alike. However, in addition to the significant wave height and the mean wave period, the three former works offer the summation of more parameterised wave spectra as well as the determination of a mean wave direction. The main drawback, considering estimates of the wave spectra based on a parametric method, is that the relative direction of the waves is only partly determined in the sense of a mean wave direction (or, in some cases, not at all). Thus, wave spreading is merely introduced by assuming a, say, ninety degree spreading around the mean wave direction with some prespecified spreading function. Moreover, as also mentioned by Tannuri et al. (2003), the parametric method is relatively expensive with respect to the computational cost, since the solution is obtained from a non-linear optimisation problem.

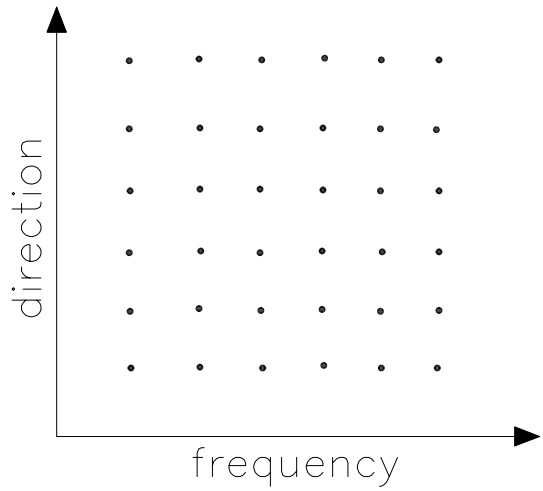

Figure 1.4: *A completely discretised wave field.*

For concept 2), that is, the estimation of fully directional wave spectra by use of measured ship motions, Webster and Dillingham (1981) introduced a kind of linear programming approach that was referred to as the Fourier transform matching method, in which the aim is to minimise the maximum deviation between measured and calculated Fourier transform coefficients. Subsequently, much work was carried out in Japan in different research fields such as oceanography, coastal and harbour engineering, naval architecture, etc., cf. Iseki (1999). In these works the extended maximum likelihood method (EMLM), the maximum entropy principle method (MEP) and the extended maximum entropy method (EMEP) were introduced as the mathematical foundation of the directional estimation, e.g. Waals et al. (2002), Isobe et al. (1984), Iseki et al. (1992), Kobune and Hashimoto (1986) and Hashimoto et al. (1994). Not all of these works, however, took into account a vessel being underway and, moreover, for those that did, the so-called triple-valued function problem, i.e. the deep-water relationship between the encounter and the wave frequency, was not accurately taken into account. Based on a Bayesian modelling method, Iseki and Ohtsu (2000) and Iseki and Terada (2002) strictly incorporated the triple-valued function problem, and the directional wave spectrum was found to be the optimum solution from a probabilistic viewpoint. The central idea in the Bayesian modelling procedure, as proposed by Akaike (1980) and utilised in the latter work by Iseki and Ohtsu (2000) and Iseki and Terada (2002), is that different kinds of prior information are introduced to take care of lack of conditions as well as to reduce the influence of noise. Compared to the other methods, that is, EMLM, MEP and EMEP, the Bayesian modelling procedure is in general considered superior, e.g. Goda (2000).

It is important to realise that Bayesian modelling – as appears from the term 'Bayesian' – introduces a stochastic point of view as regards the estimation of directional wave spectra. Thus, by introduction of likelihood functions and prior distributions, the original cost function, which is set up from the linear spectral analysis to form a least squares problem, is transformed into maximisation of a posterior distribution of the data. Obviously, another

and, so to speak, more elementary, or apparent, approach exists for estimation of the directional wave spectra compared to the Bayesian modelling. Hence, the original cost function, which is established by the linear spectral analysis, can be sought to be optimised by some direct means. However, as it is also the case for Pascoal et al. (2005), the author has no knowledge of any references for such an approach in the particular application of estimation of (directional) wave spectra. And, although Herbers and Guza (1990) operates with an approach based on 'inverse theory', Chapter 3 in the present thesis shows that Bayesian modelling and inverse theory are basically two sides of the same coin.

1.5 Limitations Due to Frequency Insensitivity

As regards ocean waves of very long wavelengths relative to the length of some ship, if this ship is excited by such waves it will (almost) only respond by following the surface elevation in a pure heave motion. Somewhat similarly, for very short wavelengths relative to the ship's length, the ship does practically not respond to such excitations at all (in this respect, the inertia of the ship does also influence). Both phenomena are illustrated in Figure 1.5.

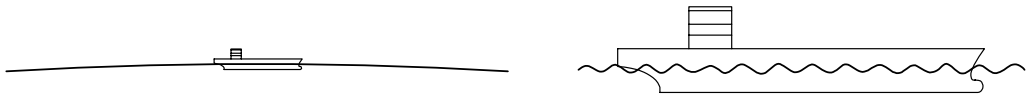

a) b)

Figure 1.5: a) *Low-frequency excitations.* b) *High-frequency excitations.*

The relation between wavelength and frequency is given by the dispersion equation, e.g. Dean and Dalrymple (1991), and for practical applications on relatively deep water, the wave frequency squared is inversely proportional to the wavelength. The above discussion on the insensitivity of ships to very long and short wavelengths, thus, directly translates into the fact that a ship will only respond very little to low- and high-frequency wave excitations. Consequently, this will have an influence when a (directional) wave spectrum is to be estimated from measured ship responses. Thus, it cannot be expected, by any means, that a ship response based method for estimation of wave spectra can predict high- or low-frequency wave components, i.e. energy, if the ship does not respond to the excitations itself. Therefore, it is important to realise that, due to different hydrodynamical behaviour of ships and, hence, their different sensitivities to low- and high-frequency excitations, then for exactly the same operational conditions and completely identical true wave spectra, the estimated wave spectra of two different ships, as regards dimensions and hydrodynamical design, will most likely deviate (slightly) from each other. The problem of deviating wave spectra, dependent on the ship being studied, is, however, not regarded as utmost important when dealt

with in the perspective of decision support. Simply because the estimated wave spectrum – based on the specific ship's responses – exactly (in theory) reflects the wave components to which the considered ship is sensitive. Hence, decision support for a specific ship may be conducted reliably even though the estimated wave spectrum lacks/overshoots energy for certain frequencies, compared to an estimated wave spectrum based on the responses of another ship.

1.6 Estimations versus the True Wave Spectrum

To follow on from the discussion in the latter section, a fundamental problem, or dilemma, as regards ocean wave spectra is that, although the wave rider buoy is considered trustworthy for practical applications in a specific location, no completely reliable means or methods, so far, exist for the determination of the *absolute true* wave spectrum at any time in any place. It should be noted that in this context, the term 'methods' does not refer to different calculation procedures within a method. Instead, the term refers to methods where the estimation of the wave spectrum is carried out on the basis of different physical devices, such as wave radar systems, satellite measurements, data from a wave rider buoy, measured ship responses, etc. To return to the subject of the absolute true wave spectrum, when methods for obtaining the wave spectrum are dealt with, it must be stressed that the outcome of a method is, thus, only an *estimate* of the true wave spectrum. Obviously, this fact adds complexity to the issues of verifying what has been estimated and to do comparisons between different methods for estimation of the wave spectrum. Consequently, redundancy in the data to be analysed is a great advantage in the sense that the more methods to compare, the better the chance of determining how the true wave spectrum may look. Unfortunately, however, the collection of useful full-scale data is related with many practical problems. Some of these problems have been experienced in the present research/project for which reason none of the results to be seen later yield a conclusive evidence on what was the true wave spectrum in the analysed situation.

1.7 Objectives and Scope of the Present Work

The overall objective of this work is to study and develop reliable procedures for determining, or estimating, the wave energy spectrum on the basis of measured ship responses. In the thesis, procedures in relation to both the non-parametric method and the parametric method will be dealt with. The emphasis is put on a ship response based non-parametric method which is applied to two different sets of full-scale data. For the first set of data, results are compared with visual observations and for the second set with results obtained from the wave radar system WAVEX. As regards the parametric method, the work described in Nielsen (2003) will be studied. This work was carried out within the joint Danish project SeaSense, SeaSense (2003).

The developed non-parametric method utilises the Bayesian modelling procedure as proposed by Akaike (1980) and the method has its foundation in the work by Iseki and Ohtsu (2000) and Iseki and Terada (2002). The latter of these works includes considerations about the equivalence of significant values in the measured and estimated response spectra. In the present work this equivalence is also included and, furthermore, if at hand from visual observations, information on the wave direction can be taken into account. Basically, the model equates, for a number of discretised points, the measured and the estimated response spectra to form a least squares problem, with a non-negativity constraint to the spectral amplitude of the underlying wave spectrum. This equation system, with the directional wave spectrum taken to be the unknowns, is generally a highly underdetermined system with an unstable solution. To overcome this problem, a constrained least squares problem is formulated and Bayesian procedures, in the sense of so-called smoothing priors, are utilised to make the solution stable. Specifically, the wave spectrum is assumed to be smoothly changing with both frequency and directionality. The theory of the developed method, called the Bayesian estimation method, is outlined in detail and aspects otherwise not dealt with in the specific and quoted literature are considered.

As regards the measured responses, an FFT procedure for the cross spectral analysis with appropriate smoothing may be applied. However, as the choice of smoothing can greatly affect the final result and due to the necessities in decision support systems for an automatic method, another procedure is used. The measured response signals are instead analysed by multivariate autoregressive (MAR) procedures that utilise work carried out within the field of control theory. As the cross spectral analysis is of utmost importance for the calculation of reliable estimates of the wave spectra, the aspects of MAR procedures are studied comprehensively. Thus, two different MAR procedures are outlined and the so-called order selection criterion is studied specifically, including a numerical example.

1.8 Structure of the Thesis

The contents of the thesis are divided into ten chapters, including this chapter. In Chapter 2 the fundamentals of decision support, or in-service monitoring, systems are dealt with, and an existing system in which work has been carried out during this project is briefly mentioned. Chapters 3, 4 and 5 are all devoted to theoretical aspects and deal with the theory in relation to the Bayesian estimation method, the parametric estimation and the cross spectral analysis, respectively. As regards the ship responses used for the estimation of wave spectra, Chapter 6 studies central elements within this area. Subsequently, Chapters 7 - 9 yield results obtained through simulated and measured ship responses. Thus, in Chapter 7 the Bayesian estimation method is analysed and verified by the study of simulated ship motions, whereas Chapters 8 and 9 deal with full-scale data for which comparisons are performed with visual observations and measurements from the wave radar system WAVEX, respectively. Finally, in Chapter 10 the conclusions are summarised and, furthermore, recommendations for future work are made.

For the sake of completeness it should also be mentioned that six appendices, Appendices A - F, are included in the thesis. The appendices all contain additional information about the calculations and analyses carried out in Chapters 7 - 9.

This page is intentionally left blank.

Chapter 2

Decision Support Systems

2.1 Introduction

The commercial competition and the general technical development lead to more and more optimised ships. Consequently, such optimisations may imply a slow drift towards the physical limits of a ship's capability and survivability, cf. Huss and Olander (1994). Especially, the latter of these points is of interest not only to the maritime but also the public society, who both require increased safety of lives and environment. A conflict, or in other words, a paramount problem is therefore how to match safety with operationally optimised ships. This issue is, among many others, studied by Francescutto (1993) and from this paper a quotation, in relation to safety consequences of optimised ships, may be mentioned: "The conclusion is that the only way to overcome the many difficulties lies in the development of a system for the time domain simulation of ship motions in a seaway, including a detailed description of the environment ...". In the present chapter such systems, denoted in-service monitoring or decision support systems, are described with the focus on requirements and properties of the systems, and on the use and/or the working of the systems.

It should be emphasised that this chapter gives only the fundamentals of in-service monitoring systems, as the focus in the present thesis is not on the entire concept of such systems. For a comprehensive description of in-service monitoring systems reference is given to e.g. Huss and Olander (1994) and the Ship Structure Committee reports Debord and Hennessy (1990) and Slaughter et al. (1997) on monitoring systems.

2.2 Requirements and Properties

2.2.1 End Users

As regards decision support systems, two categories of people can be viewed as end users of a system. These are the officers on the ship and the shipowner. In the following there will not necessarily be strictly differentiated between the two groups in relation to their requirements for a decision support system.

As a general expectation of the end users of an in-service monitoring system, it can be stated that "hull and motion monitoring, and supervision of the ship stability will improve the safety on board", which is mentioned in the final evaluation report of the Danish joint project SeaSense, cf. Nielsen (2004). Thus, by inspection of the hull loads, i.e. the deformations, and the ship stability, immediate actions can be taken to eliminate/minimise risks of potential danger. Examples of such non-desired effects are, cf. Huss and Olander (1994):

- Seasickness of passengers
- Damage to cargo due to large accelerations
- Local structural damage to forward structure due to slamming, wave impacts and green water on deck
- Shift of cargo due to a combination of roll and accelerations
- Excitation of large roll motions (parametric roll)
- Loss of stability in following waves
- Hull girder damage due to extreme wave-induced loads

Specifically, it is desired that the system is able to identify critical forthcoming events, and to give guidance in relation to speed and/or course changes to reduce the wave-induced loads. Moreover, in case of lack of stability, due to a damage, the system is to report the consequences of changes in ballast to improve the survival capacity of the ship. With respect to future events it is obvious that if reliable predictions can be made at an early stage, the operation of the ship can be made safer. The key problem is, however, that the calculation of such predictions demands detailed information about the current weather and sea conditions in terms of the on-site wave energy spectrum at anytime. Therefore, for a decision support system to work properly, a reliable estimate of the on-site wave energy spectrum is essential. Such an estimate may be obtained in several ways and, as mentioned in the Introduction in Chapter 1, this is the very topic of the present thesis, where a Bayesian estimation method based on ship response measurements is the main subject.

On the assumption that an estimate of the wave energy spectrum is at hand, the following points may be listed in order to conclude on the requirements for a decision support system. Through communication with the system interface, the ship's officers should be able to, cf. Huss and Olander (1994):

- Automatically receive warnings of predefined risk events
- On request receive guidance/support on operational decisions
- Change any of the conditioned parameters in order to analyse alternative conditions

2.2.2 Ship Type

Depending on the type of ship, different kinds of requirements are made for the in-service monitoring system. In Table 2.1 a summary of the key responses based on ship type is given. Naturally, such a list is by no means complete, and the key point is that ship characteristics should be reviewed when requirements for decision support systems are considered.

2.2.3 General Information

It is important to note that in-service monitoring systems may be without integration of a methodology for estimation of the wave energy spectrum. Obviously, the drawback of such purely surveying, or 'passive', systems, which lack an estimate of the wave spectrum, is that predictions of future events can only be based on trends and records of already measured signals. Hence, the effect of speed and/or course changes cannot be taken into account. The reason for mentioning these passive systems is that until today, most developed in-service monitoring systems are actually of this kind. Further below, additions will be given with respect to this matter.

Another issue of importance, in relation to the term 'decision support', is that of statistical versus deterministic forecasts. Thus, it is vital to stress that, when predictions of future events are made for the systems studied here, all forecasts are given in a purely statistical sense. This means that a system will not be able to predict *when* the threshold value of, say, the vertical acceleration at FP is exceeded for given operational conditions, but is only able to predict with *which probability* a threshold excess is likely to occur for the on-site operational conditions. The reason which justifies this statistical point of view is that the wave excitations, and thus the ship responses, are assumed to be a stationary stochastic process.

Table 2.1: *Typical responses to be monitored depending on ship type*, Ship Structure Committee report, Slaughter et al. (1997).

Passenger ship	• Ship motions • Noise and vibrations • Bow flare slam
Tanker/products carrier	• Amidship hull girder stress • Bow/amidships side shell stiffeners • Forefoot slam • Explosive environment
Bulk ships	• Still water hull girder stresses • Cargo hold frame stresses • Stress concentration at hatch corners • Forefoot slam
Container ships	• Stress concentration at hatch corners • Hull girder torsion • Bow flare slam • Green water on bow • Whipping/cargo accelerations
LNG/internal tank	• Forefoot slam • Temperature/explosive atmosphere • Sloshing
Barges/platforms	• Towline/mooring tension • Motions and inertial forces • Lateral motion
Naval combatant	• Bow flare slam • Firing platform deflection

2.2.4 State-of-the-Art

Today, there exists a wide variety of in-service monitoring systems, and the development as such started in the 1970's. At this time the motivation was also a question of safety, however, it was more of a general character than related to increasingly optimised ships. Thus, some of the first papers, Lindemann and Nordenstrøm (1975) and Lindemann et al. (1977), which gave a thorough treatment of the concept of surveillance systems were partly based on an inquiry among Norwegian navigators. In this inquiry it was revealed that there was a large demand for more exact knowledge of how ships respond to changes in speed and course. One of the major problems through the past has been the lack of a reliable estimate of the on-site wave energy spectrum, which is needed to assess the effect of speed and/or course changes. Therefore, many of the existing in-service monitoring systems predict forthcoming risks only on the basis of trends and statistics of already measured records. For this reason, the systems cannot take into account changing operational conditions. In recent research, methodologies to estimate the on-site wave energy spectrum have, however, been developed

and promising results have been obtained. One of these methods is to be studied extensively in the present thesis.

In-service monitoring systems have not yet become standard equipment, although some kind of real-time operational surveillance to follow/study wave-induced effects is now installed on many ships. Furthermore, most classification societies have introduced a special class notation for ships with installed hull surveillance systems, cf. Huss and Olander (1994). Based on a study carried out by Lloyd's Register of Shipping, Robinson (1990) identifies four different types of systems, or monitors, which enable ships to be operated efficiently within their design limits:

- *Seakeeping monitor*: Display of motions
- *Loading and structural monitor*: Display of still-water and wave-induced stresses, accelerations and impact loadings
- *Machinery and fuel performance monitor*: Display of shaft power, rpm and fuel consumption
- *Environmental monitor*: Display of current values (wind, temperatures, barometric pressure, water depth, calculated sea state)

It is common to all the types of monitors, with the exception of the latter, that each has its own optimum concerning the proper ship speed and heading relative to the waves. However, some of the monitors are often integrated, so that the integrated in-service monitoring system offers information which deals with several of the points stated above. The SeaSense system is of this kind and in Section 2.4 below this system is briefly mentioned.

Another system is under development in an ongoing EU project called the ADOPT, *Advanced Decision Support System for Ship Design, Operation and Training*, see ADOPT (2005). This project consists of a number of tasks, which include gathering of information relevant to decision-making during navigation, relevant to decision on environmental information of importance to the ship behaviour, etc., and in the end an integration of all the information should lead to the ADOPT Decision Support Tool.

2.3 Theoretical Procedures for Predictions

In this section it is outlined how a decision support system in principle may work, and in this connection the statistical prediction of future responses is also treated concisely.

For the sake of overview the key points in a decision support system are:

- Measurements of the ship's responses
- Knowledge of the ship's operational condition
- Linear response calculations in the frequency domain
- For non-linear responses, time series simulation is used
- A methodology for estimation of the sea state, i.e. the (directional) wave spectrum
- Statistical models for establishment of risk levels of non-desired events

2.3.1 Sensors and Response Statistics

With a set of sensors, see Figure 2.1 a), different ship responses can be measured and recorded. Thus, values can be monitored and a direct comparison can immediately be conducted with current threshold values, and furthermore trend statistics can be carried out. By integrating the sensor measurements with a mathematical model, as illustrated in Figure 2.1 b), it is possible to derive an estimate of the directional wave energy spectrum $E(\omega_e, \beta)$ with ω_e and β being the angular encounter frequency and the encounter angle relative to the wave direction, respectively. (In practical applications the wave frequency ω_0 is most often used in favour of the encounter frequency and, similarly, some angle θ relative to a fixed direction, say, the north is probably used in favour of the encounter angle.) For completeness, it should be mentioned that the wave spectrum may also be estimated by other means, e.g. wave radar systems. With the directional wave spectrum obtained, linear response statistics can readily be conducted, and in the text below the theoretical foundation for this is summarised. For reference, standard textbooks on ship responses such as Jensen (2001), Bhattacharyya (1978), and Lloyd (1998) may be consulted. Though, the specific presentation follows to a closer extent Pedersen (2000).

As stated previously, the ship responses are considered as stationary processes, which means that the statistical properties which characterise the processes do not depend on time. In the literature, stationarity of waves is typically assumed to hold within a duration of between thirty minutes and three hours, and the statistics used for describing the processes is denoted by 'short-term statistics'.

The fundamental assumption of linearity between the wave excitations and the ship responses facilitates a linear spectral analysis in the frequency domain, so that short-term statistics can be conducted. Hence, from a known general ship response R in terms of a complex-valued transfer function $\Phi_R(\omega_e, \beta)$, the theoretical relationship between the response spectrum $S_R(\omega_e)$ and the wave spectrum $E(\omega_e, \beta)$ is given by

$$S_R(\omega_e) = \int_0^{2\pi} |\Phi_R(\omega_e, \beta)|^2 E(\omega_e, \beta)\, d\beta \tag{2.1}$$

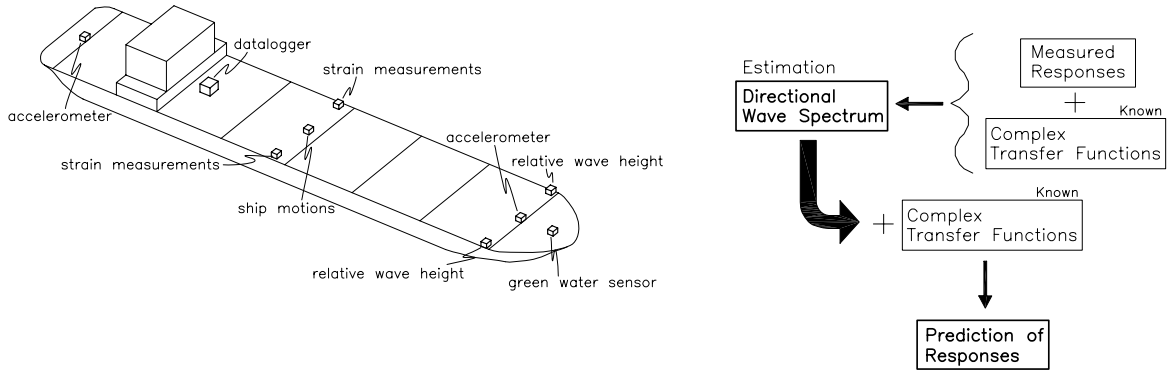

a) b)

Figure 2.1: a) *A ship mounted with a set of sensors.* b) *Illustration of a methodology for the prediction of future responses*, e.g. Iseki and Terada (2002).

Although only written as functions of the encounter frequency ω_e and the encounter angle β, other operational parameters (speed, loading condition, ...) and the sea state influence the individual functions as well.

From the response spectral density $S_R(\omega_e)$, the nth order spectral moments can be defined as

$$m_{Rn} = \int_0^\infty \omega_e^n S_R(\omega_e)\, d\omega_e \quad , \quad m = 0, 1, 2, ... \tag{2.2}$$

Based on these spectral moments, characteristics of the considered response can be derived. On the assumption that the response is narrow-banded, the distribution of the peak values can e.g. be approximated by the Rayleigh distribution

$$F_p(z) = 1 - \exp\left(-\frac{z^2}{2m_{R0}}\right) \tag{2.3}$$

Furthermore, the zero-upcrossing rate ν_0 and the peak rate ν_p may be given in terms of the spectral moments

$$\nu_0 = \frac{1}{2\pi}\sqrt{\frac{m_{R2}}{m_{R0}}} \tag{2.4}$$

$$\nu_p = \frac{1}{2\pi}\sqrt{\frac{m_{R4}}{m_{R2}}} \tag{2.5}$$

Finally, it is worth mentioning the q-quantile, $\tilde{\mu}_{N,q}$, defined as the value which the largest peak exceeds with a given small probability q. By defining the number of zero-upcrossings, N_Z, in a given period T, as

$$N_Z = \nu_0 T \tag{2.6}$$

the q-quantile can be approximated to

$$\tilde{\mu}_{N,q} \simeq s_R \sqrt{2 \ln (N_Z/q)} \tag{2.7}$$

for $N_Z \gg 1$ and $q \ll 1$, and with s_R being the standard deviation of the response found from the 0th order moment

$$s_R = \sqrt{m_{R0}} \tag{2.8}$$

Obviously, in an in-service monitoring system, the above statistical values are but a few which may be of interest to evaluate.

Another aspect of importance is which values to use as threshold values and how to determine these for the different responses. This topic will, however, not be touched and, in general, this is also an issue with sparse specific literature and a task for the proper authorities to deal with. Instead, it should be mentioned that the ADOPT project, cf. ADOPT (2005), mentioned above, has as its first task "...to decide which ship related information is relevant in decision making when navigating a ship and how to implement this information". Thus, information about and knowledge of the determination of threshold values will certainly be acquired within the project.

2.4 Example - SeaSense

As part of the present research, work was also carried out at the preliminary stage within the Danish joint project SeaSense (2003). Hence, with the fundamentals of decision support systems clarified, a real in-service monitoring system may be studied for illustrative purposes, with the focus on the presentation of results in the form of screen dumps of the user interface. For other references on real in-service monitoring systems and their practical use see e.g. Melitz et al. (1992) and Witmer and Lewis (1994).

2.4.1 Sea State and Sensors

In the system developed in SeaSense, the sea state parameters are estimated by use of a parametric method, more or less similar to the procedure derived in Chapter 4 in this thesis. The basis of the method is as illustrated in Figure 2.1 b), but for details reference is made to Chapter 4.

The monitoring program in the SeaSense system contains information about a variety of measured responses, and from the sketch in Figure 2.2 it is seen that measurements of vertical accelerations in more positions, hull girder stresses, relative wave heights, etc. take place.

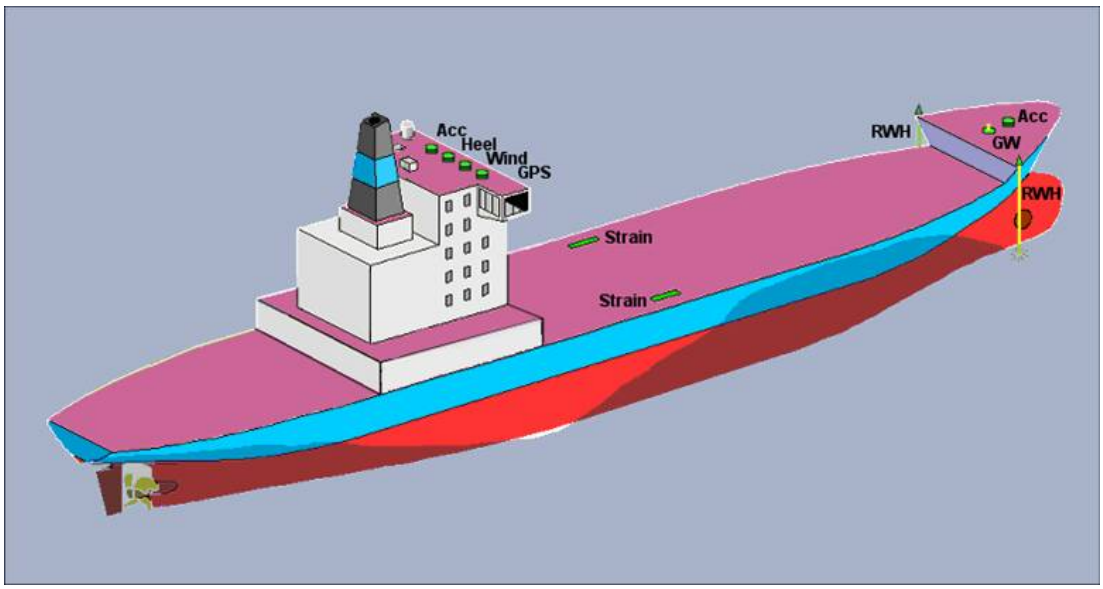

Figure 2.2: *A sketch with indication of the responses recorded.* SeaSense (2003).

2.4.2 User Interface

For an in-service monitoring system to be used efficiently and reliably, the user interface and the information given from it must be easily perceptible. This makes large demands on the presentation and the visualisation of the results and the information obtained from the measurements. However, such an assessment is not carried out here, but a number of screen dumps are presented for the particular SeaSense system in the following.

An overview of the user interface is given in Figure 2.3. From the figure (from the buttons on the right-hand side) it is seen that dependent on whether responses are to be monitored, guidance is to be given, etc., a specific button should be pressed on the user interface. Thus, two situations in relation to the responses are depicted in Figure 2.4. In the left plot motion responses are monitored, whereas the right plot shows an example of wave encounter incidences as regards bow water emergence and green water events. The plots in Figure 2.5 show examples of information given on the wave environment and on ship guidance. Ship guidance, i.e. decision support, on operational parameters, such as speed and course, is often given according to a polar diagram. In the polar diagram the ship course is read from radial lines whereas the speed is given relative to circles, so that each circle in the diagram represents a specific speed. Hence, by use of colour indications, advice can be given on speed and course in order to avoid exceeding threshold values for specific responses.

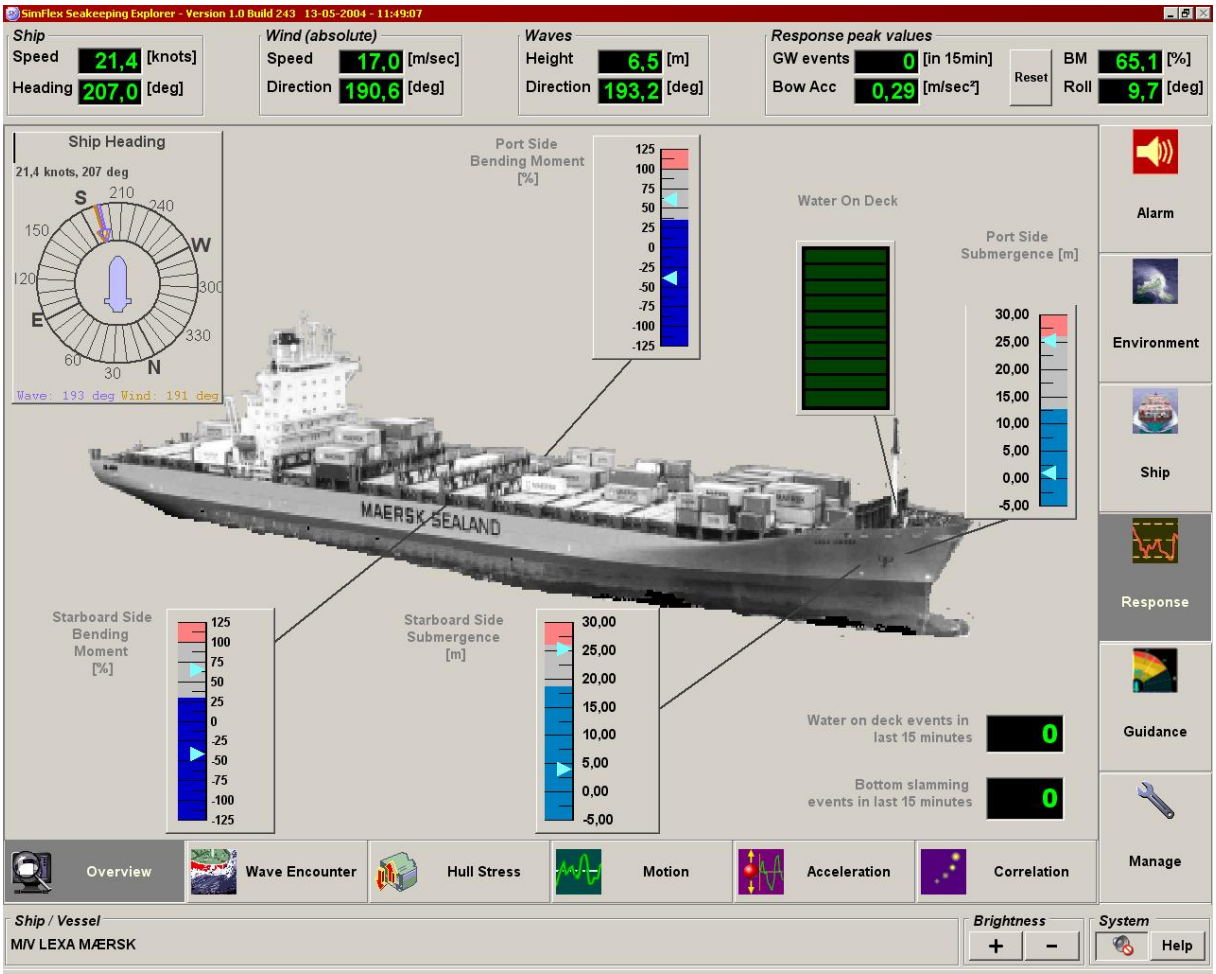

Figure 2.3: *Overview of the user interface.* SeaSense (2003).

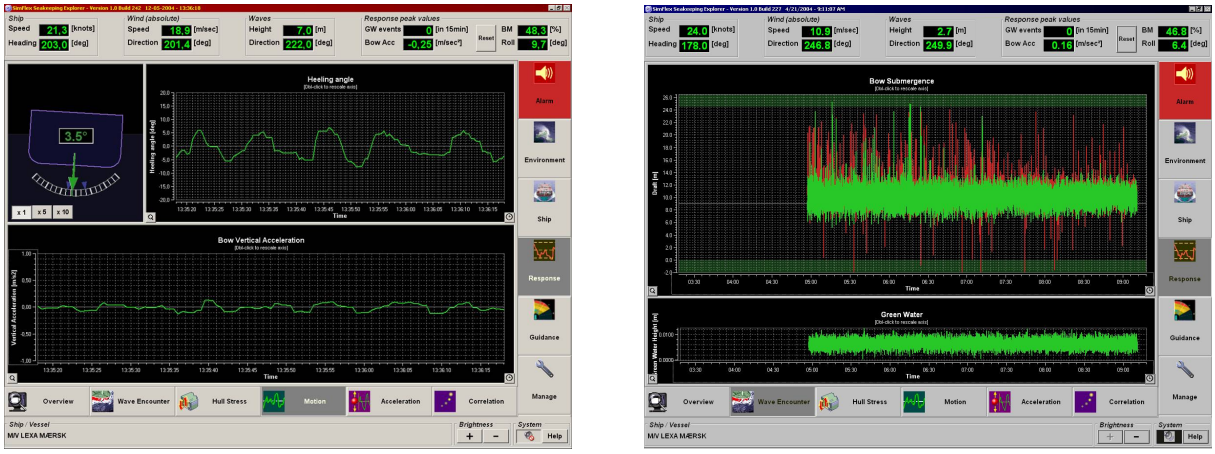

Figure 2.4: *Monitoring of responses.* SeaSense (2003).

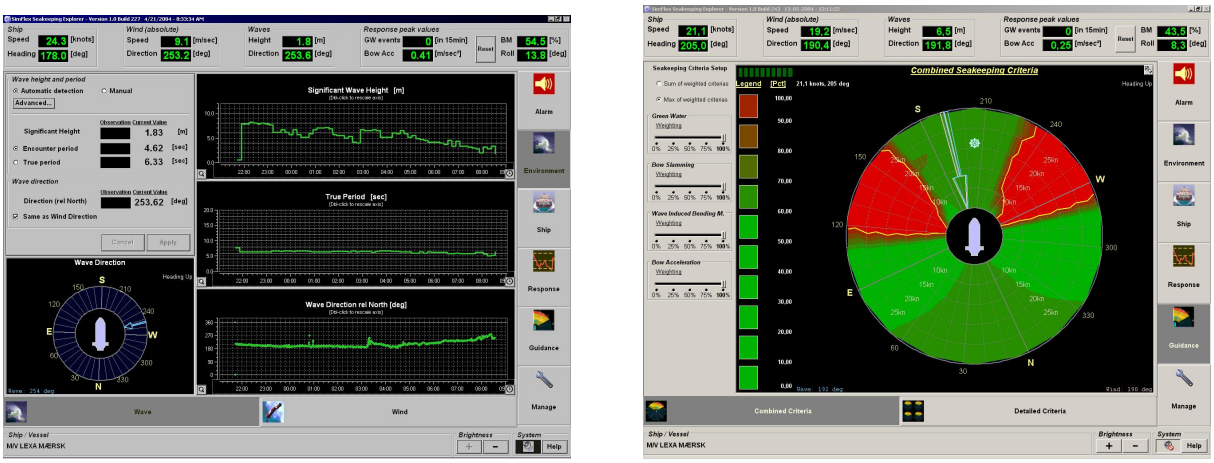

Figure 2.5: *Wave environment and ship guidance.* SeaSense (2003).

Figure 2.6: *Storm on the Atlantic Ocean and heavy wave impact during the very first test trial in the SeaSense project.*

This page is intentionally left blank.

Chapter 3

Bayesian Estimation

3.1 Introduction

With the time series of given measured ship responses, the corresponding response cross spectra, $S_{ij}(\omega_e)$, can be obtained. The measured cross spectra are functions of the encounter frequency ω_e. It should be noted that, from now on, $S_{ij}(\omega_e)$ is denoted only by 'cross spectra' as 'response' is understood unless otherwise stated. Moreover, for a specific description of the calculation of the cross spectra and a general cross spectral analysis reference is made to Chapter 5.

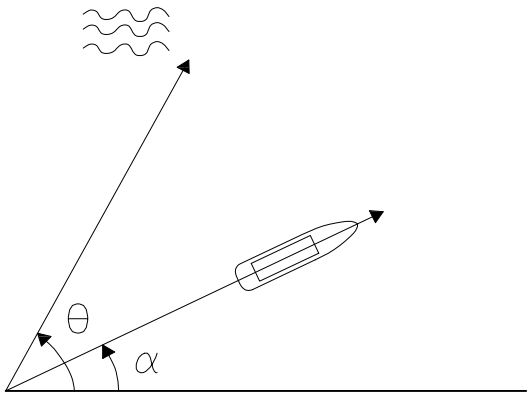

Figure 3.1: *Ship course, α, and wave direction, θ, relative to a fixed direction.*

The encounter angle β is defined as the heading of the ship relative to the waves and $\beta = \pi$ corresponds to head waves. From Figure 3.1 it is seen that when the ship course and the wave direction are measured relative to some fixed direction, the encounter angle is given by

$$\beta = \theta - \alpha \tag{3.1}$$

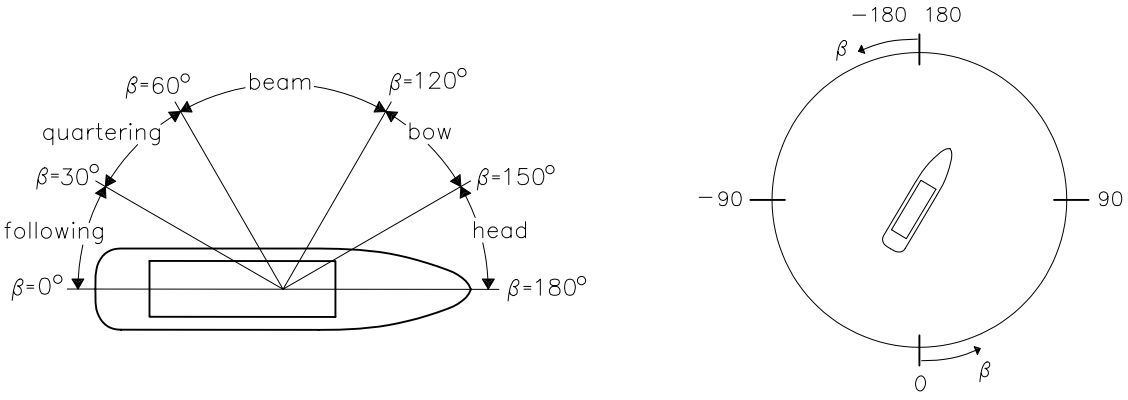

Figure 3.2: *Definition of terms as regards the encounter angles and the sign convention of* β*. Note that* β *is shown in degrees.*

As regards characteristic terms depending on the value of the encounter angle, these are illustrated in Figure 3.2.

If the ship responses are assumed to be linear with the incident waves, the complex-valued transfer functions $\Phi_i(\omega_e, \beta)$ and $\Phi_j(\omega_e, \beta)$ for the ith and jth responses yield the theoretical relationship between the ith and the jth components of the cross spectra and the directional wave spectrum $E(\omega_e, \theta)$ through the following integral equation, see e.g. Bhattacharyya (1978)

$$S_{ij}(\omega_e) = \int_{-\pi}^{\pi} \Phi_i(\omega_e, \beta)\, \overline{\Phi_j(\omega_e, \beta)} E(\omega_e, \theta)\, d\theta \tag{3.2}$$

with $\overline{\cdot}$ denoting the complex conjugate.

For convenience, the fixed direction in Figure 3.1 is taken to be coincident to the ship course so that the wave direction is given relative to the ship course, that is, $\beta = \theta$. Hence, (3.2) is rewritten

$$S_{ij}(\omega_e) = \int_{-\pi}^{\pi} \Phi_i(\omega_e, \beta)\, \overline{\Phi_j(\omega_e, \beta)} E(\omega_e, \beta)\, d\beta \tag{3.3}$$

As a general comment on (3.3) it should be noted that the directional wave spectrum $E(\omega_e, \beta)$ is convolved with, i.e. smeared out by, some known response function $\Phi_i(\omega_e, \beta)$ to give a smeared signal $S_{ij}(\omega_e)$, the cross spectra. Hence, if the opposite is done in the estimation of the directional wave spectrum, $E(\omega_e, \beta)$ is said to be deconvolved from (3.3), which task is called deconvolution. Moreover, as will be seen further below, deconvolution can be facilitated by inverse theory and/or Bayesian modelling, which are the main topics in the present chapter.

3.2 Basic Equations

The wave spectrum is advantageously estimated in the wave frequency domain, however, transformation of the right-hand side of (3.3) into a true wave frequency, ω_0, implies the so-called triple-valued function problem. This problem is governed by the deep-water relationship between the encounter and the wave frequency

$$\omega_e = \omega_0 - \omega_0^2 A \quad , \quad A = \frac{V}{g}\cos\beta \tag{3.4}$$

with V being the speed of the ship, and g the acceleration of gravity.

It should be noted that in following waves, $\beta \in [-\frac{\pi}{2}; \frac{\pi}{2}]$, for certain speeds, three wave frequencies yield the solution to the triple-valued function problem, see Figure 3.3. Therefore,

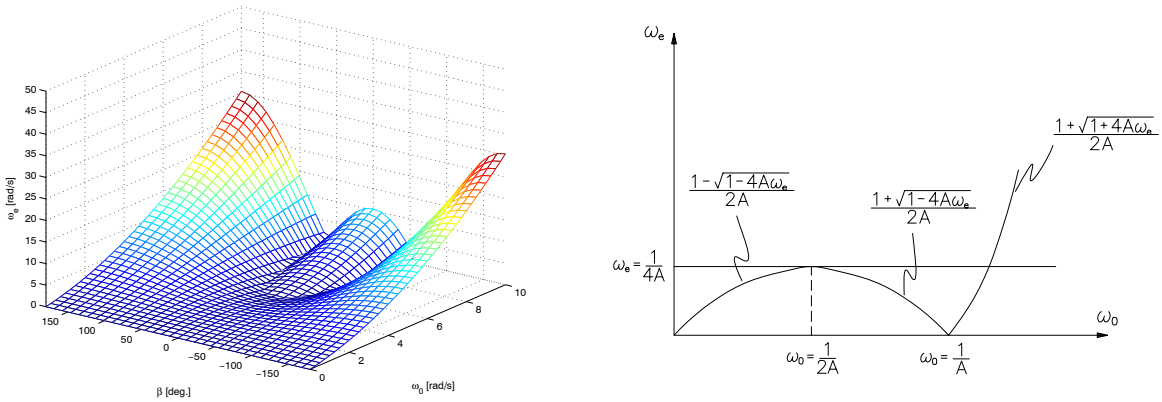

a) b)

Figure 3.3: *The relationship between encounter and wave frequencies.* a) *All-directional relationship (an arbitrary example), and* b) *a cross section at* $\beta = \theta_\alpha$ *with* $\theta_\alpha \in [-90; 90]$ deg.

in following sea and with $\omega_e < \frac{1}{4A}$, when (3.3) is transformed into the wave frequency domain, the following three wave frequencies all have to be considered, as it cannot beforehand be determined which of the frequencies is the real true one

$$\begin{aligned} \omega_{01} &= \tfrac{1-\sqrt{1-4A\omega_e}}{2A} & \left|\tfrac{d\omega_{01}}{d\omega_e}\right| &= \tfrac{1}{\sqrt{1-4A\omega_e}} \\ \omega_{02} &= \tfrac{1+\sqrt{1-4A\omega_e}}{2A} \quad , & \left|\tfrac{d\omega_{02}}{d\omega_e}\right| &= \tfrac{1}{\sqrt{1-4A\omega_e}} \\ \omega_{03} &= \tfrac{1+\sqrt{1+4A\omega_e}}{2A} & \left|\tfrac{d\omega_{03}}{d\omega_e}\right| &= \tfrac{1}{\sqrt{1+4A\omega_e}} \end{aligned} \tag{3.5}$$

Hence, the transformation into the wave frequency domain is

$$\begin{aligned} S_{ij}(\omega_e) &= \int_{\frac{\pi}{2}}^{\pi} \Phi_i(\omega_{01},\beta)\,\overline{\Phi_j(\omega_{01},\beta)}E(\omega_{01},\beta)\left|\frac{d\omega_{01}}{d\omega_e}\right|d\beta \\ &+ \int_{-\frac{\pi}{2}}^{\frac{\pi}{2}} \Phi_i(\omega_{01},\beta)\,\overline{\Phi_j(\omega_{01},\beta)}E(\omega_{01},\beta)\left|\frac{d\omega_{01}}{d\omega_e}\right|d\beta \\ &+ \int_{-\frac{\pi}{2}}^{\frac{\pi}{2}} \Phi_i(\omega_{02},\beta)\,\overline{\Phi_j(\omega_{02},\beta)}E(\omega_{02},\beta)\left|\frac{d\omega_{02}}{d\omega_e}\right|d\beta \\ &+ \int_{-\frac{\pi}{2}}^{\frac{\pi}{2}} \Phi_i(\omega_{03},\beta)\,\overline{\Phi_j(\omega_{03},\beta)}E(\omega_{03},\beta)\left|\frac{d\omega_{03}}{d\omega_e}\right|d\beta \\ &+ \int_{-\pi}^{-\frac{\pi}{2}} \Phi_i(\omega_{01},\beta)\,\overline{\Phi_j(\omega_{01},\beta)}E(\omega_{01},\beta)\left|\frac{d\omega_{01}}{d\omega_e}\right|d\beta \end{aligned} \tag{3.6}$$

where it should be stressed that the addition of the second and the third line, which correspond to following seas, is only done for $\omega_e < \frac{1}{4A}$.

3.3 Matrix Notation and Multivariate Expression

In order to perform numerical calculations the integration on the right-hand side is discretised as

$$\begin{aligned} S_{ij}(\omega_e) &= \Delta\beta \sum_{k=1}^{K} \Phi_{ik}(\omega_{01})\,\overline{\Phi_{jk}(\omega_{01})}E_k(\omega_{01}) \\ &+ \Delta\beta \sum_{k=1}^{K1} \Phi_{ik}(\omega_{02})\,\overline{\Phi_{jk}(\omega_{02})}E_k(\omega_{02}) \\ &+ \Delta\beta \sum_{k=1}^{K1} \Phi_{ik}(\omega_{03})\,\overline{\Phi_{jk}(\omega_{03})}E_k(\omega_{03}) \end{aligned} \tag{3.7}$$

where

$$\begin{aligned} &\Delta\beta = \tfrac{2\pi}{K}, \qquad E_k(\omega_{0m}) = E(\omega_{0m},\beta_k)\left|\tfrac{d\omega_{0m}}{d\omega_e}\right|_{\beta=\beta_k} \quad, m = 1,2,3 \\ &\beta_k = -\pi + (k-1)\,\Delta\beta, \qquad \Phi_{ik}(\omega_{0m}) = \Phi_i(\omega_{0m},\beta_k) \quad, m = 1,2,3 \end{aligned} \tag{3.8}$$

Here $K1$ is the number of small 'areas' which belong to following seas ($K1 \approx K/2$), and again it should be emphasised that only for $-\frac{\pi}{2} < \beta < \frac{\pi}{2}$ and $\omega_e < \frac{1}{4A}$, $S_{ij}(\omega_e)$ can be

computed directly as given by (3.7). Basically, the triple-valued function problem means that for each ω_e, and the K different headings considered, there might be up to $K + 2K1$ different combinations of frequency response functions, and likewise for the directional wave spectrum.

From the discretised format it is realised that the cross spectrum can be given in matrix notation

$$\begin{aligned}\mathbf{S}(\omega_e) &= \Delta\beta\boldsymbol{\Phi}(\omega_{01})\,\mathbf{E}(\omega_{01})\,\overline{\boldsymbol{\Phi}(\omega_{01})}^{T} \\ &\quad +\Delta\beta\boldsymbol{\Phi}(\omega_{02})\,\mathbf{E}(\omega_{02})\,\overline{\boldsymbol{\Phi}(\omega_{02})}^{T} \\ &\quad +\Delta\beta\boldsymbol{\Phi}(\omega_{03})\,\mathbf{E}(\omega_{03})\,\overline{\boldsymbol{\Phi}(\omega_{03})}^{T}\end{aligned} \tag{3.9}$$

Given e.g. three kinds of response data, η, φ and θ, then $\mathbf{S}$, $\boldsymbol{\Phi}$ and $\mathbf{E}$ are determined as

$$\mathbf{S}(\omega_e) = \begin{bmatrix} S_{\eta\eta}(\omega_e) & S_{\eta\varphi}(\omega_e) & S_{\eta\theta}(\omega_e) \\ S_{\varphi\eta}(\omega_e) & S_{\varphi\varphi}(\omega_e) & S_{\varphi\theta}(\omega_e) \\ S_{\theta\eta}(\omega_e) & S_{\theta\varphi}(\omega_e) & S_{\theta\theta}(\omega_e) \end{bmatrix} \tag{3.10}$$

$$\boldsymbol{\Phi}(\omega_{01}) = \begin{bmatrix} \Phi_{\eta 1}(\omega_{01}) & \cdots & \Phi_{\eta K}(\omega_{01}) \\ \Phi_{\varphi 1}(\omega_{01}) & \cdots & \Phi_{\varphi K}(\omega_{01}) \\ \Phi_{\theta 1}(\omega_{01}) & \cdots & \Phi_{\theta K}(\omega_{01}) \end{bmatrix} \tag{3.11}$$

$$\mathbf{E}(\omega_{01}) = \begin{bmatrix} E_1(\omega_{01}) & \cdots & 0 \\ \vdots & \ddots & \vdots \\ 0 & \cdots & E_K(\omega_{01}) \end{bmatrix} \tag{3.12}$$

$$\boldsymbol{\Phi}(\omega_{0i}) = \begin{bmatrix} \Phi_{\eta 1}(\omega_{0i}) & \cdots & \Phi_{\eta K1}(\omega_{0i}) \\ \Phi_{\varphi 1}(\omega_{0i}) & \cdots & \Phi_{\varphi K1}(\omega_{0i}) \\ \Phi_{\theta 1}(\omega_{0i}) & \cdots & \Phi_{\theta K1}(\omega_{0i}) \end{bmatrix}, \; i = 2, 3 \tag{3.13}$$

$$\mathbf{E}(\omega_{0i}) = \begin{bmatrix} E_1(\omega_{0i}) & \cdots & 0 \\ \vdots & \ddots & \vdots \\ 0 & \cdots & E_{K1}(\omega_{0i}) \end{bmatrix}, \; i = 2, 3 \tag{3.14}$$

By the calculation of $\mathbf{S}(\omega_e)$ it is observed that the cross spectrum matrix is Hermitian, i.e. $S_{ij} = \overline{S_{ji}}$, with

$$S_{ij} = C_{ij} + iQ_{ij} \tag{3.15}$$

where the even function C_{ij} is called the co-spectrum and the odd function Q_{ij} is called the quadrature-spectrum, e.g. Price and Bishop (1974).

Hence, if only the upper triangular matrix is used and real and imaginary parts are expressed separately, (3.9) can be transformed into a multivariate model expression, cf. Iseki and Terada (2002)

$$\widetilde{\mathbf{b}} = \widetilde{\mathbf{A}}\widetilde{\mathbf{f}}\left(\widetilde{\mathbf{x}}\right) + \widetilde{\mathbf{w}} \tag{3.16}$$

Here $\widetilde{\mathbf{b}}$ is the 9×1 cross spectrum vector, which is composed of real and imaginary parts of the cross spectrum matrix, i.e.

$$\widetilde{\mathbf{b}} = \begin{bmatrix} S_{\eta\eta}\left(\omega_e\right) \\ S_{\varphi\varphi}\left(\omega_e\right) \\ S_{\theta\theta}\left(\omega_e\right) \\ \mathrm{Re}\left(S_{\eta\varphi}\left(\omega_e\right)\right) \\ \mathrm{Re}\left(S_{\eta\theta}\left(\omega_e\right)\right) \\ \mathrm{Re}\left(S_{\varphi\theta}\left(\omega_e\right)\right) \\ \mathrm{Im}\left(S_{\eta\varphi}\left(\omega_e\right)\right) \\ \mathrm{Im}\left(S_{\eta\theta}\left(\omega_e\right)\right) \\ \mathrm{Im}\left(S_{\varphi\theta}\left(\omega_e\right)\right) \end{bmatrix} \tag{3.17}$$

$\widetilde{\mathbf{A}}$ denotes the $9 \times (K + 2K1)$ coefficient or system matrix composed of the products of the response functions and is given by

$$\widetilde{\mathbf{A}} = \Delta\beta \begin{bmatrix} \left|\Phi_{\eta 1}\left(\omega_{01}\right)\right|^2 \left|\frac{d\omega_{01}}{d\omega_e}\right| & \cdots & \left|\Phi_{\eta K1}\left(\omega_{03}\right)\right|^2 \left|\frac{d\omega_{03}}{d\omega_e}\right| \\ \left|\Phi_{\varphi 1}\left(\omega_{01}\right)\right|^2 \left|\frac{d\omega_{01}}{d\omega_e}\right| & \cdots & \left|\Phi_{\varphi K1}\left(\omega_{03}\right)\right|^2 \left|\frac{d\omega_{03}}{d\omega_e}\right| \\ \left|\Phi_{\theta 1}\left(\omega_{01}\right)\right|^2 \left|\frac{d\omega_{01}}{d\omega_e}\right| & \cdots & \left|\Phi_{\theta K1}\left(\omega_{03}\right)\right|^2 \left|\frac{d\omega_{03}}{d\omega_e}\right| \\ \mathrm{Re}\left(\Phi_{\eta 1}\left(\omega_{01}\right)\overline{\Phi_{\varphi 1}\left(\omega_{01}\right)}\right)\left|\frac{d\omega_{01}}{d\omega_e}\right| & \cdots & \mathrm{Re}\left(\Phi_{\eta K1}\left(\omega_{03}\right)\overline{\Phi_{\varphi K1}\left(\omega_{03}\right)}\right)\left|\frac{d\omega_{03}}{d\omega_e}\right| \\ \mathrm{Re}\left(\Phi_{\eta 1}\left(\omega_{01}\right)\overline{\Phi_{\theta 1}\left(\omega_{01}\right)}\right)\left|\frac{d\omega_{01}}{d\omega_e}\right| & \cdots & \mathrm{Re}\left(\Phi_{\eta K1}\left(\omega_{03}\right)\overline{\Phi_{\theta K1}\left(\omega_{03}\right)}\right)\left|\frac{d\omega_{03}}{d\omega_e}\right| \\ \mathrm{Re}\left(\Phi_{\varphi 1}\left(\omega_{01}\right)\overline{\Phi_{\theta 1}\left(\omega_{01}\right)}\right)\left|\frac{d\omega_{01}}{d\omega_e}\right| & \cdots & \mathrm{Re}\left(\Phi_{\varphi K1}\left(\omega_{03}\right)\overline{\Phi_{\theta K1}\left(\omega_{03}\right)}\right)\left|\frac{d\omega_{03}}{d\omega_e}\right| \\ \mathrm{Im}\left(\Phi_{\eta 1}\left(\omega_{01}\right)\overline{\Phi_{\varphi 1}\left(\omega_{01}\right)}\right)\left|\frac{d\omega_{01}}{d\omega_e}\right| & \cdots & \mathrm{Im}\left(\Phi_{\eta K1}\left(\omega_{03}\right)\overline{\Phi_{\varphi K1}\left(\omega_{03}\right)}\right)\left|\frac{d\omega_{03}}{d\omega_e}\right| \\ \mathrm{Im}\left(\Phi_{\eta 1}\left(\omega_{01}\right)\overline{\Phi_{\theta 1}\left(\omega_{01}\right)}\right)\left|\frac{d\omega_{01}}{d\omega_e}\right| & \cdots & \mathrm{Im}\left(\Phi_{\eta K1}\left(\omega_{03}\right)\overline{\Phi_{\theta K1}\left(\omega_{03}\right)}\right)\left|\frac{d\omega_{03}}{d\omega_e}\right| \\ \mathrm{Im}\left(\Phi_{\varphi 1}\left(\omega_{01}\right)\overline{\Phi_{\theta 1}\left(\omega_{01}\right)}\right)\left|\frac{d\omega_{01}}{d\omega_e}\right| & \cdots & \mathrm{Im}\left(\Phi_{\varphi K1}\left(\omega_{03}\right)\overline{\Phi_{\theta K1}\left(\omega_{03}\right)}\right)\left|\frac{d\omega_{03}}{d\omega_e}\right| \end{bmatrix} \tag{3.18}$$

while $\widetilde{\mathbf{f}}\left(\widetilde{\mathbf{x}}\right)$ is the unknown discretised directional wave spectrum, expressed as a $(K + 2K1) \times 1$ vector

$$\begin{aligned} \widetilde{\mathbf{f}}\left(\widetilde{\mathbf{x}}\right) &= \begin{bmatrix} E_1\left(\omega_{01}\right) & E_2\left(\omega_{01}\right) & \cdots & E_{K+2K1-1}\left(\omega_{03}\right) & E_{K+2K1}\left(\omega_{03}\right) \end{bmatrix}^T \\ &= \begin{bmatrix} \exp\left(x_1\right) & \exp\left(x_2\right) & \cdots & \exp\left(x_{J-1}\right) & \exp\left(x_J\right) \end{bmatrix}^T \end{aligned} \tag{3.19}$$

i.e.

$$\exp\left(x_j\right) = E_j\left(\omega_{0i}\right) \quad , \quad \begin{cases} i = 1 : j = 1, 2, ..., K \\ i = 2 : j = K+1, ..., K+K1 \\ i = 3 : j = K+K1+1, ..., K+2K1 \end{cases} \tag{3.20}$$

The exponential function acts as a non-negativity constraint and assures that the directional wave spectrum takes only values greater than zero. Finally, $\widetilde{\mathbf{w}}$ is a Gaussian white noise sequence vector with zero mean and variance $\widetilde{\sigma}^2$, introduced for stochastic reasons, so that the Bayesian modelling, which is dealt with later, is facilitated.

From the preceding it should be realised that, in general, when N kinds of response signals, i.e. time series, are considered, then

$$\begin{aligned} \text{size}\left(\widetilde{\mathbf{b}}\right) &= N^2 \times 1 \\ \text{size}\left(\widetilde{\mathbf{A}}\right) &= N^2 \times (K + 2K1) \end{aligned} \tag{3.21}$$

and from now on N kinds of time series are assumed.

3.4 Numerical Considerations

Considering numerical computations, an elementary but difficult problem exists due to the triple-valued function problem. Thus, depending on the value of the encounter frequency, the number $K + 2K1$ might, as noted previously, differ, which implies a different dimension of $\widetilde{\mathbf{A}}$ and $\widetilde{\mathbf{f}}\left(\widetilde{\mathbf{x}}\right)$, from encounter frequency to encounter frequency. One way to overcome this problem is explained in detail in the following, and furthermore it is shown how to take more encounter frequencies into account at the same time.

3.4.1 Prespecified Wave Frequencies

Basically, the idea is that a certain range of wave frequencies is specified in advance, i.e. the total number M of wave frequencies is known/chosen without considerations of the triple-valued function problem (TVFP). By allocating all of the total K heading angles to each of the chosen wave frequencies, a kind of vector that shows the organisation of heading angles and wave frequencies can be set up. The setup of this 'vector' serves only the purpose of visualisation and understanding of how the coefficient matrix $\widetilde{\mathbf{A}}$ is later to be organised. What is to be found from the 'vector' is the sequence of heading angles and wave frequencies

in which $\widetilde{\mathbf{A}}$ is evaluated. The 'vector' is determined in the following way (from now on, the index 0 is left out in the prespecified wave frequencies)

$$\begin{array}{c} (\beta_1, \omega_1) \\ (\beta_2, \omega_1) \\ \vdots \\ (\beta_K, \omega_1) \\ (\beta_1, \omega_2) \\ \vdots \\ (\beta_K, \omega_2) \\ (\beta_1, \omega_3) \\ \vdots \\ \vdots \\ (\beta_K, \omega_M) \end{array} \tag{3.22}$$

and it should be noted that the total number of element pairs is $K \cdot M$.

With the introduction of prespecified wave frequencies and the specified encounter angles, as well, the computational domain is completely discretised. Hence, in polar format, the discretisation can be visualised from Figure 3.4.

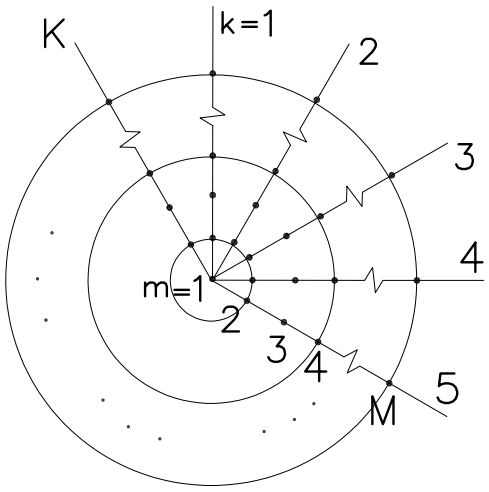

Figure 3.4: *Discretisation of wave frequencies and encounter angles.*

According to the TVFP each encounter frequency yields either one or three wave frequencies for each heading angle considered. The calculated pairs of heading angles and wave frequencies are distributed in accordance with (3.22). Obviously, the value of the wave frequency, as found from the TVFP, is with little chance found exactly as one of the specified wave frequencies in (3.22). Theoretically, however, the finer the discretisation for the specified

wave frequencies, the better the TVFP value can be approximated from (3.22). Though, in order to avoid too many prespecified wave frequencies, a weighting based on linear interpolation is introduced. Thus, by considering the situation depicted in Figure 3.5, the frequency response function is calculated as (it is assumed that the TVFP has resulted in the wave frequency ω_{01})

$$\Phi(\omega_{01}) = \frac{b}{a+b}\Phi(\omega_{\mu}) + \frac{a}{a+b}\Phi(\omega_{\mu+1}) \tag{3.23}$$

where the issue of interpolation in complex numbers, which is discussed in Chapter 6, must be remembered.

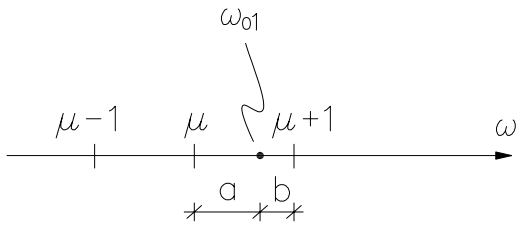

Figure 3.5: *In order to avoid too many discretised frequencies, a weighting is introduced.*

With the specified organisation of wave frequencies and heading angles, cf. (3.22), the coefficient matrix $\widetilde{\mathbf{A}}$ in the multivariate model expression no longer is of the size $N^2 \times (K + 2K1)$, but instead

$$\text{size}\left(\widetilde{\mathbf{A}}\right) = N^2 \times (K \cdot M) \tag{3.24}$$

and, indeed, the matrix may now contain a lot of zero elements.

From the organisation of $\widetilde{\mathbf{A}}$, the vector of unknown discretised values of the wave spectrum

is to be evaluated according to

$$\mathbf{f}(\mathbf{x}) = \begin{bmatrix} \exp(x_{\beta 1,\omega 1}) \\ \exp(x_{\beta 2,\omega 1}) \\ \vdots \\ \exp(x_{\beta K,\omega 1}) \\ \exp(x_{\beta 1,\omega 2}) \\ \vdots \\ \exp(x_{\beta K,\omega 2}) \\ \exp(x_{\beta 1,\omega 3}) \\ \vdots \\ \vdots \\ \exp(x_{\beta K,\omega M}) \end{bmatrix} \tag{3.25}$$

so that size($\mathbf{f}(\mathbf{x})$) = $(K \cdot M) \times 1$. Basically, this means that the $K \cdot M$ unknowns are to be solved from the N^2 equations, which, indeed, reflects a highly underdetermined equation system (typically, say, $N = 3$, and $K = 18$ and $M = 30$).

3.4.2 Considering More Encounter Frequencies

Apart from a new dimension of $\widetilde{\mathbf{A}}$ and $\mathbf{f}(\mathbf{x})$, the multivariate expression (3.16) still holds. Now, in order to deal with a set of L encounter frequencies at the same time, and by discretising the encounter frequency as

$$\omega_e = l \cdot \Delta\omega_e \quad , \quad l = 1, 2, 3, ..., L \tag{3.26}$$

the cross spectrum vector is written as

$$\mathbf{b} = \begin{bmatrix} \widetilde{\mathbf{b}}_1 \\ \widetilde{\mathbf{b}}_2 \\ \vdots \\ \widetilde{\mathbf{b}}_L \end{bmatrix} \tag{3.27}$$

where $\widetilde{\mathbf{b}}_l = \widetilde{\mathbf{b}}(l \cdot \Delta\omega_e)$ and with $\widetilde{\mathbf{b}}_l$ determined from (3.17). It should be noted that size($\mathbf{b}$) = $(N^2 \cdot L) \times 1$.

Thus, the multivariate model expression in its final version reads

$$\mathbf{b} = \mathbf{A}\mathbf{f}(\mathbf{x}) + \mathbf{w} \tag{3.28}$$

where

$$\mathbf{A} = \begin{bmatrix} \widetilde{\mathbf{A}}_1 \\ \widetilde{\mathbf{A}}_2 \\ \vdots \\ \widetilde{\mathbf{A}}_L \end{bmatrix} \quad , \quad \text{size}(\mathbf{A}) = \left(N^2 \cdot L\right) \times (K \cdot M) \tag{3.29}$$

$$\mathbf{w} = \begin{bmatrix} \widetilde{\mathbf{w}}_1 \\ \widetilde{\mathbf{w}}_2 \\ \vdots \\ \widetilde{\mathbf{w}}_L \end{bmatrix} \quad , \quad \text{size}\left(\mathbf{w}\right) = \left(N^2 \cdot L\right) \times 1 \tag{3.30}$$

with $\mathbf{w}$ being the Gaussian white noise sequence vector which has zero mean and variance σ^2.

It is seen that the inclusion of more encounter frequencies results in more equations to the equation system from which the wave spectrum is to be found. Generally, this means a less underdetermined system. Increasing the number of equations in this manner only is, however, not optimal, as new information put into the system is limited due to column degeneracy. Therefore, additional equations should be established by use of some other means. In Section 3.5 these matters are dealt with.

It should be realised that $\mathbf{A}$ contains a large amount of zero elements, but it has by no means a band diagonal form. However, due to the order of sequence of heading angles and wave frequencies in which $\mathbf{A}$ is evaluated, there will only be non-zero elements in the upper right part (not necessarily restricted to above the diagonal) of $\mathbf{A}$. This is illustrated in Figure 3.6 which shows an arbitrary example of the system matrix for a certain, although not important, speed and discretisation of encounter angles and frequencies.

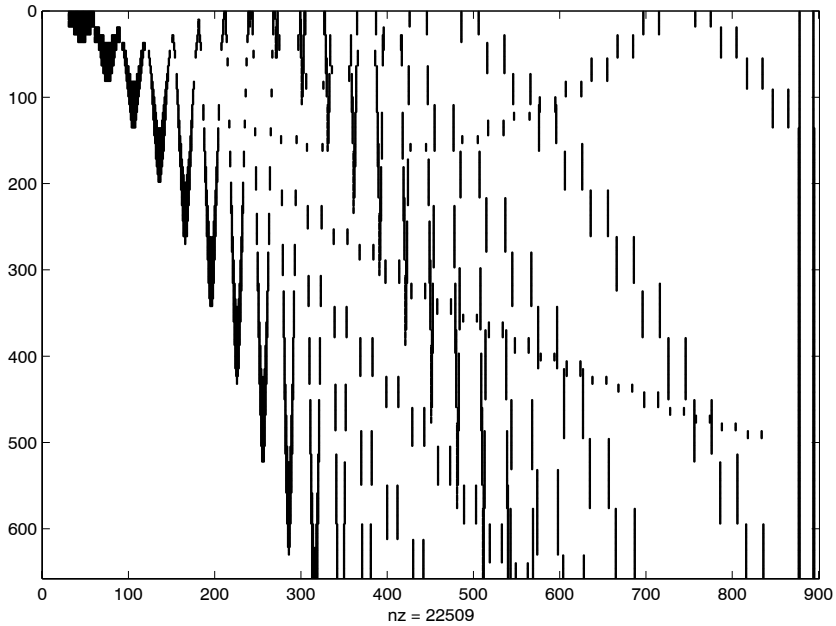

Figure 3.6: *Non-zero elements in the system matrix. 'nz' is the total number of non-zero elements; the matrix has a dimension of 657x900. (An arbitrary example)*

3.4.3 Equivalence of Energy

In addition to the equations given by (3.28), N equations can further be specified, where N, accordingly, is the number of considered response signals. Thus, as mentioned by Iseki and Terada (2002), it can be taken into account that the amount of energy in the signals should be equivalent independently of the energy being calculated from the measured cross spectra, i.e. the left-hand side of (3.3), or the theoretically estimated cross spectra, i.e. the right-hand side of (3.3). Mathematically, it can be argued that N^2 additional equations may actually be specified, since the cross spectral analysis of N responses, as mentioned, leads to a total number of N^2 different real and imaginary spectra. However, the complex-valued cross spectra, that is, the real and the imaginary parts of the off-diagonal cross spectra can have both positive and negative values which means that the area under the respective curve can be close to zero in some cases. For this reason, the diagonal spectra are only considered and, hence, N conditions/equations are specified to secure the equivalence of energy between the measured and the calculated responses. Consequently, the following equations are also taken into account

$$\int S_{ii}\left(\omega_e\right) d\omega_e = \int \int_{-\pi}^{\pi} \left|\Phi_i\left(\omega,\beta\right)\right|^2 E\left(\omega,\beta\right) d\beta d\omega \quad , \quad i = 1, ..., N \tag{3.31}$$

where it should be noted that the right-hand side is based on the wave frequency. Obviously, the introduction of these N equations has an implication for the matrix dimension of the matrices in the equation system (3.28). Thus, the number $N^2 \cdot L$ is changed to $N^2 \cdot L + N$.

From a physical point of view, the equivalence of energy of the measured and the estimated spectra is important. In the equation system (3.28), the equivalence, which is expressed by (3.31), may therefore be weighted relatively heavily.

3.5 Bayesian Modelling Procedure

In the general case, the equation system (3.28) contains more unknowns than equations, that is, the $K \cdot M$ elements in the discretised wave spectrum, $\mathbf{f}\left(\mathbf{x}\right)$, are to be solved from $N^2 \cdot L + N$ equations. Thus, the equation system is underdetermined and, consequently, it is impossible to evaluate the unknowns by ordinary multivariate procedures. Instead an evaluation can be based on the Bayesian modelling procedure as proposed by Akaike (1980), see also Iseki (1999) and Hashimoto (1997). In the following, a detailed description will be given of this modelling procedure, and as a preliminary to this treatment also some general comments are made on Bayesian statistics and modelling, and the similarity of this with inverse theory.

3.5.1 Bayesian Statistics

Given a set of n observations $\mathbf{y} = (y_1, ..., y_n)^T$ and that the data $\mathbf{y}$ has a probability or data distribution $p(\mathbf{y}|\theta)$ that depends on the values of k parameters $\theta = (\theta_1, ..., \theta_k)^T$, then Bayes' Theorem reads as follows, see e.g. Box and Tiao (1973)

$$p(\theta|\mathbf{y}) = \frac{p(\mathbf{y}|\theta)\, p(\theta)}{p(\mathbf{y})} \tag{3.32}$$

with $p(\theta|\mathbf{y})$ being the conditional distribution of the parameters θ given the data $\mathbf{y}$, and $p(\theta)$ and $p(\mathbf{y})$ being the probability distribution of θ and $\mathbf{y}$, respectively.

Obviously, from (3.32) it is seen that

$$p(\theta|\mathbf{y}) \propto p(\mathbf{y}|\theta)\, p(\theta) \tag{3.33}$$

which means that the *posterior* distribution $p(\theta|\mathbf{y})$ of θ given $\mathbf{y}$ is proportional to the product between the data distribution $p(\mathbf{y}|\theta)$ and the *prior* distribution $p(\theta)$.

According to Fisher (1922), when given the data $\mathbf{y}$, $p(\mathbf{y}|\theta)$ may be regarded as a function not of $\mathbf{y}$ but of θ. Hence, $p(\mathbf{y}|\theta)$ may be called the *likelihood function* of θ given $\mathbf{y}$ and is written $L(\theta|\mathbf{y})$. Thus, Bayes' formula is written

$$p(\theta|\mathbf{y}) \propto L(\theta|\mathbf{y})\, p(\theta) \tag{3.34}$$

3.5.2 Inverse Theory vs. Bayesian Modelling

In general, when an unknown physical process $u(x)$ is studied, the situation is often that $u(x)$ is to be determined by, or deconvolved from, a set of, say, N measurements $c_i, i = 1, 2, ..., N$ from integral equations like

$$c_i = \int r_i(x)\, u(x)\, dx + e_i \quad , \quad i = 1, 2, ..., N \tag{3.35}$$

so that $u(x)$ and c_i are related through a response function or kernel $r_i(x)$, and the measurement error e_i is taken into account. Besides, note the close similarity with (3.3). By discretising the independent variable as $x_\mu, \mu = 1, 2, ..., M$ with M being some large number and using matrix notation, the integral equation is rewritten to what could be called an inverse problem

$$\mathbf{c} = \mathbf{R}\mathbf{u} + \mathbf{e} \tag{3.36}$$

with $R_{i\mu} \equiv r_i(x_\mu)(x_{\mu+1} - x_{\mu-1})/2$. Most often (3.36) is singular with M greater than N, and a solution $\mathbf{u}$ can be sought from a least squares minimisation

$$\min \chi^2(\mathbf{u}) \equiv \min \ \|\mathbf{R}\mathbf{u} - \mathbf{c}\|^2 \tag{3.37}$$

with $\chi^2 \equiv \|\cdot\|$ being the L_2 norm. When (3.37) is solved for $\mathbf{u}$, singular value decomposition (SVD), e.g. Ientilucci (2003), is surely a secure procedure. However, the more singular values, the more non-unique the solution will be, which means an unstable, wildly oscillating, or in other ways unrealistic solution, see Press et al. (1992). Instead the solution $\mathbf{u}$ can be found from *inverse theory* that, as mentioned by Tarantola (1987) and Press et al. (1992), has as its central idea the prescription

$$\text{minimise:} \quad \chi^2(\mathbf{u}) + \lambda B(\mathbf{u}) \tag{3.38}$$

for various values of $0 < \lambda < \infty$, where $\chi^2(\mathbf{u})$ and $B(\mathbf{u})$ are positive quadratic functionals of $\mathbf{u}$. Thus, it can be shown, cf. Press et al. (1992), when a quadratic minimisation principle is combined with a quadratic constraint, and both are positive, only one of the two needs to be non-singular for the overall problem to be well posed. Often B is called the stabilising functional and it is to facilitate smoothness and/or stability of the desired solution. Regarding the optimal value of λ, which is often denoted a hyperparameter, this is to be settled by some criterion, so that the solution is reasonably smooth (increasing λ, increasingly smoothness). Moreover, in this connection it must be remembered that what is sought is *not* a hyperparameter that gives the best approximation to the measured data at the discretised points in the sense of fulfilling (3.36), as this, obviously, would be obtained for $\lambda = 0$ which, as discussed above, corresponds to an unstable solution.

Graphically the principle of inverse theory can be illustrated by Figure 3.7. In this figure, for an arbitrary inverse problem like (3.36), the hatched region shows all the feasible solutions, and of these the best solution is found to be one of the solutions located at the boundary, which is marked by the bold curve connecting the unconstrained minimum of χ^2 and the unconstrained minimum of B. Moreover, the figure illustrates that increasing the hyperparameter pulls the solution away from obtaining good agreement in favour of obtaining a smoother and more stable solution (going to the left on the bold curve).

As regards the Bayesian modelling procedure as proposed by Akaike (1980), the solution of the inverse problem (3.36) is, similar to the inverse theory, based on the method of least squares and leads to the minimisation of

$$\chi^2(\mathbf{u}) = \|\mathbf{R}\mathbf{u} - \mathbf{c}\|^2 \tag{3.39}$$

As mentioned this system is, in general, singular and Akaike (1980) suggests to minimise

$$\chi^2(\mathbf{u}) + \mu \|\mathbf{u} - \mathbf{u}_0\|^2 \tag{3.40}$$

where $\mathbf{u}_0$ denotes a particular vector of parameters containing a priori information on the problem and μ is a positive constant, i.e. the hyperparameter. However, a difficulty appears in the choice of μ, and the problem is therefore transformed into the maximisation of, cf. Akaike (1980)

$$l(\mathbf{u}) = \exp\left[-\frac{1}{2\sigma^2}\|\mathbf{R}\mathbf{u} - \mathbf{c}\|^2\right] \exp\left[-\frac{\mu}{2\sigma^2}\|\mathbf{u} - \mathbf{u}_0\|^2\right] \tag{3.41}$$

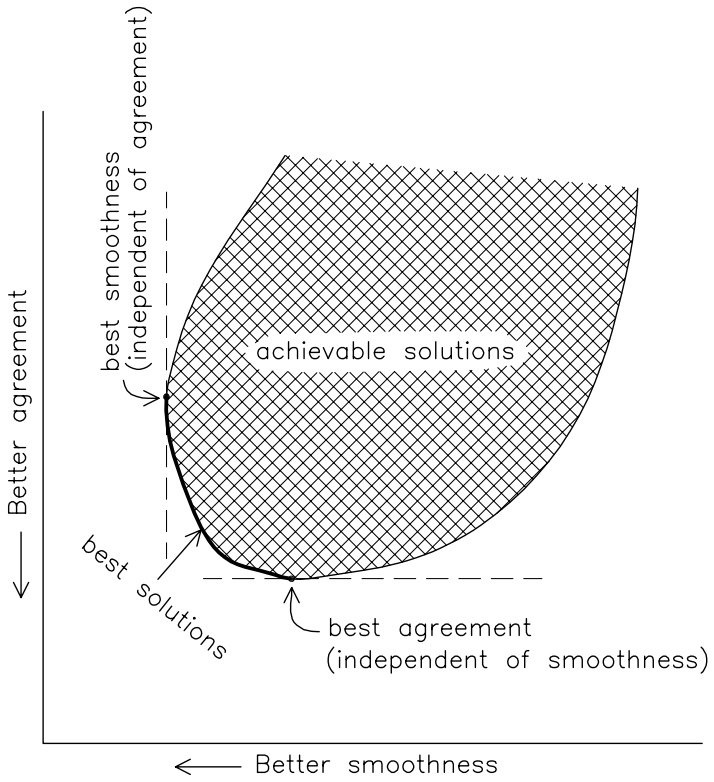

Figure 3.7: *Inverse theory and/or Bayesian modelling are basically a trade-off between two optimisations: agreement between data and solution, and smoothness or stability of the solution.* Press et al. (1992).

where σ^2 is temporarily assumed to be known. Hence, from Bayes' formula (3.34), it is seen that the solution is found to be the maximisation of the mean of the posterior distribution defined by the data distribution

$$f\left(\mathbf{c}|\sigma^2,\mathbf{u}\right)=\left(\frac{1}{2\pi\sigma^2}\right)^{\frac{N}{2}}\exp\left(-\frac{1}{2\sigma^2}\left\|\mathbf{Ru}-\mathbf{c}\right\|^2\right) \tag{3.42}$$

and the prior distribution

$$\pi\left(\mathbf{u}|\mu,\sigma^2\right)=\left(\frac{1}{2\pi\sigma^2}\right)^{\frac{M}{2}}\exp\left(-\frac{\mu}{2\sigma^2}\left\|\mathbf{u}-\mathbf{u}_0\right\|^2\right) \tag{3.43}$$

The advantage of transforming (3.40) into (3.41) is, by considering the marginal likelihood of (μ,σ^2) defined by

$$P\left(\mu,\sigma^2\right)=\int f\left(\mathbf{c}|\sigma^2,\mathbf{u}\right)\pi\left(\mathbf{u}|\mu,\sigma^2\right)d\mathbf{u} \tag{3.44}$$

then the optimal value of μ and σ^2 can be determined from what is called the method of type II maximum likelihood by Good (1965), cf. Akaike (1980). In the present situation this leads to a practical criterion for deciding on the optimal value of μ and σ^2, which is shown further below.

As it is seen, inverse theory and Bayesian modelling are basically two sides of the same coin. Thus, when inverse theory is seen through "Bayesian eyes", it seems obvious that the functional B has something to do with *a priori* expectation, or knowledge, of a solution, while the functional χ^2 has something to do with *a posteriori* knowledge. Moreover, the constant or hyperparameter λ is to form the compromise between the two functionals, i.e. agreement versus smoothness. Therefore, whether to find a solution by use of inverse theory or by use of Bayesian modelling is, in principle, equivalent. However, in the present case, the solution procedure is denoted by 'Bayesian modelling', due to the extensive use of the reference Akaike (1980), which has its theoretical background in Bayesian statistics. Finally, it should be noted that independently of the method, call it inverse theory or Bayesian modelling, the overall implication is that the initial underdetermined equation system is transformed into an overdetermined one.

The next sections return to the specific problem concerning the estimation of directional wave spectra based on Bayesian modelling, and it should be said that in some places repetitions of what has just been described may to some extent occur if the fact seems of special relevance/importance.

3.5.3 Data Distribution

From the assumption about $\mathbf{w}$ that it is Gaussian distributed with zero mean and variance σ^2, the data distribution or the likelihood function of the cross spectra data is given by the multivariate Gaussian distribution

$$l\left(\mathbf{x}|\sigma^2\right) = \left(\frac{1}{2\pi\sigma^2}\right)^{\frac{N^2\cdot L+N}{2}} \exp\left(-\frac{1}{2\sigma^2}\left\|\mathbf{A}\mathbf{f}\left(\mathbf{x}\right)-\mathbf{b}\right\|^2\right) \tag{3.45}$$

where again $\|\cdot\|$ represents the L_2 norm, and $N^2 \cdot L + N$ is the total number of integral equations formed by the product between the square of the number of measured responses, N, and the number of encounter frequencies, L, taken into account. Moreover, the addition of the N equations stemming from the equivalence of energy should also be included.

3.5.4 Prior Distribution

So far, the directional wave spectrum, $E\left(\omega,\beta\right)$, has been assumed to be piecewise constant, that is, the correlation between the energy on each of the discretised segments with area $\Delta\beta\Delta\omega$ has not yet been taken into account. However, as mentioned by Hashimoto (1997),

in actuality it is not realistic to assume that the energy distribution from segment to segment can be discontinuous. Therefore, the directional wave spectrum is, in general, considered to be a smooth and continuous function. Thus, it seems reasonable to introduce an additional condition, in the form of a prior distribution, so that local variations in $\ln\left(E\left(\omega,\beta\right)\right) = x_{k,m}$ can be well approximated by a straight line which means that the continuity and the smoothness of $E\left(\omega,\beta\right)$ are maintained in the frequency as well as in the directional range. Hence, this prior distribution, which acts as a smoothing constraint in the estimation of the directional wave spectrum, is found by requiring the second order derivative of $\ln\left(E\left(\omega,\beta\right)\right)$, with respect to ω as well as β, to be minimum. By introducing finite differences and measuring by the square of the L_2 norm, reasonable functionals to be minimised are therefore

$$\sum_{m=1}^{M}\sum_{k=1}^{K}\left(x_{k-1,m} - 2x_{k,m} + x_{k+1,m}\right)^2; \quad \left(x_{0,m} = x_{K,m},\ x_{K+1,m} = x_{1,m}\right) \tag{3.46}$$

$$\sum_{k=1}^{K}\sum_{m=2}^{M-1}\left(x_{k,m-1} - 2x_{k,m} + x_{k,m+1}\right)^2 \tag{3.47}$$

where M and K are, as above, the number of discrete wave frequencies and discrete angles of encounter, respectively.

From a more mathematical but less physical point of view, it may be said that this prior distribution, i.e. the minimisation of the functionals (3.46) and (3.47), is established from the fact that the curvature of the surface representing the directional wave spectrum is sought to be minimised.

In order to avoid excessive spectral estimation at the frequency boundaries, the sum of the power of the spectrum is minimised for $\omega \to 0$ and $\omega \to \infty$. Hence, the functional

$$\sum_{k=1}^{K}\left[\left(x_{k,1} - s_0\right)^2 + \left(x_{k,M} - s_0\right)^2\right] \tag{3.48}$$

where s_0 denotes a prespecified value is also considered. Note that the indices (here '1' and 'M') representing the wave frequency may be extended to include a larger interval, if needed, in practical computations. The reason or necessity of introducing this prior is related to practical computations as, if not introduced, problems are likely to arise due to the frequency response functions being zero (or close to) at the frequency boundaries. And, as computations have shown, this prior is very important to the estimation. With respect to the value of s_0 this might be determined from a 'reasonably' small value of the significant wave height as

$$\frac{H_s^2}{16} \simeq s_0 \cdot \left(\omega_M - \omega_1\right) \tag{3.49}$$

From an analogy to the last prior it is possible to include knowledge, if at hand from visual observations, on the wave direction. Thus, information on the wave direction can be included

in the sense that the energy from certain directions and a certain frequency range in the wave field is minimised. Hence, in a similar manner to (3.48), although with both k and m as running indices, a prior can be set up according to

$$\sum_{k=K_0}^{K_1} \sum_{m=M_0}^{M_1} \left(x_{k,m} - s_0\right)^2 \tag{3.50}$$

with K_0, K_1, M_0, and M_1 specifying the area wherein the energy is minimised.

On the above assumptions and by taking each of the prior distributions to be distributed as a Gaussian with zero mean and variance $\frac{\sigma^2}{u^2}$, the overall prior distribution is written as

$$p\left(\mathbf{x}|u,\sigma^2\right) = \left(\frac{u^2}{2\pi\sigma^2}\right)^{\frac{KM}{2}} \exp\left(-\frac{u^2}{2\sigma^2}\left\|\mathbf{D}\mathbf{x}-\mathbf{c}\right\|^2\right) \tag{3.51}$$

where u is the so-called hyperparameter that expresses the degree of smoothness as explained above, see also e.g. Akaike (1980).

The matrix $\mathbf{D}$ is composed of elements corresponding to (3.46)-(3.50). From the organisation of $\mathbf{x}$, $\mathbf{D}$ has the form

$$\mathbf{D} = \begin{bmatrix} \mathbf{D}_1 \\ \mathbf{D}_2 \\ \mathbf{D}_3 \\ \mathbf{D}_4 \end{bmatrix} \quad , \quad \text{size}\left(\mathbf{D}\right) = (3 \cdot K \cdot M) \times (K \cdot M) \tag{3.52}$$

Here $\mathbf{D}_1$ is composed as, cf. (3.46)

$$\mathbf{D}_1 = \begin{bmatrix} \mathbf{D}_1^* & \mathbf{0} & & \mathbf{0} \\ \mathbf{0} & \mathbf{D}_1^* & & \\ & & \ddots & \\ \mathbf{0} & & & \mathbf{D}_1^* \end{bmatrix} \quad , \quad \text{size}\left(\mathbf{D}_1\right) = (K \cdot M) \times (K \cdot M) \tag{3.53}$$

with

$$\mathbf{D}_1^* = \begin{bmatrix} -2 & 1 & 0 & 0 & 0 & \cdots & 1 \\ 1 & -2 & 1 & 0 & 0 & \cdots & 0 \\ 0 & 1 & -2 & 1 & 0 & \cdots & 0 \\ \vdots & & & \ddots & & & \vdots \\ 1 & 0 & 0 & \cdots & 0 & 1 & -2 \end{bmatrix} \quad , \quad \text{size}\left(\mathbf{D}_1^*\right) = K \times K \tag{3.54}$$

Regarding $\mathbf{D}_2$ this is determined from the following, cf. (3.47)

$$\mathbf{D}_2 \;=\; \begin{bmatrix} \mathbf{1} & \mathbf{-2} & \mathbf{1} & \mathbf{0} & & \mathbf{0} \\ \mathbf{0} & \mathbf{1} & \mathbf{-2} & \mathbf{1} & & \\ & & & \ddots & & \\ \mathbf{0} & & & \mathbf{1} & \mathbf{-2} & \mathbf{1} \end{bmatrix} \quad , \quad \text{size}\left(\mathbf{D}_2\right) = (K \cdot M - 2K) \times (K \cdot M) \tag{3.55}$$

where

$$\mathbf{1} = \begin{bmatrix} 1 & 0 & & \mathbf{0} \\ 0 & 1 & & \\ & & \ddots & \\ \mathbf{0} & & & 1 \end{bmatrix}, \quad -\mathbf{2} = -2 \begin{bmatrix} 1 & 0 & & \mathbf{0} \\ 0 & 1 & & \\ & & \ddots & \\ \mathbf{0} & & & 1 \end{bmatrix} \tag{3.56}$$

$$\text{size}\,(\mathbf{1}) = \text{size}\,(-\mathbf{2}) = K \times K$$

$\mathbf{D}_3$ is given by (3.48)

$$\mathbf{D}_3 = \begin{bmatrix} \mathbf{1} & \mathbf{0} & \cdots & \mathbf{0} & \mathbf{0} \\ \mathbf{0} & \mathbf{0} & \cdots & \mathbf{0} & \mathbf{1} \end{bmatrix} \quad , \quad \text{size}\,(\mathbf{D}_3) = 2K \times (K \cdot M) \tag{3.57}$$

with $\mathbf{1}$ being the $K \times K$ identity matrix as above.

As regards $\mathbf{D}_4$, this matrix cannot be specified in advance, as the setup depends on the coefficients K_0, K_1, M_0, and M_1. However, it has at most a size equal to the size of $\mathbf{D}_1$.

Concerning the vector $\mathbf{c}$ in (3.51), this is given as

$$\mathbf{c} = \begin{bmatrix} 0 \\ \vdots \\ \vdots \\ 0 \\ s_0 \\ \vdots \\ s_0 \end{bmatrix} \quad \text{size}\,(\mathbf{c}) = (3 \cdot K \cdot M) \times 1 \tag{3.58}$$

where the location of the s_0 in the last $K \cdot M$ rows depends on the coefficients K_0, K_1, M_0, and M_1.

In conclusion to the treatment of the prior distributions, it seems relevant to mention that since three functionals are introduced, three different hyperparameters, as a matter of fact, are to be considered. However, as the computational cost in connection with the optimisation of the hyperparameters is relatively large, compared to the final outcome of the directional estimation when considering three different hyperparameters, only one hyperparameter is dealt with. Especially, the computational cost is important in the study of practical decision support systems. Therefore, the optimisation is done for only one hyperparameter.

3.5.5 Posterior Distribution

According to Bayes' theorem (3.34), the posterior distribution of the discretised spectrum is constituted by the data distribution and the prior distribution as

$$p_{\text{post}}\left(\mathbf{x}|\sigma^2, u\right) \propto l\left(\mathbf{x}|\sigma^2\right) \cdot p\left(\mathbf{x}|u, \sigma^2\right) \tag{3.59}$$

so that

$$p_{\text{post}}\left(\mathbf{x}|\sigma^2,u\right) \propto \left(\frac{1}{2\pi\sigma^2}\right)^{\frac{N^2\cdot L+N}{2}} \left(\frac{u^2}{2\pi\sigma^2}\right)^{\frac{KM}{2}} \cdot$$

$$\exp\left(-\frac{1}{2\sigma^2}\left(\|\mathbf{A}\mathbf{f}\left(\mathbf{x}\right)-\mathbf{b}\|^2+u^2\|\mathbf{D}\mathbf{x}-\mathbf{c}\|^2\right)\right)$$

$$= \left(\frac{1}{2\pi\sigma^2}\right)^{\frac{N^2\cdot L+N}{2}} \left(\frac{u^2}{2\pi\sigma^2}\right)^{\frac{KM}{2}} \exp\left(-\frac{1}{2\sigma^2}S\left(\mathbf{x}\right)\right) \tag{3.60}$$

where

$$S\left(\mathbf{x}\right) = \|\mathbf{A}\mathbf{f}\left(\mathbf{x}\right)-\mathbf{b}\|^2+u^2\|\mathbf{D}\mathbf{x}-\mathbf{c}\|^2 \tag{3.61}$$

Obviously, for given $\mathbf{b}$, σ^2 and u, the maximum posterior distribution of $\mathbf{x}$ can be obtained by minimising $S\left(\mathbf{x}\right)$. As already mentioned above, this minimisation can be interpreted as a constrained least squares method, which is generally used for solving inverse problems, cf. Dimri (1992) and Akaike (1980). However, before dealing with the specific theory proposed by Akaike (1980), $S\left(\mathbf{x}\right)$ is rewritten.

Due to the exponential functions, $\mathbf{f}\left(\mathbf{x}\right)$ is non-linear in $\mathbf{x}$, but by using a Taylor expansion around $\mathbf{x}_0$, $\mathbf{f}\left(\mathbf{x}\right)$ is linearised as

$$\mathbf{f}\left(\mathbf{x}\right) = \mathbf{f}\left(\mathbf{x}_0\right)+\mathbf{F}\left(\mathbf{x}_0\right)\left(\mathbf{x}-\mathbf{x}_0\right) \tag{3.62}$$

where the $(K\cdot M)\times(K\cdot M)$ diagonal matrix

$$\mathbf{F}\left(\mathbf{x}\right) = \begin{bmatrix} \exp\left(x_{\beta 1,\omega 1}\right) & & & \mathbf{0} \\ & \exp\left(x_{\beta 2,\omega 1}\right) & & \\ & & \ddots & \\ \mathbf{0} & & & \exp\left(x_{\beta K,\omega M}\right) \end{bmatrix} \tag{3.63}$$

Thus, introducing (3.62) into (3.61) gives

$$S\left(\mathbf{x}\right) = \|\mathbf{A}^*\mathbf{x}-\mathbf{b}^*\|^2+u^2\|\mathbf{D}\mathbf{x}-\mathbf{c}\|^2 \tag{3.64}$$

with

$$\mathbf{A}^* = \mathbf{A}\mathbf{F}\left(\mathbf{x}_0\right) \tag{3.65}$$

$$\mathbf{b}^* = \mathbf{b}-\mathbf{A}\mathbf{f}\left(\mathbf{x}_0\right)+\mathbf{A}\mathbf{F}\left(\mathbf{x}_0\right)\mathbf{x}_0 \tag{3.66}$$

Hence, $S\left(\mathbf{x}\right)$ is rewritten by the following matrix manipulation

$$S\left(\mathbf{x}\right) = \|\mathbf{G}\mathbf{x}-\mathbf{d}\|^2 \tag{3.67}$$

where

$$\mathbf{G} = \begin{bmatrix} \mathbf{A}^* \\ u\mathbf{D} \end{bmatrix}, \quad \mathbf{d} = \begin{bmatrix} \mathbf{b}^* \\ u\mathbf{c} \end{bmatrix} \tag{3.68}$$

and for convenience size($\mathbf{G}$) = $\alpha \times \beta$ and size($\mathbf{d}$) = $\alpha \times 1$ are assumed, although the exact size of $\mathbf{G}$ and $\mathbf{d}$ may be found from size($\mathbf{A}^*$) and size($\mathbf{D}$).

As seen from the rewriting of $S(\mathbf{x})$, both $\mathbf{A}^*$ and $\mathbf{b}^*$ depend on the initial value $\mathbf{x}_0$. This means that a solution to the minimisation of $S(\mathbf{x})$ cannot be calculated directly but must be found from iteration. How to perform this iteration is explained in more detail in a section below. However, it is noteworthy that the minimisation of $S(\mathbf{x})$ is equivalent to the least squares problem for an equation system with more equations than unknowns, i.e. the system is, as mentioned above, overdetermined. In general, such systems can be solved by various techniques, among others the use of normal equations, QR factorization, and singular value decomposition (SVD). The solution procedure by normal equations and, especially, QR factorisation will be considered in more detail below. Though, due to the robustness of SVD in the cases of near-rank deficiency or actual rank deficiency, this method should also be mentioned as a possibility of calculating the solution to the minimisation of $S(\mathbf{x})$. However, as will be noted below, rank deficiency is not considered to be a problem for the present equation system and, as well, due to the relatively high computational cost of SVD, this procedure is not to be applied. Before considering the exact solution procedure it is shown how to calculate the optimum hyperparameter u.

3.6 Akaike's Bayesian Information Criterion

In order to determine the optimum hyperparameter, u, and the variance, σ^2, Akaike (1980) proposed a criterion known as Akaike's Bayesian Information Criterion, or abbreviated ABIC. Thus, the determination of u and σ is based on the minimisation of ABIC, which in its general form is given by

$$\text{ABIC} = -2\ln \int p_{\text{post}}(\mathbf{y}|...)\, d\mathbf{y} \tag{3.69}$$

i.e. the minimisation of minus twice the logarithm to the marginal likelihood of the parameter(s) which may be in question. In general, such a minimisation, equivalently maximisation, of a likelihood calls for an approximation due to the high dimensional integral. This matter is an entire subject of its own and is treated among many others by Davison (1986). At present, however, the focus will only be on the exact calculation of (3.69).

Introducing (3.60) in (3.69), ABIC for the present case becomes

$$\begin{aligned} \text{ABIC} \;=\; & \left(N^2 \cdot L + N\right) \ln\left(2\pi\sigma^2\right) - K \cdot M \ln\left(u^2\right) - \\ & 2\ln \int \left(\frac{1}{2\pi\sigma^2}\right)^{\frac{KM}{2}} \exp\left(-\frac{1}{2\sigma^2} S(\mathbf{x})\right) d\mathbf{x} \end{aligned} \tag{3.70}$$

By dealing with the high dimensional integral in (3.70), $S(\mathbf{x}) = \|\mathbf{G}\mathbf{x} - \mathbf{d}\|^2$ is rewritten. Thus, by defining $\hat{\mathbf{x}}$ as the estimate of $\mathbf{x}$ that minimises S, the best solution, $\mathbf{G}\hat{\mathbf{x}}$, is closer to $\mathbf{d}$ than any other vector. Therefore, S can be decomposed in the following way, cf. Oda and Shibuya (1996)

$$\begin{aligned} S(\mathbf{x}) &= \|\mathbf{G}\hat{\mathbf{x}} - \mathbf{d}\|^2 + \|\mathbf{G}(\mathbf{x} - \hat{\mathbf{x}})\|^2 \\ &= S^* + \|\mathbf{G}(\mathbf{x} - \hat{\mathbf{x}})\|^2 \end{aligned} \tag{3.71}$$

with

$$S^*(\hat{\mathbf{x}}) = \|\mathbf{G}\hat{\mathbf{x}} - \mathbf{d}\|^2 \tag{3.72}$$

Hence, for the integral in (3.70), use of Laplace's approximation for high dimensional integrals, e.g. Vonesh (1996) and Shun and McCullagh (1995), yields

$$\begin{aligned} &\int \left(\frac{1}{2\pi\sigma^2}\right)^{\frac{KM}{2}} \exp\left(-\frac{1}{2\sigma^2}S\right) d\mathbf{x} = \exp\left(-\frac{S^*}{2\sigma^2}\right) \cdot \\ &\int \left(\frac{1}{2\pi\sigma^2}\right)^{\frac{KM}{2}} \exp\left(-\frac{1}{2\sigma^2}\|\mathbf{G}(\mathbf{x} - \hat{\mathbf{x}})\|^2\right) d\mathbf{x} \\ &= \exp\left(-\frac{S^*}{2\sigma^2}\right) \cdot \det\left(\mathbf{G}^T\mathbf{G}\right)^{-\frac{1}{2}} \end{aligned} \tag{3.73}$$

where $\det(\mathbf{Z})$ denotes the determinant of matrix $\mathbf{Z}$.

Thus, ABIC becomes

$$\mathrm{ABIC} = \left(N^2 \cdot L + N\right) \ln\left(2\pi\sigma^2\right) - K \cdot M \ln\left(u^2\right) + \frac{S^*}{\sigma^2} + \ln\left(\det\left(\mathbf{G}^T\mathbf{G}\right)\right) \tag{3.74}$$

In order to determine the value of σ^2 which minimises ABIC, differentiation with respect to σ^2 implies

$$\frac{N^2 \cdot L + N}{2\pi\sigma^2} \cdot 2\pi - \frac{S^*}{\left(\sigma^2\right)^2} = 0 \tag{3.75}$$

Hence,

$$\sigma^2_{\min} = \frac{S^*}{N^2 \cdot L + N} \tag{3.76}$$

is the value which minimises ABIC, and the final form of Akaike's Bayesian Information Criterion reads

$$\mathrm{ABIC} = \left(N^2 \cdot L + N\right) \ln\left(2\pi\sigma^2_{\min}\right) - K \cdot M \ln\left(u^2\right)$$

$$+\left(N^2 \cdot L + N\right) + \ln\left(\det\left(\mathbf{G}^T\mathbf{G}\right)\right) \tag{3.77}$$

By interpreting $\ln(u)$ as a free parameter, the minimum ABIC can be searched for in the $\ln(u)$-space, and it is emphasised that both $\sigma_{\min} = \sigma_{\min}(\ln(u); ...)$ and $\mathbf{G} = \mathbf{G}(\ln(u); ...)$ are functions of $\ln(u)$. In general, though, it should be noticed that for given $\ln(u)$, $\mathbf{x}$ can be calculated from the minimisation of $S(\mathbf{x})$, cf. (3.67), which means that $\sigma_{\min}$ is found from (3.76) and, hence, ABIC only depends on $\ln(u)$.

In the next section it is described in detail how to do the minimisation of $S(\mathbf{x})$ and how to calculate ABIC.

3.7 Solution Procedure

On the assumption that $\mathbf{G} \in \mathbb{R}^{\alpha\times\beta}$ has full column rank (that is $\text{rank}(\mathbf{G}) = \beta$) the least squares solution $\hat{\mathbf{x}}$, i.e. the minimisation of $S(\mathbf{x})$, $\frac{\partial S(\mathbf{x})}{\partial \mathbf{x}_i} = 0$, can be found from the normal equations as given by, cf. (3.67)

$$\mathbf{G}^T\mathbf{G}\mathbf{x} = \mathbf{G}^T\mathbf{d} \tag{3.78}$$

which can be solved by calculating the Cholesky factorisation of $\mathbf{G}$. However, in the present case the solution to the least squares problem will be based on the QR factorisation of $\mathbf{G}$ by use of the Householder orthogonalisation/transformation. This is so, because advantageous manipulations of $\mathbf{G}$ can be performed by the QR factorisation, and since in the near-rank deficient case, the QR factorisation based on the Householder Transformation yields a more accurate solution compared to the normal equations, e.g. Lawson and Hanson (1974). In the following, the solution procedure based on the QR factorisation will be explained, and with respect to the theory used, reference is made to Golub and Loan (1996).

Manipulation of $S(\mathbf{x})$, cf. (3.67), may be done by introducing a matrix $\mathbf{B}$ composed of $\mathbf{G}$ with the addition of one column taken as $\mathbf{d}$, i.e.

$$\mathbf{B} = \left[\begin{array}{cc} \mathbf{G} & \mathbf{d} \end{array}\right] \quad , \quad \text{size}(\mathbf{B}) = \alpha \times (\beta + 1) \tag{3.79}$$

By successive use of the Householder orthogonalisation, an orthogonal matrix $\mathbf{Q} \in \mathbb{R}^{\alpha\times\alpha}$ and an upper triangular matrix $\mathbf{R}^* \in \mathbb{R}^{\alpha\times(\beta+1)}$ can be calculated so that

$$\mathbf{B} = \mathbf{Q}\mathbf{R}^* \tag{3.80}$$

with the coefficient matrix $\mathbf{R}^*$ given as

$$\mathbf{R}^* = \left[\begin{array}{cccc} r_{1,1} & \cdots & r_{1,\beta} & r_{1,\beta+1} \\ 0 & \ddots & \vdots & \vdots \\ \vdots & & r_{\beta,\beta} & r_{\beta,\beta+1} \\ 0 & \cdots & 0 & r_{\beta+1,\beta+1} \\ \mathbf{0} & \cdots & \mathbf{0} & \mathbf{0} \end{array}\right] \tag{3.81}$$

where it is assumed that $\mathbf{G}$ - and hence $\mathbf{B}$ - has full column rank, i.e. $\text{rank}(\mathbf{B}) = \beta + 1$.

By defining

$$\mathbf{R} = \begin{bmatrix} r_{1,1} & \cdots & r_{1,\beta} \\ & \ddots & \vdots \\ \mathbf{0} & & r_{\beta,\beta} \end{bmatrix} \quad , \quad \mathbf{s} = \begin{bmatrix} r_{1,\beta+1} \\ \vdots \\ r_{\beta,\beta+1} \end{bmatrix} \tag{3.82}$$

$\mathbf{R}^*$ is written as

$$\mathbf{R}^* = \begin{bmatrix} & \mathbf{R} & & \mathbf{s} \\ 0 & \cdots & 0 & r_{\beta+1,\beta+1} \\ \mathbf{0} & \cdots & \mathbf{0} & \mathbf{0} \end{bmatrix} \tag{3.83}$$

Moreover,

$$\mathbf{R}^* = \mathbf{Q}^{-1}\mathbf{B} = \mathbf{Q}^{-1} \begin{bmatrix} \mathbf{G} & \mathbf{d} \end{bmatrix} \tag{3.84}$$

Hence, since the L_2 norm is preserved during orthogonal transformation, and as an orthogonal matrix has an inverse equal to its transpose, $S(\mathbf{x})$, cf. (3.67), can be rewritten

$$\begin{aligned} S(\mathbf{x}) &= \left\| \mathbf{Q}^T (\mathbf{G}\mathbf{x} - \mathbf{d}) \right\|^2 \\ &= \left\| \mathbf{R}\mathbf{x} - \mathbf{s} \right\|^2 + r^2_{\beta+1,\beta+1} \end{aligned} \tag{3.85}$$

Thus, as $r^2_{\beta+1,\beta+1}$ is independent of $\mathbf{x}$, the minimisation of $S(\mathbf{x})$ is obtained by solving

$$\mathbf{R}\mathbf{x} = \mathbf{s} \tag{3.86}$$

that is

$$\begin{bmatrix} r_{1,1} & \cdots & r_{1,\beta} \\ & \ddots & \vdots \\ \mathbf{0} & & r_{\beta,\beta} \end{bmatrix} \begin{bmatrix} x_1 \\ \vdots \\ x_\beta \end{bmatrix} = \begin{bmatrix} r_{1,\beta+1} \\ \vdots \\ r_{\beta,\beta+1} \end{bmatrix} \tag{3.87}$$

which can easily be solved by use of backward substitution. Moreover, it should be noted that the minimum variance $\sigma^2_{\min}$ of the residuals, cf. (3.76), is calculated from

$$\sigma^2_{\min} = \frac{r^2_{\beta+1,\beta+1}}{N^2 \cdot L + N} \tag{3.88}$$

Finally, it should also be noted that, since

$$\mathbf{G} = \mathbf{Q} \begin{bmatrix} \mathbf{R} \\ \mathbf{0} \end{bmatrix} \tag{3.89}$$

the determinant in (3.77) can be calculated from the following

$$\begin{aligned}\det\left(\mathbf{G}^T\mathbf{G}\right) &= \det\left(\begin{bmatrix}\mathbf{R}\\ \mathbf{0}\end{bmatrix}^T \mathbf{Q}^T\mathbf{Q}\begin{bmatrix}\mathbf{R}\\ \mathbf{0}\end{bmatrix}\right)\\ &= \det\left(\mathbf{R}^T\mathbf{R}\right)\\ &= \det\left(\mathbf{R}^T\right)\det\left(\mathbf{R}\right)\\ &= \prod_i r_{i,i}^2 \end{aligned} \tag{3.90}$$

which should be utilised, as a conventional matrix computation method for obtaining the determinant of the product $\mathbf{G}^T\mathbf{G}$ very likely leads to a floating point exception, when digital computers are used, cf. Hashimoto (1997).

Hence, in summary, the QR factorisation implies a convenient solution procedure for the minimisation of $S(\mathbf{x})$ and, furthermore, it leads to an appropriate simplification of the calculation of ABIC. Thus, by introducing the number of columns in $\mathbf{G}$, i.e. $\beta = K \cdot M$, cf. (3.68), the minimisation of $S(\mathbf{x})$ is obtained by solving

$$\begin{bmatrix} r_{1,1} & \cdots & r_{1,K\cdot M}\\ & \ddots & \vdots\\ \mathbf{0} & & r_{K\cdot M,K\cdot M}\end{bmatrix}\begin{bmatrix} x_1\\ \vdots\\ x_{K\cdot M}\end{bmatrix} = \begin{bmatrix} r_{1,K\cdot M+1}\\ \vdots\\ r_{K\cdot M,K\cdot M+1}\end{bmatrix} \tag{3.91}$$

and ABIC is calculated as follows, cf. (3.77)

$$\begin{aligned}&\mathrm{ABIC} = \left(N^2\cdot L + N\right)\left(\ln\left(2\pi\frac{r_{K\cdot M+1,K\cdot M+1}^2}{N^2\cdot L+N}\right)+1\right)\\ &-2\cdot K\cdot M\ln\left(u\right)+\sum_{i=1}^{K\cdot M}\ln\left(r_{i,i}^2\right)\end{aligned} \tag{3.92}$$

3.8 Calculation of the Directional Wave Spectra

For the sake of completeness and overview, the tasks related to the estimation of directional wave spectra are summarised, and just below a point schedule shows, more or less, the exact calculation procedure. Furthermore, some numerical techniques used in the calculation are introduced at the end.

Based on the QR factorisation, the estimate $\hat{\mathbf{x}}$ that minimises S can be computed by (3.91), and hence ABIC can be calculated from (3.92). Then, if all of the procedures above are repeated for sufficiently many $\ln(u)$, ABIC can be plotted as a function of $\ln(u)$. Thus, the minimum ABIC is searched, and for the belonging $\ln(u_{\min})$, the best estimate $\mathbf{x}_{\text{final}}$ is calculated. Finally, the directional wave spectrum is found by substituting $\mathbf{x}_{\text{final}}$ into (3.25).

In schematic form the determination of the directional wave spectrum proceeds as follows, see also Figure 3.8:

1. An initial guess $\mathbf{x}_0^*$, e.g. $x_{k,m} = \ln \frac{1}{2\pi}$, for the wave spectrum is made. For $i = 1, 2, ...P$, with an appropriate large value of P, a range of the hyperparameter u_i is calculated as follows, cf. Hashimoto (1997)

   $$u_i = a \cdot b^i \tag{3.93}$$

   where a and b are constant coefficients, e.g. $a = 1$, and $b = 0.5$.

2. Put $i = 1$ and do (3) and (4) below in chronological order.

3. Based on $\mathbf{x}_0^*$ and u_i, $\mathbf{G}$ and $\mathbf{d}$ are set up according to (3.68). From (3.91) a better solution, $\mathbf{x}_1^*$, to $\hat{\mathbf{x}}_i$ is calculated. Based on u_i and the new solution $\mathbf{x}_1^*$, $\mathbf{G}$ and $\mathbf{d}$ are set up again. Hence, (3.91) yields the solution $\mathbf{x}_2^*$. This iteration continues until convergence is achieved; i.e $\hat{\mathbf{x}}_i = \mathbf{x}_j^*$ with e.g. $\frac{\left\|\mathbf{x}_j^* - \mathbf{x}_{j-1}^*\right\|}{\left\|\mathbf{x}_j^*\right\|} < \varepsilon$.

4. Based on $\hat{\mathbf{x}}_i$ and u_i, calculate ABIC_i by (3.92).

5. Put $i = i + 1$ and repeat (3) and (4) until $i = P$.

6. From the corresponding pairs u_i and ABIC_i, determine the value of the hyperparameter $u_{\min}$ that minimises ABIC.

7. Use $u_{\min}$ to compute $\mathbf{x}_{\text{final}}$ from (3.91), similarly to point (3) above.

8. Determine the directional wave spectrum by substituting $\mathbf{x}_{\text{final}}$ into (3.25).

3.8.1 Numerical Techniques

When the basic equation system is set up, cf. (3.3), N different time series, or signals, are considered. Obviously, the standard deviation of these N signals will, in some cases, be of a very different magnitude depending on the kind of signals being recorded. Hence, the solution of the equation system will be much affected by this fact, which is reflected by a poor agreement between the solution and the data for the signals with the relatively smallest standard deviation. Conversely, the solutions corresponding to the signals with the relatively

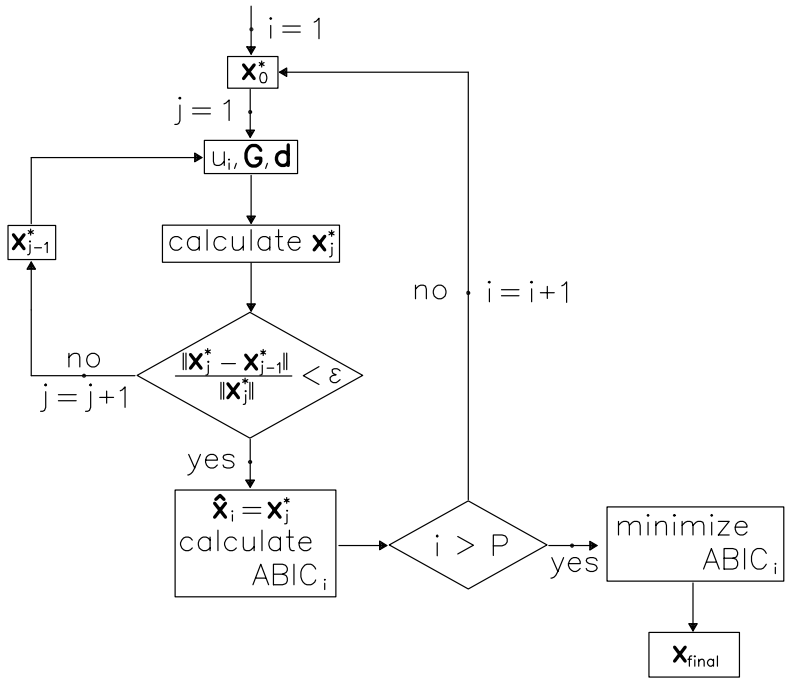

Figure 3.8: *Graphical illustration of the Bayesian estimation.*

largest standard deviation will approximate the data in a better way. In order to overcome this problem the equation system must be normalised. Thus, if it is remembered that the cross spectra, in general, are complex, cf. (3.15)

$$S_{ij}(\omega_e) = C_{ij}(\omega_e) + iQ_{ij}(\omega_e) \tag{3.94}$$

Bendat and Piersol (2000) suggests to normalise the cross spectra according to

$$\begin{aligned} \widehat{C}_{ij}(\omega_e) &= \frac{C_{ij}(\omega_e)}{\sqrt{\frac{1}{2}\left[S_{ii}(\omega_e)S_{jj}(\omega_e) + C_{ij}(\omega_e)^2 - Q_{ij}(\omega_e)^2\right]}} \\ \widehat{Q}_{ij}(\omega_e) &= \frac{Q_{ij}(\omega_e)}{\sqrt{\frac{1}{2}\left[S_{ii}(\omega_e)S_{jj}(\omega_e) - C_{ij}(\omega_e)^2 + Q_{ij}(\omega_e)^2\right]}} \end{aligned} \tag{3.95}$$

Normalising the equation system has also the implication that the optimal value of the hyperparameter assumes almost the same magnitude in all cases for similar data.

Regarding the minimisation to find the optimal hyperparameter, as sketched in point (6) in the above schedule, this minimisation is performed by use of the method of Golden Section Search, see for instance Press et al. (1992).

This page is intentionally left blank.

Chapter 4

Parametric Estimation

4.1 Introduction

The wave energy spectrum can also be estimated from a procedure which takes the wave spectrum to be comprised of one or more parameterised – theoretically known – wave spectra. In this chapter such a procedure for estimation of the wave spectrum is outlined. Conceptually, the procedure is similar to the Bayesian modelling method. For this reason, reference is given to Chapter 3 for details on fundamentals, which include the governing equations, the relationship between encounter and wave frequencies, the discretisation of the wave field, etc.

Basically, the relationship between the measured response spectra and the directional wave spectrum is given by expression (3.28), including information on the equivalence of energy. In expression (3.28), a white noise sequence vector $\mathbf{w}$ is introduced in order to facilitate the Bayesian modelling. Without the introduction of white noise, no assumption is made on the error between the measured and the calculated response spectra which means that the directional wave spectrum $\mathbf{f} = E(\omega, \beta)$ can be sought in the least squares sense by solving

$$\min\chi^2 \equiv \min\|\mathbf{Af} - \mathbf{b}\|^2 \tag{4.1}$$

with $\chi = \|\cdot\|$ being the L_2 norm.

4.2 Parameterised Wave Spectra

Parameterised wave spectra, e.g. Goda (2000), are typically considered reliable for describing the variation with frequency of ocean wave spectra. Moreover, the angular spread of wave spectra can be described by certain parameters, e.g. Longuet-Higgins et al. (1961) and Goda

(2000). On this assumption, the wave spectrum to be estimated from equation (4.1) is based on the following ten-parameter bimodal spectrum, e.g. Tannuri et al. (2003) and Hogben and Cobb (1986)

$$\begin{aligned} E(\omega,\theta) &= \frac{1}{4}\sum_{i=1}^{2}\frac{\left(\frac{4\lambda_i+1}{4}\omega_{p,i}^4\right)^{\lambda_i}}{\Gamma(\lambda_i)}\frac{H_{s,i}^2}{\omega^{4\lambda_i+1}}A(s_i)\cdot \\ &\quad \cos^{2s_i}\left(\frac{\theta-\theta_{mean,i}}{2}\right)\exp\left[-\frac{4\lambda_i+1}{4}\left(\frac{\omega_{p,i}}{\omega}\right)^4\right] \end{aligned} \tag{4.2}$$

with H_s being the significant wave height, λ is the shape parameter of the spectrum, θ_{mean} is the mean wave direction, ω_p is the angular peak frequency, and s represents the spreading parameter.

$$A(s) = \frac{2^{2s-1}\Gamma^2(s+1)}{\pi\Gamma(2s+1)} \tag{4.3}$$

is a constant introduced to normalise the area under the $\cos^{2s}$ curve and Γ denotes the Gamma function.

The wave spectrum, (4.2), basically considers a sea component ($i = 1$) and a swell component ($i = 2$), and on this basis it is, in theory, possible to model most ocean wave spectra, e.g. Hogben and Cobb (1986). Hence, by application of (4.2), and taking the wave direction to be coincident to the encounter angle, the solution of equation (4.1) implies a non-linear optimisation problem from which the best-fit-values can be determined.

4.3 Frequency Dependent Spreading

From measurements, cf. Longuet-Higgins et al. (1961) and Mitsuyasu et al. (1975), the spreading parameter s is found to vary with frequency. In the present Parametric method the frequency dependency of the spreading parameter is included in the sense that s takes a maximum value around the spectral peak frequency, whereas s decreases for frequencies both lower and higher than the peak frequency. According to Goda (2000) the spreading parameter can basically be modelled as

$$s = \begin{cases} \text{ceil}\left[(\omega/\omega_p)^5\, s_{max}\right], & \omega \le \omega_p \\ \text{ceil}\left[(\omega/\omega_p)^{-2.5}\, s_{max}\right], & \omega > \omega_p \end{cases} \tag{4.4}$$

where the peak value of s, denoted s_{max}, has been introduced as the principal parameter.

Compared to the original proposal by Goda (2000), ceil[ ] has been introduced in (4.4). Thus, ceil[ ] rounds towards plus infinity and is a numerical technique utilised here to stabilise the

optimisation. As regards s_{max}, the following values for engineering applications have been recommended, cf. Goda (2000)

$$s_{max} = \begin{cases} 10 & \text{, wind waves} \\ 25 & \text{, swell with short decay distance} \\ 75 & \text{, swell with long decay distance} \end{cases} \tag{4.5}$$

4.4 Estimated Parameters

In conclusion, the optimal wave spectrum estimated by the Parametric method is found from the optimisation of the parameters

$$\{ \; H_{s,1} \quad \lambda_1 \quad \theta_{mean,1} \quad \omega_{p,1} \quad s_{max,1} \quad H_{s,2} \quad \lambda_2 \quad \theta_{mean,2} \quad \omega_{p,2} \quad s_{max,2} \; \} \tag{4.6}$$

As has been discussed, the parametric modelling basically assumes the wave spectrum to be composed of a sea and a swell part. In case of unimodal seas, however, the method should predict a negligible value for one of the significant wave heights ($H_{s,1}$ or $H_{s,2}$).

To close this chapter it should be noted that results of the outlined parametric method is presented in Chapter 9.

This page is intentionally left blank.

Chapter 5

Cross Spectral Analysis

5.1 Introduction

As regards spectral analysis of time series, the Fast Fourier Transformation (FFT) offers an easily applicable tool for the calculation of power and cross spectral densities, i.e. periodograms. However, as the periodogram is a high variance estimate of the power at a given frequency, see e.g. Penny (2000), the estimated spectrum will be very spiky. This is seen from the example in Figure 5.1 and Figure 5.2 which show part of a recorded pitch signal (normalised with the standard deviation) and the corresponding power spectrum, respectively (data from Shioji-Maru (2004)).

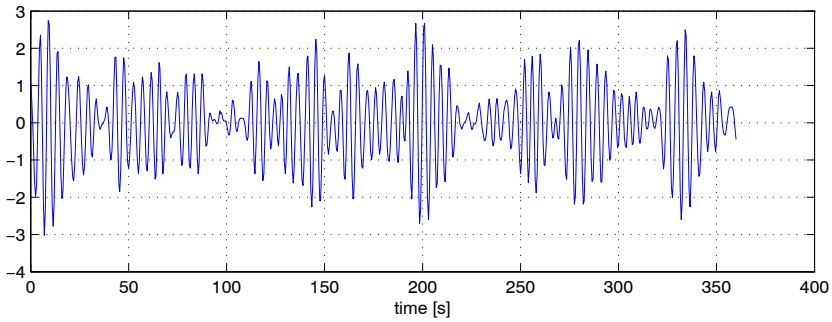

Figure 5.1: *Graphical illustration of the considered time series.*

Furthermore, the phenomenon of spectral leakage means that power is lost from a given frequency to other frequency bins in the FFT signal, due to the use of a finite data stream and also because of the linearly fixed frequencies used in the FFT procedure.

As regards deconvolution, the periodogram being a high variance estimate of the power implies that reliable results cannot be obtained, as well as spectral leakage reduces the

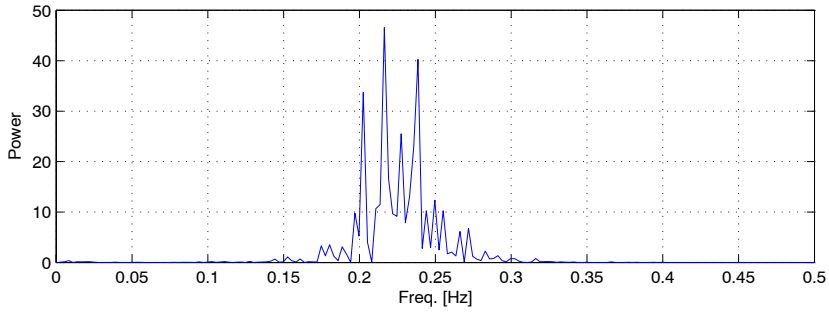

Figure 5.2: *The corresponding power spectrum for the time series.*

accuracy. Thus, if the cross spectral analysis is based on the FFT procedure, methods or techniques that compensate for the two mentioned problems have to be used. In general, such techniques involve segmentation with possible overlap of the time series and the use of window functions to take care of respectively the spiky spectrum and the spectral leakage. However, the main problem with these techniques is that manual choices - such as the type of window function, the size of the window, the number of samples by which the segments overlap, etc. - for the procedures can greatly affect the result. This is seen from the example in Figure 5.3 which depicts the power spectrum of the signal in Figure 5.1 for three different setups of segmentation. All of the periodograms are produced with a Hann window, e.g. Press et al. (1992), and the segments overlap each other with 100 samples. The only difference is the window size, which is 400, 300 and 200 samples, respectively. As seen the results are quite different, and consequently the results as obtained from deconvolution will vary depending on the window size used.

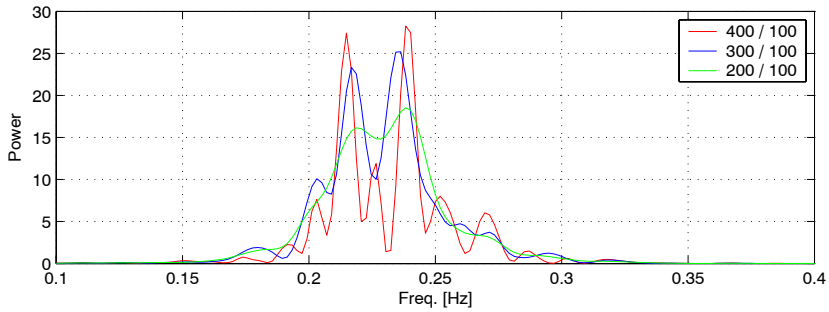

Figure 5.3: *The power spectrum for different numbers of segments. Note the difference in scale on the axes when compared to Figure 5.2.*

From the point of view of deconvolution, the present example suggests using a window size of 200 samples. However, it should be realised that use of a smaller window size would make the spectrum smoother. The problem is therefore: for which window size is the optimal situation achieved? Unfortunately, by application of FFT procedures, the answer cannot be given in general, and it should be noted that the smaller the window size - and thus the

smoother a spectrum - the more frequency dependent information might be lost. Therefore, it cannot be recommended to use periodograms based on FFT to carry out the spectral analysis in decision support systems. Instead, the spectral analysis can be carried out by use of multivariate autoregressive modelling (MAR). In the following sections this will be explained in detail.

5.2 Basics of MAR Modelling

As noted by Penny (2000), the MAR spectral estimation has two distinct advantages over methods based on the FFT: 1) the power can be estimated over a continuous range of frequencies and 2) the power estimates have less variance.

Basically, a MAR model tries to describe/estimate the current value of variables of the set of considered time series from a weighted linear sum of previous values of the considered time series. Depending on the number p of preceding values which the model takes into account, the model is said to be of order p. Such a multivariate autoregressive process is a rather simple, although effective, approach to do time series analysis, cf. Harrison et al. (2003). However, concerning decision support systems, as pointed out by Akaike (1971), in relation to control of dynamical systems, the decision of the order forms a crucial point of the autoregressive process.

In the sections below the mathematical theory of multivariate autoregressive modelling is described. The main references for the present treatment are Akaike and Nakagawa (1988), Akaike (1971) and Neumaier and Schneider (2001), but Marple (1987), Åström (1970) and Himmelblau (1970) may be consulted for a more general description of stochastic control theory.

5.3 Spectral Estimation

It is assumed that K stationary time series have been obtained and that these are stored in the vector $\mathbf{x}$ of the size$(\mathbf{x}) = K \times 1$

$$\mathbf{x} = \begin{bmatrix} x_1 \\ x_2 \\ \vdots \\ x_K \end{bmatrix} \tag{5.1}$$

so that each element corresponds to a given measured time series, $x_i\,(s \cdot \Delta t)$, $s = 0, 1, 2, ..., N$ and Δt being the sampling time. For convenience, Δt is from now on taken to equal 1 unless otherwise stated.

By modelling the $x_i(s)$ from the previous M values of x_j , $j = 1, 2, ..., K$, the following multivariate autoregressive representation is established

$$x_i(s) = \sum_{m=1}^{M} \sum_{j=1}^{K} A_{ij}(m)\, x_j(s-m) + \varepsilon_i(s) \quad , \quad i = 1, 2, ..., K \tag{5.2}$$

which in matrix notation is written as

$$\mathbf{x}(s) = \sum_{m=1}^{M} \mathbf{A}(m)\, \mathbf{x}(s-m) + \mathbf{u}(s) \tag{5.3}$$

where $\mathbf{A}(m)$ is a $K \times K$ matrix of the so-called MAR coefficients and $\mathbf{u} = \left[\begin{array}{cccc} \varepsilon_1 & \varepsilon_2 & \dots & \varepsilon_K \end{array} \right]^T$ contains the residual white noise elements between the measured and modelled values of $x_i(s)$. These white noise variables are introduced in the MAR procedure for stochastic reasons.

For a schematic visualisation of the MAR process, (5.3) is rewritten as

$$\mathbf{x}(s) = \mathbf{W}\mathbf{y}_s + \mathbf{u}(s) \tag{5.4}$$

where

$$\mathbf{y}_s = \left[\begin{array}{c} \mathbf{x}(s-1) \\ \mathbf{x}(s-2) \\ \vdots \\ \mathbf{x}(s-M) \end{array} \right] \tag{5.5}$$

are the M previous multivariate time series samples, and $\mathbf{W}$ is a $K \times (K \cdot M)$ matrix of the MAR coefficients, or weights

$$\mathbf{W} = \left[\begin{array}{cccc} \mathbf{A}(1) & \mathbf{A}(2) & \cdots & \mathbf{A}(M) \end{array} \right] \tag{5.6}$$

Figure 5.4 a) illustrates the MAR modelling with the K-dimensional time series $\mathbf{x}(s)$ modelled by $\mathbf{W}\mathbf{y}_s$ plus the residual error $\mathbf{u}(s)$. From Figure 5.4 b) it is seen that $\mathbf{W}$ is the matrix containing the weights (MAR coefficients) that characterise the interactions among the elements of M. The matrix consists of M layers (one for each time lag used in the model) with each layer being a $K \times K$ matrix of weights. The M layers of $\mathbf{W}$ have been placed in sequential order at the bottom of the figure, and it is symbolised how the diagonal elements are "self-connections" while the off-diagonals reflect the dependence between different variables in the original K-dimensional time series, cf. Harrison et al. (2003).

In the spectral estimation, x_i in (5.2) is modelled as a linear combination of the M preceding values of x_j , $j = 1, 2, ..., K$, and the MAR coefficients are determined as the best linear predictors for a sufficiently large M. The corresponding $\varepsilon_i(s)$ may practically be

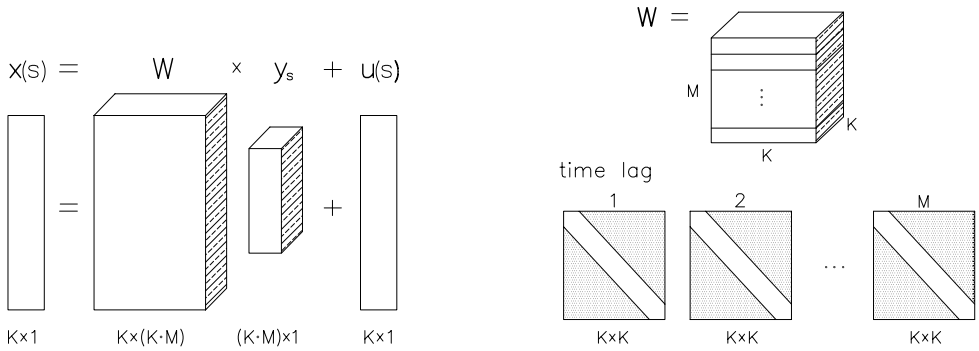

Figure 5.4: *A schematic visualisation of the MAR process.* Harrison et al. (2003).

considered to be uncorrelated with all the past values of $x_i(s)$, cf. Akaike and Nakagawa (1988), and thus, as $\varepsilon_i(s-m)$ with $m \geq 1$ is given by a linear combination of the past values $x(s-m), x(s-m-1), ...$, the covariance between $\varepsilon_i(s)$ and $\varepsilon_i(s-m)$ will be zero. Therefore, the residual white noise vector has a covariance matrix given by

$$R_{\varepsilon_i\varepsilon_j}(m) = \begin{cases} \sigma_{ij} & , m = 0 \\ 0 & , m = 1, 2, ... \end{cases} \tag{5.7}$$

with σ_{ij} being the covariance between $\varepsilon_i(s)$ and $\varepsilon_j(s)$.

With the expression in (5.7) a very simple relationship is found for the cross spectral densities, $p_{\varepsilon_i\varepsilon_j}(f)$, of the white noise signals, as

$$\begin{aligned} p_{\varepsilon_i\varepsilon_j}(f) &= \sum_{m=-\infty}^{\infty} R_{\varepsilon_i\varepsilon_j}(m) \exp(-i2\pi f m) \\ &= \sigma_{ij} \end{aligned} \tag{5.8}$$

where $i = \sqrt{-1}$ in the exponential expression.

As regards the residuals, and putting $A_{ij}(0) = -\delta_{ij}$, with δ_{ij} being Kronecker's delta (i.e. $\delta_{ij} = 1$, $i = j$, and $= 0$ otherwise), it is seen that

$$\varepsilon_i(s) = -\sum_{m=0}^{M}\sum_{j=1}^{K} A_{ij}(m)\, x_j(s-m) \tag{5.9}$$

which shows - as stated above - that $\varepsilon_i(s)$ is found from a linear transformation of $x_j(s)$. Moreover, it should be noted that $A_{ij}(m)$ corresponds to the impulse response function when a continuous one-dimensional case is considered

$$z(t) = \int_{-\infty}^{\infty} y(t-\tau)\, h(\tau)\, d\tau \tag{5.10}$$

Here the original $y(t-\tau)$ undergoes a linear transformation through the impulse response function $h(\tau)$. Thus, the power spectral density at frequency g, $p_{zz}(g)$, of $z(t)$ is given by, e.g. Akaike and Nakagawa (1988)

$$p_{zz}(g) = |B(g)|^2 p_{yy}(g) \quad , \quad -\infty < g < \infty \tag{5.11}$$

with $p_{yy}(g)$ being the power spectral density of $y(t)$, and

$$B(g) = \int_{-\infty}^{\infty} h(\tau) \exp(-i2\pi g\tau)\, d\tau \tag{5.12}$$

being the frequency response function found as the Fourier transform of the impulse response function $h(\tau)$.

By observing this similarity between the present multivariate case and the equivalent one-dimensional case, and noting that in the multivariate case the cross spectral densities between the errors $\varepsilon_i(s)$ and $\varepsilon_j(s)$ are complex, the elements of the cross spectral error densities can be written

$$p_{\varepsilon_i\varepsilon_j}(f) = \sum_{u=1}^{K}\sum_{v=1}^{K} A_{iu}(f)\, p_{uv}(f)\, \overline{A_{jv}(f)} \quad , \quad i,j = 1,2,...,K \tag{5.13}$$

with $\overline{\cdot}$ denoting the complex conjugate. $A_{iu}(t)$ is found from a Fourier transformation

$$A_{\alpha\beta}(f) = \sum_{m=0}^{M} A_{\alpha\beta}(m) \exp(-i2\pi fm) \quad , \quad \alpha,\beta = 1,2,...,K \tag{5.14}$$

with $A_{\alpha\beta}(m=0) = -\delta_{\alpha\beta}$ so that $\mathbf{A}(m=0)$ is the $K \times K$ minus identity matrix. (Be aware of the similar symbol $A_{\alpha\beta}(f)$ used for the Fourier transform of $A_{\alpha\beta}(m)$.)

Further, by introducing (5.8) in (5.13), the following expression is obtained

$$\sigma_{ij} = \sum_{u=1}^{K}\sum_{v=1}^{K} A_{iu}(f)\, p_{uv}(f)\, \overline{A_{jv}(f)} \quad , \quad i,j = 1,2,...,K \tag{5.15}$$

which by use of matrices can be rewritten. Thus, by letting $\mathbf{\Sigma}$, $\mathbf{A}(f)$ and $\mathbf{P}(f)$ be the matrices whose (i,j)th elements are given by σ_{ij}, $A_{ij}(f)$ and $p_{ij}(f)$ (the cross spectral density of $x_i(s)$ and $x_j(s)$), respectively, (5.15) reads

$$\mathbf{\Sigma} = \mathbf{A}(f)\, \mathbf{P}(f)\, \overline{\mathbf{A}(f)}^T \tag{5.16}$$

Hence, in the case that $\mathbf{A}(f)$ is non-singular, the cross spectral density can be found from

$$\mathbf{P}(f) = \mathbf{A}(f)^{-1}\, \mathbf{\Sigma} \overline{\mathbf{A}(f)}^{-T} \tag{5.17}$$

The latter result shows that once an autoregressive formulation, as expression (5.2), has been established, the cross spectra of K stationary time series are completely specified. However, the determination remains of the optimal MAR coefficients $A_{ij}(m)$ for the order M denoted by $A_{Mij}(m)$, $m = 1,2,...,M$.

5.4 Determination of the MAR Coefficients

The optimal MAR parameters can be computed by minimising the mean square of $\varepsilon_i(s)$. The mean square is given as (by use of some algebra)

$$\overline{\varepsilon_i(s)}^2 = \frac{1}{N}\sum_{s=1}^{N}\varepsilon_i(s)^2 =$$

$$R_{ij}(0) + \sum_{n=1}^{M}\sum_{l=1}^{K}\sum_{m=1}^{M}\sum_{j=1}^{K} A_{Mij}(m)\, A_{Mil}(m)\, R_{jl}(m-n)$$

$$-2\sum_{m=1}^{M}\sum_{j=1}^{K} A_{Mij}(m)\, R_{ij}(m) \tag{5.18}$$

corresponding to the least squares estimate, $\widehat{A}_{Mij}(m)$, of the true solution $A_{Mij}(m)$. Differentiation with respect to the MAR coefficients leads to the equation system

$$\sum_{m=1}^{M}\sum_{j=1}^{K} A_{Mij}(m)\, R_{jl}(m-n) = R_{il}(n) \quad ,$$

$$l = 1, 2, ..., K \quad , \quad n = 1, 2, ..., M \tag{5.19}$$

which is an $(M \times K)$-dimensional simultaneous first order equation. Such systems are difficult to solve numerically for large K and M, cf. Akaike and Nakagawa (1988), and furthermore, as the optimal order M_{opt} is not known in advance, it is necessary to solve (5.19) for a range of orders $M = 1, 2, ..., L$, for which reason the amount of computations becomes very large. However, instead of solving directly for the least squares estimates, $\widehat{A}_{Mij}(m)$, $m = 1, 2, ..., M$, an efficient recursive computational procedure derived by Whittle (1963) can be applied. Basically, this procedure is a generalisation of the univariate recursive method by Durbin (1960) for the fitting of autoregressive schemes of successively increasing order. Thus, in practical applications, with knowledge of the covariance functions, $C(x_i(n-m), x_j(n-l))$, the autoregressive model can be fitted with second order moments equal to the covariances up to the order M and for this purpose, Whittle's recursive computational procedure is efficient.

Further below, a recursive procedure similar to that of Whittle's is discussed, but attention is also given to a method that solves (5.19) in a direct manner by a stepwise algorithm. Both procedures have been implemented. As regards the latter a pre-developed MatLab package by Schneider and Neumaier (2001) is applied to find the optimal MAR coefficients. Subsequently, an additional cross spectral analysis is carried out according to (5.17). Before dealing with each of the two procedures, however, the important aspect of how to choose the optimal order of the MAR process is discussed.

5.5 Choice of the Optimal Order

The determination of the optimal model order is of great importance and the determination forms usually the most delicate part of the MAR analysis. In the literature several of so-called model order selection criteria can be found, see e.g. Lütkepohl (1985) for an overview. Basically, such order criteria are functions of the logarithm of the determinant of the white noise covariance matrix $\mathbf{\Sigma}$. The criteria, in general, take into account the model order, M, the number of data points, N, in the time series, and the number of considered time series, K. From a mathematical point of view, see Penny and Roberts (2002), the setup of the order criteria can be explained from what is known as the negative variational free energy, $F(M)$. This quantity thus provides a lower bound on the log evidence which, by definition, yields the likelihood of the considered model. Hence, by maximising the free energy, an estimate of the optimal order can be found. Regarding the negative variational free energy, this can, in completely general terms, be written

$$F(M) = L + P \tag{5.20}$$

where L is the average log-likelihood of the data, having to do with the 'accuracy', and P is a divergence term, acting as a penalty term which penalises more complex models. See Penny and Roberts (2002) for details.

As a concrete order selection criterion for choosing the optimal order, Akaike (1971) suggested that this can be taken to be the value that yields the minimum of the $MFPE$ (multiple final prediction error) function

$$MFPE(M) = \left(1 + \frac{M \cdot K + 1}{N}\right)^{K} \left(1 - \frac{M \cdot K + 1}{N}\right)^{-K} \det(\mathbf{\Sigma}) \tag{5.21}$$

where $\det(\mathbf{Z})$ denotes the determinant of matrix $\mathbf{Z}$, and $\mathbf{\Sigma}$ is the white noise covariance matrix. That is, compared to the variational free energy, $\det(\mathbf{\Sigma})$ denotes the 'accuracy' term while the complexity of the model is expressed by the parameters M, N and K. As mentioned by Lütkepohl (1993), for an increased order M, $\det(\mathbf{\Sigma})$ declines whereas the multiplicative term $\left(1 + \frac{MK+1}{N}\right)\left(1 - \frac{MK+1}{N}\right)^{-1}$ increases, and the order is obtained as the value for which these two forces are balanced optimally.

Another selection criterion for the optimal order is based on the Bayesian Information Criterion (BIC), e.g. Neumaier and Schneider (2001) and Penny and Roberts (2002), where the optimal order is found for the maximum of

$$BIC(M) = -\frac{N}{2}\log(\det(\mathbf{\Sigma})) - \frac{M \cdot K \cdot K}{2}\log(N) \tag{5.22}$$

Note that the overall structure of the two criteria is to some degree identical, though with the log working on the BIC.

As already mentioned, more order selection criteria exist, but in the present work only the two listed above are implemented and utilised. However, choosing these is also in agreement with the study by Lütkepohl (1985), which, in general, found that the $MFPE$ and the BIC criteria are well-working order selection criteria and to some extent superior to others.

5.6 Recursive Computational Procedure

In the following, it is sketched how to determine the MAR coefficients from the so-called recursive procedure. The method follows closely Akaike and Nakagawa (1988).

1. It is assumed that K sets of time series

$$\begin{matrix} x_1(s \cdot \Delta t) \\ x_2(s \cdot \Delta t) \\ \vdots \\ x_K(s \cdot \Delta t) \end{matrix} \quad , \quad s = 1, 2, ..., N \tag{5.23}$$

   are given, and that all of the time series are equidistantly spaced with the same time sampling Δt.

2. For all the sets the mean value (with $\Delta t = 1$)

$$\mu_i = \frac{1}{N} \sum_{s=1}^{N} x_i(s) \quad , \quad i = 1, 2, ..., K \tag{5.24}$$

   is calculated, and $x_i(s)$, $s = 1, 2, ..., N$, is redefined by

$$x_i(s) = x_i(s) - \mu_i \quad , \quad i = 1, 2, ..., K \tag{5.25}$$

3. For $i, j = 1, 2, ..., K$, the $K \times K$ covariance matrix $\mathbf{C}$ is calculated for different lags l, and the elements are given by

$$C_{ij}(l) = \frac{1}{N} \sum_{s=1}^{N-l} x_i(s+l)\, x_j(s) \quad , \quad l = 1, 2, ..., L \tag{5.26}$$

   and from now on all calculations concern matrices of size $K \times K$.

4. Initialise arrays of matrices $\mathbf{A}_M(m) = \mathbf{B}_M(m) = \mathbf{0}$ for $m, M = 1, 2, ..., L$.

5. From the recursive procedure below, $\mathbf{A}_M(m)$, $m = 1, 2, ..., M$, and $\mathbf{D}_M$ are calculated for $M = 0, 1, ..., L$:

$$\mathbf{D}_M = \mathbf{C}(0) - \sum_{m=1}^{M} \mathbf{A}_M(m)\, \mathbf{C}(m)^T \tag{5.27}$$

$$\mathbf{E}_M = \mathbf{C}(M+1) - \sum_{m=1}^{M} \mathbf{A}_M(m)\,\mathbf{C}(M+1-m) \tag{5.28}$$

$$\mathbf{F}_M = \mathbf{C}(0) - \sum_{m=1}^{M} \mathbf{B}_M(m)\,\mathbf{C}(m)^T \tag{5.29}$$

$$\mathbf{D}_M^* = \mathbf{E}_M \mathbf{F}_M^{-1} \tag{5.30}$$

$$\mathbf{E}_M^* = \mathbf{E}_M^T \mathbf{D}_M^{-1} \tag{5.31}$$

$$\mathbf{A}_{M+1}(m) = \begin{cases} \mathbf{A}_M(m) - \mathbf{D}_M^* \mathbf{B}_M(M+1-m) & , \quad m = 1,2,...,M \\ \mathbf{D}_M^* & , \quad m = M+1 \end{cases} \tag{5.32}$$

$$\mathbf{B}_{M+1}(m) = \begin{cases} \mathbf{B}_M(m) - \mathbf{E}_M^* \mathbf{A}_M(M+1-m) & , \quad m = 1,2,...,M \\ \mathbf{E}_M^* & , \quad m = M+1 \end{cases} \tag{5.33}$$

6. Compute also the model order selection criterion, which is $MFPE$ or BIC, for each $M = 0,1,...,L$

$$MFPE(M) = \left(1 + \frac{M \cdot K + 1}{N}\right)^K \left(1 - \frac{M \cdot K + 1}{N}\right)^{-K} \det(\mathbf{D}_M) \tag{5.34}$$

$$BIC(M) = -\frac{N}{2} \log(\det(\mathbf{D}_M)) - \frac{M \cdot K \cdot K}{2} \log(N) \tag{5.35}$$

Note that $\mathbf{D}_M$ is substituted for the covariance matrix, $\mathbf{\Sigma}$, of the white noise. This issue is studied in more detail by e.g. Tjøstheim and Paulsen (1983) and Mentz et al. (1988), and based on both asymptotic theory and simulations their studies indicate that the residual covariance matrix $\mathbf{D}_M$ is a fairly reliable estimator of the white noise covariance matrix $\mathbf{\Sigma}$, cf. Neumaier and Schneider (2001).

7. The optimal order and, thus, the MAR coefficients are chosen for the value of $M = M_{\text{opt}}$ which yields the minimum of $MFPE$ (or the maximum of BIC). At the end of the chapter, numerical examples are given to study the behaviour of the two criteria.

8. Based on (5.17), an estimate of the cross spectral density matrix $\mathbf{P}(f)$ can be calculated

$$\mathbf{P}(f) = \mathbf{A}_{M_{\text{opt}}}(f)^{-1}\,\mathbf{D}_{M_{\text{opt}}}\,\overline{\mathbf{A}_{M_{\text{opt}}}(f)}^{-T} \tag{5.36}$$

Note that, according to point (7) above, M is replaced by M_{opt} and $\mathbf{A}(m)$ by $\mathbf{A}_{M_{\text{opt}}}(m)$ in (5.17). Moreover, $\mathbf{D}_{M_{\text{opt}}}$ replaces $\mathbf{\Sigma}$.

5.7 Stepwise Least Squares Algorithm

Although the above procedure for estimating the MAR coefficients and carrying out the cross spectral analysis is efficient, it should be noted that other procedures exist. For example, Neumaier and Schneider (2001) deals with a so-called stepwise least squares (LS) algorithm for the estimation of the parameters of the MAR model. Basically, this algorithm uses a QR factorisation of an augmented data matrix of the MAR coefficients to evaluate, for a sequence of successive orders, a criterion for the selection of the model order and to compute the parameters of the MAR model of the optimal order. Though, being of high complexity, this method has as an accessible outcome the possibility of obtaining confidence intervals on the MAR parameters. Moreover, it facilitates the estimation of the so-called eigenmodes of the MAR process. Such eigenmodes can be used to derive dynamical characteristics of the system being studied and, especially, in the fields of geosciences where the interest is focused on different oscillation patterns this is of importance. Thus, components of the system that are associated with the dynamical characteristics can be identified, see e.g. Hasselmann (1988) for details.

In the following, an outline of the theory related to the estimation of the MAR coefficients by the stepwise LS algorithm will be given. For reference, see Neumaier and Schneider (2001).

5.7.1 LS Estimates for Fixed Order

From a MAR model, cf. (5.4), of order M with $N + p$ time samples for each of the K time series,

$$\mathbf{x}_s = \mathbf{W}\mathbf{y}_s + \mathbf{u}_s \quad , \quad s = 1, 2, ..., N \tag{5.37}$$

the augmented data matrix reads

$$\mathbf{W} = \left[\begin{array}{cccc} \mathbf{A}(1) & \mathbf{A}(2) & \cdots & \mathbf{A}(M) \end{array} \right] \quad , \quad \text{size}(\mathbf{W}) = K \times (K \cdot M) \tag{5.38}$$

and the 'predicting' vector is

$$\mathbf{y}_s = \left[\begin{array}{c} \mathbf{x}_{s-1} \\ \mathbf{x}_{s-2} \\ \vdots \\ \mathbf{x}_{s-M} \end{array} \right] \quad , \quad \text{size}(\mathbf{y}_s) = n_M \times 1 \tag{5.39}$$

where $n_M = K \cdot M$.

By solving

$$\min\left(\|\mathbf{x}_s - \mathbf{W}\mathbf{y}_s\|^2\right) \tag{5.40}$$

for the MAR coefficients of $\mathbf{W}$ in terms of the moment matrices

$$\mathbf{X} = \sum_{s=1}^{N} \mathbf{y}_s \mathbf{y}_s^T \ , \qquad \mathbf{Y} = \sum_{s=1}^{N} \mathbf{x}_s \mathbf{x}_s^T \ , \qquad \mathbf{Z} = \sum_{s=1}^{N} \mathbf{x}_s \mathbf{y}_s^T \ , \tag{5.41}$$

the least squares estimate of $\mathbf{W}$ can be written as follows, see Lütkepohl (1993)

$$\hat{\mathbf{W}} = \mathbf{Z}\mathbf{X}^{-1} \tag{5.42}$$

The residual covariance matrix $\hat{\mathbf{C}}$ (which corresponds to $\mathbf{D}_M$ in the recursive procedure, cf. (5.27)),

$$\hat{\mathbf{C}} = \frac{1}{N - K \cdot M} \sum_{s=1}^{N} \hat{\mathbf{u}}_s \hat{\mathbf{u}}_s^T \tag{5.43}$$

with

$$\hat{\mathbf{u}}_s = \mathbf{x}_s - \hat{\mathbf{W}} \mathbf{y}_s \tag{5.44}$$

is an estimate of the noise covariance matrix $\mathbf{C}$ (which corresponds to $\mathbf{\Sigma}$ in the recursive procedure), and it can be expressed as

$$\hat{\mathbf{C}} = \frac{1}{N - K \cdot M} \left(\mathbf{Y} - \mathbf{Z}\mathbf{X}^{-1}\mathbf{Z}^T \right) \tag{5.45}$$

It can be shown that the residual covariance matrix $\hat{\mathbf{C}}$ is proportional to a Schur complement, e.g. Golub and Loan (1996), of the matrix

$$\mathbf{\Gamma} = \begin{bmatrix} \mathbf{X} & \mathbf{Z}^T \\ \mathbf{Z} & \mathbf{Y} \end{bmatrix} \tag{5.46}$$

which is the moment matrix $\mathbf{\Gamma} = \mathbf{K}^T\mathbf{K}$ (from a Cholesky factorisation) with

$$\mathbf{K} = \begin{bmatrix} \mathbf{y}_1^T & \mathbf{x}_1^T \\ \vdots & \vdots \\ \mathbf{y}_N^T & \mathbf{x}_N^T \end{bmatrix} \tag{5.47}$$

From this matrix, a QR factorisation yields

$$\mathbf{K} = \mathbf{Q}\mathbf{R} \tag{5.48}$$

with

$$\mathbf{R} = \begin{bmatrix} \mathbf{R}_{11} & \mathbf{R}_{12} \\ \mathbf{0} & \mathbf{R}_{22} \end{bmatrix} \tag{5.49}$$

Applying this result to the Cholesky factorisation (as $\mathbf{Q}^T\mathbf{Q} = \mathbf{I}$)

$$\mathbf{\Gamma} = \mathbf{K}^T\mathbf{K} = \mathbf{R}^T\mathbf{R} \tag{5.50}$$

leads to the following expression for the moment matrix $\mathbf{\Gamma}$

$$\begin{bmatrix} \mathbf{X} & \mathbf{Z}^T \\ \mathbf{Z} & \mathbf{Y} \end{bmatrix} = \begin{bmatrix} \mathbf{R}_{11}^T\mathbf{R}_{11} & \mathbf{R}_{11}^T\mathbf{R}_{12} \\ \mathbf{R}_{12}^T\mathbf{R}_{11} & \mathbf{R}_{12}^T\mathbf{R}_{12} + \mathbf{R}_{22}^T\mathbf{R}_{22} \end{bmatrix} \tag{5.51}$$

Thus, it is seen that the least squares estimate of the MAR coefficients, cf. (5.42), is represented as

$$\hat{\mathbf{W}} = \left(\mathbf{R}_{11}^{-1}\mathbf{R}_{12}\right)^T \tag{5.52}$$

and the residual covariance matrix, cf. (5.45), is given by

$$\hat{\mathbf{C}} = \frac{1}{N - K \cdot M}\mathbf{R}_{22}^T\mathbf{R}_{22} \tag{5.53}$$

5.7.2 Downdating the LS Estimates

To choose the optimal order, the computation of an order selection criterion is needed for each of the orders, here taken to be limited as $M_{\min} \leq M \leq M_{\max}$. However, instead of calculating the residual covariance matrix by a separate QR factorisation for each of the orders, an approximation of the residual covariance matrix can be computed for a model order $M < M_{\max}$by downdating the QR factorisation for a model of order $M_{\max}$.

It should be mentioned that the following derivation is rather concise and gives only the very fundamentals. See Neumaier and Schneider (2001) for details.

To downdate the QR factorisation for a model of order M to a structurally similar factorisation for a model of order $M' = M - 1$, the structure of the data matrix $\mathbf{K}$, cf. (5.47)

$$\mathbf{K} = \begin{bmatrix} \mathbf{K}_1 & \mathbf{K}_2 \end{bmatrix}, \quad \mathbf{K}_1 = \begin{bmatrix} \mathbf{y}_1^T \\ \vdots \\ \mathbf{y}_N^T \end{bmatrix}, \quad \mathbf{K}_2 = \begin{bmatrix} \mathbf{x}_1^T \\ \vdots \\ \mathbf{x}_N^T \end{bmatrix} \tag{5.54}$$

should be used. Hence, a data matrix $\mathbf{K}' = \begin{bmatrix} \mathbf{K}_1' & \mathbf{K}_2 \end{bmatrix}$ for a model of order $M' = M - 1$ follows, approximately, from the data matrix $\mathbf{K} = \begin{bmatrix} \mathbf{K}_1 & \mathbf{K}_2 \end{bmatrix}$ for a model of order M by removing from the submatrix $\mathbf{K}_1 = \begin{bmatrix} \mathbf{K}_1' & \mathbf{K}_1'' \end{bmatrix}$ of the predictors $\mathbf{y}_s$ the K trailing columns $\mathbf{K}_1''$. The QR factorisation of the data matrix $\mathbf{K}'$ then follows from the QR factorisation of $\mathbf{K}$ by partioning the submatrices $\mathbf{R}_{11}$ and $\mathbf{R}_{12}$ of $\mathbf{R}$, considering the K trailing rows and columns of $\mathbf{R}_{11}$ and the K trailing rows of $\mathbf{R}_{12}$ separately

$$\mathbf{R}_{11} = \begin{bmatrix} \mathbf{R}_{11}' & \mathbf{R}_{11}'' \\ \mathbf{0} & \mathbf{R}_{11}''' \end{bmatrix}, \quad \mathbf{R}_{12} = \begin{bmatrix} \mathbf{R}_{12}' \\ \mathbf{R}_{12}'' \end{bmatrix} \tag{5.55}$$

Thus, the QR factorisation of $\mathbf{K}$ becomes

$$\mathbf{K} = \begin{bmatrix} \mathbf{K}_1' & \mathbf{K}_1'' & \mathbf{K}_2 \end{bmatrix} = \mathbf{Q} \begin{bmatrix} \mathbf{R}_{11}' & \mathbf{R}_{11}'' & \mathbf{R}_{12}' \\ \mathbf{0} & \mathbf{R}_{11}''' & \mathbf{R}_{12}'' \\ \mathbf{0} & \mathbf{0} & \mathbf{R}_{22} \end{bmatrix} \tag{5.56}$$

and by dropping the K columns belonging to the submatrix $\mathbf{K}_{11}''$, the factorisation of the downdated data matrix is obtained

$$\mathbf{K}' = \begin{bmatrix} \mathbf{K}_1' & \mathbf{K}_2 \end{bmatrix} = \mathbf{Q} \begin{bmatrix} \mathbf{R}_{11}' & \mathbf{R}_{12}' \\ \mathbf{0} & \mathbf{R}_{12}'' \\ \mathbf{0} & \mathbf{R}_{22} \end{bmatrix} \tag{5.57}$$

With this factorisation the residual covariance matrix becomes

$$\begin{aligned} \hat{\mathbf{C}}_{M-1} &= \frac{1}{N - K \cdot M} \left(\mathbf{R}_{22}^T \mathbf{R}_{22} + \mathbf{R}_{12}''^T \mathbf{R}_{12}'' \right) \\ &= \hat{\mathbf{C}}_M + \frac{1}{N - K \cdot M} \mathbf{R}_{12}''^T \mathbf{R}_{12}'' \end{aligned} \tag{5.58}$$

so that a downdating formula for the residual covariance matrix has been obtained.

The downdating procedure can be iterated, that is, starting from a QR factorisation for a model of order $M_{\max}$ and stepwise downdating the factorisation until the minimum order $M_{\min}$ is reached. Hence, by applying an order selection criterion, such as the $MFPE$ or BIC, the optimal order can be chosen. Thus, from the optimal order, the least squares estimates of the MAR coefficients, cf. (5.52), is found by replacing the maximally sized submatrices $\mathbf{R}_{11}$ and $\mathbf{R}_{12}$ by their leading submatrices of size $n_{M_{\text{opt}}}$, see Neumaier and Schneider (2001). Subsequently, the cross spectral density matrix $\mathbf{P}(f)$ is derived from (5.17) by replacing $\mathbf{A}(f)$ and $\mathbf{\Sigma}$ with $\hat{\mathbf{W}}_{M_{\text{opt}}}$ and $\hat{\mathbf{C}}_{M_{\text{opt}}}$, respectively.

Now, after dealing with the theoretical aspects of the multivariate autoregressive modelling and the cross spectral analysis, a numerical example will be considered.

5.8 Numerical Example

5.8.1 Time Series Generation

As an introduction it is to be outlined how to generate K time series based on a MAR model of order p. Thus, a K-dimensional vector $\mathbf{y}(s) = \begin{bmatrix} y_1(s) & y_2(s) & \dots & y_K(s) \end{bmatrix}^T$ with $\Delta t = 1$ is prescribed as

$$\mathbf{y}(s) = \sum_{m=1}^{p} \mathbf{A}(m)\, \mathbf{y}(s-m) + \mathbf{u}(s) \tag{5.59}$$

which means that the process is characterised by the MAR coefficients

$$\mathbf{A}(1) \ , \mathbf{A}(2) \ , \ \ldots \ , \mathbf{A}(p) \tag{5.60}$$

which all must be given/known in advance. Moreover, the process is characterised by the white noise covariance matrix $\mathbf{\Sigma}$, which is given too, and hence the white noise vector is calculated from, e.g. Lütkepohl (1993)

$$\mathbf{u}(s) = \mathbf{L}\mu(s) \tag{5.61}$$

where $\mu(s) = \left[\ \mu_1(s) \quad \mu_2(s) \quad \ldots \quad \mu_K(s) \ \right]^T$ denotes a vector of random numbers which are independent realisations of a random variable with mean 0 and variance 1, and with the lower triangular matrix $\mathbf{L}$ found from the Cholesky decomposition of $\mathbf{\Sigma}$

$$\mathbf{\Sigma} = \mathbf{L}\mathbf{L}^T \tag{5.62}$$

5.8.2 Behaviour of Order Criteria

As an example, three real time series, corresponding to the responses pitch, roll and vertical acceleration at FP, for the research and training, the ship Shioji-Maru, are considered (data from Shioji-Maru (2004)). For details on the Shioji-Maru see Chapter 7. In Figure 5.5 the responses are shown and it is seen that the time series have a duration of six minutes.

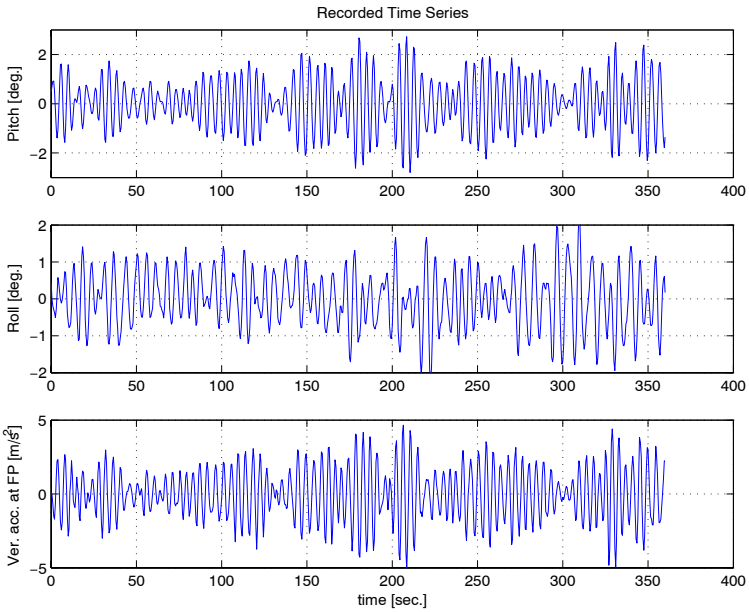

Figure 5.5: *Three responses: pitch, roll, and vertical acceleration at FP form the basis of the example.*

Now, by modelling the time series as a MAR model, i.e. determining the MAR coefficients and the covariance matrix, for a range of orders (2nd to 18th), and then generating 100 samples of time series for each order, and subsequently applying both the recursive procedure and the stepwise least squares algorithm to the set of data, it can be observed how well the model order selection criteria, (5.21) and (5.22), behave. That is, the study is based on the following tasks:

1. In order to model the three time series, the MAR coefficients and the covariance matrix are calculated for 2nd to 18th order models.
2. Based on the MAR coefficients, $\mathbf{A}(i)$, and the white noise covariance matrix, $\mathbf{\Sigma}$, time series are generated as outlined in the preceding subsection. 100 sets of time series are simulated for each order.
3. For each order the recursive procedure and the stepwise LS algorithm are applied to the generated time series for which the correct order is known (those specified in point (1)).
4. Compared to the correct order it is seen how often the order selection criteria choose this order.

The outcome of the study is seen in Figure 5.6 and Figure 5.7. From Figure 5.6 a) and b) it is seen that when the time series are modelled as a, say, 4th order MAR model, the $MFPE$, when the recursive procedure is used for the analysis, only selects the correct model order in approximately 45% of the times, whereas the BIC criterion estimates the correct model order in 95% of the times. There is a clear indication that for the low orders the BIC criterion is superior to the $MFPE$. For the higher order models, the $MFPE$ criterion is best as regards choice of the model order. Considering the stepwise LS algorithm, from Figure 5.6 c) and d), a similar trend is noted. It is seen that the higher the order, the harder it is for the model order selection criteria to choose the correct model order. The reason for this is that the number of data points, $N = 800$, in the time series is held constant. The ratio of data points to coefficients (that depend on the order) has therefore reduced. This has the effect of making the model order curves, that is, the order selection criterion as a function of the order, less peaky at higher order, cf. Penny and Roberts (2002).

The ability of the order criterion to choose the correct order, as seen from Figure 5.6, is important. However, it may be argued, especially in practical applications with no prior knowledge of the correct/optimal order, it is of more importance that the order selection criterion 'just' on average, including deviation from this, determines the optimal order. Thus, a study of Figure 5.7 reveals that although the $MFPE$ criterion in some cases is less good than the BIC in predicting the correct order, the mean of the orders selected by the $MFPE$, in general, is closer to the correct order than the mean of the orders for the BIC, and, furthermore, the standard deviation is smallest for the $MFPE$. Hence, in conclusion to the present study it seems that in a completely general situation, when MAR modelling

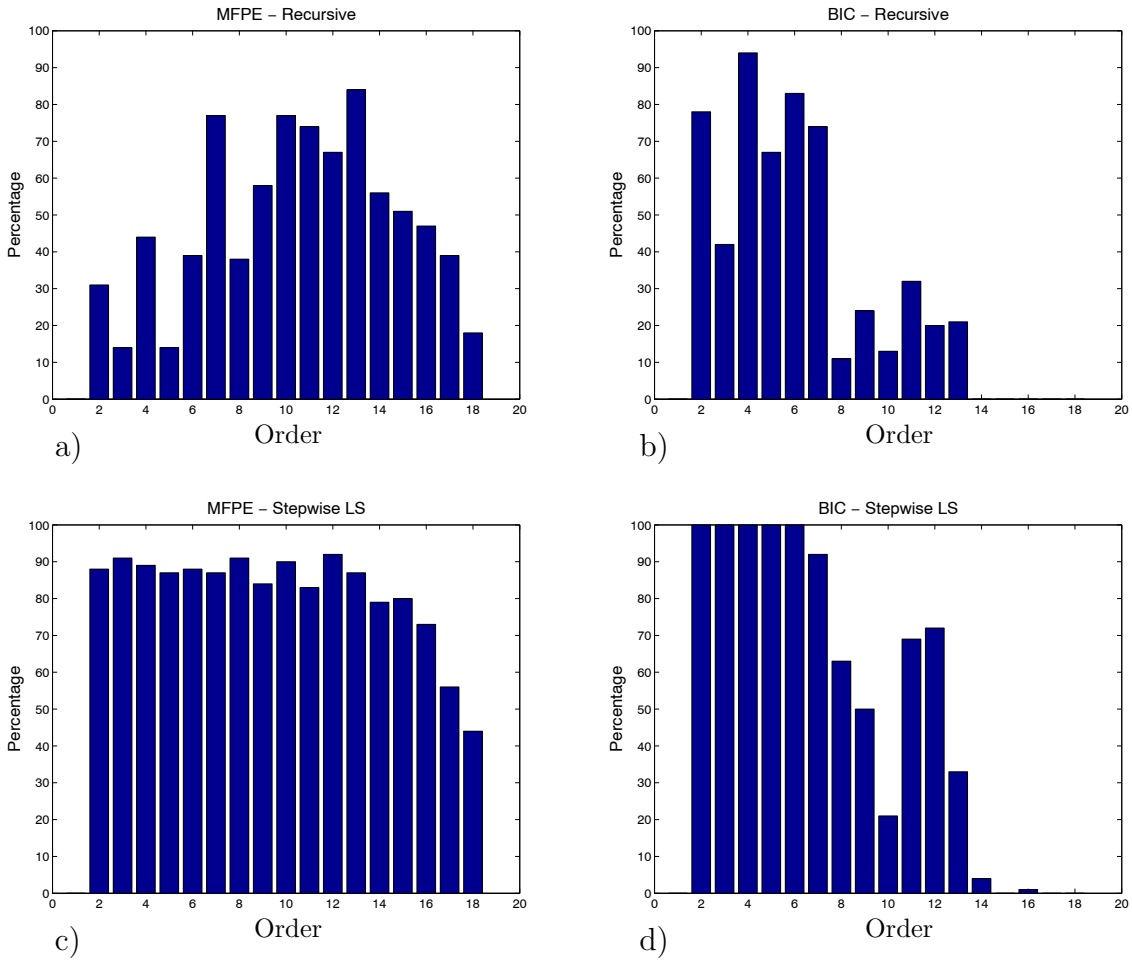

Figure 5.6: *The percentage of times the specific criterion chooses the correct model order.* a) *$MFPE$ from the recursive procedure,* b) *BIC from the recursive procedure,* c) *$MFPE$ from the stepwise LS algorithm, and* d) *BIC from the stepwise LS algorithm.*

and cross spectral analysis are carried out, the $MFPE$ criterion is the most suitable order selection criterion, as it is able to select the optimal order with fairly good accuracy for both low and high orders.

To finish the example, the cross spectral analysis is carried out for the three time series shown in Figure 5.5. The analysis is based on both the recursive procedure and the stepwise LS algorithm. In both cases the optimal order is estimated by the $MFPE$ criterion as well as the BIC. Thus, when the $MFPE$ criterion is applied to both of the calculation methods, an optimal order of $M_{\text{MFPE}} = 12$ is chosen whereas the BIC estimates the optimal order as $M_{\text{BIC}} = 4$ in the two cases. Just below, a few words will be said about which order to believe in as the 'true' optimal one, but for the sake of clarity and completeness Figure 5.8 and Figure 5.9 show the calculated cross spectra for the order of 4 and 12, respectively.

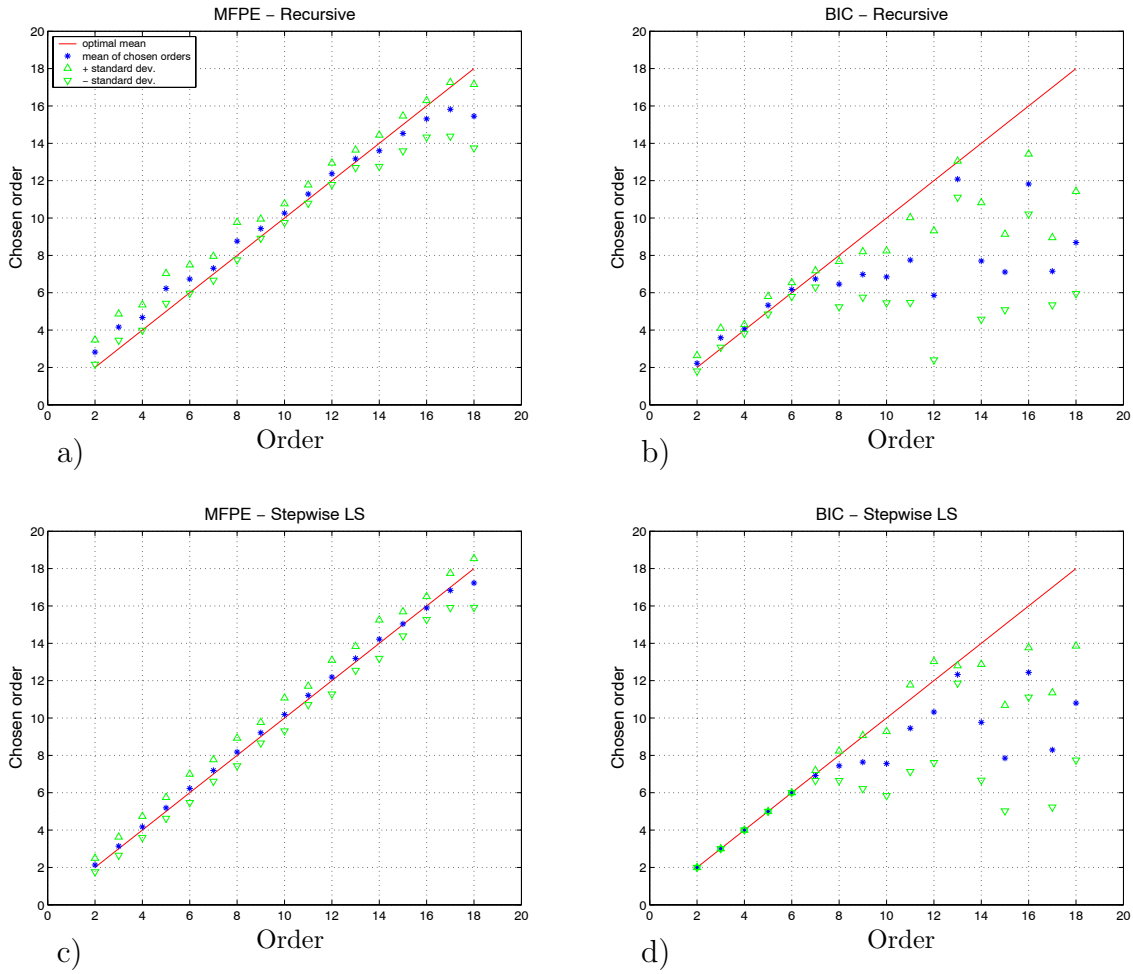

Figure 5.7: *Mean and standard deviations of selected orders.*
a) *MFPE from the recursive procedure,* b) *BIC from the recursive procedure,* c) *MFPE from the stepwise LS algorithm, and* d) *BIC from the stepwise LS algorithm.*

In both cases the recursive procedure and the stepwise LS algorithm are compared. Note that the 'off-diagonal' spectra have real and imaginary parts and are each other's symmetric conjugate.

As seen from the figures the recursive procedure and the stepwise LS algorithm yield almost identical results, although there seems to be slightly more energy preserved when the cross spectral analysis is carried out with the latter of the two methods. The differences are much more outspoken when the cases of order $M = 4$ and $M = 12$ are compared. Thus, it is very notable that the pitch/pitch cross spectrum exhibits two peaks for $M = 12$, cf. Figure 5.9, whereas this is not the case for $M = 4$, cf. Figure 5.8. Obviously, this fact is no reason for concluding that the optimal order *is* really 12 rather than 4, but by focusing on, say, the pitch/pitch spectrum, the FFT-based spectrum, i.e. Figure 5.3 at the very beginning of the

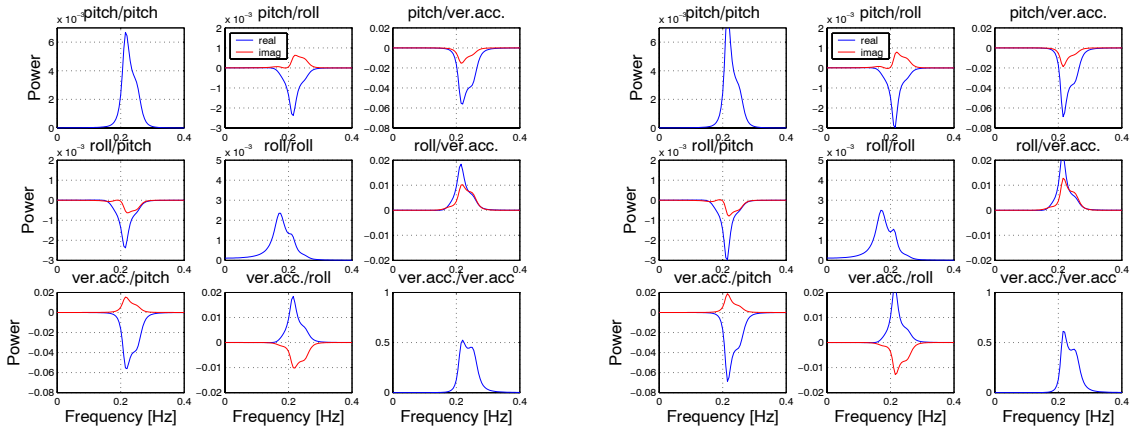

a) b)

Figure 5.8: *The cross spectra calculated for order* $M = 4$*.*
a) *The recursive procedure and* b) *the stepwise LS algorithm.*

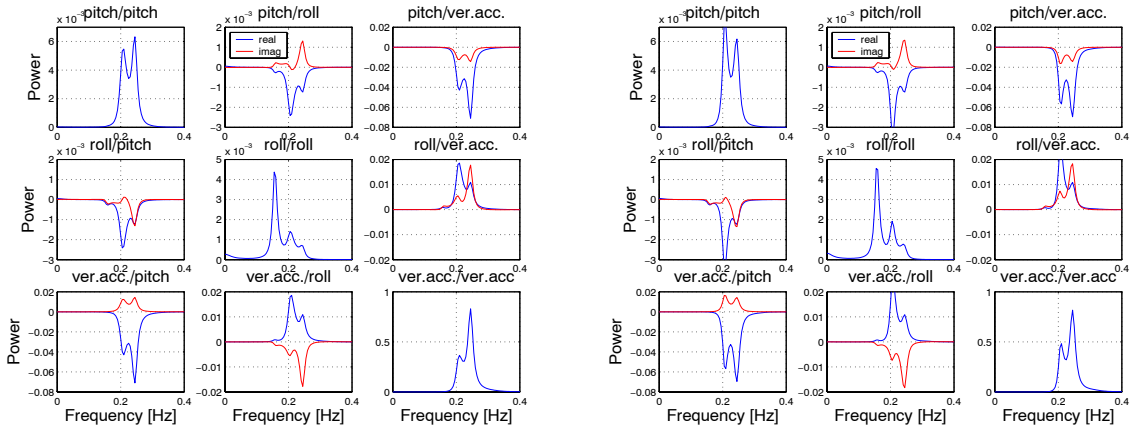

a) b)

Figure 5.9: *The cross spectra calculated for order* $M = 12$*.* a) *The recursive procedure and* b) *the stepwise LS algorithm.*

present chapter, also suggests two distinct peaks (it is understood here that the same set of data is analysed).

5.9 The Recursive Procedure vs. the LS Algorithm

From the derivations in the preceding sections it is hard to justify which one of the two MAR procedures – the recursive or the stepwise least squares algorithm – should be chosen in favour of the other. The recursive procedure is less complicated in the view of a programming aspect, whereas the LS algorithm has properties which could be of favour in the dynamical analysis of system. It has, however, turned out that the LS algorithm is slightly faster as

regards computational time, which in general is low (in the order of 10 seconds for three sets of time series). For this reason the stepwise LS algorithm is applied to the cross spectral analysis of the response measurements studied in the following chapters. Furthermore, it can be argued that the numerical example suggests the use of the LS algorithm, since Figure 5.6 illustrates better prediction of the correct order by the LS algorithm compared to the recursive procedure. As regards the order selection criterion Figure 5.7 favours the $MFPE$.

Chapter 6

Response Signals

6.1 Introduction

In this chapter response signals and transfer functions are discussed in more detail. This includes: what kind of signals to use, the number of signals to use, generally observed problems with response signals, calculation/treatment of the corresponding transfer functions, etc.

6.2 In-hand Time Series

Before details on the above-mentioned aspects of the response signals are considered, an important issue is to be dealt with. This issue is related to the acquisition in time of the responses. Ideally, for a real-time in-service monitoring system installed on a ship, sensors are measuring continuously and, hence, in the treatment of the response signals, continuously running time series are to be considered. However, when the estimation of wave spectra is dealt with, a certain amount of data is necessary for the success of a reliable estimate of the on-site spectrum. Moreover, due to the physics of ocean waves, the change in space and time of the on-site wave spectrum can be assumed to be slow, with reservations about course and speed changes of the ship. Consequently, it is not assumed to be of vital importance to have a continuously running update of the estimated wave spectrum. Instead, the wave spectrum is updated only on a, say, 15 minutes basis. Thus, for the tasks related to the estimation of wave spectra, the treatment/procedures do not have to handle running time series, but instead the procedures must be able to handle time series which are already in hand, and this simplifies the procedures.

6.3 Type of Responses

In principle, it can be said that any type of response signal may be utilised in the wave spectrum estimation as long as a linear complex-valued transfer function exists, that is, can be calculated. However, it is believed that the highest rate of success is achieved when global ship responses, such as pitch, roll, vertically wave-induced bending moment, etc., are used. This means that response signals of e.g. pressure transducers in the hull should not be considered in the estimation, as local effects may affect such a response.

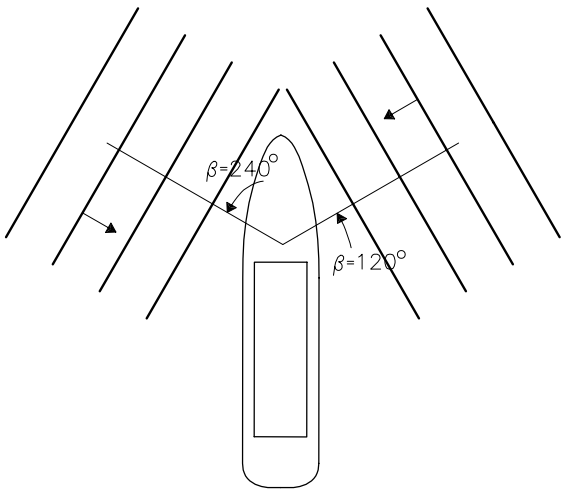

Figure 6.1: *Some transfer functions are symmetric with respect to port and starboard.*

As regards transfer functions, it is important to realise that many responses are invariant in the encounter angle in the sense that, when 180 deg. is head sea, no difference is found in the phase lag independently of an encounter angle equal to, say, 120 deg. or 240 deg. is studied, see Figure 6.1. The implication of this may, in principle, lead to a mirror image of the directional wave spectrum, see Figure 6.2, so that the direction of the waves, as read from the estimated directional spectrum, is wrong. Therefore, it should be sought to operate with, at least, one response with a transfer function which has port/starboard asymmetry such as e.g. sway and roll. It is understood here that complex-valued transfer functions are utilised, so that the amplitude as well as the phase of the responses are reflected.

Another aspect of ship responses and the corresponding complex transfer functions is that of insensitivity to low- and high-frequency wave excitations. For this reason it is advantageously to use responses which do not all exhibit sensitivity to wave excitations of the same frequency interval. Thus, the response of the relative wave height, for example, yields information at higher wave frequencies which means that information can be attained at frequencies above which the vessel hardly respond.

With respect to the number of responses to be taken into account for optimal estimation, a unique answer cannot be given. In more studies, including this, it has, however, been

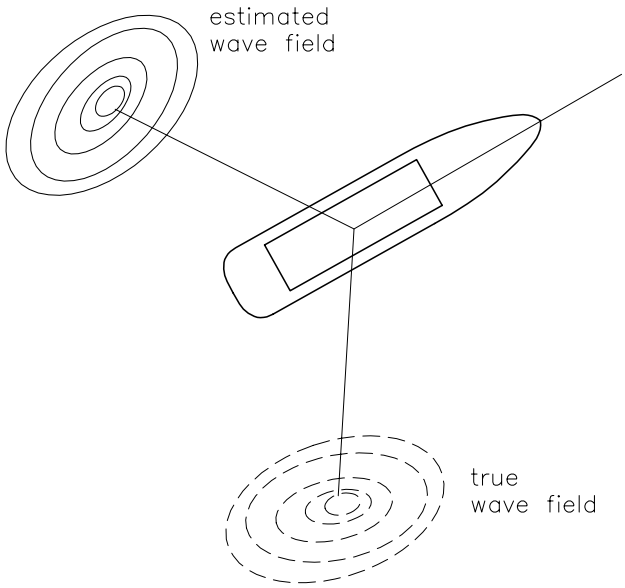

Figure 6.2: *The estimated wave field may be found to be on the wrong side when port/starboard invariant transfer functions are used.*

concluded that the use of three types of responses is the best compromise to obtain accurate estimations, cf. Aschehoug (2003), Tannuri et al. (2003) and Iseki and Terada (2002). The reason is that fewer responses lead to ambiguities in the solution, and more responses do not necessarily increase the accuracy much, although the computational costs are increased significantly.

6.4 Basic Treatment of Response Signals

Obviously, a range of problems may be encountered when response signals in the form of time series are measured and analysed. The present section serves only to illustrate a few of these problems. For clarity, it should be noted that all time series are handled as vectors. Thus, from the original data stream, the specific response signal and the associated time signal are stored as vectors $\mathbf{x}$ and $\mathbf{t}$, respectively.

6.4.1 Time Synchronisation

From experience it is known that when more sensors are integrated in an in-service monitoring system, time synchronisation between the different sensors may have to be introduced. The outcome of such a time synchronisation is illustrated in Figure 6.3, which shows part

of a strain response recorded amidships on a container ship, Nielsen (2003). In the specific situation, the time synchronisation happened approximately every 80 sec. with a resulting jump of the order of 0.7 sec. 'back in time', see Figure 6.3. In the lower plot of the figure a zoom is shown of the circled area in the upper plot. Obviously, this step back in time must be repaired.

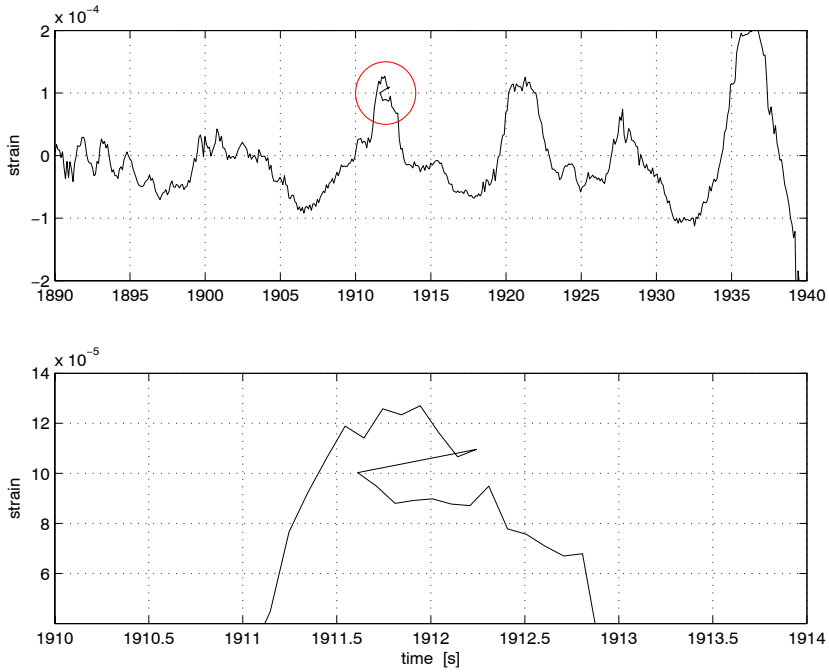

Figure 6.3: *Step back in time due to time synchronisation.*

6.4.2 Equidistant Time Steps and Filtering

In theory, the values in $\mathbf{t}$ should be spaced equidistantly according to the inverse of the sampling rate, f_s^{-1}. However, the sampling rate is, in general, not truly constant but varies slightly around a mean value which is the practical sampling rate as given by the manufacturer of the measuring device. In order to take care of such problems a linear spline with a constant sampling rate equal to the rate given by the manufacturer can be fitted through the data. The theory of splines is not dealt with here, instead reference is made to the literature, e.g. de Boer (1979) and Farin (1990).

6.4.3 Filtering

In order to reduce the amount of noise in the signals, and since the overall interest – in relation to estimation of wave spectra – is in the frequency range where the wave energy is

distributed, the response signals may have to be filtered. For details on filtering reference is made to the literature, see e.g. Press et al. (1992) and Oppenheim and Schafer (1989). In the present analysis one of MatLab's built-in procedures for bandpass filters is implemented and can be used. This procedure is based on an Infinite Impulse Response (IIR) filter and uses an elliptic digital filter in a direct form II transposed implementation of the standard difference equation, cf. Oppenheim and Schafer (1989).

The necessity to use a bandpass filter is illustrated in Figure 6.4. This figure shows a non-dimensionalised power spectrum of a strain response, Nielsen (2003). The calculation of the power spectrum, which at present is calculated by the Fast Fourier Transformation (FFT) for the purpose of visualisation, is dealt with in the next section. With respect to the discussion on the necessity to use a bandpass filter, it is observed that for the very low frequencies, noise is present as the spectrum does not go towards zero, which should be the case. Moreover, it is seen that the power spectrum exhibits a (small) 'bump' at the frequencies around $f_e = 0.65$Hz. This peak, however, is not the result of the wave-induced bending moment but reflects the energy due to vibrations of the ship's hull as a consequence of springing. The observation is in good agreement with the lowest eigenfrequency $f_{\text{eigen}} = 0.65$Hz of the ship's hull, see Nielsen (2003). In summary, in order to deal with only the energy as directly transferred by the waves, and hence to deal with the energy contained in the wave spectrum, a bandpass filter can be applied to the response signals.

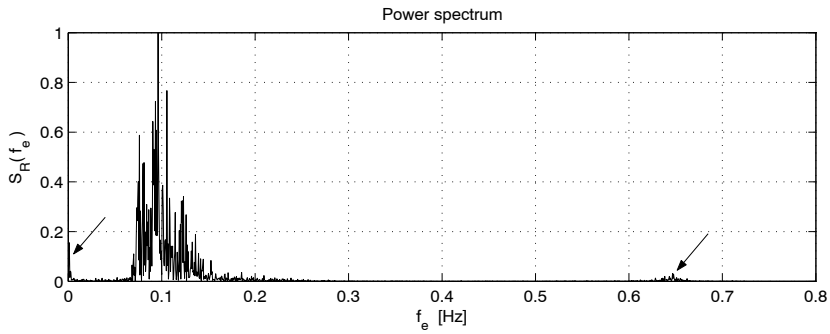

Figure 6.4: *Low and high frequency energies due to noise and springing, respectively, are marked by arrows.*

In addition, when the signal is filtered, another implication is that outliers and/or non-physical values in the responses are discarded.

6.4.4 Cross Spectral Analysis

As seen previously, the cross spectral analysis is fundamental when wave spectra are estimated, cf. (3.3). For this reason Chapter 5 was devoted to the cross spectral analysis and how to facilitate it by use of multivariate autoregressive modelling and, therefore, the topic is not treated as such in this section. However, as some of the preliminary studies performed on

the estimation of wave spectra involved a cross spectral analysis from the FFT, the method based on FFT is to be described very briefly.

A spectrum of the response energy can be obtained by conducting an ordinary FFT on the time signal of the response. This yields, however, a non-smooth graph of the spectrum, see e.g. Figure 6.4, and for further computations the necessity of a smooth spectrum is paramount. Hence, data windows and segmentation, see e.g. Press et al. (1992), have to be applied in order to smoothen the spectrum. In such cases, methods developed in the WAFO package at NTNU and Lund University can be applied, see Brodtkorb et al. (2000). Furthermore, MatLab has efficient procedures for the cross spectral analysis, cf. the routines `psd` and `csd`, e.g. Rabiner and Gold (1975) and Welch (1967).

6.5 Estimation of the Wave Height

Except being of interest in itself as a response signal to be used to estimate the wave spectrum, the acceleration signal may also be used to determine the ship's vertical motion, i.e. the displacement history relative to a fixed datum. Thus, in combination with the relative freeboard, an estimate of the actual wave height can be obtained without use of any transfer functions.

Before the specific routines are discussed it should be mentioned that as the complete time series - which are of relatively short duration - are already in hand, the methods developed here are somewhat simplified compared to the situation when new data continues to arrive. In the latter case modifications are needed, and procedures like recursive least squares, e.g. Strang (1986), could be applied.

6.5.1 Integration of Acceleration Signal

Although the double integration of the acceleration signal, in theory, is straightforward, practical problems arise due to the unknown initial conditions with respect to velocity and displacement. To overcome this problem, the acceleration signal is integrated twice with no concern about the initial conditions. Hence, the following expression for the displacement at time t_i is obtained

$$x_i = x_0 + v_0 t_i + \widetilde{x}_i \tag{6.1}$$

where $\widetilde{x}_i$ is the acceleration signal numerically integrated twice from $t = 0$ to $t = t_i$.

The evaluation of the conditions x_0 and v_0 is left. These conditions should not be confused with the true physical initial conditions. Instead, x_0 and v_0 can be interpreted as a translation and a rotation, respectively, of the double integrated acceleration signal. Basically, this

means that (6.1) expresses a kind of trend removal of the double integration, so that the root mean square value of the displacement is minimised.

The determination of x_0 and v_0 is obtained by minimising the square sum of (6.1) over K time steps

$$S = \sum_{i=1}^{K} (x_0 + v_0 t_i + \widetilde{x}_i)^2 \tag{6.2}$$

which leads to the equations

$$\frac{1}{2}\frac{\partial S}{\partial x_0} = \sum_{i=1}^{K} (x_0 + v_0 t_i + \widetilde{x}_i) = 0 \tag{6.3}$$

$$\frac{1}{2}\frac{\partial S}{\partial v_0} = \sum_{i=1}^{K} \left(x_0 t_i + v_0 t_i^2 + \widetilde{x}_i t_i\right) = 0 \tag{6.4}$$

These equations are transformed into a linear equation system in x_0 and v_0

$$\begin{bmatrix} K & \sum t_i \\ \sum t_i & \sum t_i^2 \end{bmatrix} \begin{bmatrix} x_0 \\ v_0 \end{bmatrix} = - \begin{bmatrix} \sum \widetilde{x}_i \\ \sum \widetilde{x}_i t_i \end{bmatrix} \tag{6.5}$$

The method above only in the overall global sense assures that the displacement has zero mean, whereas on a local scale the displacement history may have a mean value (much) different from zero, see Figure 6.5.

This phenomenon is resolved by fitting a piecewise linear interpolation to the data with the individual straight lines determined by a procedure similar to (6.2)-(6.5) with time intervals of the order of 100 sec. (approximately 10 periods). Subsequently, the final displacement history is found as the difference between the displacement from (6.1) and the linear interpolation, see Figure 6.5.

It may be argued that a better fit is obtained by fitting a cubic spline, since the kinks in the piecewise linear interpolation lead to infinite curvatures at the connection points. However, as manipulation with a cubic spline interpolation influences the acceleration, due to the second order derivative of a cubic spline being non-zero, the introduction of a cubic spline will raise another problem.

6.5.2 Determination of Wave Height

With knowledge of the displacement history of the accelerometer and the position of it, combined with the distance between the deck edge and the sea surface measured as the relative freeboard, the wave elevation can be estimated. The calculation is straightforward,

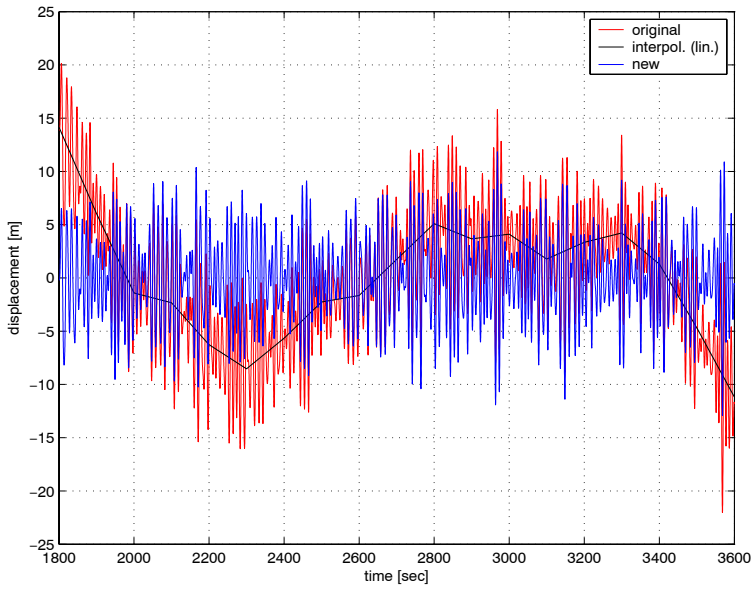

Figure 6.5: *Displacement history of data from* Nielsen (2003).

though it is paramount that the discrete times at which the displacement and the freeboard are evaluated are identical.

A practical problem for some freeboard measuring-sensors is that the signal in severe and rough seas may be 'saturated'. Thus, data drop-outs may occur when the distance between the measuring device and the water surface is less than a few metres. Unfortunately, 'saturation' may also happen due to sprays of water which is illustrated in Figures 6.6 and 6.7, with data from Nielsen (2003). Hence, in some situations, the signal of the (relative) wave height may be very erratic, or the signal may, as mentioned, suffer from actual data drop-outs.

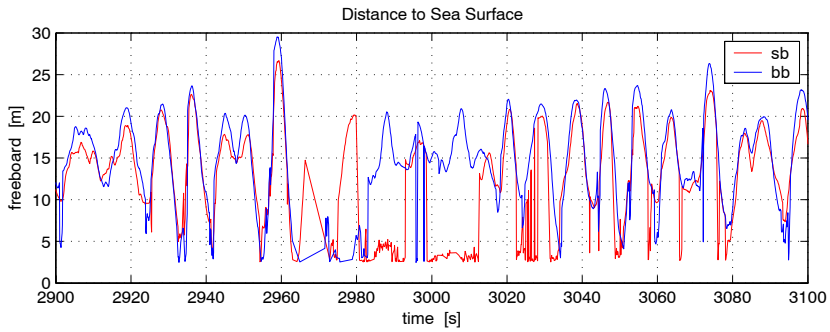

Figure 6.6: *'Saturation' of the signal.* 'sb' *denotes starboard and* 'bb' *denotes port.*

Problems of this nature, related to the specific measuring device, may be resolved by use of other types of devices. For example, in an Italian project, see Bollero et al. (2004), the relative freeboard is measured by measuring the hydrostatic pressure in specific positions on

Figure 6.7: *Wave impact with major spray.*

the hull. It should, however, be noted that independently of the type of measuring device, other types of physical phenomena, such as bottom emergence, may lead to data drop-outs. Therefore, for a thorough treatment in the study of algorithms for determination of the wave height, some kind of reconstruction algorithm should be imposed to treat the data for drop-outs. In the Ship Structure Committee report Atwater (1990), on the development of a shipboard wave height sensor, this matter is dealt with in detail.

6.6 Complex-valued Transfer Functions

As seen from (3.3), listed again for the sake of clarity

$$S_{ij}(\omega_e) = \int_{-\pi}^{\pi} \Phi_i(\omega_e, \beta)\, \overline{\Phi_j(\omega_e, \beta)} E(\omega_e, \beta)\, d\beta \tag{6.6}$$

the theoretical foundation for the estimation of a wave spectrum $E(\omega_e, \beta)$ based on ship responses $S_{ij}(\omega_e)$ is given by the complex-valued transfer functions $\Phi_i(\omega_e, \beta)$. For this reason, reliable and accurate calculations of the transfer functions for the considered ship are needed. This section discusses how to obtain the transfer functions and how to include them in the wave spectrum estimation.

Linear frequency domain strip theory, like that based on the theory by Salvesen et al. (1970), is a computationally efficient method to obtain transfer functions, and a vast number of investigations have proved its reliability, see for instance the Proceedings of the 18th International

Towing Tank Conference ITT (1987), Hutchison (1990), and Folsø (2004). However, with the increase in computer power, more advanced theories in the form of three-dimensional time domain codes are also applicable. Moreover, it should be mentioned that the transfer functions may be derived by measurements.

When actual decision support systems for specific ships are dealt with, all complex-valued transfer functions may be calculated in advance for a range of discretised encounter angles and appropriate intervals of other operational parameters. Hence, by multidimensional interpolation, estimates of the complex transfer functions can be quickly obtained, see Figure 6.8.

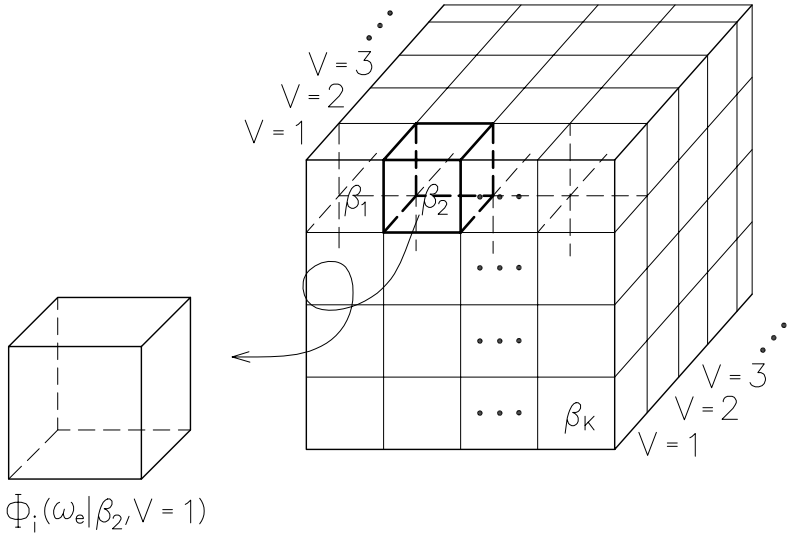

Figure 6.8: *The transfer functions may be obtained by interpolation in a test array. Here this is illustrated with the ship speed as the only operational parameter in addition to the encounter angle. In practice, more operational parameters will exist.*

It is worth to mention that if a ship in its operational use is known to have a large interval on each of its operational parameters which disfavours – for some reason – multidimensional interpolation, semi-analytical, so-called, closed-form expressions, Jensen et al. (2004), can be used instead. Thus, fast predictions can be made of the responses for the exact operational conditions.

In the wave spectrum estimations in the present study, the complex-valued transfer functions are calculated from linear frequency domain strip theory or a 3-D time domain code, depending on the ship being studied. In all cases, however, the transfer functions are calculated in advance and, subsequently, multidimensional interpolation in test arrays, as shown in Figure 6.8, is used when the estimation of the wave spectrum is conducted. As regards the interpolation in the transfer functions or, in general, in complex vectors, it is important to realise, as pointed out by among others Aschim (2002), that direct interpolation in the

real and imaginary part may typically cause errors close to the natural periods. Therefore, the appropriate practice is to perform the interpolation in the absolute values $|\Phi|$ and phases ψ of the complex transfer functions

$$|\Phi| = \sqrt{\mathrm{Re}\,(\Phi)^2 + \mathrm{Im}\,(\Phi)^2} \tag{6.7}$$

$$\psi = \tan^{-1}\left(\frac{\mathrm{Im}\,(\Phi)}{\mathrm{Re}\,(\Phi)}\right) \tag{6.8}$$

Hence, when the interpolated values are obtained, the complex transfer functions are reestablished by transforming back to complex numbers

$$\mathrm{Re}\,(\Phi) = |\Phi|\cos(\psi) \tag{6.9}$$

$$\mathrm{Im}\,(\Phi) = |\Phi|\sin(\psi) \tag{6.10}$$

This page is intentionally left blank.

Chapter 7

Numerical Test Cases

7.1 Introduction

In order to test the Bayesian estimation procedure, simulated stationary stochastic time series of different ship responses can be generated on the basis of a known one-dimensional wave spectrum. Thus, it is possible to check the program code for many kinds of errors and to some extent also the applicability and correctness of the Bayesian estimation. In the following, it is outlined how the generation of a stochastic time series for an arbitrary ship response can be performed, and then, succeedingly, estimations are calculated.

It should be mentioned that the generated time series correspond to a specific heading between the ship and the waves, as a one-dimensional wave spectrum is considered. Thus, the estimations carried out for the generated time series contain no information about wave directionality. However, in the final section in the present chapter, the generated time series are treated as though they stem from a directional wave field, which means that a directional wave spectrum is sought to be determined.

7.2 Simulation of Time Series

It is assumed that some specific ship is under investigation, and a general ship response R is considered. On the basis of a hydrodynamic computation (strip theory, three-dimensional hydrodynamic computation, measurements, etc.), the complex transfer function, $\Phi_R(\omega_e, \beta)$, as a function of the encounter frequency and the encounter angle can be obtained for given operational parameters. Hence, for a given heading and speed, a stochastic time series for the response R can be calculated as, see e.g. Denis and Pierson (1953)

$$R(t) = \sum_{i=1}^{N} a_i \left|\Phi_R(\omega_{e,i})\right| \cos\left(\omega_{e,i} t + \varepsilon_i\right) \tag{7.1}$$

where N represents the number of discretised encounter frequencies (which should theoretically be infinity), ε_i is a stochastic variable so that $0 < \varepsilon_i \leq 2\pi$, and the wave amplitude a_i is calculated from

$$a_i = \sqrt{2E\left(\omega_{0,i}\right)\Delta\omega_0} \tag{7.2}$$

Here $\omega_{0,i}$ denotes the wave frequency for the corresponding encounter frequency, or vice versa, while $\Delta\omega_0$ is the step length in the sequence of wave frequencies. $E\left(\omega_{0,i}\right)$ is the wave spectrum which will also be a function of among other things the significant wave height, H_s, and the zero-upcrossing period, T_z.

As regards (7.1), it should be noted that for an equidistant frequency discretisation, the signal $R\left(t\right)$ will repeat itself after a period of $\frac{2\pi}{\Delta\omega_0}$. Thus, in order to avoid this problem, the frequency discretisation is taken to be non-equidistant,

$$\omega_{i+1} = \omega_i + c \cdot p_i \tag{7.3}$$

with c as an 'appropriately' small factor while p_i denotes a stochastic variable with values between 0 and 1.

7.3 One-dimensional Estimations

In the tests carried out, time series have been simulated for the research and training ship the Shioji-Maru, see Table 7.1, which belongs to the Tokyo University of Marine Science and Technology.

Table 7.1: *Principal particulars of the Shioji-Maru.*

Length, L_{pp}	46.00 m
Breadth, B_{mld}	10.00 m
Draught, T	2.65 m
Displacement	659.4 t

Until now both the wave and the encounter frequencies have been expressed in terms of the angular frequency $\omega = 2\pi f$. However, in practical computations it is often more convenient to use the frequency f, and from now on the wave and the encounter frequencies will be given as f_0 and f_e, respectively.

Below, a case will be studied corresponding to quartering sea ($\beta = 60$ deg.), e.g. Figure 3.2. Thus, for a ship speed of 8.5 knots, the problem of three wave frequencies for the corresponding encounter frequency takes place for $f_e < 0.18$Hz, cf. (3.4) and (3.5). Hence, it is a good example to test how the Bayesian method handles the triple-valued function

problem. For information, Appendix D contains two similar examples for bow sea where the true wave spectrum has both one and two peaks.

In the Bayesian estimation three responses form the basis. The responses to be considered are the ship motions heave, pitch, and roll. It should be noted that the waves are assumed to be long-crested, and the wave spectrum used for the time series generation is taken to be a special case of the generalised JONSWAP spectrum, namely a Pierson Moskowitz (PM) spectrum, see for instance Jensen et al. (2004), with the following parameters

$$\begin{aligned} H_s &= 2 \text{ m} \\ T_z &= 8 \text{ sec.} \end{aligned} \tag{7.4}$$

As a consequence of the one-dimensional wave spectrum, directionality of the waves is not considered in the tests. Hence, what is to be obtained from the tests is a direct comparison of the energy distribution with frequency between the wave spectrum as estimated from the Bayesian procedure and the true PM wave spectrum, characterised by the parameters in (7.4).

7.3.1 Quartering Sea

In Figures 7.1 and 7.2 the amplitude of the frequency response functions, i.e. $|\Phi_R(f_{e,i})|$, and the corresponding time series for heave, pitch, and roll are shown. As seen from Figure 7.2 an hour of time has been simulated, and in the Bayesian estimation all data of that period is used. It should be noted that in reality, that is, for full-scale data, 60 minutes of acquisition time should not be considered, since the operational conditions are hardly constant within a period of this length.

As a comment on the complex transfer functions, $\Phi_R(f_{e,i})$, it can be mentioned that these are calculated by the New Strip Method, Strip-calculations (2004). For a detailed analysis of the frequency response functions reference is made to Appendix A, where the amplitudes of the transfer functions are depicted for a range of encounter angles and speeds.

The Bayesian estimation method yields the wave spectrum, which is found as the optimal solution of the equation system (3.61), for the minimum value of ABIC, cf. (3.69). In Figure 7.3 the ABIC values are plotted as function of the natural logarithm of the hyperparameter u. From the figure it is seen that ABIC draws a downward convex curve, which attains a minimum of -1591 at $\ln u = -2.42$ corresponding to $u = 0.089$. Thus, the estimated wave spectrum assumes the form shown in Figure 7.4, where, for comparison, the true Pierson Moskowitz spectrum is depicted as well. In the figure the red curve is the true Pierson Moskowitz spectrum and the blue graph is the estimated wave spectrum as obtained from the Bayesian estimation. Based on the plots it can be concluded that the Bayesian estimation procedure is capable of producing the correct solution. Note that the spectra are plotted as function of the wave frequency f_0.

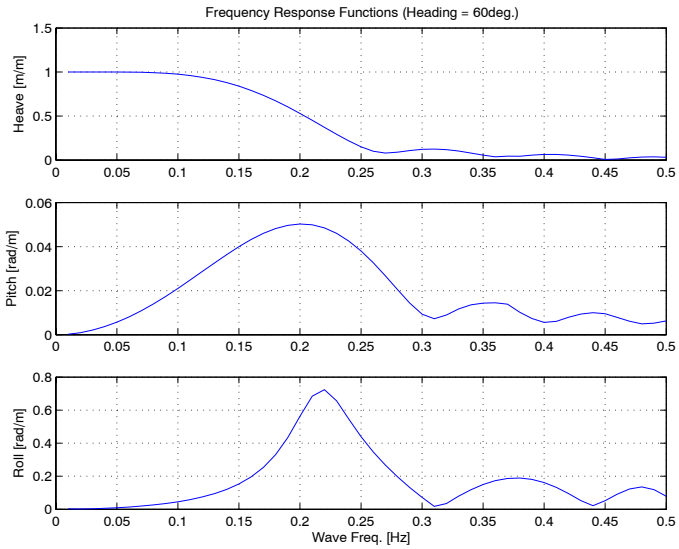

Figure 7.1: *Amplitudes of the frequency response functions for heave pitch, and roll. The ship speed is 8.5 knots.*

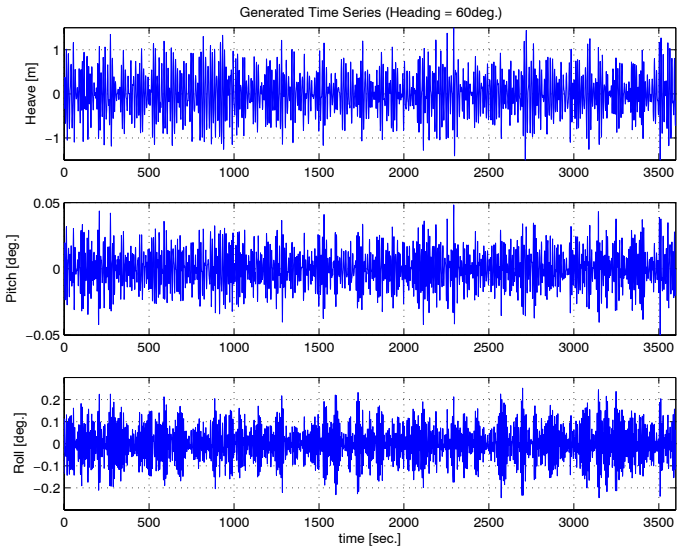

Figure 7.2: *The time series of the responses, which form the basis of the Bayesian estimation.*

As seen from the comparison between the two graphs in Figure 7.4, very good agreement exists. This is, indeed, reflected in the value of the significant wave height, which is found from the area under the spectrum as, e.g. Jensen (2001)

$$H_s = 4\left(\int E\left(f_0\right) df_0\right)^{\frac{1}{2}} \tag{7.5}$$

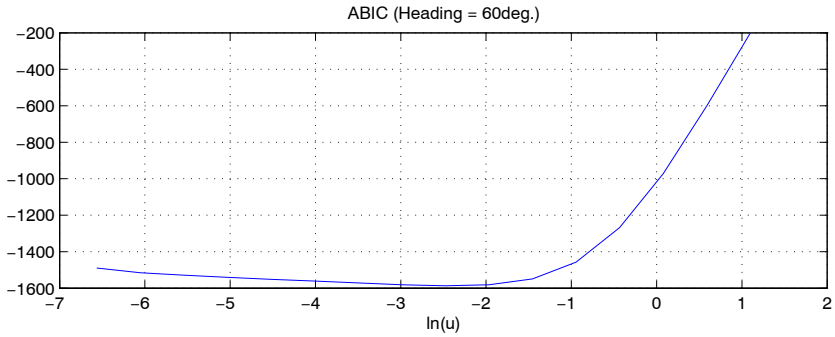

Figure 7.3: *ABIC as function of the hyperparameter.*

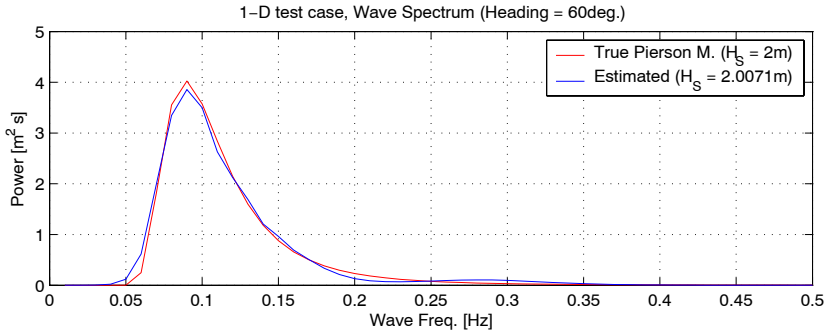

Figure 7.4: *The true and estimated wave spectra for quartering sea. Note that the spectrum is given as function of the wave frequency.*

Thus, the relative deviation in the significant wave height for the two cases amounts to 0.4%, see the legend of Figure 7.4.

In Figure 7.5 the estimated wave spectrum is plotted for different values of the hyperparameter. From this figure it is seen that, especially for the lowest value of u, the solution approximates the wave spectrum badly. Thus, the figure shows the significance of the hyperparameter since for the lowest value of u, the smoothness of the solution is completely lacking. The legend 'optimal' corresponds to the minimum of ABIC for $u = 0.089$, and the three comparative cases are, in decreasing order, $u = 3.00$, $u = 1.08$, and $u = 0.01$.

As a consequence of the very good estimation of the wave spectrum for the optimal value of the hyperparameter, the estimated response spectra are also very close to the 'measured' ones, that is, the generated response spectra. The comparisons are seen in Figure 7.6. It should be noted that these spectra are shown as function of the encounter frequency f_e.

As regards the calculation of the estimated response spectra, this is done by multiplying the coefficient matrix, $\mathbf{A}$, with the estimated wave spectrum, $\mathbf{f}(\mathbf{x}_{\text{estim}})$, suggested by the

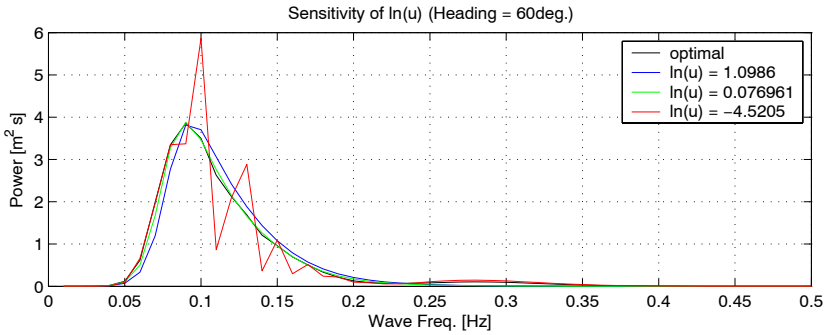

Figure 7.5: *The estimated wave spectrum for different values of the hyperparameter.*

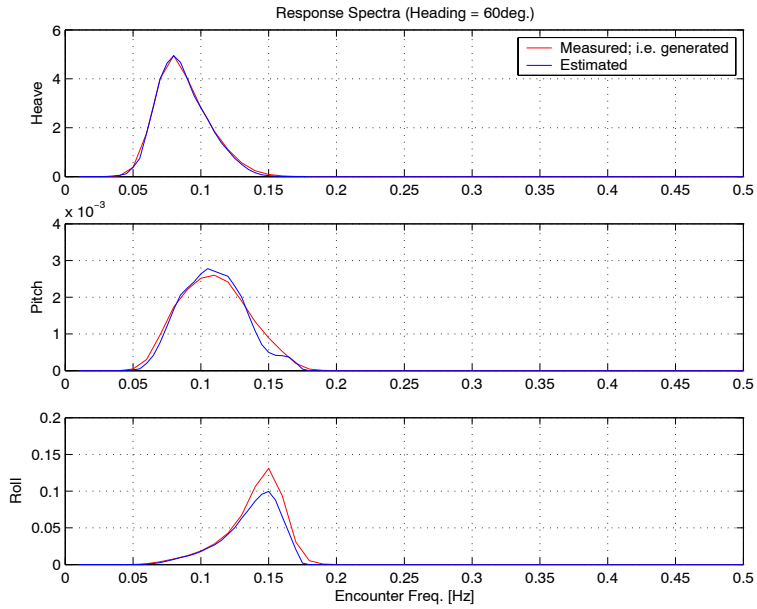

Figure 7.6: *Comparison of the generated and estimated response spectra. Note that the spectra are depicted as function of the encounter frequency. Units:* Heave [m^2s], Pitch [rad^2s], Roll [rad^2s]

multivariate model, however, without taking into account the white noise, cf. (3.28)

$$\mathbf{b}_{\text{estim}} = \mathbf{A}\mathbf{f}\left(\mathbf{x}_{\text{estim}}\right) \tag{7.6}$$

Hence, the true wave frequency is properly re-transformed into the encounter frequency through the triple-valued function problem.

In general, even for the same ship course and speed, i.e. the same coefficient matrix $\mathbf{A}$, it should be noted that since the estimated wave spectrum is found to be the optimal solution of the minimisation of (cf. (3.61))

$$S\left(\mathbf{x}\right) = \left\|\mathbf{A}\mathbf{f}\left(\mathbf{x}_{\text{estim}}\right) - \mathbf{b}_{\text{measured}}\right\|^2 + u^2 \left\|\mathbf{D}\mathbf{x}_{\text{estim}} - \mathbf{c}\right\|^2 \tag{7.7}$$

a perfect agreement cannot be expected between $\mathbf{b}_{\text{estim}}$ and $\mathbf{b}_{\text{measured}}$. Moreover, in practical applications of decision support systems, it would be of minor interest to estimate the already measured response spectra. Instead, the estimation of the response spectra is important in case the ship course and/or speed are changed on the assumption that the estimated wave spectrum is valid forward in time of, say, half an hour. However, in the present example, with knowledge of the true wave spectrum, it makes sense only to compare this wave spectrum with the estimated one, and, in the case of good agreement between the two, see how well the measured (i.e. generated) response spectra are approximated by carrying out the calculation as stated in (7.6).

7.4 Directional Estimations

The generated time series are now treated as though they stem from full-scale measurements. This means that no assumptions/choices are made in relation to the encounter angle between the ship and the waves and, thus, the entire directional area (0-360 deg.) is considered in the estimation. Hence, a completely directional wave spectrum is to be estimated even though the generated time series correspond to waves propagating from one specific direction, which theoretically corresponds to the energy in the wave spectrum being concentrated on a radial line in a polar plot with (f_0, β) as the polar coordinates, cf. Figure 7.7.

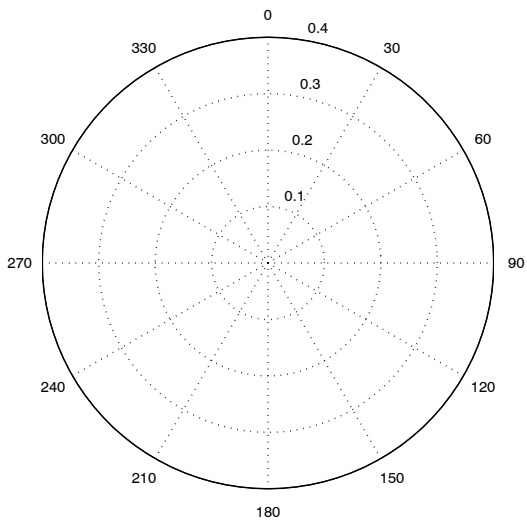

Figure 7.7: *The polar plot used for visualisation of the directional wave spectrum as a function of* (f_0, β).

Below, four cases will be studied where each case is based on the PM spectrum with $H_s = 2$ m and $T_z = 8$ sec., as dealt with above. The only difference between the four cases is that for the time series generation, four different encounter angles are used: 1) 180 deg., 2) 150 deg., 3) 90 deg., and 4) 60 deg. In each case the ship is assumed to be on a route straight

west, for which reason the absolute wave directions, relative to the north, are as listed in Table 7.2. It should be noted that the directions are given for approaching waves.

Table 7.2: *The encounter angle and the corresponding absolute wave direction used for the generation of the time series.*

Case	Enc. angle	Abs. wave dir.
1	180 deg.	270 deg.
2	150 deg.	300 deg.
3	90 deg.	0 deg.
4	60 deg.	30 deg.

In Figures 7.8 and 7.9 the directional estimations and the integrated frequency spectra, respectively, are shown for the four cases, and in Table 7.3 the important parameters for the estimated wave spectra are noted. As regards the zero-upcrossing period T_z, this is found from the spectral moments

$$T_z = \sqrt{\frac{m_0}{m_2}} \tag{7.8}$$

with

$$m_n = \int_0^\infty f_0^n \int_{-\pi}^{\pi} E\left(f_0, \beta\right) d\beta df_0 \tag{7.9}$$

Table 7.3: *Estimated wave parameters.*

Case	Wave direction	H_s	T_z
1	270 deg.	2.2 m	8.0 sec.
2	300 deg.	1.9 m	8.1 sec.
3	0 deg.	2.2 m	9.0 sec.
4	30 deg.	2.0 m	8.1 sec.

As seen from Figure 7.8 and Table 7.3, the Bayesian estimation captures the overall wave parameters including the wave direction with high accuracy. Thus, from the polar plots, the directional distribution seems to be in good agreement with the true absolute wave direction as listed in Table 7.2. However, it is noted that a perfect symmetric shape of the directional spectra is not observed in any of the cases. In this connection it should be realised that the wave spectrum distributes, or spreads, the energy around the mean wave direction due to the prior distributions, which secure a smooth change in direction as well as in frequency. To study the agreement between the estimated wave spectra and the true PM spectrum in more detail, Figure 7.9 is useful. From this figure it is seen that, although not as good as in

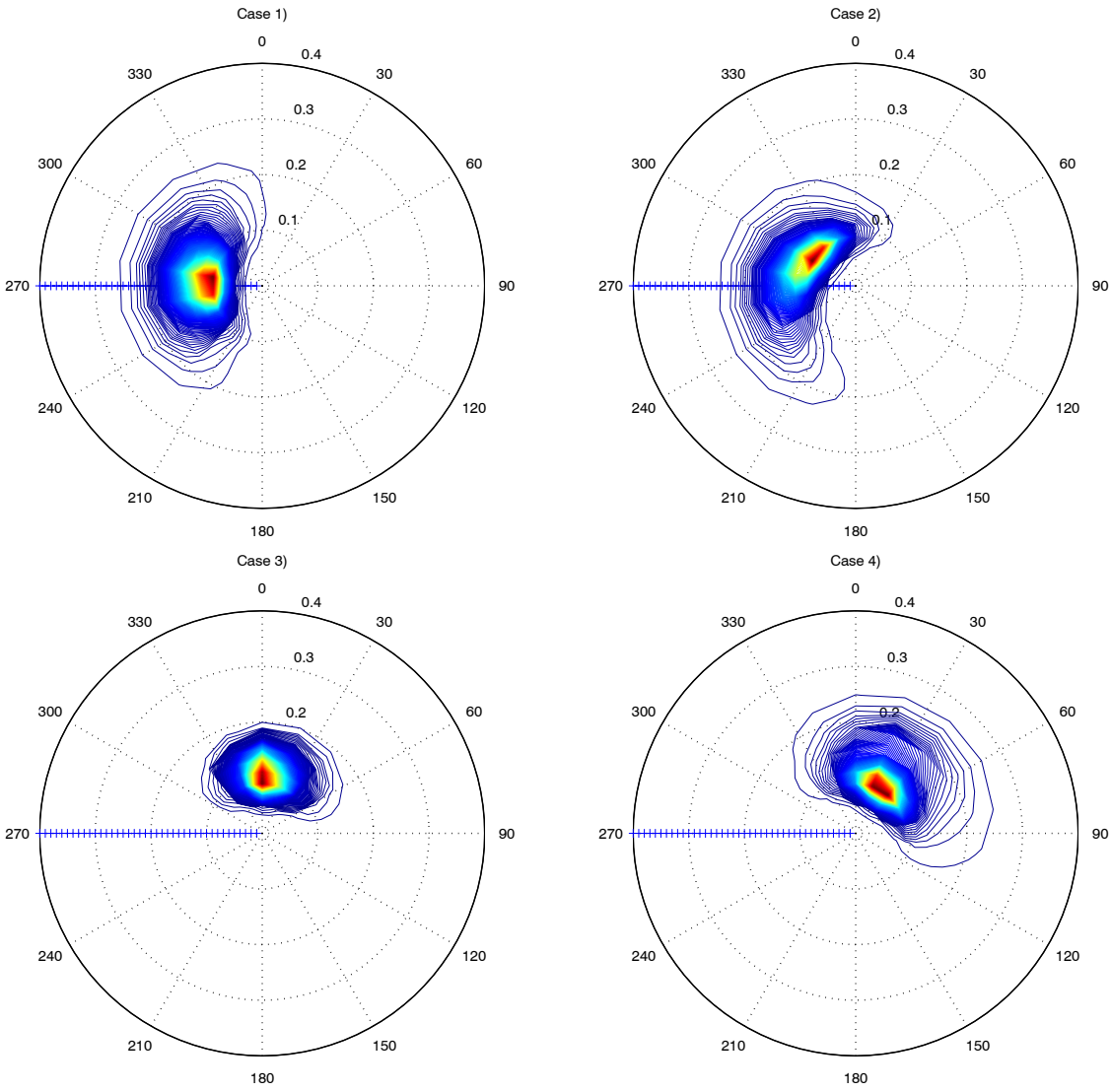

Figure 7.8: *Estimation of directional wave spectra for the four cases.*

the one-dimensional case, Section 7.3, the Bayesian method is again capable of estimating the true wave spectrum.

7.4.1 Frequency Insensitivity

To close on the numerical simulations, it is interesting to note that the less sensitivity to low- and high-frequency excitations is reflected when numerical simulations are studied. This is illustrated in Figure 7.10 which shows the errors on the wave parameters as function of the zero-upcrossing period. Thus, for each T_z-value, ship motions have been simulated for an

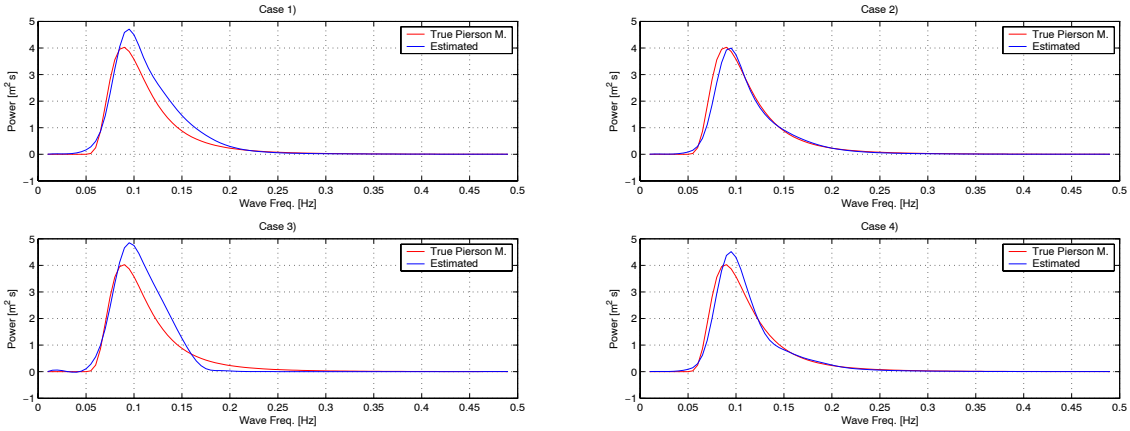

Figure 7.9: *The integrated 1-D frequency spectra for the four cases.*

encounter angle equal 60 deg. and a significant wave height of 2 m. Subsequently, the wave spectrum and the corresponding wave parameters have been estimated, as done above, and then depicted versus the zero-upcrossing period. From Figure 7.10 it is evidently seen that there is a loss of accuracy for small and large wave periods, which is explained by the fact that the ship responds little to such waves. Similar examples with the same overall results, however with the emphasis on a parametric estimation procedure, are seen in Tannuri et al. (2003).

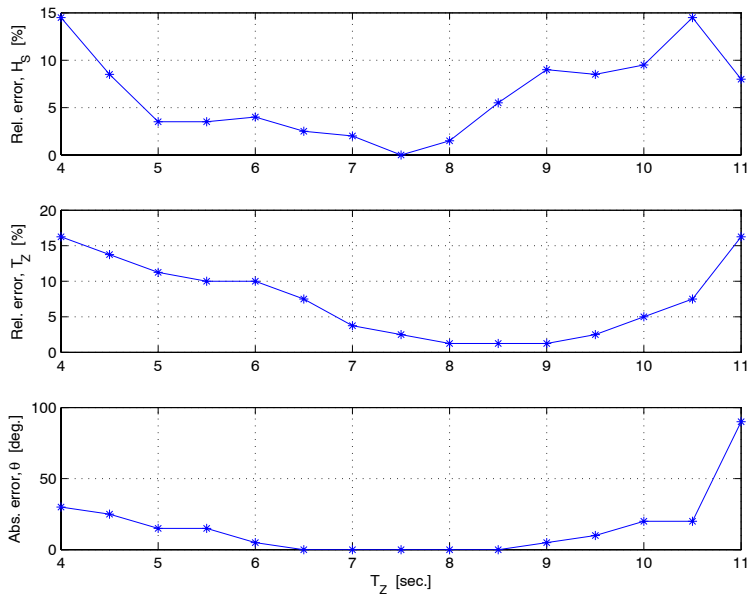

Figure 7.10: *Maximum estimation errors on characteristic wave parameters as function of the zero-upcrossing period.* $H_s = 2\text{m}$ *and* $\beta = 60\text{deg.}$ *are used in the generation of the time series.*

7.5 Conclusions

Based on simulated global ship responses, examples have shown that the Bayesian estimation with a high rate of success can predict the underlying wave spectrum used for the generation of the responses. In one example, a Pierson Moskowitz spectrum was analysed with success, and as seen from Appendix D a wave spectrum with two peaks can be estimated as well. Moreover, generated time series, based on a one-dimensional wave spectrum, were treated as though they stemmed from a directional wave field. Also in these cases the Bayesian estimation gave not only the correct integrated one-dimensional frequency spectrum, but also the correct absolute wave direction.

All in all, the Bayesian estimation method has proved to be capable of estimating directional wave spectra. However, it is important to realise that in numerical examples a perfect relationship exists between the measured responses and the transfer functions, that is, the 'measured' responses are generated by utilisation of the transfer functions. Furthermore, due to the latter, linearity is assured as well and in numerical examples no unknown kinds of noise phenomena are present. For full-scale data a similar good agreement between the true existing wave spectrum and the estimated spectrum cannot be expected. Another problem is that information on the absolute true wave spectrum is difficult to obtain. Thus, comparisons have to be made with other kinds of estimations and/or visual observations. In the next two chapters some of these problems will be treated as full-scale data is to be studied.

This page is intentionally left blank.

Chapter 8

Full-Scale Data - Comparisons with Visual Observations

8.1 Introduction

From a series of full-scale trials, Shioji-Maru (2004), conducted with the research and training ship the Shioji-Maru, cf. Table 7.1, full-scale data now forms the basis of the Bayesian estimation. The measurement conditions are summarised in Table 8.1 and, as seen, four sets of data are analysed. The wave direction applies to approaching waves and is given relative to the north. In Figure 8.1 the trajectory of the ship is shown, and it should be noted that each set of data corresponds to a certain course.

Table 8.1: *Measurement conditions.*

Data	Course	Speed	Wave dir.	Wave height	Wave period
A	270 deg.	8.5 knots	235 deg.	1.6 m	7 sec.
B	60 deg.	9.5 knots	250 deg.	1.3 m	7 sec.
C	220 deg.	7.0 knots	220 deg.	1.8 m	7 sec.
D	90 deg.	8.5 knots	240 deg.	1.3 m	7 sec.

In the Bayesian estimation the data sets are considered one at a time, and specifically the data consists of three measured ship responses: the pitch and the roll motions, and the vertical acceleration at FP. In Figure 8.2 the amplitude of the frequency response functions are plotted in polar format, both as function of the wave frequency and of the relative wave encounter angle. In the plots, the radial line at 180 deg. corresponds to the case of head waves. It should also be noted that all the plots apply to a speed of 8.5 knots. However, little variation is seen for the other speeds as given in Table 8.1. For a detailed inspection of the frequency response functions reference is made to Appendix A. It should be noticed that

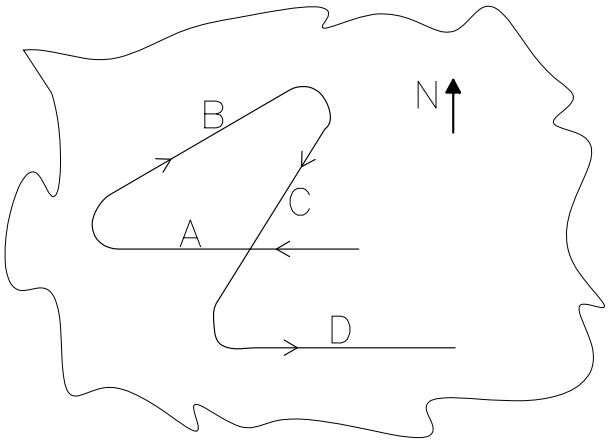

Figure 8.1: *Trajectory of the Shioji-Maru.*

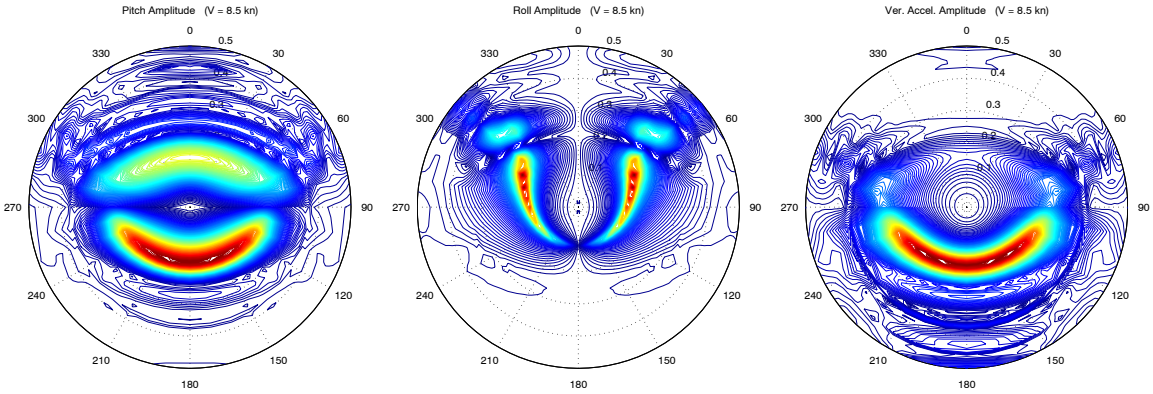

a) b) c)

Figure 8.2: *The amplitudes of the frequency response functions of the Shioji-Maru depicted in polar plots.* a) *pitch,* b) *roll, and* c) *vertical acceleration at FP; all shown for* $V = 8.5$ *knots. 180 deg. is head waves.*

the author himself has not carried out the calculations of the frequency response functions, for which reason sensitivity analyses of the functions have not been conducted.

The recorded time series have a duration of six minutes in each set of data, and Figure 8.3 illustrates an example of the time series for the three responses. In Section B.2 of Appendix B all the time series are visualised for the four data sets which are analysed. Moreover, it should be noted that the cross spectral analysis is carried out by use of the stepwise least squares algorithm, cf. Section 5.7, and the optimal order is determined according to the multiple final prediction error ($MFPE$) described in Section 5.5.

As a general comment on the recorded data, the measurements took place in Tateyama Bay, which is located on the inside of the mouth of Tokyo Bay, Japan, sheltered from the Pacific

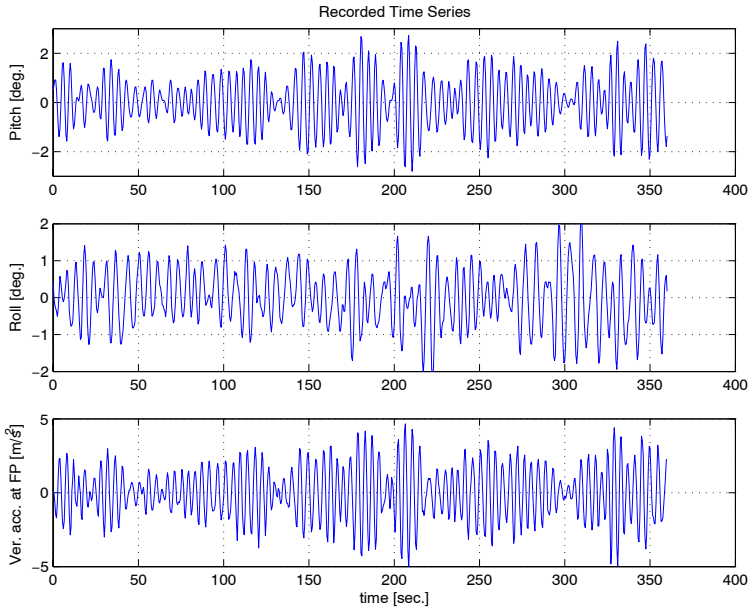

Figure 8.3: *Three responses, pitch, roll, and vertical acceleration at FP, form the basis of the Bayesian estimation.*

Ocean. Thus, the experimental area is primarily influenced by wind waves with a little fetch.

8.2 Bayesian Estimation

In the following, the directional wave spectrum is estimated for each set of data characterised by the measurement conditions given in Table 8.1. Table 8.2 yields the results of the Bayesian estimations in respect of wave parameters and Figures 8.4 and 8.5 visualise the wave spectrum. In Table 8.2 the mean wave period T_s is calculated from the spectral moments, cf. (7.9)

$$T_s = \frac{m_0}{m_1} \tag{8.1}$$

As regards the wave direction listed in Table 8.2, 'Wave dir.' yields, similarly to Table 8.1, the values relative to the north, from which direction the waves are approaching. 'Wave dir.' is taken to be the direction of the main peak in the directional spectrum, i.e. the peak with most energy in its surrounding area. Thus, it is likely that the best agreement with the visually observed wave direction is found for this direction, which can be considered to be the dominant wave direction. On the other hand, an estimated mean wave direction, in the energy sense, can also be calculated. Hence, by defining, similarly to the spectral moments,

so-called directional moments, d_n

$$d_n = \int_{-\pi}^{\pi} \beta^n \int_0^{\infty} E\left(f_0, \beta\right) df_0 d\beta \tag{8.2}$$

the energy mean direction is given by

$$\frac{d_1}{d_0} \tag{8.3}$$

Table 8.2: *Estimated parameters.*

Data	Wave dir. (peak)	Energy mean dir.	H_s	T_s
A	250 deg.	245 deg.	1.0 m	5.9 sec.
B	220 deg.	190 deg.	0.8 m	7.5 sec.
C	235 deg.	230 deg.	1.0 m	6.0 sec.
D	235 deg.	200 deg.	0.7 m	8.2 sec.

8.2.1 Wave Parameters

From comparisons of the parameters in Tables 8.1 and 8.2 and by studying Figures 8.4 and 8.5, it is seen that with respect to the dominant wave direction, the Bayesian estimation yields results in reasonable agreement with the visual observations. Furthermore, the mean wave period is found from the estimation with a fair accuracy relative to the observations. On the other hand, the significant wave height is only estimated at values at about 60 percent of the visual observations for all the data sets. The latter fact suggests that the amount of energy in the estimations is too low, a fact which will be dealt with in more detail in the subsection below. It should be noted that 'the significant wave height', as such, is a mathematical definition and, hence, visual observations do not necessarily reflect this quantity. Moreover, making visual observations of wave heights, and sea state parameters in general, is by no means an easy task and, naturally, the observations contain a certain amount of uncertainty. More comments will be given below on wave heights and the energy in the responses. Furthermore, the very last subsection discusses the apparent fact that for Data B and D, the wave spectrum contains energy in a frequency-directional area not seen for Data A and C, cf. Figure 8.4.

8.2.2 Response Spectra

As regards the energy in the estimated ship responses, Figure 8.6 should be studied. In this figure comparisons of the measured and the estimated response spectra are seen, and

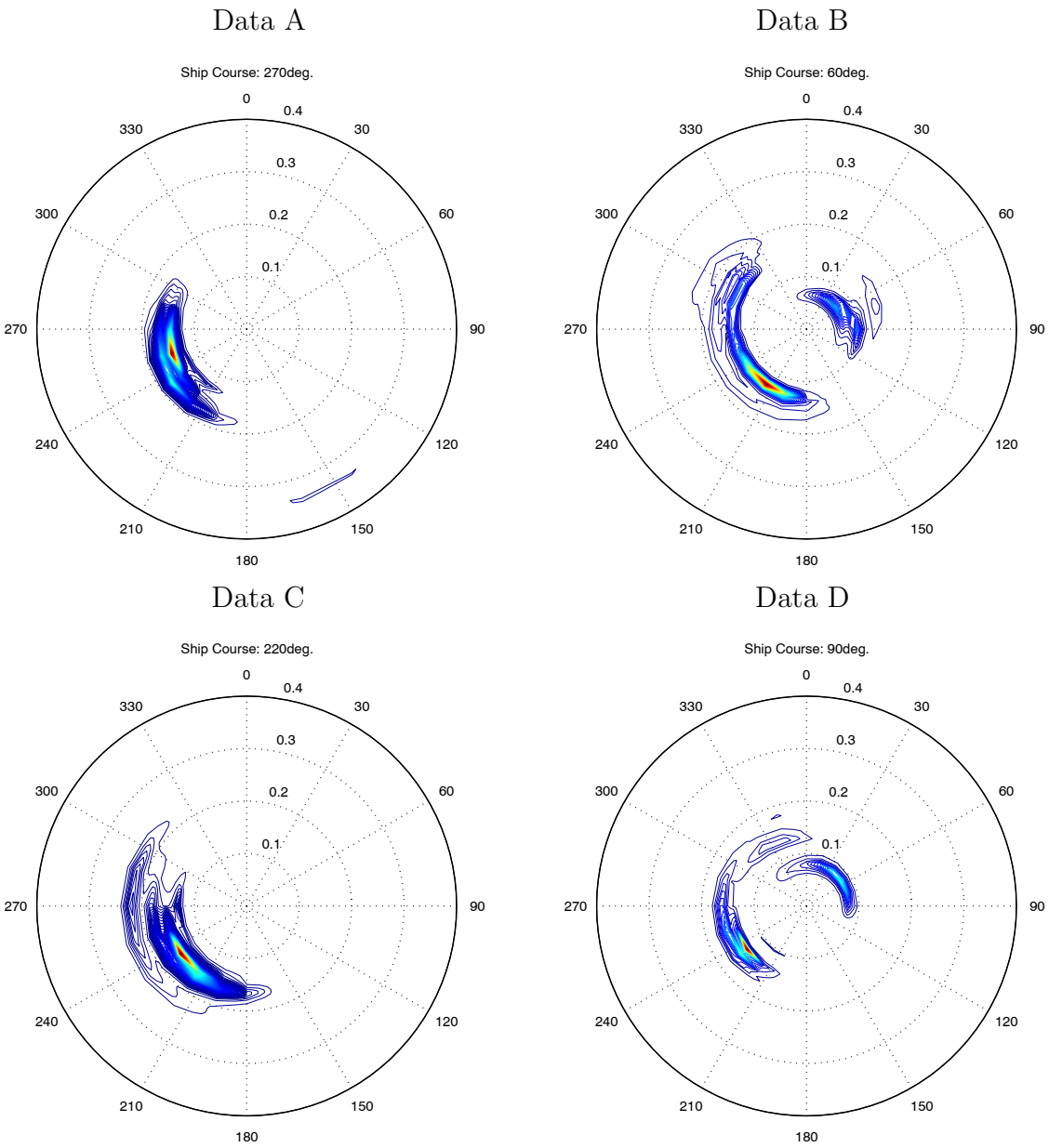

Figure 8.4: *The estimated directional wave spectra for the four data sets.*

notably the estimated response spectra for the vertical acceleration deviate from the measurements. In particular, this is illustrated in Table 8.3, which shows the relative deviation on the variance, calculated as the area of the individual response spectra, for the considered responses. That is, the relative deviation in percentage is given by

$$\mathrm{dev}_{Var} = \frac{\mathrm{Var}_{\mathrm{estimated}} - \mathrm{Var}_{\mathrm{measured}}}{\mathrm{Var}_{\mathrm{measured}}} \cdot 100\% \tag{8.4}$$

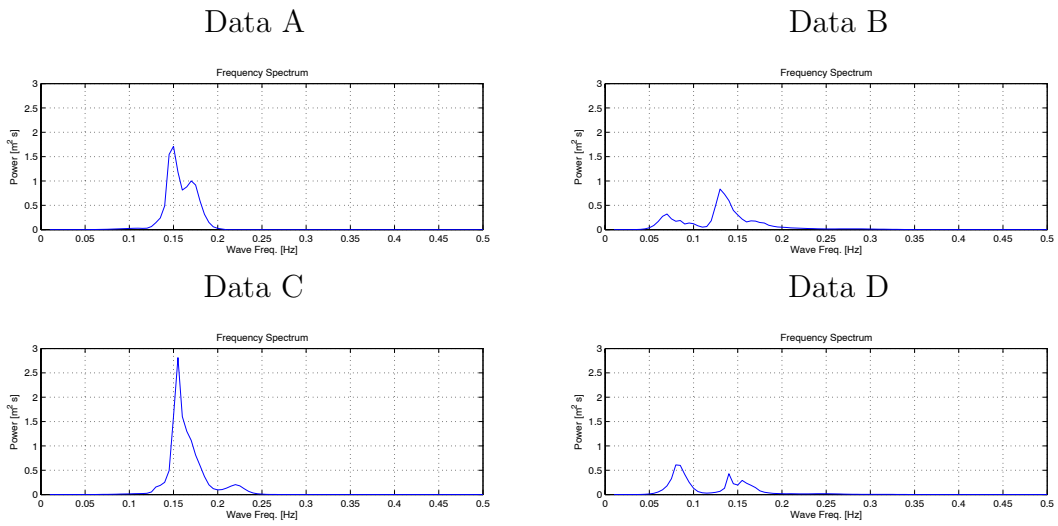

Figure 8.5: *Integrated 1-D wave spectra for the four data sets. Spectra seen as function of the wave frequency.*

In the table, the absolute values of the variances for the measured spectra, i.e. responses, are also listed. From the table it is seen that in all cases the variances of the vertical acceleration are approximately 50% less for the estimated spectra compared to the measured ones. For the pitch and the roll motions, on the contrary, there is no similar general trend. Thus, it is noted that for both of these responses, the variances of the estimated responses are in some cases larger, and in some cases smaller than the variances of the measured responses; without a unique relation between the cases.

Table 8.3: *Deviation on variance for the estimated responses. Figures relative to the measured absolute variances, which are also listed.*

	Pitch		Roll		Ver. Acc.	
Data	Dev.	Var. [rad^2]	Dev.	Var. [rad^2]	Dev.	Var. [(m/s^2)^2]
A	20%	$35 \cdot 10^{-5}$	2%	$1.9 \cdot 10^{-4}$	-51%	$350 \cdot 10^{-4}$
B	-38%	$9.6 \cdot 10^{-5}$	16%	$3.8 \cdot 10^{-4}$	-48%	$7.5 \cdot 10^{-4}$
C	23%	$42 \cdot 10^{-5}$	-3%	$2.9 \cdot 10^{-4}$	-49%	$370 \cdot 10^{-4}$
D	-15%	$4.3 \cdot 10^{-5}$	7%	$2.5 \cdot 10^{-4}$	-43%	$4.8 \cdot 10^{-4}$

With respect to the deviations between the measured and the estimated response spectra, it is important to remember the discussion on the way of calculating the estimated response spectra, cf. expression (7.6) and (7.7). Therefore, a perfect agreement is, in general, not expected when the measured spectra are compared with the estimated spectra. From the just presented full-scale data it can, however, be concluded that, compared to the simulated data studied previously, more noise interferes with the full-scale data, for which reason the

estimated response spectra approximate the measured spectra less well compared to what was the case for the simulated data in Chapter 7. Moreover, the better agreement for the

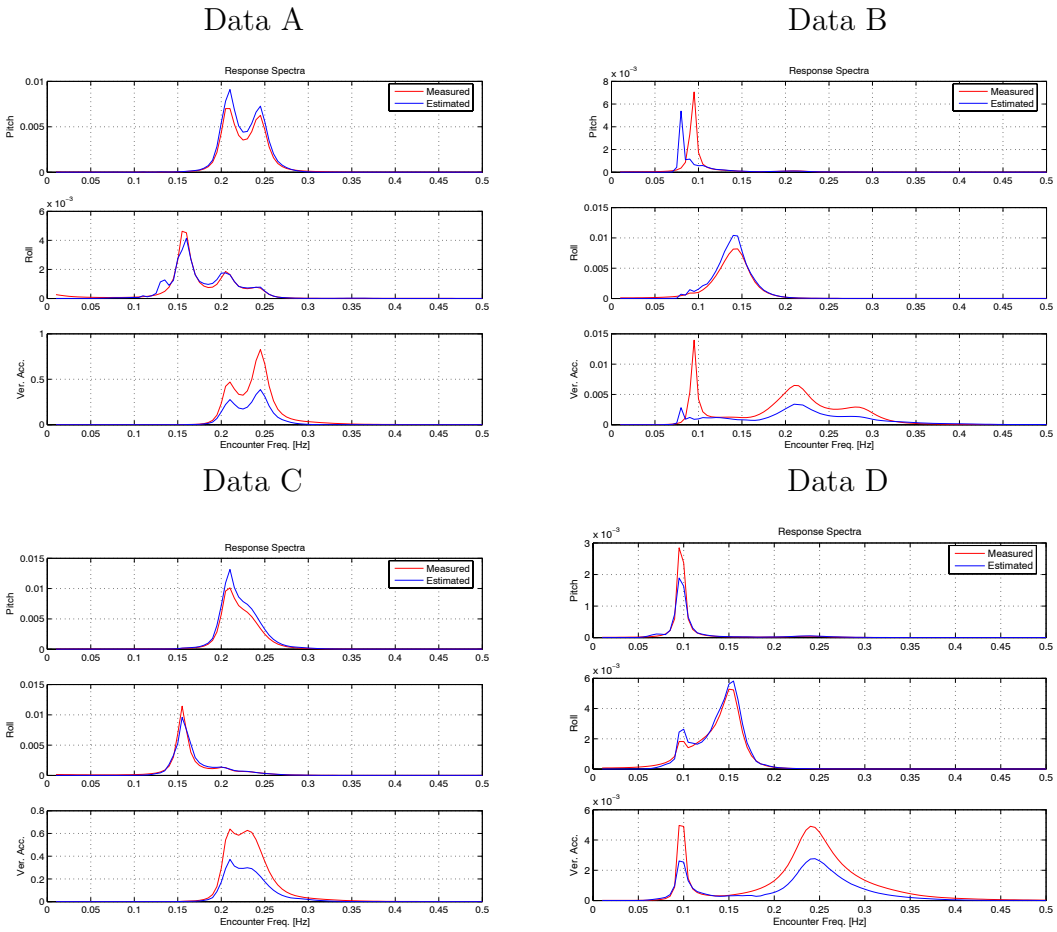

Figure 8.6: *Comparisons of measured and estimated response spectra for the four data sets, illustrated as function of the encounter frequency. Note the difference in scale. Units:* Pitch [rad^{2}s], Roll [rad^{2}s], Ver. Acc. [m^2/s^3]

simulated data can be explained by a perfect relation between the measured (generated) responses and the wave spectrum through the complex transfer functions. That is, the simulated data was generated *by using* the complex transfer functions, whereas for the full-scale data, the complex transfer functions *are assumed* to relate the responses with the wave spectrum. To return to the actual differences between the measured and the estimated response spectra for the just analysed full-scale data, a perfect agreement is, as mentioned, not expected for the individual response spectra. Instead, the Bayesian method is to give an agreement between the measured and the estimated response spectra that holds on average, that is, for one response the variance for the estimation may be smaller than that for the measured one, and vice versa for another response. Based on the numbers in Table 8.3, this is seen to be the case, although the smaller figures for the vertical acceleration appear to dominate slightly, relative to the other two responses. The reason for the response of

the vertical acceleration consistently being estimated to be too small could be that the transfer function for this response is too small compared to what it should be. Hence, on the assumption of this hypothesis and from a study of an example where the Bayesian estimation is only based on the vertical acceleration, it is expected to estimate a larger significant wave height compared to what is the case when all responses are taken into account. On the contrary, doing the Bayesian estimation with only, say, the pitch and the roll motions, an increase in the significant wave height is not expected. In Figure 8.7 the outcome of such examples is illustrated. The examples are based on Data A and in the figure, a) shows the results when the estimation is based on the pitch and the roll motions, respectively, and b) shows the outcome when only the vertical acceleration is taken into account. In the figure both the integrated frequency spectrum and the response spectra are plotted and, indeed, as

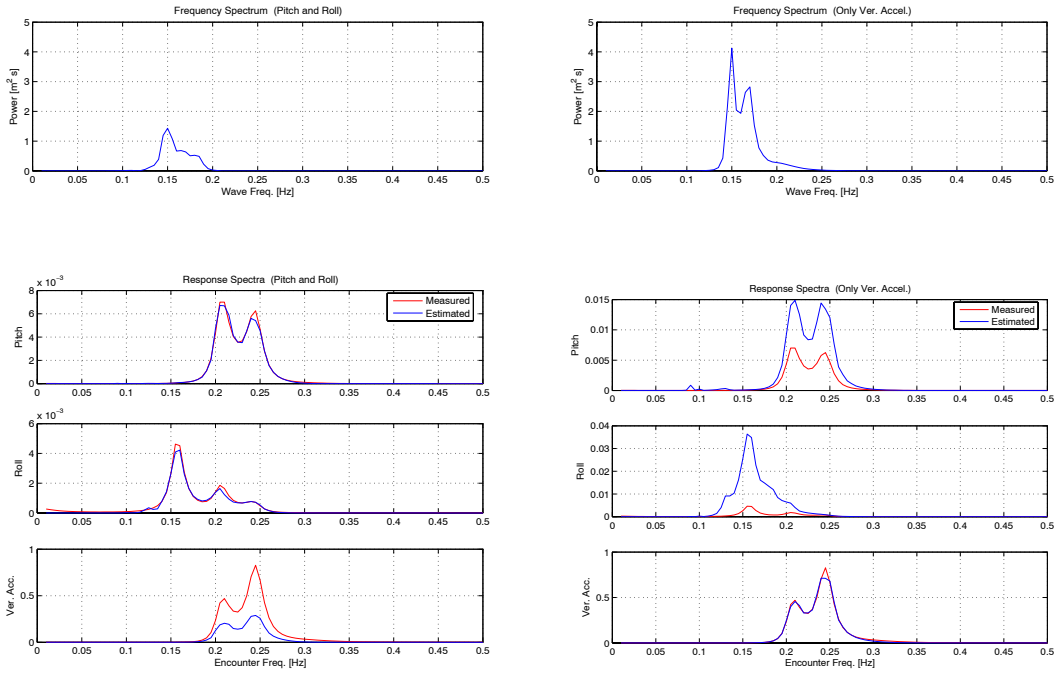

a) Based on pitch and roll b) Based on ver. acceleration

Figure 8.7: *Estimations taking into account two and one responses, respectively. Note the difference in scale for the response spectra for the two cases. Units:* Pitch [rad^{2}s], Roll [rad^{2}s], Ver. Acc. [m^2/s^3]

expected, the wave spectrum contains the most energy in case b). Related to the significant wave height, case a) and b) yield

$$\begin{aligned} H_s^{\text{a)}} &= 0.9 \text{ m} \\ H_s^{\text{b)}} &= 1.4 \text{ m} \end{aligned} \tag{8.5}$$

which confirms the expectation of the magnitude of the significant wave height, cf Table 8.2. Moreover, it is seen that the estimated response spectra for the pitch and the roll motions

almost exactly approximate the measured response spectra for these motions in case a), and similarly for the vertical acceleration in case b). Furthermore, it is noted that, when the estimation of the wave spectrum is based on either the pitch and the roll motion, or the vertical acceleration, the other response spectra are estimated to be less good compared to the situation with all the responses taken into account in the estimation, cf. Figure 8.6. However, due to the coupling between pitch and vertical acceleration, an estimation based on one of these motions also gives a reasonable estimate for the other, at least with the correct shape.

In summary of Figure 8.7 a) and b) it can - for the specific data - be argued that only one response is necessary to obtain reasonable results for the wave height and the integrated frequency spectrum. It is important, though, to note that as regards the directionality of the wave field, poor information is given when only one response is taken into account, which is seen in Figure 8.8. Especially, this is seen for port/starboard symmetric responses as is the

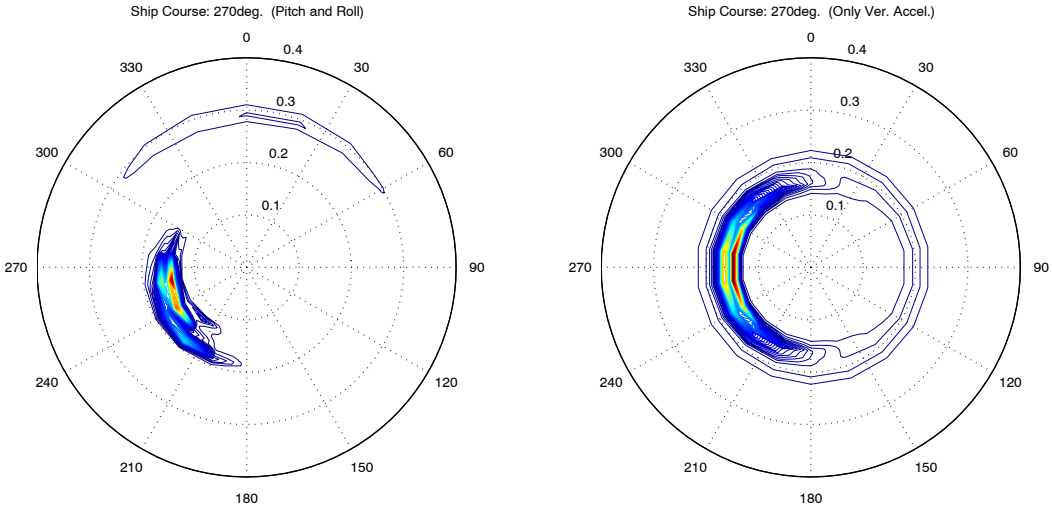

a) Based on pitch and roll b) Based on ver. acceleration

Figure 8.8: *Estimations taking into account two and one responses, respectively. Note the port/starboard symmetry for the estimation based on only the vertical acceleration at FP.*

case in Figure 8.8 b). In a more general perspective the examples illustrate the importance of reliable and accurate frequency response functions. Thus, the Bayesian estimation yields a solution that holds in the overall, or average, sense for the considered responses. Hence, three responses, with equally accurate transfer functions, are by all means optimal for the estimation. However, if the transfer function of one of the responses lacks accurateness compared to the measured signal, the estimation is not completely disturbed by this. Instead, the Bayesian method seeks an estimate of the wave spectrum that adapts the best possible way for all the considered responses; or in other words, the Bayesian method finds the solution that gives the best possible relation between all three (or how many it may be) measured responses and their corresponding frequency response functions. This is so on the assumption that the responses are weighted equally. On the other hand, it is seen that in

the extreme case, with two signals weighted by a factor of zero, i.e. the signals are not taken into account, the Bayesian estimation yields a solution which matches the measured non-zero weighted response almost 100%. This is the case even though the estimated wave spectrum is not believed to agree very well with the true wave spectrum, especially when directionality is also considered.

8.2.3 Following versus Head Waves

In the plots of the estimated directional wave spectra, see Figure 8.4, the ship course is inscribed on top of each plot. Hence, from these plots and Figure 8.1 of the trajectory, it is observed that data sets A and C correspond to bow and head waves, whereas in the case of data sets B and D, the ship experienced quartering and following waves. This is, as already mentioned, in good agreement with the visual observations listed in Table 8.1. However, it should be noted that in the case of quartering and following seas, i.e. data sets B and D, the estimated directional spectra appear quite different from the cases of bow and head sea, i.e. data sets A and C. Thus, it is observed that in the latter cases, the directional wave spectrum is fully adjoined with only one peak. Conversely, for data sets B and D the estimated directional wave spectrum exhibits two main peaks, and with the individual peaks completely separated from each other. An explanation for these differences is not straightforward when only taking into account the present examples/data. Therefore, whether it is the Bayesian estimation as such which is due to the dissimilarities, or if the dissimilarities can be explained from different physical conditions from data set to data set is difficult to say. However, in view of the fact that all the data sets, more or less, are recorded within the same area, cf. Figure 8.1, and the fact that each data set is recorded only a few minutes later than the preceding set, something suggests that the Bayesian estimation yields different results depending on the direction of the waves relative to the ship. If this is the case, a possible explanation may be sought in the fundamental relation, given by the complex-valued transfer functions, between the responses and the excitation. From a study of the frequency response functions for the considered responses, see Figure 8.2 and as well Appendix A, it is thus observed that in general, and in particular for following waves, the Shioji-Maru is little sensitive to the low-frequency excitations. Therefore, on the assumption that there really *is* wave energy concentrated in the area - that is, the area surrounding the frequency of 0.08Hz and a direction corresponding to approximately 60 deg., highlighted by the red circle in Figure 8.9 - as only seen for data sets B and D, it can be argued that for data sets A and C, where the ship is in following waves for the considered area of wave energy, the corresponding encounter frequency for the excitations is so low that the ship is not affected by those excitations. Consequently, the wave energy for the specific area is not 'caught' by the Bayesian estimation when the data corresponding to trials A and C is dealt with. On the contrary, for data sets B and D with the ship encountering the waves at a higher frequency, due to head waves, the examined area *is* reflected in the estimation.

From similar reasoning it may also be explained why the energy in the dominant frequency-directional area for data sets B and D is estimated to be smaller compared to what is seen

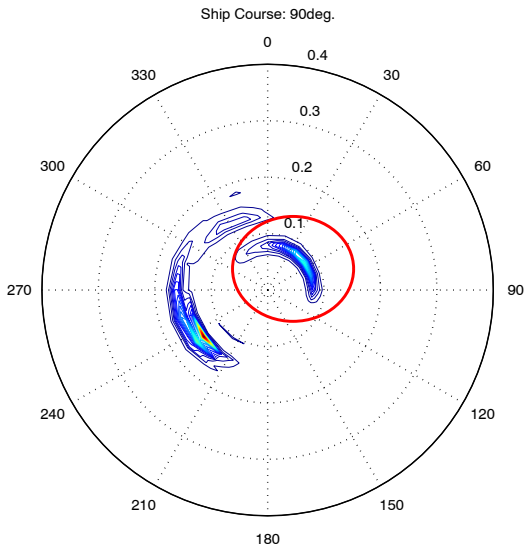

Figure 8.9: *Circled area being wave energy only estimated for Data B and D.*

for data sets A and C. Thus, the waves propagating from a direction around 240 deg. are for Data B and D experienced as following waves, so that the excitations, due to these waves, do not affect the ship as much as when the ship encounters the waves more or less head on, as for Data A and C.

The differences between the excitations felt by the ship for following and head waves are evidently seen in Table 8.3. From the table it appears that both the pitch motion and the vertical acceleration have an energy content that is several times larger for Data A and C compared to B and D. Especially, it is observed that for the vertical acceleration, the ratio between the (measured) variance for data set A relative to B, and C relative to D, is as much as 47 and 77, respectively. As regards the low-frequency peak in the estimated wave spectrum for Data B and D, the result of this peak is notably seen from the response spectra, see Figure 8.6, for the pitch motion and the vertical acceleration, and as well from the roll motion for Data D. Thus, for data set D, by assuming an encounter angle of 150 deg., a wave frequency of $f_0 = 0.08$Hz is transformed into an encounter frequency of $f_e = 0.10$Hz, which exactly corresponds to the location of the low-frequency peak in the response spectra, cf. Data D in Figure 8.6.

In conclusion to the subject of following waves versus head waves, it is apparent that the Bayesian method has problems in estimating a unique directional wave spectrum when different ship courses are analysed. This may be seen as a general problem for the method but, on the other hand, it is also important to remember what would be the case in practical applications considering decision support. In such cases it is unlikely that the ship's officers consider a change in ship course of more than, maybe, 45 deg. as an option to reduce the ship responses. Hence, the estimated wave spectrum, which is derived *only* on the basis of waves or excitations which *affect* the ship, is probably not to change much for the new ship

course. (It is understood here that it is the same set of responses which are used to estimate the wave spectrum in all the cases.) In the examples this small sensitivity to not-too-large course changes is, indeed, seen in comparisons of Data A with Data C and Data B with Data D, respectively. For those comparisons, only very small changes in the directional wave spectrum are noted, see Figure 8.4 as well as Table 8.2.

Finally, it should be mentioned that a more mathematical/theoretical explanation for the difference in energy distribution of the wave spectra observed for Data A and C compared to Data B and D has been considered. This explanation has to do with the fact that the TVFP leads to three wave frequencies in following seas for certain encounter frequencies. Hence, for Data B and D, the waves, which are observed for directions between 210 deg. and 240 deg., are experienced as following waves for the specific ship courses. As regards the fundamental equation system, the solution (i.e. the directional wave spectrum) means that the coefficients corresponding to the spectral values of the wave spectrum for the specific discretised points in the area of the red circle, cf. Figure 8.9, apparently have *such* a weight so that the optimal solution is obtained for non-zero spectral values for these points. Since this explanation has to do with the very mathematical solution of the problem, it cannot be investigated in more detail.

8.3 Conclusions

As seen from the analysed full-scale data in the present chapter, the comparisons conducted show a satisfactory agreement between visual observations and estimations by the Bayesian estimation method. Thus, both the wave direction and the mean wave period were estimated with reasonable accuracy. The significant wave height was, however, estimated on the lower side in all cases compared to the visual observation. Apart from the fact that uncertainties are present in visual observations, deviations in the wave height were also dealt with in connection with the influence of the transfer functions. Hence, from investigations related to the energy in the response spectra, it was illustrated how the Bayesian estimation yields a solution that is the best possible on average, relative to all the considered responses.

It was seen that in following waves the Bayesian method - for the specific ship considered - had difficulties in 'capturing' low-frequency waves. The explanation was the fact that the investigated ship, in general, is little sensitive to low-frequency excitations. On the face of it, this is a problem since the estimated wave spectrum does not reflect the true distribution of energy within the wave field, that is, swell components may in some cases be disregarded even though being present in reality. However, seen from a practical point of view, i.e. in the context of decision support, the apparent lack of energy - restricted to a certain low-frequency range - in the estimated wave spectrum does not necessarily have a large influence if decision support is to be given for the specific responses used to estimate the wave spectrum. Simply due to the fact that if the ship is not sensitive to low-frequency wave excitations for the considered responses, decision support for these responses can be done as well by just

taking into account a wave spectrum which does not contain the specific low-frequency wave components. It must, however, be underlined that the situation is somewhat different if decision support should be given with respect to responses not used for the estimation of the wave spectrum. Such responses may exhibit a different frequency-wise behaviour for which reason the use of a wave spectrum, which lacks energy for certain directions and frequencies, will (may) lead to wrong conclusions as regards decision support for these responses.

This page is intentionally left blank.

Chapter 9

Full-Scale Data - Comparisons with WAVEX

9.1 Introduction

Directional wave spectra can be estimated by other methods and devices. One of such methods is based on the backscatter image produced when microwaves are projected on the ocean surface, e.g. Reichert et al. (1998) and Borge et al. (2000). In the present chapter, comparisons of the Bayesian-estimated directional wave spectra are made with estimations from the wave radar system WAVEX, see e.g. the technical manual of MIROS (1998). Unfortunately, however, no visual observations were made, so redundancy is by no means obtained.

The motion measurements, which form the basis of the estimations, have been carried out on a container ship with dimensions as seen in Table 9.1. The responses used to estimate the wave spectra are the three global motions heave, roll and pitch, respectively. At this stage, the author feels it is necessary to mention that the sway response could be suggested instead of the roll response for reasons which will be dealt with later. However, as practical problems were observed for the sway response in the beginning of the present analysis, this response was discarded. The problems were resolved, though, and estimations with the sway response in place of the roll have been carried out and will be presented and discussed later.

Table 9.1: *Main dimensions of the considered ship.*

Length, L_{pp}	275.0 m
Breadth, B_{mld}	40.0 m
Draught, T	12.0 m
Displacement	50,000 t

As will be seen from the results presented below, nine sets of data have been investigated. In Table 9.2 the analysed data sets are sorted by the date of origin and it is important to note that each data set has a time duration of 15 minutes. The specific acquisition time is taken in the middle of a 30 minutes period, which is the period on which the WAVEX estimation is based. During the acquisition of the response signals, the operational conditions were (nearly) constant. Time series of the responses are visualised in Section B.3 of Appendix B.

Table 9.2 presents also the ship's position which is given by the latitude and the longitude of the location, and from Figure 9.1 it is seen that all data sets have been recorded in the Pacific Ocean. As a general comment on the data it should be noted that none of the sets have been recorded during particularly light sea states. The reason for this is that the recording system, i.e. the monitoring system, saves only entire time histories of the hundred so-called worst cases (with a duration of 30 minutes) experienced within a month. Otherwise, only statistical values are stored.

Table 9.2: *Overview of analysed data.*

Data	Date	Time	Latitude	Longitude	Abs. Course	Speed
A	03/07 2003	22.00	38°51 N	155°43 E	64.1°	12.1 m/s
B	04/07 2003	05.00	39°55 N	157°25 E	64.0°	12.3 m/s
C	04/07 2003	07.00	40°34 N	158°48 E	64.5°	12.4 m/s
D	06/07 2003	02.00	47°30 N	159°55 E	71.7°	12.0 m/s
E	24/09 2003	03.00	31°15 N	131°44 E	62.5°	10.0 m/s
F	30/09 2003	06.00	47°43 N	156°55 W	87.9°	12.2 m/s
G	10/10 2003	01.00	34°21 N	122°14 W	265.4°	10.9 m/s
H	10/10 2003	06.00	34°15 N	123°70 W	264.3°	10.8 m/s
I	18/02 2004	16.00	54°04 N	172°31 E	259.7°	11.0 m/s

As regards the cross spectral analysis of the responses, it should be noted that this is carried out by use of the stepwise least squares algorithm, cf. Section 5.7, and the optimal order is determined according to the multiple final prediction error ($MFPE$) described in Section 5.5.

With respect to the frequency response functions for the considered responses, detailed information is found in Appendix A, where the amplitudes of the frequency response functions are plotted for a range of encounter angles and for five different sets of operational parameters. The complex-valued transfer functions have been calculated by the three-dimensional time domain code WASIM. In Figure 9.2 the variation with heading and frequency of the amplitudes for heave, roll and pitch, respectively, are visualised in polar plots for one set of the operational parameters. It should be mentioned that the author himself has not carried out the calculations of the transfer functions, for which reason sensitivity analyses of the transfer functions have not been conducted.

In Sections 9.2 and 9.4, the final outcome of the directional estimations for the wave spectra found by the Bayesian method is presented and compared with estimations by WAVEX.

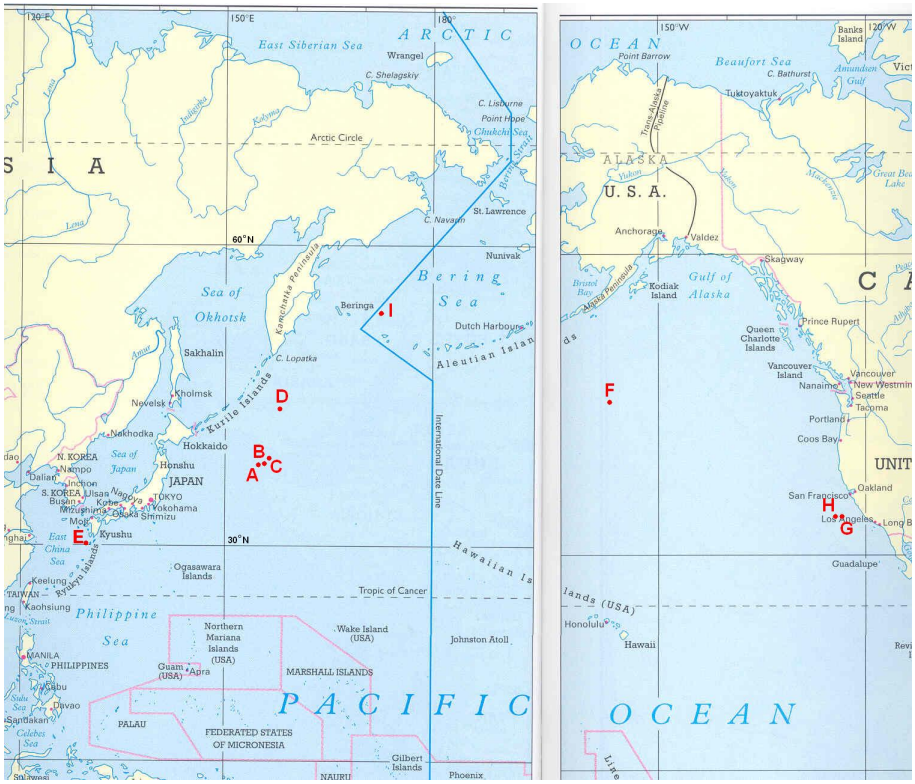

Figure 9.1: *Ship position for the recorded data. Map scanned from* Lloyd's Maritime Atlas Aldworth (1997).

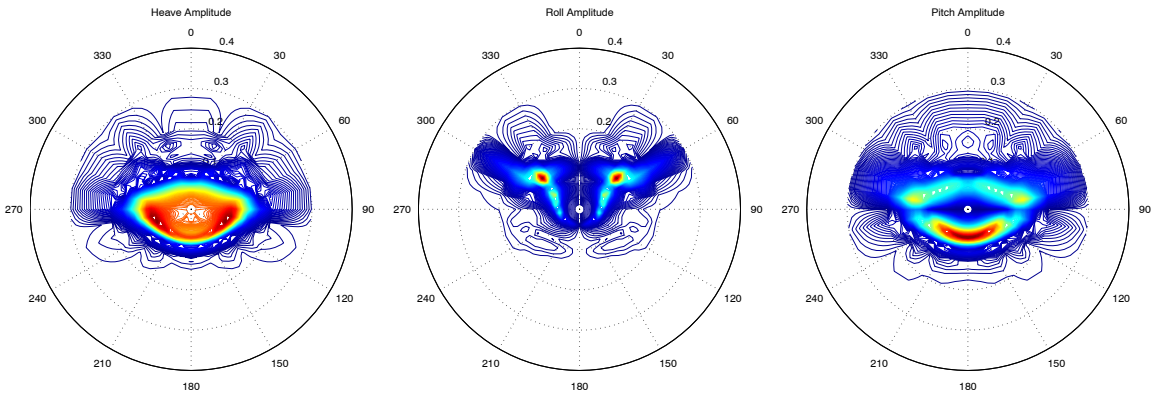

a) b) c)

Figure 9.2: *Visualisation of the amplitudes of the frequency response functions.* a) *heave,* b) *roll, and* c) *pitch. 180 deg. is head waves.*

Furthermore, attention is given to the measured and the estimated response spectra. In the sections all the results for the nine data sets are presented schematically and discussed. It should, however, be noted that the relevant plots of directional wave spectra etc. for each

data set are found in Section 9.3. In that section, the results are visualised by three figures: namely one figure with two polar plots which illustrate the directional wave spectrum estimated by the Bayesian modelling procedure and by WAVEX, a second figure that shows the integrated frequency wave spectrum, and, finally, a third figure which presents the comparison between the measured and the calculated response spectra for both the Bayesian procedure and WAVEX. The discussion carried out in the two sections, Section 9.2 and Section 9.4, treats the results in an overall sense. This means that the presented results reflect only the outcome obtained from the optimal solution of the Bayesian estimation, without consideration of individual parameters and conditions. In a subsequent section, Section 9.5, the focus will be on elements which influence the (optimum) solution to the Bayesian estimation. Thus, different kinds of parameter studies will be conducted where e.g. the influence of the hyperparameter is investigated.

9.2 Wave Parameters

9.2.1 Bayesian vs. WAVEX

The nine data sets listed in Table 9.2 are analysed by the Bayesian estimation method and the analysis leads to the wave parameters presented in Table 9.3, see also Section 9.3. The significant wave height H_s is calculated according to (7.5), and the mean wave period is found from (8.1). In the table, numbers are also given for the estimations produced by WAVEX. Thus, results from the former method are denoted by 'BAY' whereas parameters calculated from WAVEX are denoted by 'WAV'. As regards the rightmost 2 x 2 columns, which relate to the directionality of the wave field, these numbers are relative in the sense that they are given relative to the ship's longitudinal axis. The definition follows from WAVEX, so that head waves are experienced for directions around 0 deg. ($\sim$ 360 deg.) and following waves are observed for directions around 180 deg. It should be noted that 'Peak dir.' represents the direction of the main peak, whereas 'Energy dir.' denotes the energy mean direction, cf. (8.3).

From a study of the numbers in Tables 9.3 and 9.4 it is seen that, in general, the agreement between the wave parameters estimated by the Bayesian method and by WAVEX is reasonable. However, the best agreement is notably found for Data A, B, C and D. As regards the absolute difference in the directions, there is also fair agreement between the results. For Data E, F, G, H and I, the agreement is less good between the Bayesian estimates and the WAVEX estimates. Thus, the maximum deviations on the significant wave height and the mean wave period are 36% and -18%, respectively. The reason for the less good agreement in these cases could be the existence of severer sea states compared to the sea states for Data A, B, C and D. It is seen that both the Bayesian method and the WAVEX estimate substantially higher values for H_s, when the last five sets in Table 9.3 are compared with the first four data sets. This tendency is also seen from the response spectra presented in Section 9.3 and is as well reflected in the visualisation of the time series shown in Section

Table 9.3: *Estimated wave parameters from Bayesian estimation and obtained from WAVEX.*

	H_s [m]		T_s [sec.]		Peak dir. [deg.]		Energy dir. [deg.]	
Data	BAY	WAV	BAY	WAV	BAY	WAV	BAY	WAV
A	2.7	3.0	7.5	6.9	300	285	240	260
B	2.5	2.5	7.1	6.8	240	225	230	240
C	2.3	2.6	7.0	6.5	240	240	230	230
D	2.4	2.5	7.0	6.6	160	110	160	110
E	3.6	4.9	8.2	9.2	0	340	350	350
F	4.0	4.8	7.8	8.6	180	200	170	170
G	3.3	4.5	10.2	8.7	285	60	280	55
H	3.6	4.4	9.0	8.8	280	40	300	60
I	5.7	7.2	13.1	10.8	180	190	170	180

Table 9.4: *Deviation between estimated wave parameters from Bayesian estimation and obtained from WAVEX, relative to the Bayesian results.*

Data	H_s	T_s	Peak dir. [deg.]	Energy dir. [deg.]
A	11%	-8%	15	20
B	0	-4%	15	10
C	13%	-7%	0	0
D	4%	-6%	50	50
E	36%	12%	20	10
F	20%	10%	20	0
G	36%	-15%	135	135
H	22%	-2%	120	120
I	26%	-18%	10	10

B.3 of Appendix B. Hence, the assumed linearity between the ship responses and the waves might be less good in the last five cases, a fact which would influence the Bayesian results since linearity is fundamental for the method to be reliable. On the other hand, it is believed that due to the high inertia of the ship, the errors in the Bayesian estimation should decrease as the wave period increases. The reason is that the ship acts as a filter and therefore the ship will filter the high-frequency wave components which induce no significant motions. To judge the increasing deviations between the Bayesian estimates and the WAVEX results observed for Data E, F, G, H, I compared to Data A, B, C, D, it is thus important to keep the filtering aspect in mind as well.

Returning to the deviations between the Bayesian and the WAVEX results in each individual set of data, cf. Table 9.4, it should be noted that with respect to the significant wave height, WAVEX yields always results which are larger than those obtained by the Bayesian method, in particular this applies to Data E, F, G, H, and I. The general trend of larger significant wave heights estimated by WAVEX is difficult to explain since, on the face of

it, it may be the Bayesian estimations which exhibit too little energy or it may be the WAVEX results which exhibit too much energy. As will be seen in a subsequent section, studies of the energy contained within the response spectra suggest that energy is lacking when measurements and estimations based on the Bayesian results are compared. The same trend is, however, seen in some of the cases for the estimated response spectra based on the WAVEX results, although the tendency is not as unique as for the Bayesian results. Therefore, more detailed investigations and analyses would be required to settle on the discrepancy in the significant wave height estimated by the Bayesian method and by WAVEX. In the end, this would require additional knowledge of the on-site sea state in the given situation, and unfortunately this information cannot be attained. In conclusion on the significant wave height, which reflects the energy hold by the wave spectrum, it should be noted that the integrated frequency wave spectra, see Section 9.3, for the Bayesian and the WAVEX estimations deviate primarily in the sense of more broad-banded spectra for the latter estimations.

As regards the mean wave period, Tables 9.3 and 9.4 show no consistent trend in the deviations between the Bayesian estimates and the WAVEX estimates and, in general, the magnitude of these deviations must be considered acceptable from an engineering point of view.

For the peak wave directions and the energy mean directions, see the figures of the estimated directional wave spectra in Section 9.3 as well as Table 9.3, the agreement between the Bayesian method and WAVEX is also found to be reasonably. However, both for Data G and H there seems to be a conflict whether waves are approaching from one side or the other side of the ship. Thus, the Bayesian estimation has waves approaching on the port side whereas WAVEX yields waves entering from the starboard side, nearly as though the two estimations are mirror images of each other around the ship's longitudinal axis. It is by no means easy to give a reason for this controversy since nothing is changed in the computational setup for the two cases and different weighting of the signals, although not shown, does also not reveal better agreement. Furthermore, it is seen that the agreement between the integrated frequency spectra, see Figures 9.24 and 9.27, for the Bayesian and the WAVEX estimations for Data G and H is just as good as for the other seven cases. This fact and the estimations being kind of mirror images of each other indicate that the problem is restricted to a port/starboard relation. An apparent and straightforward explanation for the discrepancy could therefore be related to port/starboard symmetric frequency response functions used in the Bayesian estimation. Thus, the problem may be considered to be similar to what is illustrated in Figure 6.2 in Chapter 6. However, as the roll response is used as one of the responses in the present data analysis, the port/starboard asymmetry is reflected in the Bayesian estimation. In this context it should be remembered that by use of complex-valued transfer functions, the amplitude as well as the phase of the responses are taken into account. For this reason the controversy in the wave direction for Data G and Data H has also not to do with the phase shift of the roll transfer function experienced at frequencies close to the natural roll frequency in beam seas. An estimate, e.g. Lloyd (1998), of the natural roll frequency of the ship is found to be $f_r \simeq 0.06$Hz ($\sim T_r \simeq 15$sec.) and Figure 9.3, which depicts the roll phase angle, confirms, more or less, this value and

illustrates the mentioned shift in phase.

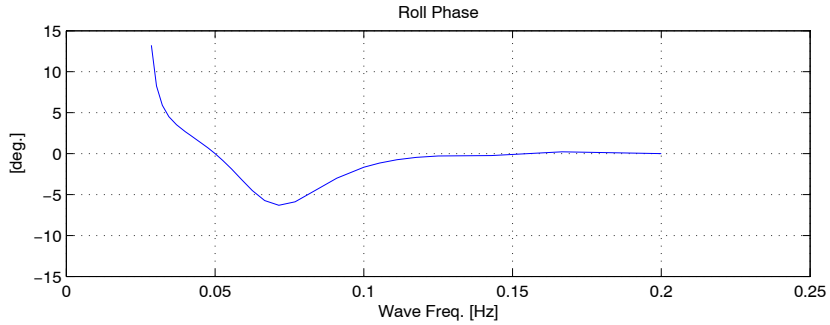

Figure 9.3: *The phase angle of the roll transfer function for an encounter angle equal to 90 deg. The operational conditions correspond to Data G and H.*

It can thus be excluded that the roll response as such has to do with the controversy in the wave direction observed for the two data sets. For this reason it would be interesting to do the Bayesian estimations with the roll response replaced by another response, e.g. the sway response which is also an odd function and therefore exhibits port/starboard asymmetry as well. Section F.2 in Appendix F illustrates such estimations with the roll replaced by the sway, and Table 9.5 presents the estimated wave parameters for these estimations including the wave parameters from the roll based estimations, cf. Table 9.3.

Table 9.5: *Estimated wave parameters from the Bayesian method with the responses {heave, sway and pitch} and {heave, roll and pitch}.*

Data	A	B	C	D	E	F	G	H	I
H_s [m] (sway)	2.4	2.3	2.0	2.2	3.1	3.9	3.4	3.7	7.2
H_s [m] (roll)	2.7	2.5	2.3	2.4	3.6	4.0	3.3	3.6	5.7
T_s [sec.] (sway)	8.1	8.1	7.6	8.0	9.5	8.9	9.5	9.5	10.1
T_s [sec.] (roll)	7.5	7.1	7.0	7.0	8.2	7.8	10.2	9.0	13.1

In general, the sway based wave parameters deviate only slightly compared to the estimations where the roll response is used. Similarly, the directional distribution of energy, cf. the directional wave spectra in Sections 9.3 and F.2, is more or less identical, independently if the roll or the sway response is used in the Bayesian estimations. As regards Data G and Data H, the sway based estimations, cf. Figures F.19 and F.22, do not specifically confirm the roll based Bayesian estimations and nor do they specifically indicate results in favour of the WAVEX estimations. Thus, it is seen that the sway based estimations have waves approaching from the starboard side as well as the port side. In this respect it can be argued that the discrepancy in the directional distribution of energy is less notable when the sway based results are compared with WAVEX. In conclusion on the controversy in the wave

direction, it cannot be decisively stated whether waves in reality were entering on the port or the starboard side. More comments on the sway vs. roll based estimations are found in one of the subsections in Section 9.5.

Although no evidence was found on the wave propagation in Data G and H, a hypothetical experiment may illustrate what could have been the case if visual observations, e.g. by the ship's officers, were at hand. Thus, as an imaginary example, the waves *are* assumed to enter on the starboard side due to input from visual observations. The result is seen in Figure 9.4, 'BAYESIAN - MANIPULATED', and is obtained by minimising the wave energy within the wave field corresponding to waves entering from the port side. For the sake of completeness, the estimated wave parameters in the present example are almost identical to those seen in Table 9.3 for Data H (BAY). The figures are $H_s = 3.4$ m and $T_s = 9.6$ sec.

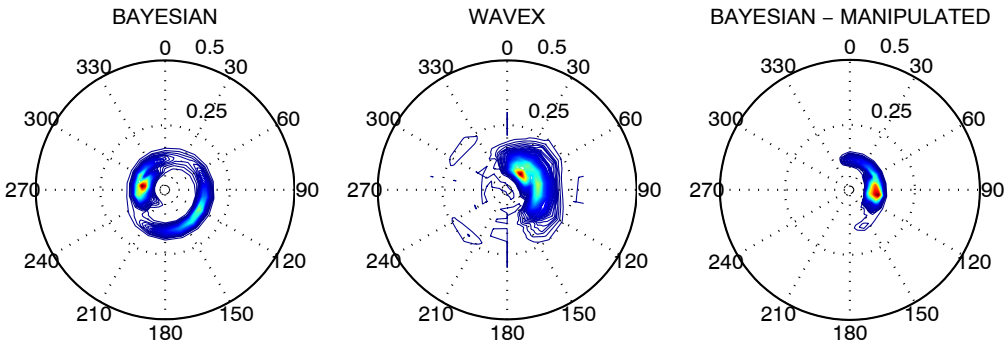

Figure 9.4: *The estimated wave spectra for Data H when the estimation is carried out with and without manipulation with respect to the wave direction. The relative ship course is 0 deg., and the wave field is depicted as approaching waves.*

Based on the above discussion on wave heights, wave periods and directions, it is not possible to conclude that the estimations given by WAVEX are correct and those by the Bayesian estimation method are wrong, or vice versa. To draw such conclusions knowledge of the absolute true wave spectrum would be needed, which raises a central problem: means to obtain the on-site – and absolute true – wave spectrum at any time do not exist. For this reason, redundancy in the data in the form of a third estimate of the wave spectra, e.g. from a wave buoy in the event this was passed during operation, would have been desirable. Unfortunately, redundancy has not been present in the data, and therefore it should only be said that one method may be more correct than the other, although the agreements between the two kind of estimations were reasonable. In Section 9.4, a discussion based on the response spectra will go further into detail on the deviations between the Bayesian

estimates and the WAVEX results.

9.2.2 Parametric Estimations

For comparison, wave parameters have also been estimated by the parametric method described in Chapter 4. It should be noted that the wave spectra are not visualised which means that the results of the Parametric method serve only as comparative means with respect to the actual wave parameters. However, Section F.3 in Appendix F shows a comparison of the directional wave spectra estimated by the three methods.

In Table 9.6 the wave parameters found by optimisation of the ten parameters given in expression (4.6) are listed.

Table 9.6: *Wave parameters from the optimisation: the peak wave period T_p, the significant wave height H_s, the (mean) wave direction θ_m, the shape factor λ, and the spreading parameter s_{max}.*

	T_p	[sec.]	H_s	[m]	θ_m	[deg.]	λ		s_{max}	
Data	spec1	spec2	spec1	spec2	spec1	spec2	spec1	spec2	spec1	spec2
A	7.69	9.09	1.7	1.7	220	295	4.0	1.0	10	75
B	9.12	7.71	1.2	1.9	295	240	1.0	4.0	25	75
C	16.5	7.63	0.4	1.7	295	240	1.0	4.0	25	75
D	16.7	7.26	0.7	1.2	55	130	1.0	4.0	10	25
E	14.3	12.5	0.4	3.4	135	5	1.0	4.0	25	75
F	14.2	7.64	1.9	2.8	130	145	4.0	3.7	10	10
G	10.0	16.7	2.8	2.2	265	0	1.6	4.0	75	75
H	14.4	8.33	2.7	2.6	295	250	2.5	4.0	75	75
I	14.4	20.0	7.0	2.4	180	305	4.0	2.8	25	75

In order to compare the Bayesian and the Parametric method, Table 9.7 should be studied. The results of the Parametric method are denoted 'OPT'. From a study of the numbers in Table 9.7 it is seen that, in general, there is a good agreement between the Bayesian and the Parametric method. However, notable differences (in the relative sense) are observed for the significant wave height of Data C, D and I. This goes also for the mean wave period of Data E and F. With regard to the primary wave direction and the overall distribution of energy of the estimations of the two modelling procedures, cf. Section F.3, the consistency is reasonable. Especially, it seems that the introduced frequency-dependency, cf. (4.4), of the spreading parameter of the Parametric modelling yields directional estimations which exhibit somewhat similar properties as seen for the Bayesian estimations. At this stage it is worth to mention that, although not shown, the introduction of a frequency-dependent spreading leads actually to results which are in better agreement with the Bayesian as well as the WAVEX estimates compared to what is seen without the frequency-dependency of

Table 9.7: *Comparison of wave parameters: the significant wave height H_s, the mean wave period T_s, and the primary (mean) wave direction θ_m.*

	H_s [m]			T_s [sec.]			θ_m [deg.]		
Data	BAY	OPT	WAV	BAY	OPT	WAV	BAY	OPT	WAV
A	2.7	2.5	3.0	7.5	7.2	6.9	200	220	280
B	2.5	2.3	2.5	7.1	7.3	6.8	240	240	225
C	2.3	1.7	2.6	7.1	7.4	6.5	240	240	240
D	2.4	1.4	2.5	7.0	8.3	6.6	160	130	115
E	3.6	3.4	4.9	8.2	11.3	9.2	0	5	330
F	4.0	3.4	4.8	7.8	8.6	8.6	180	145	180
G	3.3	3.5	4.5	10.2	10.7	8.7	280	265	60
H	3.6	3.7	4.4	9.0	9.5	8.8	280	295	35
I	5.7	7.4	7.2	13.1	13.0	10.8	185	180	190

the spreading parameter; both with respect to the wave parameters and the distribution of energy.

9.3 Comparative Plots

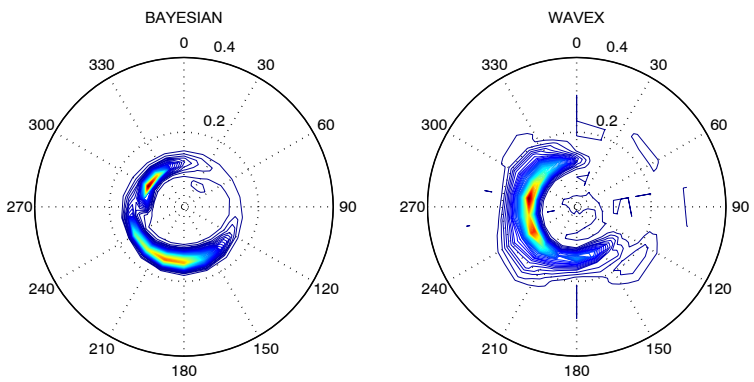

Figure 9.5: *The estimated wave spectra for Data A. Relative ship course is 0 deg., and wave field is depicted as approaching waves.*

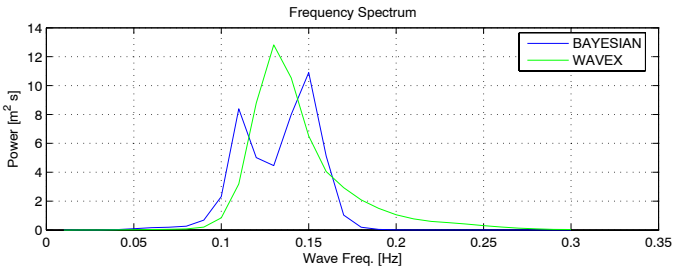

Figure 9.6: *Integrated frequency spectra for Data A.*

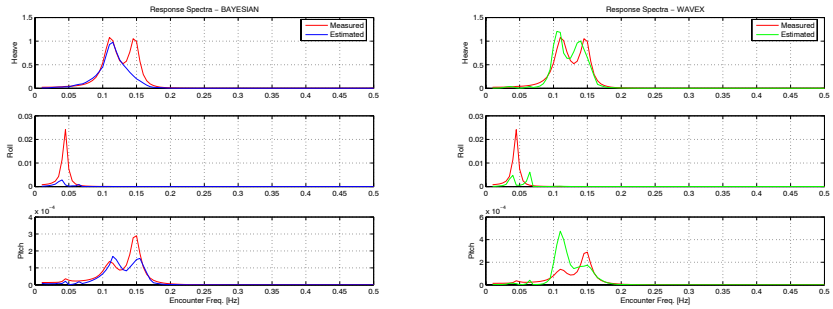

Figure 9.7: *Response spectra for Data A; measured and 'estimated' with the latter based on the estimated wave spectra. Units:* Heave [m^2s], Roll [rad^2s], Pitch [rad^2s]

Data B

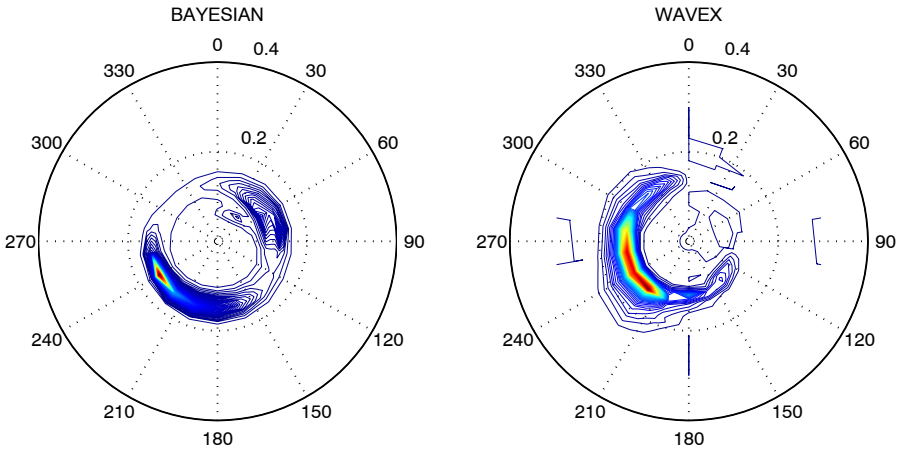

Figure 9.8: *The estimated wave spectra for Data B. Relative ship course is 0 deg., and wave field is depicted as approaching waves.*

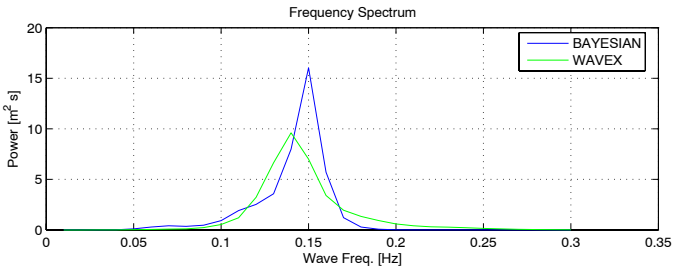

Figure 9.9: *Integrated frequency spectra for Data B.*

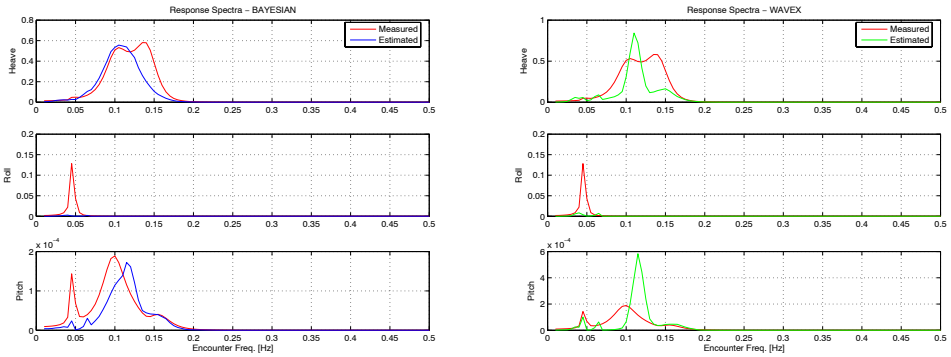

Figure 9.10: *Response spectra for Data B; measured and 'estimated' with the latter based on the estimated wave spectra. Units:* Heave [m^2s], Roll [rad^2s], Pitch [rad^2s]

Data C

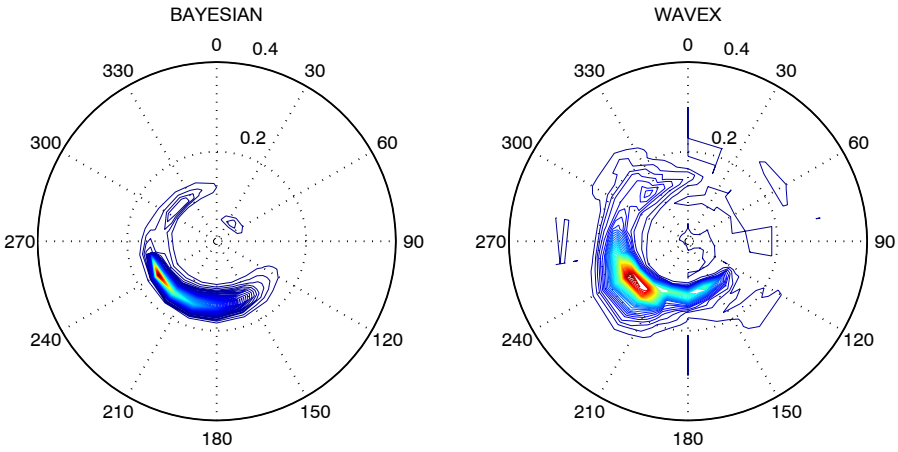

Figure 9.11: *The estimated wave spectra for Data C. Relative ship course is 0 deg., and wave field is depicted as approaching waves.*

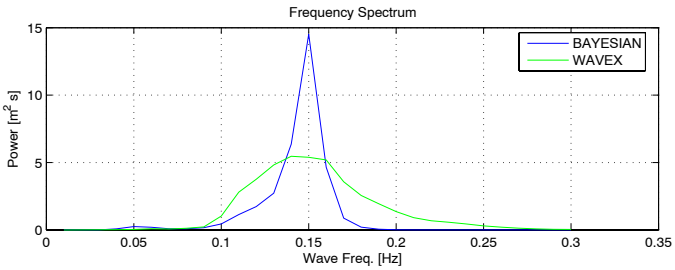

Figure 9.12: *Integrated frequency spectra for Data C.*

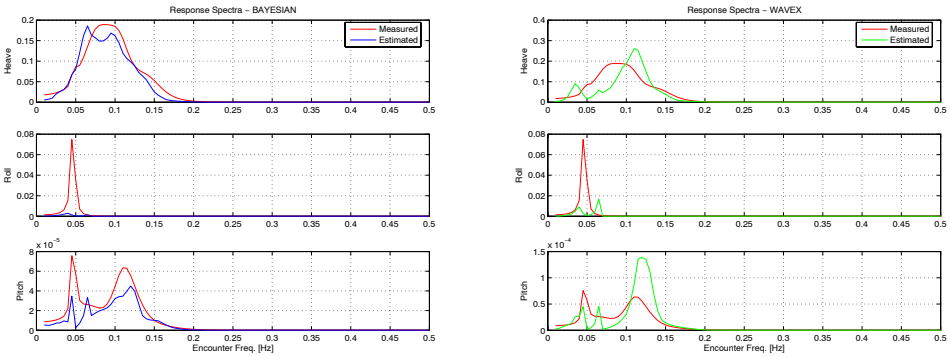

Figure 9.13: *Response spectra for Data C; measured and 'estimated' with the latter based on the estimated wave spectra. Note the difference in scales for some of the responses. Units:* Heave [m^2s], Roll [rad^2s], Pitch [rad^2s]

Data D

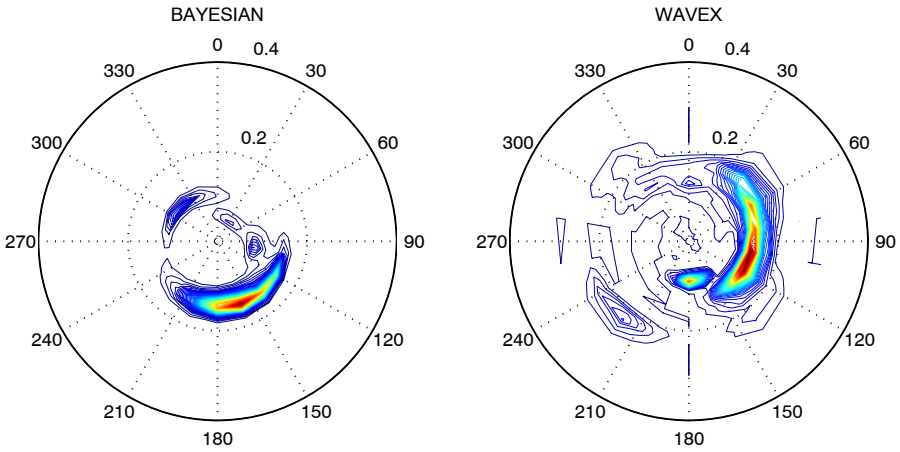

Figure 9.14: *The estimated wave spectra for Data D. Relative ship course is 0 deg., and wave field is depicted as approaching waves.*

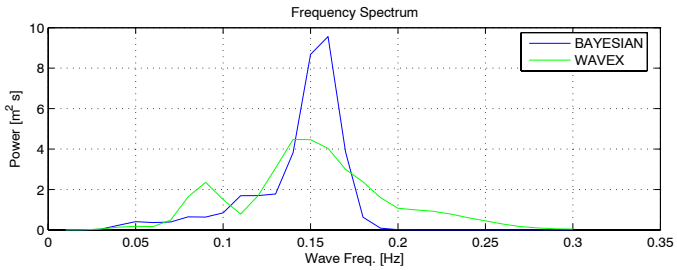

Figure 9.15: *Integrated frequency spectra for Data D.*

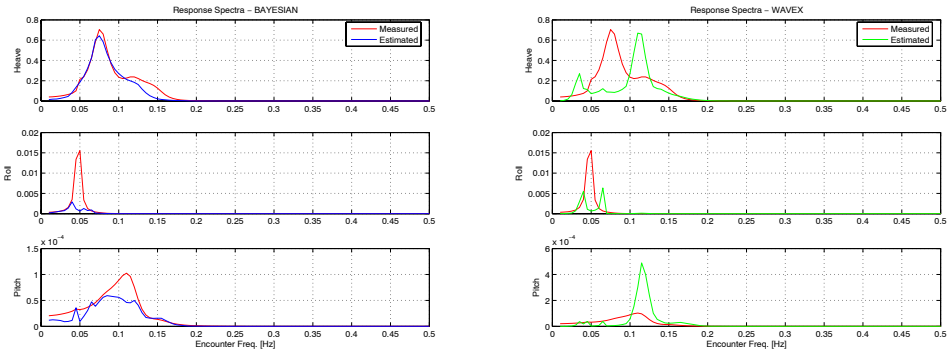

Figure 9.16: *Response spectra for Data D; measured and 'estimated' with the latter based on the estimated wave spectra. Note the difference in scales for some of the responses. Units:* Heave [m^2s], Roll [rad^2s], Pitch [rad^2s]

Data E

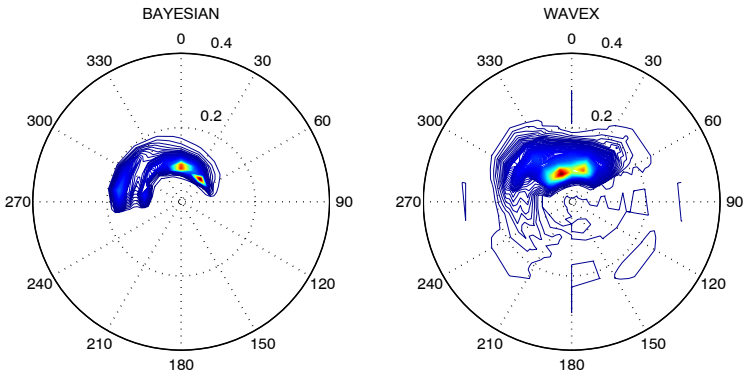

Figure 9.17: *The estimated wave spectra for Data E. Relative ship course is 0 deg., and wave field is depicted as approaching waves.*

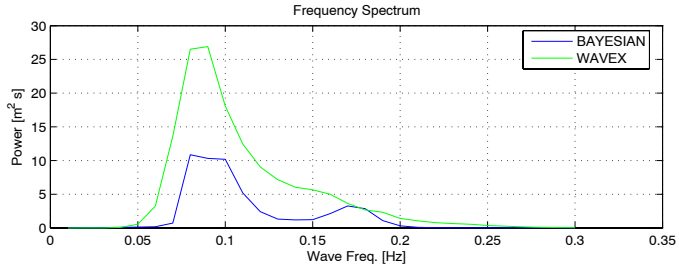

Figure 9.18: *Integrated frequency spectra for Data E.*

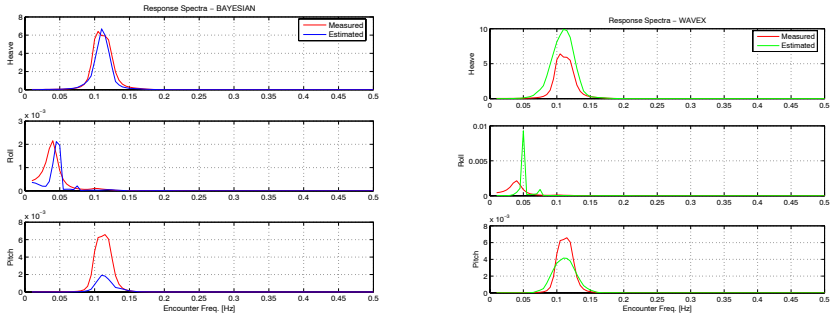

Figure 9.19: *Response spectra for Data E; measured and 'estimated' with the latter based on the estimated wave spectra. Note the difference in scales. Units:* Heave [m^2s], Roll [rad^2s], Pitch [rad^2s]

Data F

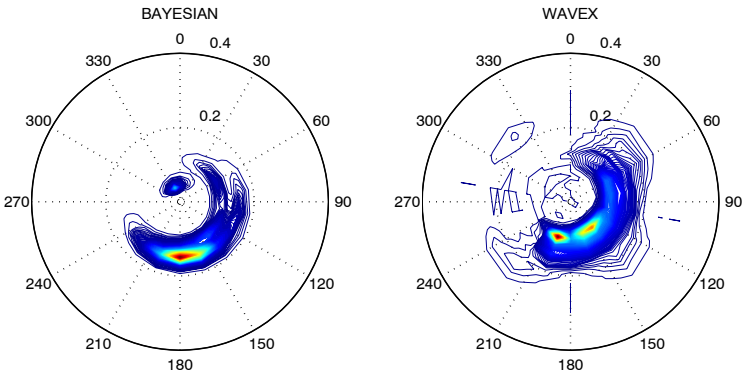

Figure 9.20: *The estimated wave spectra for Data F. Relative ship course is 0 deg., and wave field is depicted as approaching waves.*

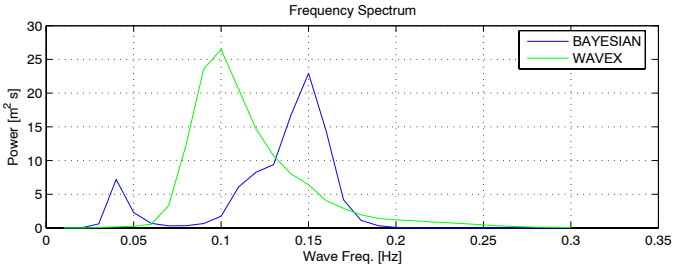

Figure 9.21: *Integrated frequency spectra for Data F.*

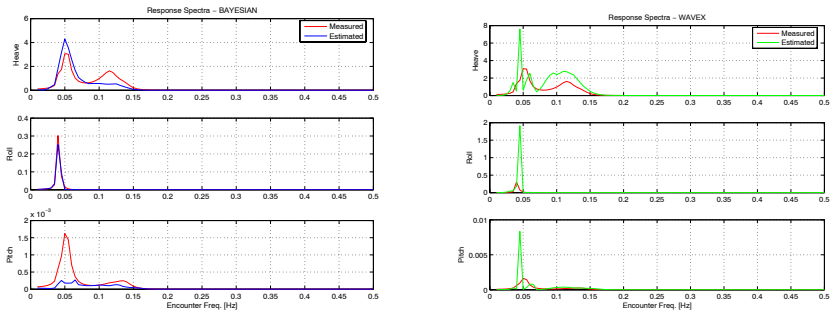

Figure 9.22: *Response spectra for Data F; measured and 'estimated' with the latter based on the estimated wave spectra. Note the difference in scales. Units:* Heave [m^2s], Roll [rad^2s], Pitch [rad^2s]

Data G

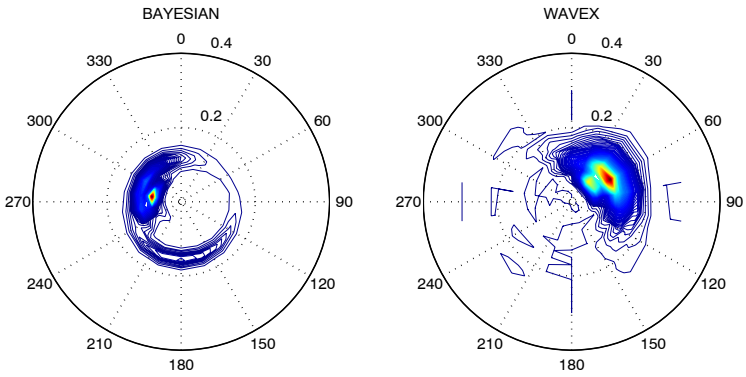

Figure 9.23: *The estimated wave spectra for Data G. Relative ship course is 0 deg., and wave field is depicted as approaching waves.*

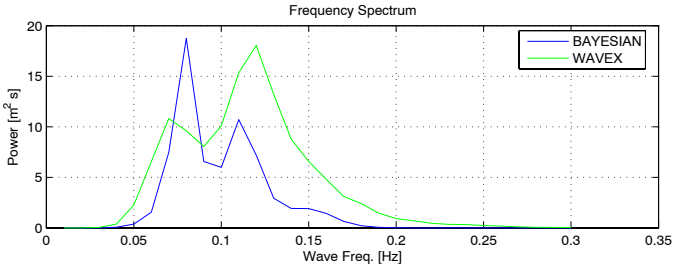

Figure 9.24: *Integrated frequency spectra for Data G.*

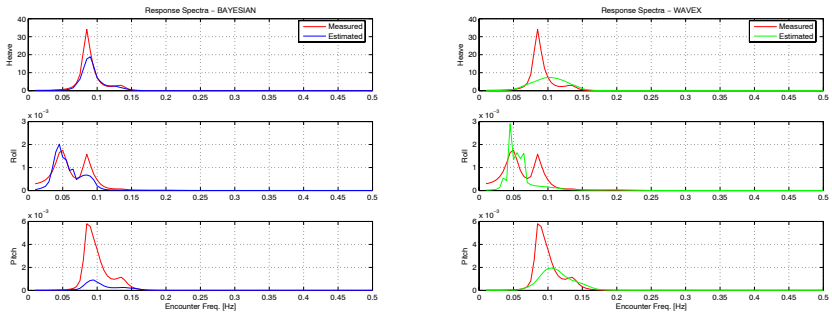

Figure 9.25: *Response spectra for Data G; measured and 'estimated' with the latter based on the estimated wave spectra. Note the difference in scales for some of the responses. Units:* Heave [m^{2}s], Roll [rad^{2}s], Pitch [rad^{2}s]

Data H

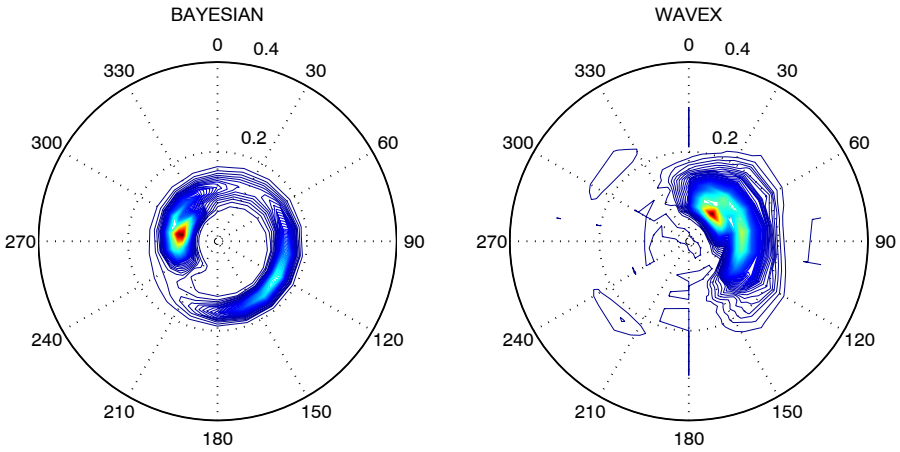

Figure 9.26: *The estimated wave spectra for Data H. Relative ship course is 0 deg., and wave field is depicted as approaching waves.*

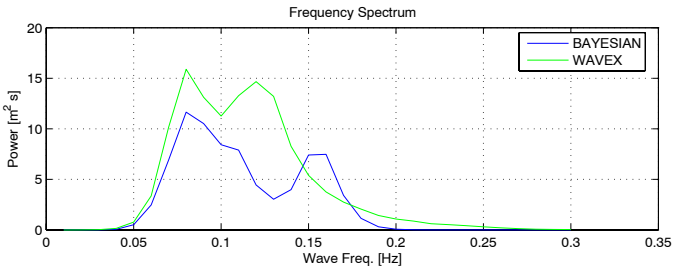

Figure 9.27: *Integrated frequency spectra for Data H.*

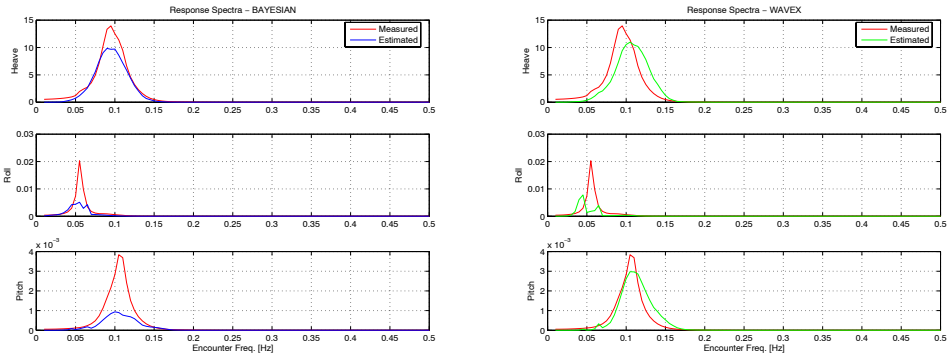

Figure 9.28: *Response spectra for Data H; measured and 'estimated' with the latter based on the estimated wave spectra. Note the difference in scales for some of the responses. Units:* Heave [m^2s], Roll [rad^2s], Pitch [rad^2s]

Data I

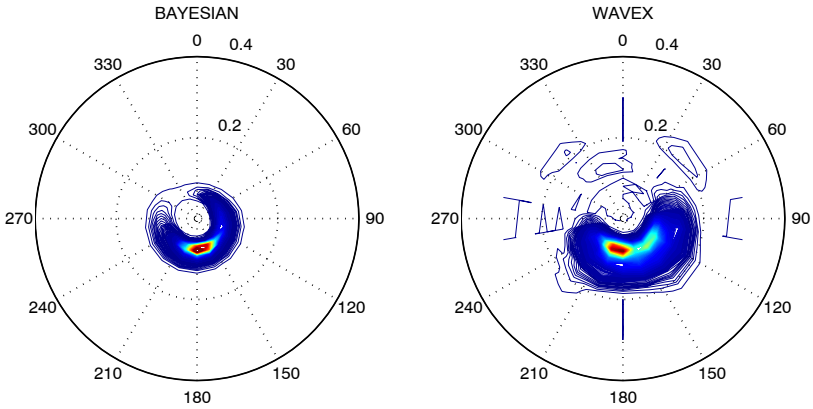

Figure 9.29: *The estimated wave spectra for Data I. Relative ship course is 0 deg., and wave field is depicted as approaching waves.*

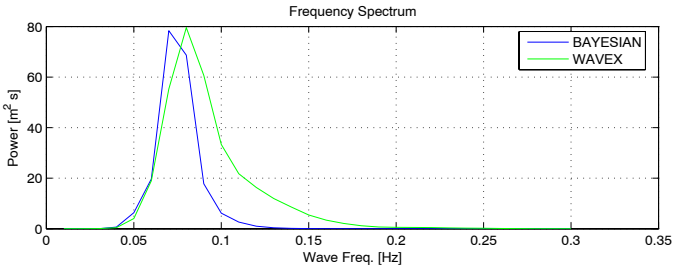

Figure 9.30: *Integrated frequency spectra for Data I.*

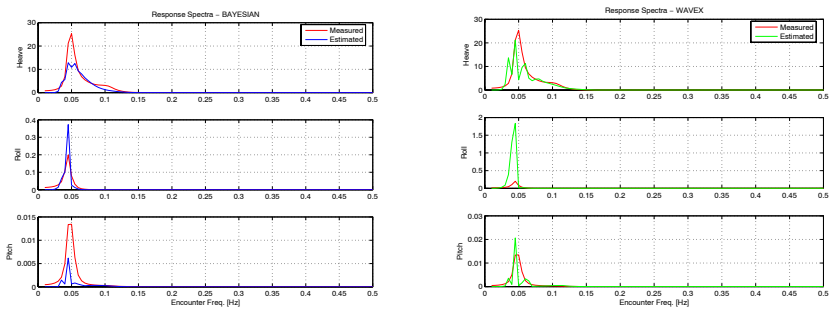

Figure 9.31: *Response spectra for Data I; measured and 'estimated' with the latter based on the estimated wave spectra. Note the difference in scales for some of the responses. Units:* Heave [m^{2}s], Roll [rad^{2}s], Pitch [rad^{2}s]

9.4 Response Spectra

In order to compare the measured and the estimated response spectra the two lower figures on the pages in Section 9.3 should be studied. In these figures the red graph represents the measured response spectra, which are obviously identical in each of the sets of figures. The blue and the green graph in the left and the right figures, respectively, represent the estimated response spectra. The left figure illustrates the results based on the Bayesian-estimated wave spectrum and the right figure shows the results of the WAVEX estimation, and for this reason deviations are seen when these response spectra are compared with each other.

In general, there is little difference whether the measured response spectra are approximated on the basis of the Bayesian- or the WAVEX-based wave spectrum, see also Tables 9.8 and 9.9. However, for specific data sets and responses it is the Bayesian based response spectra which approximate the measured spectra the best. This is not surprising, since

Table 9.8: *Deviation on variance for the considered responses. Figures relative to the measured variance.*

	Heave		Roll		Pitch	
Data	BAY	WAV	BAY	WAV	BAY	WAV
A	-22%	0.2%	-84%	-65%	-25%	28%
B	-17%	-38%	-96%	-87%	-30%	18%
C	-11%	-14%	-92%	-73%	-32%	20%
D	-15%	-27%	-72%	-56%	-30%	59%
E	-20%	86%	-35%	4.0%	-72%	-14%
F	-5.8%	63%	-5.5%	330%	-64%	57%
G	-20%	-34%	-11%	-30%	-77%	-41%
H	-18%	-8.5%	-49%	-51%	-62%	6.2%
I	-31%	-18%	15%	527%	-71%	-29%

the Bayesian results are based on the factually measured response spectra. However, better overall agreement were actually to be expected between the measured and the estimated response spectra for the Bayesian cases (i.e. an agreement similar to that seen in Chapter 8). With the focus on only the Bayesian results in the following, it is observed that especially for the roll and the pitch motions a relatively poor agreement is found between the measured and the estimated spectra. Moreover, from a study of the Bayesian results in Table 9.8, it is seen that nor in the overall perspective is the agreement particularly good as all three responses at the same time are estimated with variances less than the measured variances for each set of data. This is in contrast to the observations for the full-scale data analysed in Chapter 8, cf. Table 8.3, where the errors on the variances were, so to say, equally distributed. The reason for the present contradiction has been investigated intensively but, disappointingly, no satisfactory explanation has been found. The reason is, however, believed

Table 9.9: *Measured variance, calculated from the response spectrum.*

Data	Heave [m^2]	Roll [rad^2]	Pitch [rad^2]
A	$5.7 \cdot 10^{-2}$	$3.1 \cdot 10^{-4}$	$1.3 \cdot 10^{-5}$
B	$4.0 \cdot 10^{-2}$	$13 \cdot 10^{-4}$	$1.1 \cdot 10^{-5}$
C	$1.5 \cdot 10^{-2}$	$8.3 \cdot 10^{-4}$	$0.46 \cdot 10^{-5}$
D	$3.6 \cdot 10^{-2}$	$2.1 \cdot 10^{-4}$	$0.69 \cdot 10^{-5}$
E	$22 \cdot 10^{-2}$	$0.60 \cdot 10^{-4}$	$20 \cdot 10^{-5}$
F	$14 \cdot 10^{-2}$	$19 \cdot 10^{-4}$	$4.7 \cdot 10^{-5}$
G	$72 \cdot 10^{-2}$	$0.88 \cdot 10^{-4}$	$18 \cdot 10^{-5}$
H	$61 \cdot 10^{-2}$	$3.0 \cdot 10^{-4}$	$13 \cdot 10^{-5}$
I	$65 \cdot 10^{-2}$	$30 \cdot 10^{-4}$	$26 \cdot 10^{-5}$

to be found in the mathematics of the solution procedure derived in Chapter 3 and not in the physics behind the procedure. This is so, because no matter whether the frequency response functions are (completely) wrong, whether non-linearities in reality dominate the relation between excitations and responses, whether the cross spectral analysis contains errors, etc., the solution $\mathbf{x}$, i.e. the estimated wave spectrum, is basically found by minimising (cf. expression (3.61) in Chapter 3

$$\|\mathbf{A}\mathbf{f}(\mathbf{x}) - \mathbf{b}\|^2 + u^2 \|\mathbf{D}\mathbf{x} - \mathbf{c}\|^2 \tag{9.1}$$

Hence, the solution, although maybe unstable and completely unrealistic, will in the best possible way approximate the measured response spectra contained in the vector $\mathbf{b}$, by proper multiplication and with reservation about smoothing. Theoretically, *the* best agreement is therefore expected for a hyperparameter equal to zero, which implies a singular equation system that cannot be solved by QR factorisation. However, even for the smallest possible hyperparameter, which facilitates QR factorisation, it has been tested that the agreement between the measured and the estimated variances of the responses for the data set in the present chapter is not as good as observed for the data in Chapter 8, and the errors are not equally distributed. It is therefore difficult to give a specific reason for the rather poor agreement between the measured and the estimated response spectra seen for the Bayesian estimation. In Section 9.5 more attention is given to the subject in respect of a parameter study.

For the WAVEX results, the discrepancies between the measured and the estimated response spectra can be explained more easily, since three reasons may be specified: 1) the WAVEX estimate of the wave spectrum is not correct, 2) the calculated frequency response functions are not correct, and 3) the response measurements are influenced by errors. The author does not go into further detail on the WAVEX results, however, it is important to note that although deviations are present in specific cases between the Bayesian and the WAVEX results, the agreement of the shape and the location of peaks of the response spectra seems reasonable.

9.5 Parameter Study

In the preceding sections, the results were all obtained from the optimum solution of the Bayesian modelling procedure, and attention was not given to individual parameters or conditions influencing the solution. In this section, the focus will be on different kinds of parameters and conditions, and the sensitivity of the solution to these parameters and conditions is investigated. It should be mentioned that, unless otherwise stated, the considered responses are heave, roll and pitch.

9.5.1 Hyperparameter

The determination of the optimum hyperparameter is an important aspect in the Bayesian estimation. For Data A, ABIC is plotted as function of the hyperparameter and the result is seen in Figure 9.32. The optimal hyperparameter is determined as $u = 0.22$, which is

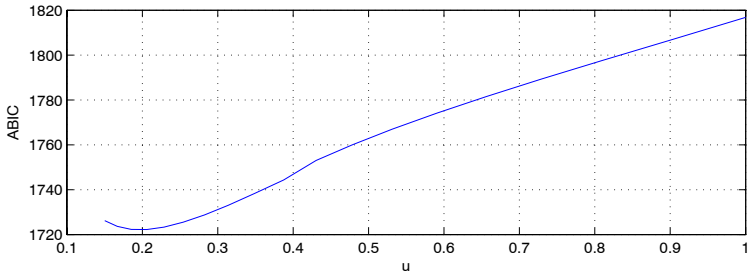

Figure 9.32: *ABIC as function of the hyperparameter.*

found for the minimum value of ABIC, and for this value the Bayesian estimation yields $H_s = 2.7$m and $T_s = 7.5$sec., as seen in Table 9.3 for Data A. To study the influence of the hyperparameter on the wave parameters (of Data A), Table 9.10 should be considered. From the table it is seen that a consistent, although inverse, trend exists for the significant wave height and the mean wave period in the sense of decreasing and increasing values, respectively, for an increase in the hyperparameter.

Table 9.10: *Influence of the hyperparameter on the significant wave height and the mean wave period. Note: optimum hyperparameter not shown.*

u	0.15	0.19	0.23	0.28	0.35	0.43	0.53	0.66	0.81	1.00
H_s [m]	3.1	2.8	2.7	2.6	2.6	2.4	2.3	2.2	2.1	2.1
T_s [sec.]	6.7	7.5	7.5	7.5	7.6	7.7	7.7	7.8	7.8	7.9

In Chapter 3 it was described how the hyperparameter reflects a compromise between agreement of the solution with data and smoothness of the solution. Therefore, the tendency

of increasing significant wave height for decreasing values of the hyperparameter is in good agreement with the analysis conducted in Section 9.4, which showed that the estimated response spectra exhibited too little energy compared to the measured spectra. Hence, the best agreement between the measured and the estimated response spectra is obtained for the lowest value of the hyperparameter in Table 9.10. However, the corresponding solution, which is the directional wave spectrum, is generally too non-smooth or non-physically, which is seen from Figure 9.33 (compare with Figure 9.5). This is also seen in Figure 9.34 which shows the integrated frequency wave spectrum for different values of the hyperparameter. Finally, it should be mentioned that the solution does not converge for lower values of the hyperparameter than seen in Table 9.10. Indeed, this fact indicates that the equation system is close to being singular so that QR factorisation cannot be applied to obtain a solution.

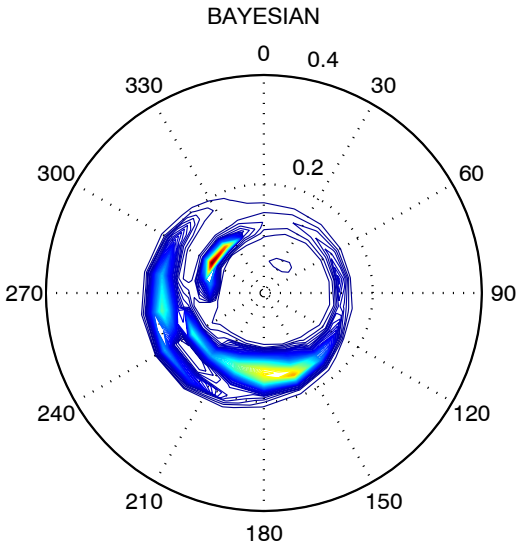

Figure 9.33: *Directional wave spectrum for the lowest value of the hyperparameter.*

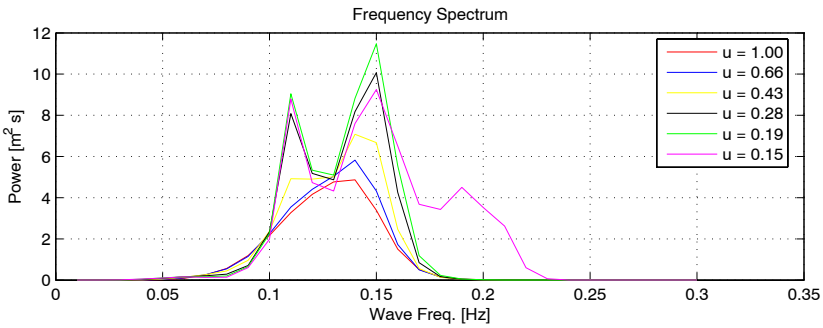

Figure 9.34: *The integrated frequency wave spectrum for different values of the hyperparameter.*

9.5.2 Discretisation

In order to solve for the directional wave spectrum, the wave field is discretised into a number of directions, K, and a number of wave frequencies, M, cf. Figure 3.4 in Chapter 3. In all of the estimations carried out so far in the present chapter, the wave field has been discretised into $K = 18$ directions and $M = 30$ wave frequencies. In Table 9.11 the variation of the wave parameters is seen for different setups of the discretisation for Data A. As it appears from

Table 9.11: *The sensitivity of the solution to the discretisation. The figures are based on Data A, and the numbers in bold correspond to the discretisation used in the preceding calculations.*

K	12			18			36		
M	20	30	60	20	30	60	20	30	60
H_s [m]	2.6	2.7	2.5	2.6	**2.7**	2.7	2.8	2.9	2.8
T_s [sec.]	8.2	8.0	8.1	7.8	**7.5**	7.4	7.9	7.5	7.5

the table, the solution is not particularly sensitive to the discretisation. Thus, it should be observed that no general trend is seen in the significant wave height or the mean wave period, neither by increasing the number of frequencies nor by increasing the number of directions, and, although not shown, the same applies to the directional distribution of energy. Based on this study, it is therefore considered as reasonable to use a discretisation corresponding to $K = 18$ and $M = 30$. Hence, the discretisation is fine enough to yield results which capture properties in both the directional and the frequency ranges and, at the same time, the solution is obtained fairly cheaply as regards CPU time; in the order of a couple of minutes with a 2.0GHz Pentium processor.

9.5.3 Normalisation

The normalisation of the equation system, cf. (3.95) and repeated here for the sake of completeness,

$$\begin{aligned} \widehat{C}_{ij}\left(\omega_e\right) &= \frac{C_{ij}(\omega_e)}{\sqrt{\frac{1}{2}\left[S_{ii}(\omega_e)S_{jj}(\omega_e)+C_{ij}(\omega_e)^2-Q_{ij}(\omega_e)^2\right]}} \\ \widehat{Q}_{ij}\left(\omega_e\right) &= \frac{Q_{ij}(\omega_e)}{\sqrt{\frac{1}{2}\left[S_{ii}(\omega_e)S_{jj}(\omega_e)-C_{ij}(\omega_e)^2+Q_{ij}(\omega_e)^2\right]}} \end{aligned} \tag{9.2}$$

has two functions: 1) it has the implication that for similar sets of data, e.g. Data A, Data B,..., Data I as studied in this chapter, the optimum hyperparameter assumes almost the same value in each set, which means a reduced calculation time of the optimal solution, and 2) it secures, at least theoretically, that none of the equations dominate the system, independently of the standard deviation of the underlying response.

As regards 1), the optimal hyperparameter assumes values varying between 0.20 and 0.25 for the nine data sets when the normalisation is applied to the equation system. On the contrary, the optimum values of the hyperparameter vary significantly, relatively to the interval just stated, when the normalisation is not applied. This is seen in Table 9.12, which shows both the optimal hyperparameter and the estimated wave parameters for the nine data sets, not taking into account the normalisation. The larger interval of optimal hyperparameters for

Table 9.12: *Estimated wave parameters and optimal hyperparameters for the case of a non-normalised equation system.*

Data	A	B	C	D	E	F	G	H	I
u^{optim}	0.05	0.05	0.04	0.02	0.33	0.08	0.58	0.13	0.16
H_s [m]	2.6	3.2	2.7	2.1	3.1	5.5	4.1	3.7	5.5
T_s [sec.]	7.4	6.8	6.7	7.2	11.0	7.0	11.8	10.9	13.6

the nine data sets means increased computational time in each of the considered data sets, since for the individual data set an estimated wave spectrum must be determined for a large range of values of the hyperparameter before the optimum solution can be sought for.

From Table 9.12 it should also be noted that the wave parameters vary slightly compared to the case of a normalised equation system, cf. Table 9.3. There is, however, no consistent trend whether the parameters from the non-normalised equation system are larger or smaller than the ones from the normalised system.

With respect to the response spectra, the normalisation involves an interesting aspect. Thus, as seen from (9.2), it should be noted that the real (mathematically speaking) diagonal response spectra, i.e. the heave-heave, the roll-roll and the pitch-pitch, are all normalised to 1, which implies point 2) above. Hence, the estimated response spectra may also be calculated from the directional wave spectrum by multiplication by a normalised coefficient matrix, cf. (7.6) in Chapter 7, so that a comparison could be made to reveal how well the estimated response spectra approximate 1. For Data A such normalised response spectra are seen in Figure 9.35 (note that the term 'normalised' in this context has nothing to do with the equation system). With respect to the cut-off frequencies, these are determined so that none of the non-normalised response spectra have values less than 5% of the smallest maximum value of the three responses in between the two frequencies. That is, only response values above a certain noise-level is taken into account.

The spectra seen in Figure 9.35 should, theoretically, vary around the value of 1. By integration of the normalised response spectra S_{norm}, the average value of each spectra are calculated as

$$\frac{1}{f_{max} - f_{min}} \int_{f_{min}}^{f_{max}} S_{norm}(f) df \tag{9.3}$$

and in Table 9.13 average values are shown for all data sets.

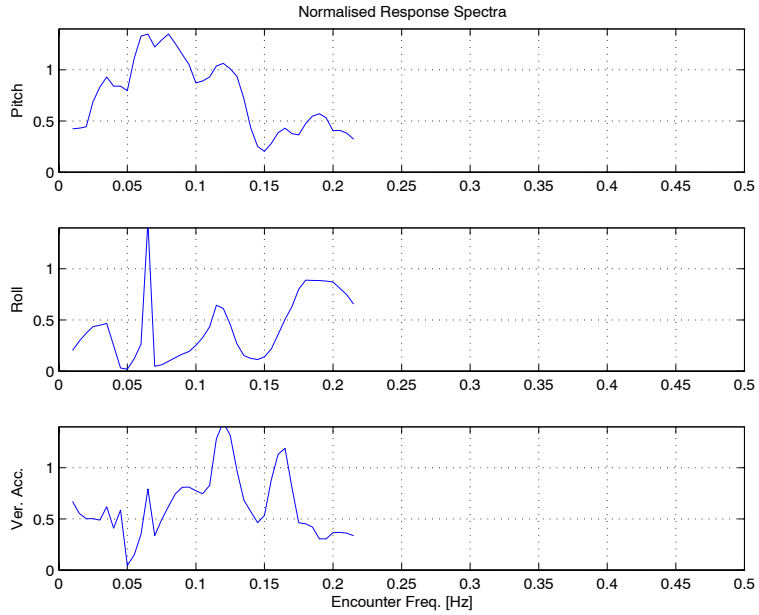

Figure 9.35: *Normalised response spectra (Data A).*

Table 9.13: *Average values of the normalised estimated response spectra.*

Data	A	B	C	D	E	F	G	H	I
Heave	0.74	0.77	0.71	0.63	0.80	0.77	0.66	0.60	0.60
Roll	0.42	0.33	0.30	0.43	0.64	0.44	0.55	0.54	0.29
Pitch	0.63	0.67	0.69	0.67	0.42	0.54	0.33	0.50	0.45

The agreement with the theoretical value 1 is not impressive and it should be noted that all the numbers for the individual sets of data are less than 1. This fact contradicts the central idea in the Bayesian modelling, where the errors are supposed to be equally distributed.

The present analysis does, basically, not reveal other aspects than those already seen in Section 9.4. However, it could be interesting to see if the relatively poor agreement between the measured and the estimated response spectra has to do with the normalisation of the equation system. In Figure 9.36 the response spectra for Data A are therefore plotted in the case of a non-normalised equation system, i.e. without application of (9.2). Somewhat surprisingly it is seen that, compared to the case of a normalised equation system, cf. Figure 9.7, the estimated response spectra approximate the measured ones better (except for the roll response) in the present case; the case of a non-normalised equation system. In Appendix F similar plots to those seen in the figures in Section 9.3, are shown for the optimal solutions to the non-normalised equation systems for Data A - Data I. From the figures it is revealed that the directional distribution of energy in the wave spectra is more or less identical to the cases of a normalised equation system. As regards the response spectra, there seems to be a slightly better agreement between the estimated and the measured spectra (except for

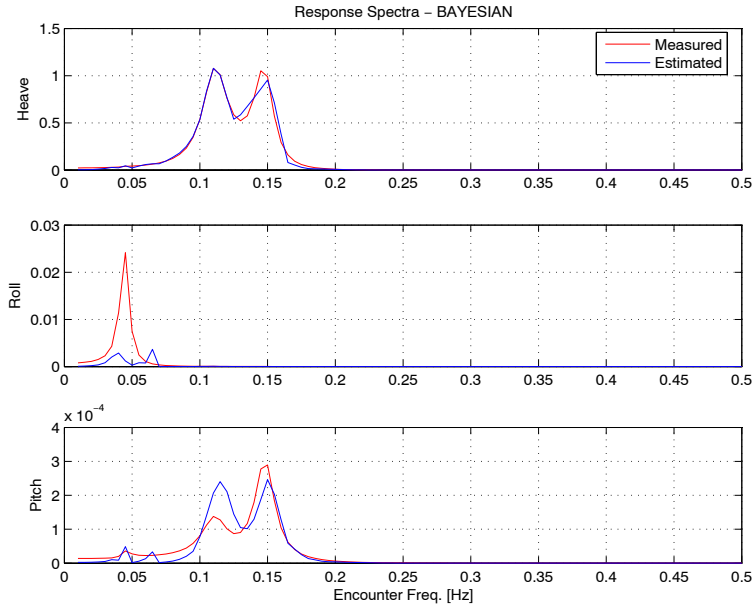

Figure 9.36: *Response spectra calculated without normalising the equation system. Units:* Heave [m^{2}s], Roll [rad^{2}s], Pitch [rad^{2}s]

the roll motion) for cases without the normalisation given by (9.2).

For the specific full-scale data studied in this chapter it thus seems to be just as good to obtain the solution without applying the normalisation (9.2). Seen from a more general perspective, the normalisation is, however, believed to be advantageous due to its influence on the optimum hyperparameter, as mentioned in point 1) above, and since the normalisation implies a dimensionless equation system. Furthermore, with respect to the poor agreement between the measured and the estimated response spectra, it may also be a special case for the full-scale data analysed in the present chapter, since no problems of this nature were seen for the full-scale data of the Shioji-Maru studied in Chapter 8. Thus, in addition to that chapter, Table 9.14 and Section E.2 in Appendix E show that the normalised estimated response spectra for the Shioji-Maru are close to the theoretical value 1 and, moreover, with a somewhat equal distribution of the errors.

Table 9.14: *Average values of the normalised estimated response spectra for the Shioji-Maru.*

Data	A	B	C	D
Pitch	1.23	1.02	1.25	1.18
Roll	1.05	1.12	1.07	1.06
Ver. acc.	0.57	0.56	0.55	0.68

9.5.4 Sway versus Roll

In a previous section estimations were also carried out with the roll response replaced by the sway response. These estimations lead to the wave parameters presented in Table 9.5 and the figures shown in Section F.2 in Appendix F.

In relation to parametric estimations of wave spectra from motion measurements of FPSOs, Tannuri et al. (2003) argues correctly that the roll motion, in general, has a non-linear and resonant behaviour and, furthermore, that the roll motion is extremely sensitive to load variations. Tannuri et al. (2003) and Pascoal et al. (2005) therefore propose to use the sway response instead of the roll, as the frequency response function of sway is less sensitive to loading conditions.

The present author will not argue against the above mentioned statements. However, it should be noted that, based on the estimations carried out in this thesis, it seems hard to justify whether the one response should be proposed in favour of the other. Thus, the roll and the sway based wave parameters deviate only slightly from each other, cf. Table 9.5, and with no consistent trend in the deviations when compared with the wave parameters estimated by WAVEX. Moreover, the directional distribution of energy is seen to be (almost) identical, although the sway based estimations, in contrast to the roll based estimations, have waves entering from both the port and the starboard side for Data G and H. Similarly, the main or the peak wave direction is observed to be equal for the roll based and the sway based cases for Data B, C and D, although with a more smooth directional distribution of energy for the roll based estimations. As regards the measured and the estimated response spectra, cf. Sections 9.3 and F.2, the sway based results yield an overall agreement similar to that seen for the roll based results. That is, the heave response spectrum is estimated relatively close to the measured spectrum in all the data sets, whereas for the sway and the pitch responses the agreement is rather poor in some of the cases. As a comment to the measured response spectra, which are based on the multivariate autoregressive procedure derived in Chapter 5, it should be remembered that, since the individual response is modelled by previous values of all the responses, cf. (5.2), slight deviations can be present in the measured response spectra for the individual data set (A, B, ..., I), dependent on if the roll or the sway response is taken into account.

In conclusion on the present analysis, a conclusive accedence to the proposal made by Tannuri et al. (2003) and Pascoal et al. (2005) cannot be made, as the present analysis does not directly confirm to utilise sway in favour of roll. It is, however, important to note that both of these studies were based on cases with zero forward speed which may have had an influence on the roll-versus-sway question.

In general, there are some important facts, though, which should be addressed when the question of sway vs. roll are discussed. Thus, in addition to the disadvantages of roll mentioned by Tannuri et al. (2003), the sway response may be well-approximated by assuming a linear relationship with the wave excitations. Moreover, the sway response is more broad-banded compared to roll. On the other hand, the sway response has no restoring term for

which reason the response can be difficult to calculate accurately. Hence, in summary and from a general point of view, the sway response may be considered better to use than roll as regards estimation of wave spectra based on ship responses.

9.6 Conclusions

In this chapter motion measurements of a container ship were analysed and based on the measured responses heave, roll and pitch, directional wave spectra were estimated by the Bayesian modelling procedure for nine sets of data. For all the sets of data, information on the wave spectra was also given by estimations from the wave radar system WAVEX.

In general, the agreement between the Bayesian and the WAVEX results was reasonable. Thus, it was seen that the wave parameters, as regards the significant wave height and the mean wave period, were estimated with a reasonable consistency in the individual sets of data. However, deviations were observed in some of the cases. These cases were all characterised by quite severe sea states, which means that the linear assumption between the wave excitations and the ship responses could be less good in these data sets. Hence, the Bayesian results may be badly influenced, since linearity is fundamental for the method to be reliable. With respect to the peak wave direction and the energy mean direction, the directional wave spectra for the Bayesian method and the WAVEX results revealed a satisfactory agreement, although two data sets showed deviations as regards of waves entering on the starboard side or the port side. A specific reason for the discrepancies could not be given, in particular, it was emphasised that the phase shift of the roll frequency response function is taken into account, since complex transfer functions are used. In the same connection, wave spectra were also estimated by replacing the roll response by the sway. No particular deviations or controversies were observed between the two cases.

The measured response spectra were approximated relatively poorly by using the estimated wave spectra, especially compared to what was seen in Chapter 8 for another set of full-scale measurements. With the focus on the Bayesian results, a specific reason could not be given for the less good agreement between the measured and the estimated response spectra.

This page is intentionally left blank.

Chapter 10

Conclusions and Recommendations

10.1 Conclusions

The objective of the present work has been to develop methods for estimating the directional wave energy spectrum on the basis of measured ship responses. From a survey and a study of literature on existing methods, a parametric and a non-parametric method were developed. The parametric method is based on a summation of a number of generalised JONSWAP spectra, whereas the non-parametric method estimates the directional wave spectrum in a number of discretised points of the wave field, which is divided into a set of frequencies and, as well, a set of directions. For both methods, linear spectral analysis is applied to the motion measurements to set up equations from which the wave energy spectrum may be determined.

As the primary interest of estimation of on-site directional wave spectra is in decision support systems for safe navigation of ships, it is paramount that all procedures and methods are automated. Hence, the cross spectral analysis is performed by use of multivariate autoregressive (MAR) procedures, which facilitate an automatic and optimal determination of the cross spectra of the responses. In the work, a detailed derivation of two MAR procedures was carried out.

In the thesis, focus was put on the non-parametric estimation method, called the Bayesian estimation method, or just the Bayesian method. The method is based on Bayesian procedures and has as its only assumption about the directional wave spectrum that the spectrum is smoothly changing in both the frequency and the directional range. In order to verify and study the method in detail, analyses of simulated data and full-scale data were conducted.

The analysis of simulated data can be summarised by the following points:

- From a theoretically known wave spectrum, ship responses were generated.

- Based on the generated ship responses, the Bayesian method was capable of yielding a nearly perfect estimate of the underlying wave spectrum.
- As a result of the good estimation of the wave spectrum, the 'measured', i.e. the generated, response spectra could be approximated with very good agreement.
- Problems in relation to following (quartering) waves were not observed.

As regards full-scale data, data sets from two different ships were investigated. For one ship, the Shioji-Maru, a research and training vessel, motion measurements of the pitch and the roll motions and the vertical acceleration at FP were recorded during four test trials and formed the basis of the estimations of wave spectra. Similarly, for the other ship, a container ship, measurements of the heave, the roll and the pitch motions during crossings on the Pacific Ocean were used for estimation of directional wave spectra. Unfortunately, neither of the data sets for the ships included conclusive evidence on the true on-site directional wave spectra in any of the cases. Thus, comparisons of the wave parameters were made with visual observations and with estimations from the wave radar system WAVEX for the Shioji-Maru and the container ship, respectively.

For the analysed full-scale data of the Shioji-Maru, the conclusions to be drawn are

- Compared to visual observations, as regards the wave period and the wave propagation, good agreement was seen for the estimated wave parameters.
- In general, the wave height was estimated on the lower side compared to the observations. Discrepancies were explained partly by uncertainties in the measurements and partly by the influence of the frequency response functions.
- In cases of low-frequency excitations (in following waves), the Bayesian method had difficulties in 'capturing' the wave energy.
- Based on the estimated wave spectra, the measured response spectra were well-approximated by multiplication with the linear complex-valued transfer functions.

For the container ship, the following points should be noted:

- Nine data sets were analysed by the Bayesian estimation method and for all the data sets, estimations of the wave spectra were also in hand from WAVEX.
- With respect to the significant wave height and the mean wave period reasonable agreement was observed for the cases characterised by the lowest sea states. For the severer sea states less good agreement was seen.

- Although the peak wave direction and the energy mean direction were estimated relatively consistently by the Bayesian method and by WAVEX, two data sets revealed a controversy in the wave propagation of the two methods. A specific reason for the controversy in wave propagation could not be given.
- Estimations of the wave spectra were also conducted by use of the sway response instead of the roll. No significant deviations were observed between the two cases.
- Due to lack of redundancy in the data, it was not settled which estimations – the ones from WAVEX or the ones from the Bayesian method – if any, were the correct ones.
- As regards the response spectra, the estimated spectra, based on the Bayesian estimation, approximated the measured spectra less good in some cases. For the WAVEX estimations, similar comparisons were observed.
- For the Bayesian-estimated response spectra, the use of a normalised versus a non-normalised equation system was investigated. Although a slightly better agreement was seen for the results based on the non-normalised equations for the specific data, it is in general recommended to use a normalised equation system.

With the focus on specific full-scale data in the preceding, the overall conclusions of the present work are

- The Bayesian estimation method is capable of estimating directional wave spectra from measured ship responses.
- The accurateness of the frequency response functions is of utmost importance to obtain reliable estimations of the wave spectra.
- It is paramount that at least one of the responses has an asymmetric frequency response function with respect to port/starboard entering waves. It is understood here that complex-valued transfer functions are utilised, so that the amplitude as well as the phase of the responses are reflected by the frequency response function.
- The present analysis did not suggest to use the roll response in favour of the sway response, or vice versa. However, in general the sway response has properties which may be preferred compared to the properties of the roll response.
- As a result of insensitivity to low- and high-frequency wave excitations, different hydrodynamically designed ships, the responses of which are recorded for decision support, may estimate different directional wave spectra, even for the same wave-environmental and operational conditions.
- Reasonable agreement has been observed for the Bayesian estimation method when estimated wave parameters and directional distributions of energy have been compared with visual observations and results from a wave radar system.

- Problems in relation to the agreement between the measured response spectra and the estimated response spectra have been observed in certain cases. A specific explanation for the problems could not been given.
- From sensitivity analyses it has been investigated how different parameters and conditions influence the estimated directional wave spectrum. The weighting of the considered responses and the so-called hyperparameter are of importance to the solution. A refinement of the discretisation of the wave field is, however, less important.

10.2 Recommendations for Future Work

The Bayesian estimation method in itself may be improved and, from a more general point of view, recommendations for future means of or methods for estimation of directional wave spectra can also be suggested.

10.2.1 The Bayesian Estimation Method

As regards the Bayesian method, conclusive evidence on its reliability is difficult to obtain from full-scale measurements. Detailed and comprehensive model-scale experiments would therefore be interesting to analyse. Based on such experiments with the operational conditions, the frequency response functions and the wave spectrum known exactly, the reliability of the method could be verified and, furthermore, certain characteristic parameters to tune the method in order to improve the accuracy might be found.

Due to computational costs, only one hyperparameter has been introduced to weight the prior distributions. In reality, each of the prior distributions, i.e. smoothing in the frequency, smoothing in the directions, and weighting of the minimisation at the boundaries, should be related to its own hyperparameter. By development of more efficient mathematical procedures for determination of the optimal solution (or by utilisation of the increasing power of computers), a number of hyperparameters might, thus, be included.

In the method, both the wave excitations and the ship responses are assumed to be stationary stochastic processes. This assumption is reasonable for the wave excitations for relatively short periods of time and, as well, for the ship responses when the operational conditions (speed, course, trim, ...) are held constant. For changing operational conditions, the ship responses should, however, be considered as non-stationary stochastic processes. This implies that means of doing time-varying cross spectral analysis and estimation of wave spectra ought to be introduced. Recently, Iseki (2004) has suggested an extended method, based on time-varying vector autoregressive (TVVAR) coefficient modelling, e.g. Kitagawa and Gersh (1985) and Jiang and Kitagawa (1993), to include time-varying estimation of wave spectra. Seen from a theoretical point of view, the methodology is very interesting but at

the same time the method is also relatively expensive as regards CPU time. Therefore, more efficient solution procedures need to be established, cf. Iseki (2004), before implementation of a time-varying method should be considered in connection with decision support systems. Moreover, with respect to practical application, it is probably possible for the ship's officers to keep the operational conditions (nearly) constant in periods of 5 to 20 minutes, so that the ship responses are stationary during the time of data recording for the estimation of the wave spectrum.

With respect to the non-negativity constraint, cf. (3.19), which assures spectral values greater than zero, it should be noted that Pascoal et al. (2005) proposes another coordinate transformation based on $\mathbf{f}(\mathbf{x}) = \mathbf{x}^2$ due to reported numerical problems with (3.19). Such problems have not been observed by the present author, but it is worth noting, as mentioned by Pascoal et al. (2005), that the search in $\mathbf{x}$ will be restrained to either positive or negative values for the transformation $\mathbf{f}(\mathbf{x}) = \mathbf{x}^2$. Hence, this transformation could be likely to reduce the computational time of the solution for which reason it would be interesting to implement.

10.2.2 Estimations of Wave Spectra

For non-parametric estimation methods based on a discretisation of the wave field with respect to frequency and direction, the fundamental equation system will in general be underdetermined, which results in an unstable and/or unrealistic solution. In the present work, and similar work in the literature, the introduction of a probabilistic viewpoint – in the sense of Bayesian modelling – secures a stable solution. A more direct approach without the stochastic point of view for estimation of directional wave spectra would therefore be interesting to investigate. Unfortunately, the author has no specific ideas of the basis of such an approach, nor has the literature, for which reason efforts should be put in future work to come up with means or methods for estimation of wave spectra not relying on the probabilistic viewpoint.

As regards in-service monitoring systems, these usually offer several numbers of ship responses to be monitored. In the event of an integrated estimation method of wave spectra there would therefore, basically, be the same number of responses to base the estimation on. However, as mentioned in Chapter 6, many studies indicate that three responses is advantageous to apply for the estimation. This means that some combination of responses may be better than others, depending on the given circumstances. Hence, at a very preliminary stage and maybe as a somewhat hypothetical thought, it has been considered if neural networks by some means could be applied to decide on which combination of responses would be optimal under given circumstances.

Parameterised wave spectra, such as the generalised JONSWAP, are typically considered reliable for describing the variation with frequency of ocean wave spectra. In the parametric method described in the present work and for similar methods described in the literature, the directionality of the waves is, however, restricted in area (i.e. frequencies and directions)

and predetermined in its shape. This is considered as a problem and it could therefore be interesting to do investigations by a combination of the non-parametric and the parametric estimation methods, so that the estimated wave spectra, frequency-wise, have properties from one or the summation of more parameterised wave spectra, whereas no restrictions would exist directional-wise on the estimated wave spectra.

References

(1987), *Proceedings of the 18th International Towing Tank Conference*, Kobe, Japan.

ADOPT (2005), ADOPT, the project's web site can be found at http://adopt.rtdproject.net.

Akaike, H. (1971), Autoregressive Model Fitting for Control, *Annals of the Institute of Statistical Mathematics*, 23:163–180.

Akaike, H. (1980), Likelihood and Bayes Procedure, in Bernado, J. M., Groot, M. H. D., Lindley, D. U. and Smith, A. F. M. (editors), *Bayesian Statistics*, pp. 143–166, University Press, Valencia.

Akaike, H. and Nakagawa, T. (1988), *Statistical Analysis and Control of Dynamic Systems*, KTK Scientific Publishers.

Aldworth, P. (editor) (1997), *Lloyd's Maritime Atlas*, LLP Ltd, Colchester, 19th edition.

Aschehoug, M. (2003), Scientific Paper on The Sea State Estimation Methodology, Technical report, SIREHNA, France, paper prepared in the HullMon+ project.

Aschim, A. (2002), Specification of Linear Motion Module in Active Operator System, Technical report, Det Norske Veritas AS, report 2002-1274.

Åström, K. (1970), *Introduction to Stochastic Control Theory*, Academic Press.

Atwater, R. (1990), Shipboard Wave Height Sensor, Technical report, Ship Structure Committee, report SSC-362.

Bendat, J. and Piersol, A. (2000), *Random Data - Analysis and Measurement Procedures*, John Wiley & Sons, Inc., 3rd edition.

Bhattacharyya, R. (1978), *Dynamics of Marine Vehicles*, John Wiley & Sons.

de Boer, C. (1979), *A Practical Guide to Splines*, Springer-Verlag.

Bollero, A., Pescetto, A. and Simone, S. (2004), Hull Stress Monitoring of Italian Navy's Frigate: Results After First Year Campaign, in *2nd Conference on Emerging Machinery and Structural Condition Monitoring Technologies for Defence Applications*, Halifax, Nova Scotia, Canada.

Borge, J., Gonzáles, R., Hessner, K., Reichert, K. and Soares, C. (2000), Estimation of Sea State Directional Spectra by Using Marine Radar Imaging of Sea Surface, in *Proceedings of ETCE/OMAE2000 Joint Conference*, New Orleans, Louisiana, USA.

Box, G. and Tiao, G. (1973), *Bayesian Inference in Statistical Analysis*, Addison-Wesley Publishing Company, 1st edition.

Brodtkorb, P., Johannesson, P., Lindgren, G., Rychlik, I., Ryden, J., Sjö, E. and Sköld, M. (2000), WAFO - a Matlab Toolbox for Analysis of Random Waves and Loads, the WAFO package can be downloaded freely on the internet.

Davison, A. (1986), Approximate Predictive Likelihood, *Biometrika*, 73:323–332.

Dean, R. and Dalrymple, R. (1991), *Water Wave Mechanics for Engineers and Scientists*, volume 2 of *Advanced Series on Ocean Engineering*, World Scientific.

Debord, F. and Hennessy, B. (1990), Development of a Generalized Onboard Response Monitoring System, Technical report, Ship Structure Committee, report SSC-349.

Denis, M. S. and Pierson, W. (1953), On the Motion of Ships in Confused Seas, *Trans. SNAME*, 61.

Dimri, V. (1992), *Deconvolution and Inverse Theory: Application to Geophysical Problems*, Elsevier.

Durbin, J. (1960), The Fitting of Time-series Models, *Review of the International Statistical Institute*, 28:233–244.

Ewans, K. (1998), Observations of the Directional Spectrum of Fetch-Limited Waves, *Journal of Physical Oceanography*, 28:495–512.

Ewans, K. and van der Vlugt, T. (1999), Estimating Bimodal Frequency-direction Spectra From Surface Buoy Data Recorded During Tropical Cyclones, *Journal of Offshore Mechanics and Arctic Engineering*, 121:172–180.

Farin, G. (1990), *Curves and Surfaces for Computer Aided Geometric Design*, Academic Press, 2nd edition.

Fisher, R. (1922), On the Mathematical Foundations of Theoretical Statistics, *Phil. Trans. Roy. Soc., Series A*, 222.

Folsø, R. (2004), *Comfort Optimization of High-speed Passenger Ferries*, Ph.D. thesis, Maritime Engineering, Department of Mechanical Engineering, Technical University of Denmark.

Francescutto, A. (1993), Is It Really Impossible to Design Safe Ships?, *Trans. RINA*, 135:163–168.

Goda, Y. (2000), *Random Seas and Design of Maritime Structures*, volume 15 of *Advanced Series on Ocean Engineering*, World Scientific.

Golub, G. and Loan, C. V. (1996), *Matrix Computations*, The John Hopkins University Press, 3rd edition.

Good, I. (1965), *The Estimation of Probablities*, M.I.T. Press.

Gran, S. (1992), A Course in Ocean Engineering, *Development in Marine Engineering*, 8.

Harrison, L., Penny, W. and Friston, K. (2003), Multivariate Autoregressive modeling of fMRI Time Series, *NeuroImage*, 19:1477–1491.

Hashimoto, N. (1997), Analysis of The Directional Wave Spectrum From Field Data, in Liu, P.-F. (editor), *Advances in Coastal and Ocean Engineering*, volume 3, pp. 103–143, World Scientific.

Hashimoto, N., Nagai, T. and Asai, T. (1994), Extension of the Maximum Entropy Principle Method for Directional Wave Spectrum Estimation, in *Proceedings of 24th ICCE*, pp. 232–246, Kobe, Japan.

Hasselmann, K. (1988), PIPs and POPs: The Reduction of Complex Dynamical Systems Using Principal Interaction and Oscillation Patterns, *Journal of Geophysical Research*, 93:11015–11021.

Herbers, T. and Guza, R. (1990), Estimation of Directional Wave Spectra from Multicomponent Observations, *Journal of Physical Oceanography*, 20:1703–1724.

Himmelblau, D. (1970), *Process Analysis by Statistical Method*, John Wiley & Sons.

Hogben, N. and Cobb, F. (1986), Parametric Modelling of Directional Wave Spectra, in *Proceedings of 18th Offshore Technology Conference*, Houston, Texas.

Hua, J. and Palmquist, M. (1994), Wave Estimation through Ship Motion Measurement, Technical report, Naval Architecture, Department of Vehicle Engineering, Royal Institute of Technology.

Huss, M. and Olander, A. (1994), Theoretical Seakeeping Predictions On Board Ships - A System for Operational Guidance and Real Time Surveillance, Technical report, Naval Architecture, Department of Vehicle Engineering, Royal Institute of Technology.

Hutchison, B. (1990), Seakeeping Studies: A Status Report, *Trans. SNAME*, 98:263–317.

Ientilucci, E. (2003), Using the Singular Value Decomposition, Technical report, Chester F. Carlson Center for Imaging Science, Rochester Institute of Technology.

Iseki, T. (1999), Estimation of Directional Wave Spectra Using Ship Motion Data, in Akaike, H. (editor), *The Practice of Time Series Analysis*, pp. 115–130, Springer-Verlag.

Iseki, T. (2004), Extended Bayesian Estimation of Directional Wave Spectra, in *Proceedings of 23rd Int. Conf. on Offshore Mechanics and Arctic Engineering (OMAE)*, Vancouver, Canada.

Iseki, T. and Ohtsu, K. (2000), Bayesian Estimation of Directional Wave Spectra Based on Ship Motions, *Control Engineering Practice*, 8:215–219.

Iseki, T., Ohtsu, K. and Fujino, M. (1992), A Study on Estimation of Directional Spectra Based on Ship Motions, *Journal of Japan Institute of Navigation*, 86:179–188.

Iseki, T. and Terada, D. (2002), Bayesian Estimation of Directional Wave Spectra for Ship Guidance Systems, *International Journal of Offshore and Polar Engineering*, 12:25–30.

Isobe, M., Kondo, K. and Horikawa, K. (1984), Extension of MLM for Estimating Directional Wave Spectrum, in *Proceedings of Symposium on Description and Modeling of Directional Seas*, volume A-6.

Jensen, J. (2001), *Load and Global Response of Ships*, volume 4 of *Elsevier Ocean Engineering Book Series*, Elsevier.

Jensen, J., Mansour, A. and Olsen, A. (2004), Estimation of Ship Motions Using Closed-form Expressions, *Ocean Engineering*, 31:61–85.

Jiang, X. and Kitagawa, G. (1993), A Time Varying Coefficient Vector AR Modeling of Nonstationary Covariance Time Series, *Signal Processing*, 33(3):315–331.

Kitagawa, G. and Gersh, W. (1985), A Smoothness Priors Time Varying AR Coefficient Modeling of Nonstationary Covariance Time Series, *IEEE Transaction on Automatic Control*, AC-30(1):48–56.

Kobune, K. and Hashimoto, N. (1986), Estimation of Directional Spectra from the Maximum Entropy Principle, in *Proceedings of 5th Int. Offshore Mechanics and Arctic Engineering (OMAE) Symposium*, pp. 80–85, Tokyo, Japan.

Lawson, C. and Hanson, R. (1974), *Solving Least Squares Problems*, Prentice Hall.

Lindemann, K. and Nordenstrøm, N. (1975), A System for Ship Handling in Rough Weather, in *Proceedings of Fourth Ship Control System Symposium*, volume 7, pp. 45–68, Royal Netherlands Naval College.

Lindemann, K., Odland, J. and Strengehagen, J. (1977), On the Application of Hull Surveillance Systems for Increased Safety and Improved Structural Utilization in Rough Weather, *Trans. SNAME*, 85:131–158.

Lloyd, A. (1998), *Seakeeping*, Ellis Horwood, 2nd edition.

Longuet-Higgins, M., Cartwright, D. and Smith, N. (1961), Observations of the Directional Spectrum of Sea Waves Using the Motions of a Floating Buoy, *Ocean Wave Spectra*, pp. 111–136.

Lütkepohl, H. (1985), Comparison of Criteria for Estimating the Order of a Vector Autoregressive Process, *Journal of Time Series Anal.*, 6:35–52.

Lütkepohl, H. (1993), *Introduction to Multiple Time Series Analysis*, Springer-Verlag, 2nd edition.

Marple, S. (1987), *Digital Spectral Analysis with Applications*, Prentice-Hall.

MatLab (2005), MatLab Help Tutorial, taken from MatLab R14.

Melitz, D., Robertson, E. and Davison, N. (1992), Performance Management of VLCCs - An Owner's Approach, *Society of Naval Architects and Marine Engineers, Marine Technology*, 29(4):250–262.

Mentz, R., Morettin, P. and Toloi, C. (1988), On Residual Variance estimation in Autoregressive Models, *Journal of Time Series Anal.*, 19:187–208.

MIROS (1998), WAVEX - Principles of Operation, technical documentation by MIROS.

Mitsuyasu, H., hansen, olsen and passer (1975), Observation of the Directional Spectrum of Ocean Waves Using a Cloverleaf Buoy, *Journal of Physical Oceanography*, 5:750–760.

Neumaier, A. and Schneider, T. (2001), Estimation of Parameters and Eigenmodes of Multivariate Autoregressive Models, *ACM Transactions on Mathematical Software*, 27(1):27–57.

Nielsen, J. (2004), SeaSense - Slut Rapport, Technical report, Force Technology, final report on the joint project SeaSense between Søværnets Materielkommando, DTU, Lyngsø Marine, Force Technology, and Maersk. (The report is in Danish.).

Nielsen, U. (2003), Analysis of Full Scale Data - Estimation of Wave Spectra, Technical report, Section of Maritime Engineering, MEK, Technical University of Denmark, data recorded during the joint project SeaSense.

Oda, H. and Shibuya, H. (1996), Deconvolution of Long-core Paleomagnetic Data of Ocean Drilling Program by Akaike's Bayesian Information Criterion Minimization, *Journal of Geophysical Research*, 101:2815–2834.

Oppenheim, A. and Schafer, R. (1989), *Discrete-Time Signal Processing*, Prentice-Hall.

Pascoal, R., Soares, C. and Sørensen, A. (2005), Ocean Wave Spectral Estimation Using Vessel Wave Frequency Motions, in *Proceedings of OMAE2005*, Halkidiki, Greece.

Pedersen, T. (2000), *Wave Load Prediction - a Design Tool*, Ph.D. thesis, Department of Naval Architecture and Offshore Engineering, Technical University of Denmark.

Penny, W. (2000), Signal Processing Course, lecture notes, Course offered at the Department of Imaging Neuroscience, University College London.

Penny, W. and Roberts, S. (2002), Bayesian Multivariate Autoregressive Models with Structured Priors, *IEE Proceedings on Vision, Image and Signal Processing*, 149(1):33–41.

Press, W., Flannery, B., Teukolsky, S. and Vetterling, W. (1992), *Numerical Recipes in FORTRAN77: The Art of Scientific Computing*, Cambridge University Press, 2nd edition.

Price, W. and Bishop, R. (1974), *Probalistic Theory of Ship Dynamics*, Chapman and Hall.

Rabiner, L. and Gold, B. (1975), *Theory and Application of Digital Signal Processing*, Prentice-Hall.

Reichert, K., Borge, J. and Dittmer, J. (1998), WaMos II: An Operational Wave Monitoring System, in *Proceedings - Oceanology International '98*, Brighton, UK.

Robinson, D. (1990), Voyage Data Recorders - Operating with Safety and Efficiency, in *Proceedings of IMAS90: Marine Technology and the Environment*, London, Institute of Marine Engineers.

Salvesen, N., Tuck, E. and Faltinsen, O. (1970), Ship Motions and Sea Loads, *Trans. SNAME*, 78:250–287.

Schneider, T. and Neumaier, A. (2001), Algorithm 808: ARfit - A Matlab Package for the Estimation of Parameters and Eigenmodes of Multivariate Autoregressive Models, *ACM Transactions on Mathematical Software*, 27(1):58–65.

SeaSense (2003), SeaSense, a joint Danish project between Søværnets Materielkommando, DTU, Lyngsø Marine, Force Technology, and Maersk. A research project concerning a specific in-service monitoring system for decision support.

Shioji-Maru (2004), Data recorded in Tateyama Bay, Japan, the data has kindly been offered by the Tokyo University of Marine Science and Technology. The data originates from the research and training ship Shioji-Maru.

Shun, Z. and McCullagh, P. (1995), Laplace Approximation of High Dimensional Integrals, *Journal of Royal Statistical Society*, 57:749–760.

Slaughter, S., Cheung, M., Sucharski, D. and Cowper, B. (1997), State of the Art in Hull Monitoring Systems, Technical report, Ship Structure Committee, report SSC-401.

Strang, G. (1986), *Introduction to Applied Mathematics*, Wellesley-Cambridge Press.

Strip-calculations (2004), 2-D Strip Calculations, the calculations were carried out at the Tokyo University of Marine Science and Technology by Associate Professor Toshio Iseki.

Tannuri, E., Sparano, J., Simos, A. and Cruz, J. D. (2003), Estimating Directional Wave Spectrum Based on Stationary Ship Motion Measurements, *Applied Ocean Research*, 25:243–261.

Tarantola, A. (1987), *Inverse Problem Theory: Methods for Data Fitting and Model Parameter Estimation*, Elsevier.

Tjøstheim, D. and Paulsen, J. (1983), Bias of Some Commonly Used Time Series Estimates, *Biometrika*, 70:389–399.

Vonesh, E. (1996), A Note on the Use of Laplace's Approximation for Nonlinear Mixed-effects Models, *Biometrika*, 83:447–452.

Waals, O., Aalbers, A. and Pinkster, J. (2002), Maximum Likelihood Method as a Means to Estimate The Directional Wave Spectrum and The Mean Wave Drift Force on a Dynamically Positioned Vessel, in *Proceedings of OMAE2002*, Oslo, Norway.

Webster, W. and Dillingham, J. (1981), Determination of Directional Seas From Ship Motions, in *Proceedings of Directional Wave Spectra Application '81*, Berkeley, CA.

Welch, P. (June 1967), The Use of Fast Fourier Transform for the Estimation of Power Spectra: A Method Based on Time Averaging Over Short, Modified Periodograms, *IEEE Trans. Audio Electroacoust.*, AU-15:70–73.

Whittle, P. (1963), On the Fitting of Multivariate Autoregressions, and the Approximate Canonical Factorization of a Spectral Density Matrix, *Biometrika*, 50:129–134.

Witmer, D. and Lewis, J. (1994), Operational and Scientific Hull Structure Monitoring on TAPS Trade Tankers, *Trans. SNAME*, 102:501–533.

This page is intentionally left blank.

Appendix A

Transfer Functions

A.1 Introduction

The present appendix shows the frequency response functions of the two ships, the responses of which were dealt with in the thesis. Due to confidentiality, no specifications can be given for the hydrodynamical data of the containership. It should be mentioned that all the plots illustrate the amplitude of the frequency response functions, as these are complex functions that can be represented by an amplitude and a phase angle. As regards the encounter angle, this is given so that head waves correspond to 180 deg.

A.2 The Shioji-Maru

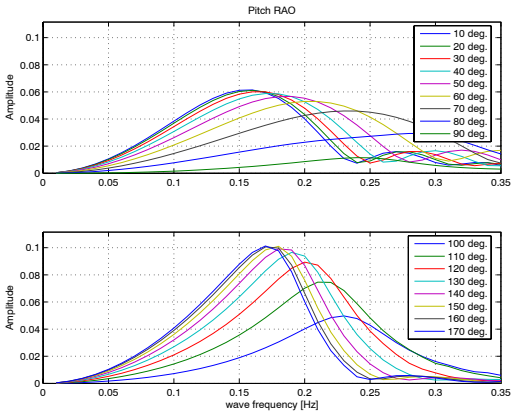

Figure A.1: *Amplitudes of the RAO for pitch.* $V = 7.0 knots$

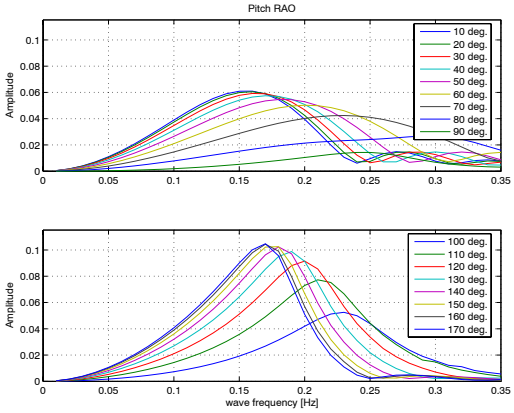

Figure A.2: *Amplitudes of the RAO for pitch.* $V = 8.5 knots$

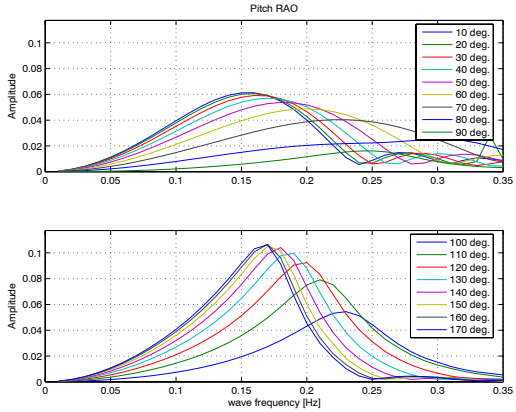

Figure A.3: *Amplitudes of the RAO for pitch.* $V = 9.5knots$

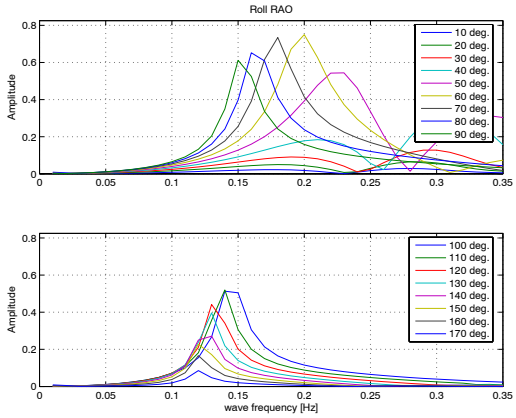

Figure A.4: *Amplitudes of the RAO for roll.* $V = 7.0knots$

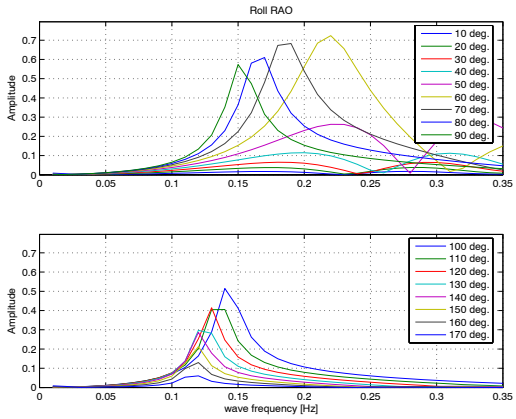

Figure A.5: *Amplitudes of the RAO for roll.* $V = 8.5knots$

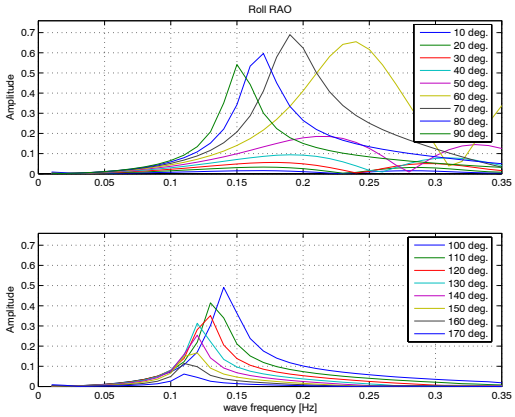

Figure A.6: *Amplitudes of the RAO for roll.* $V = 9.5knots$

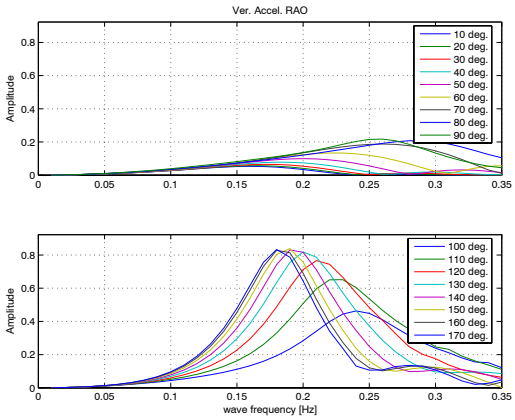

Figure A.7: *Amplitudes of the RAO for the vertical acceleration at FP.* $V = 7.0knots$

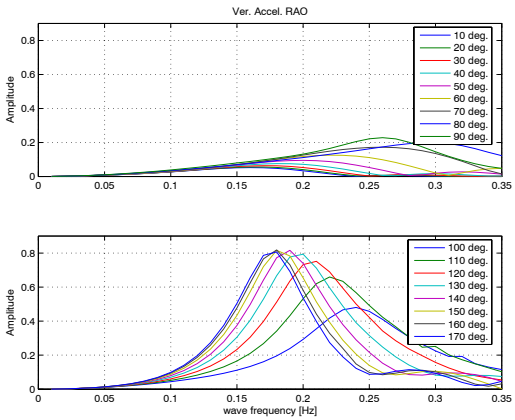

Figure A.8: *Amplitudes of the RAO for the vertical acceleration at FP.* $V = 8.5knots$

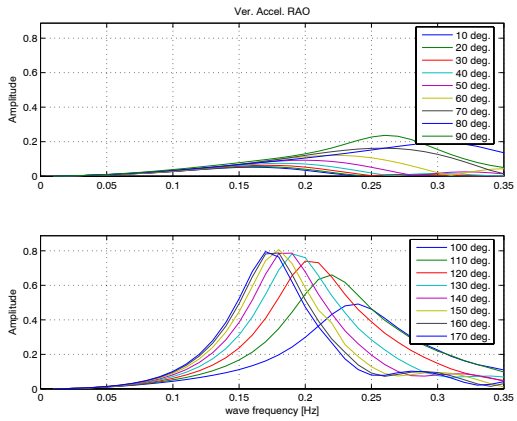

Figure A.9: *Amplitudes of the RAO for the vertical acceleration at FP.* $V = 9.5 knots$

A.3 The Container Ship

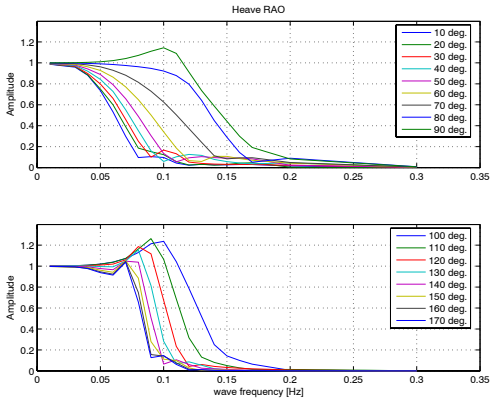

Figure A.10: *Amplitudes of the RAO for heave. Set 1.*

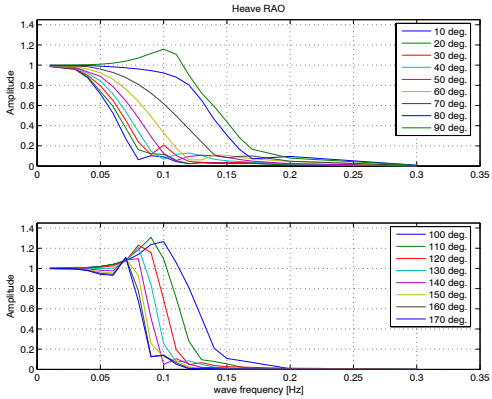

Figure A.11: *Amplitudes of the RAO for heave. Set 2.*

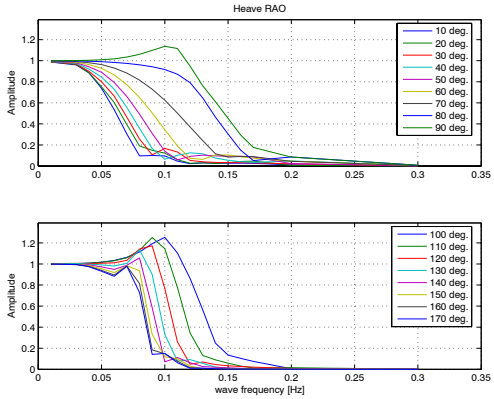

Figure A.12: *Amplitudes of the RAO for heave. Set 3.*

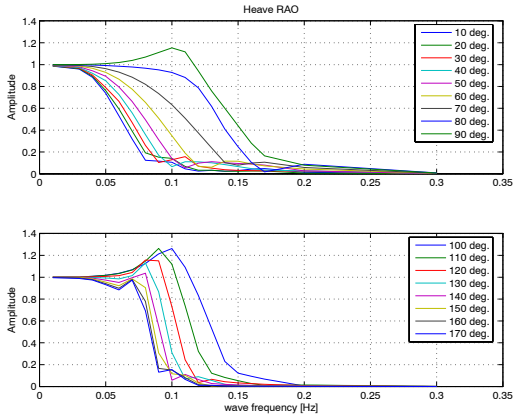

Figure A.13: *Amplitudes of the RAO for heave. Set 4.*

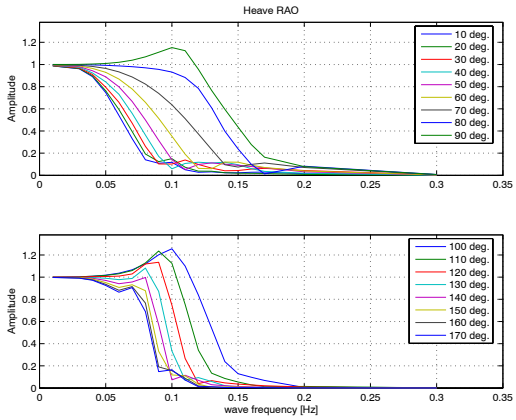

Figure A.14: *Amplitudes of the RAO for heave. Set 5.*

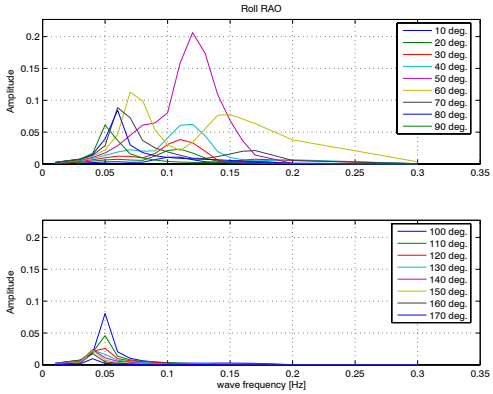

Figure A.15: *Amplitudes of the RAO for roll. Set 1.*

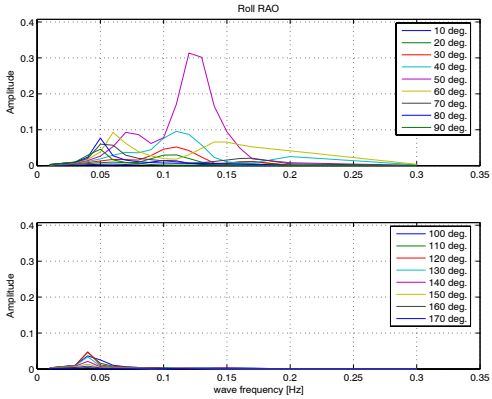

Figure A.16: *Amplitudes of the RAO for roll. Set 2.*

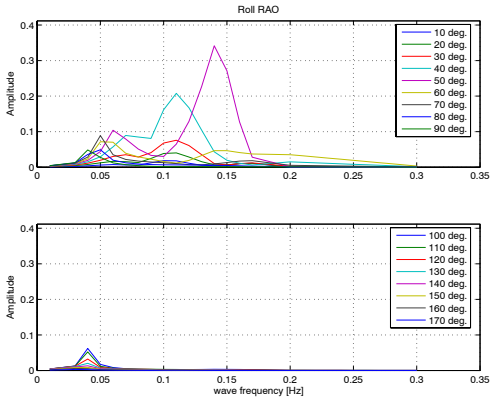

Figure A.17: *Amplitudes of the RAO for roll. Set 3.*

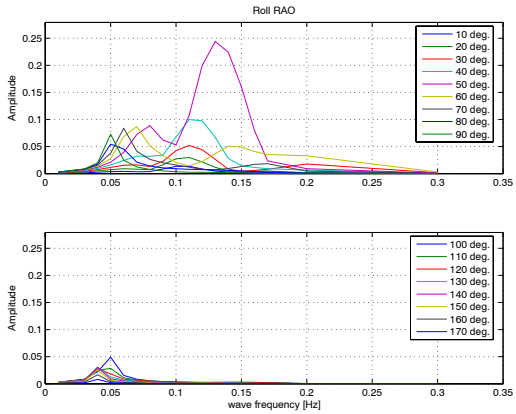

Figure A.18: *Amplitudes of the RAO for roll. Set 4.*

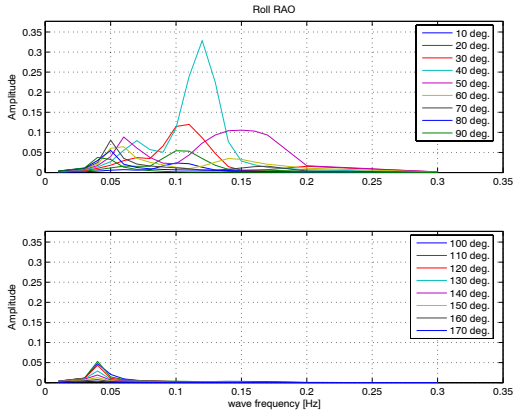

Figure A.19: *Amplitudes of the RAO for roll. Set 5.*

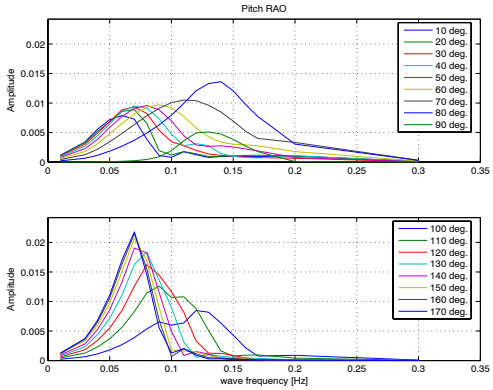

Figure A.20: *Amplitudes of the RAO for pitch. Set 1.*

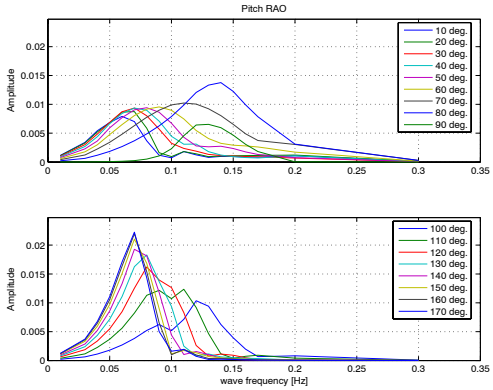

Figure A.21: *Amplitudes of the RAO for pitch. Set 2.*

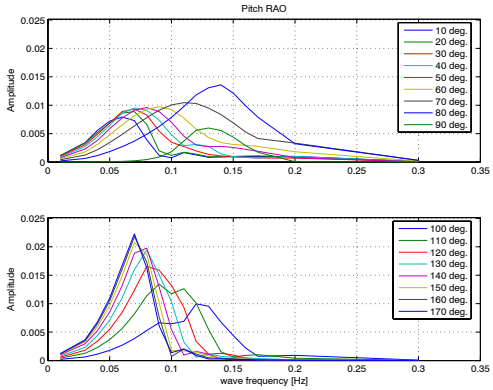

Figure A.22: *Amplitudes of the RAO for pitch. Set 3.*

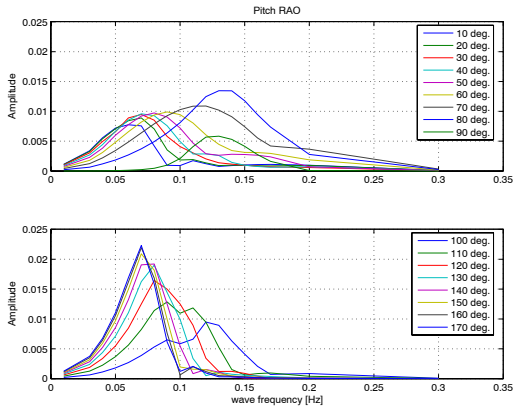

Figure A.23: *Amplitudes of the RAO for pitch. Set 4.*

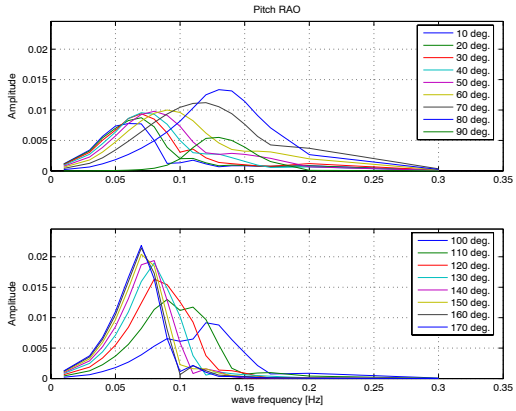

Figure A.24: *Amplitudes of the RAO for pitch. Set 5.*

This page is intentionally left blank.

Appendix B

Time Series

B.1 Introduction

The data sets which were analysed in Chapters 8 and 9 stem from motion measurements of different ship responses. Specifically, these measurements are recorded as time histories of the pitch, the roll and the vertical acceleration at FP for the Shioji-Maru, and as time histories of the heave, the roll and the pitch motions for the container ship. In the following pages, the time histories are visualised for each of the analysed data sets. It should be noted that the time series of the container ship illustrate periods of 30 minutes, although the specific acquisition times used for the estimations are 15 minutes and taken in the middle of the 30 minutes periods.

B.2 The Shioji-Maru

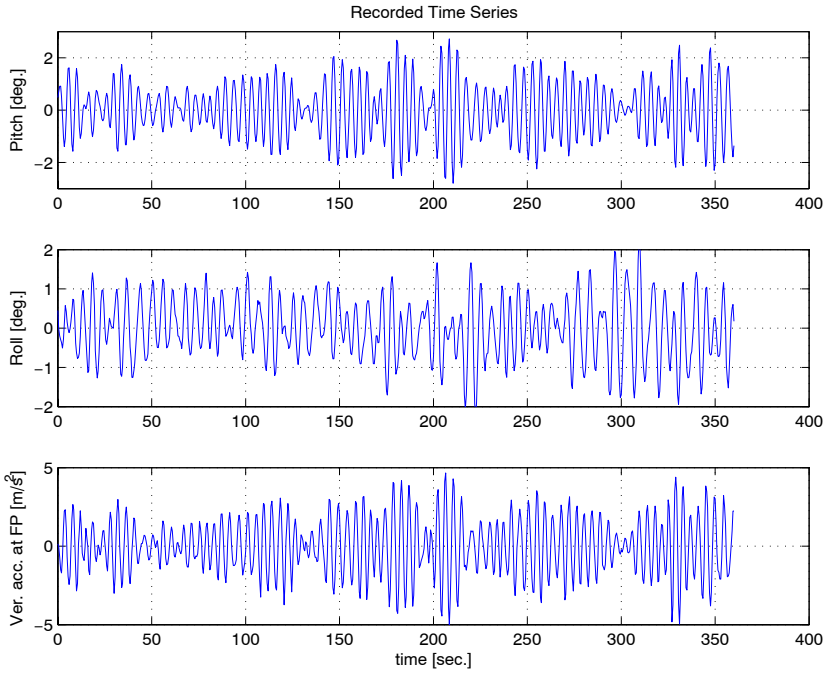

Figure B.1: *Time series for the responses of Data A.*

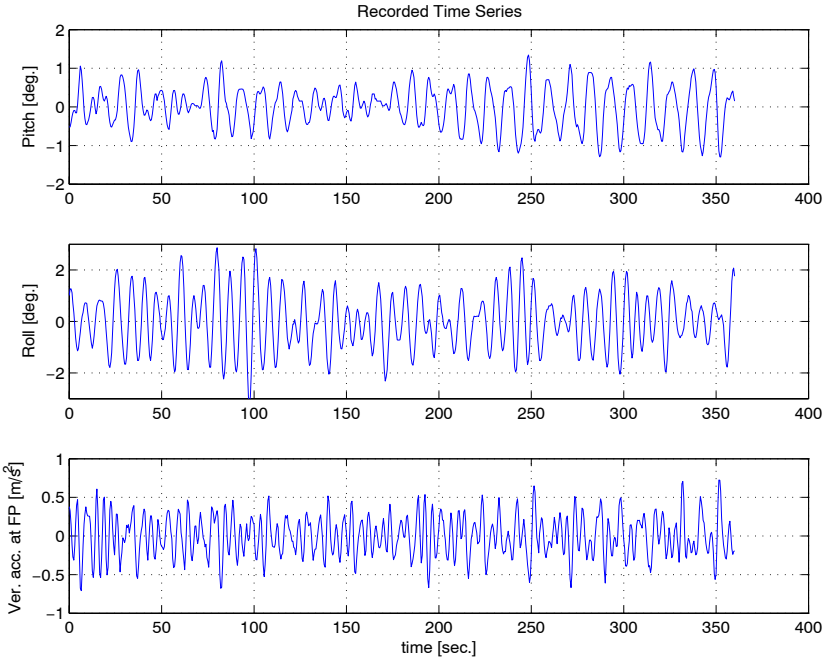

Figure B.2: *Time series for the responses of Data B.*

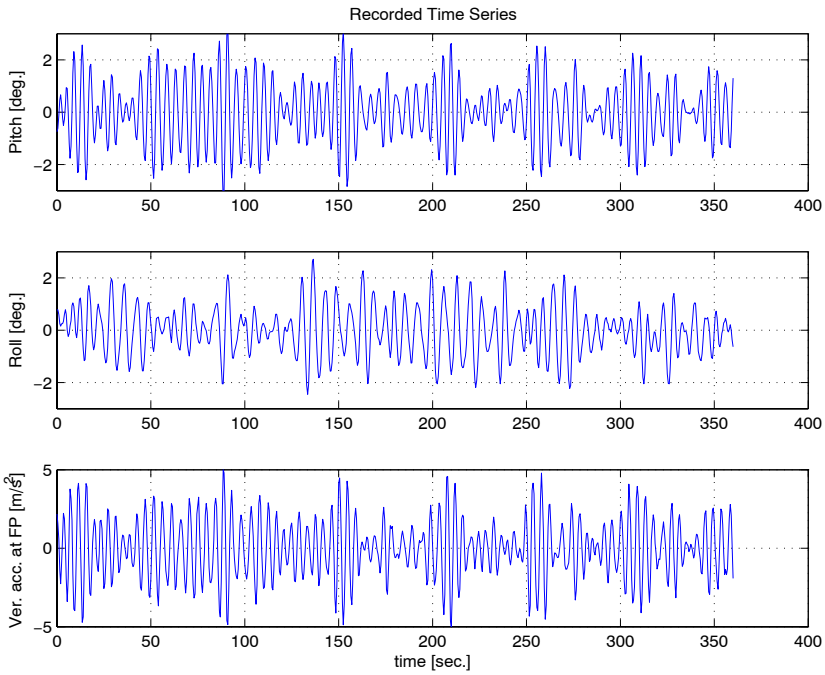

Figure B.3: *Time series for the responses of Data C.*

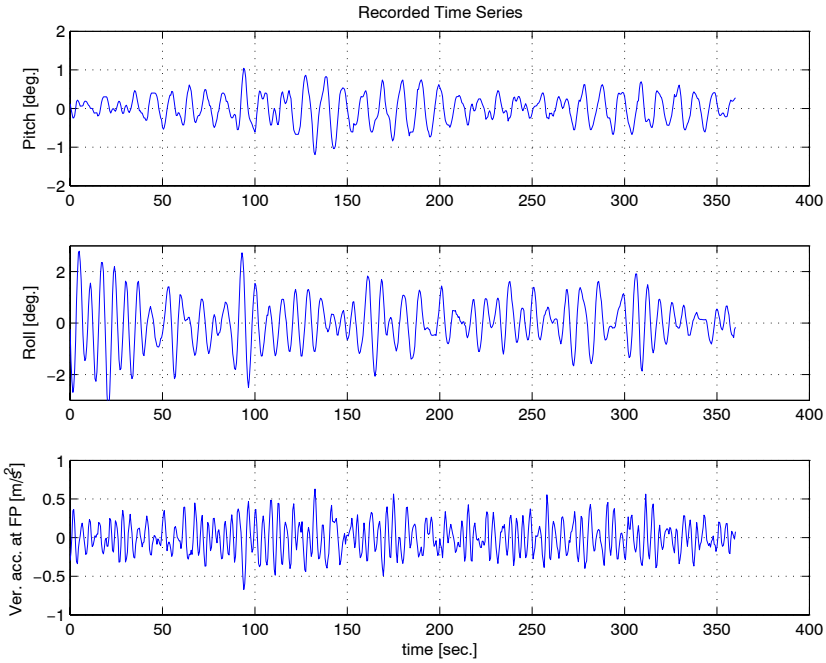

Figure B.4: *Time series for the responses of Data D.*

B.3 The Container Ship

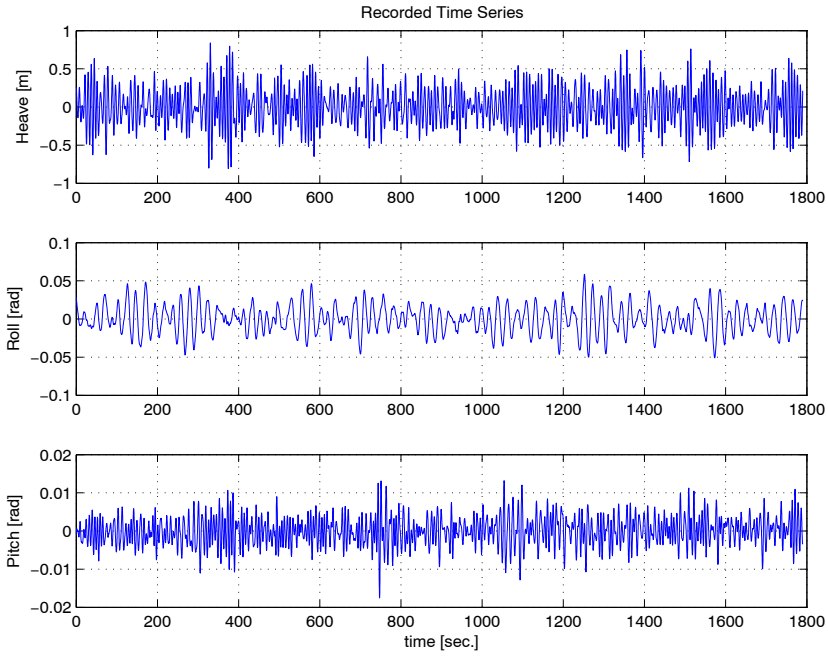

Figure B.5: *Time series for the responses of Data A.*

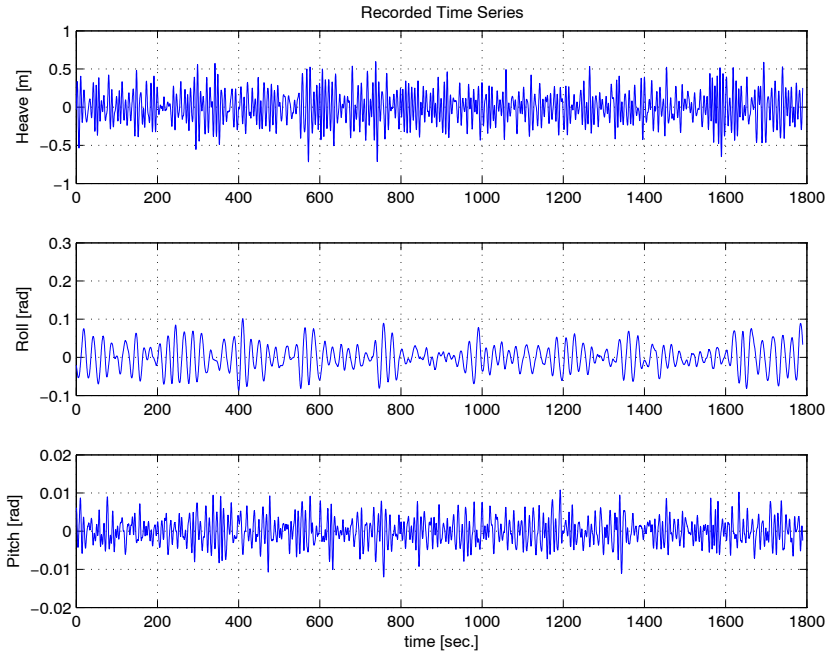

Figure B.6: *Time series for the responses of Data B.*

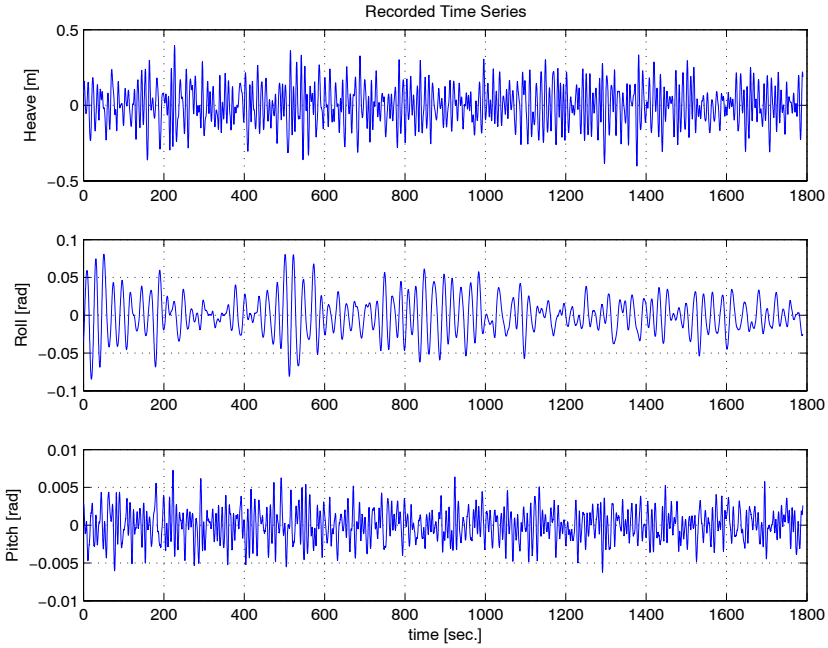

Figure B.7: *Time series for the responses of Data C.*

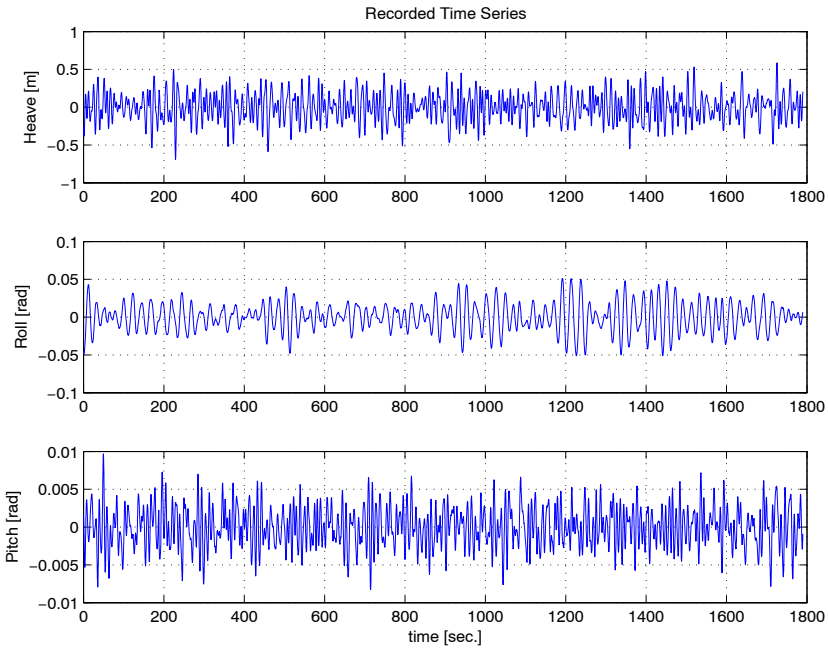

Figure B.8: *Time series for the responses of Data D.*

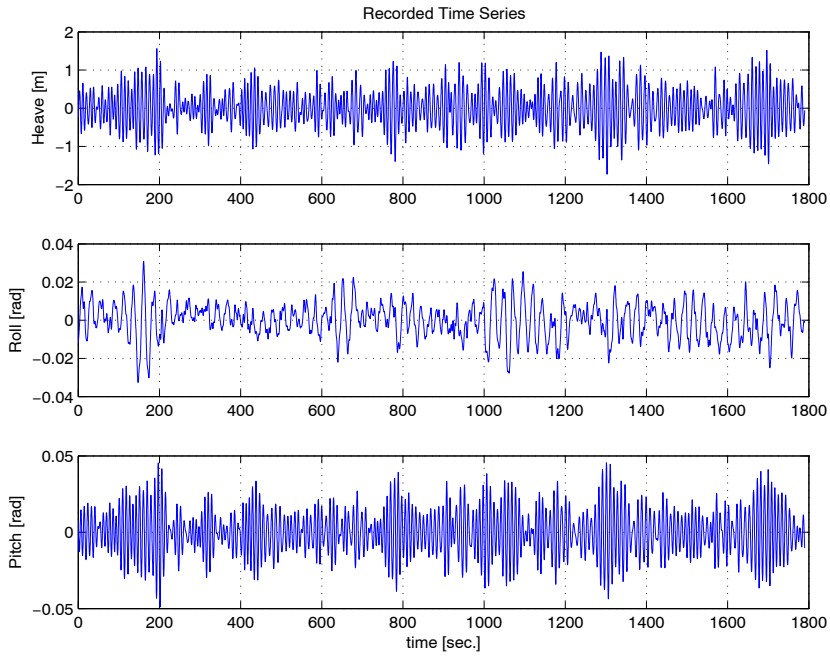

Figure B.9: *Time series for the responses of Data E.*

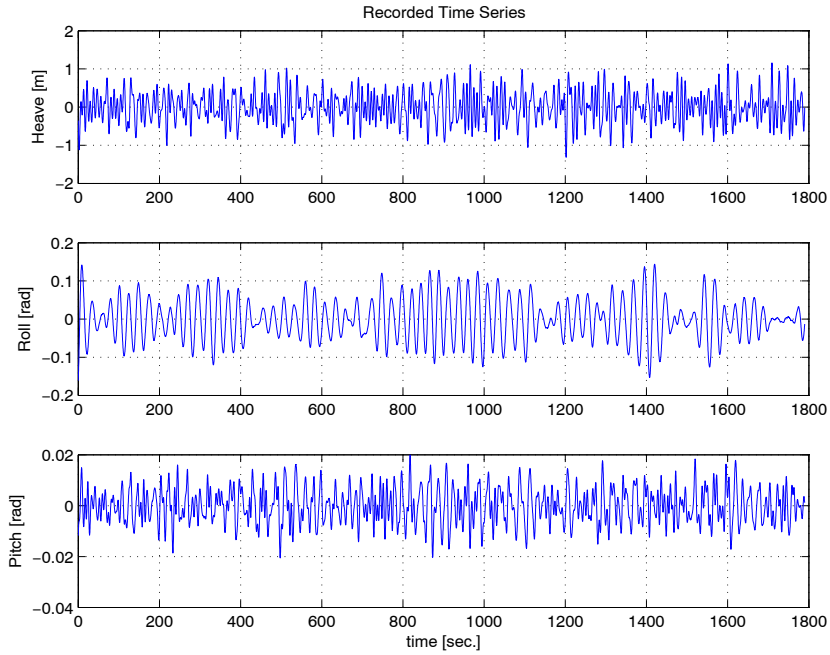

Figure B.10: *Time series for the responses of Data F.*

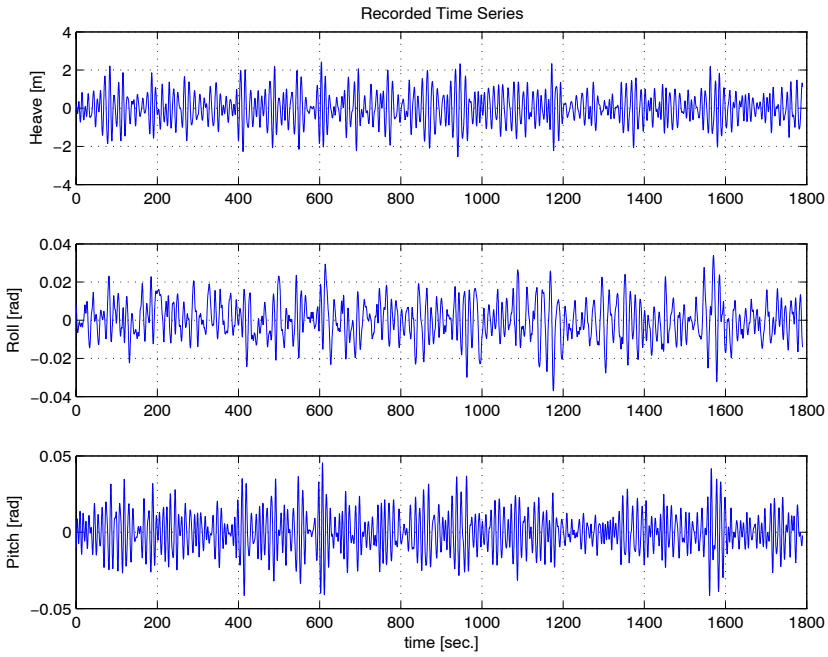

Figure B.11: *Time series for the responses of Data G.*

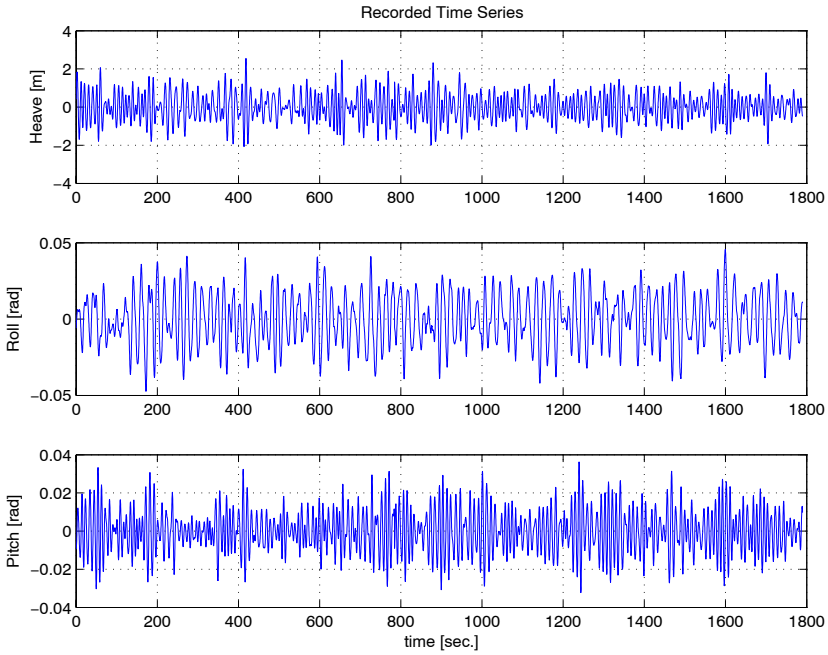

Figure B.12: *Time series for the responses of Data H.*

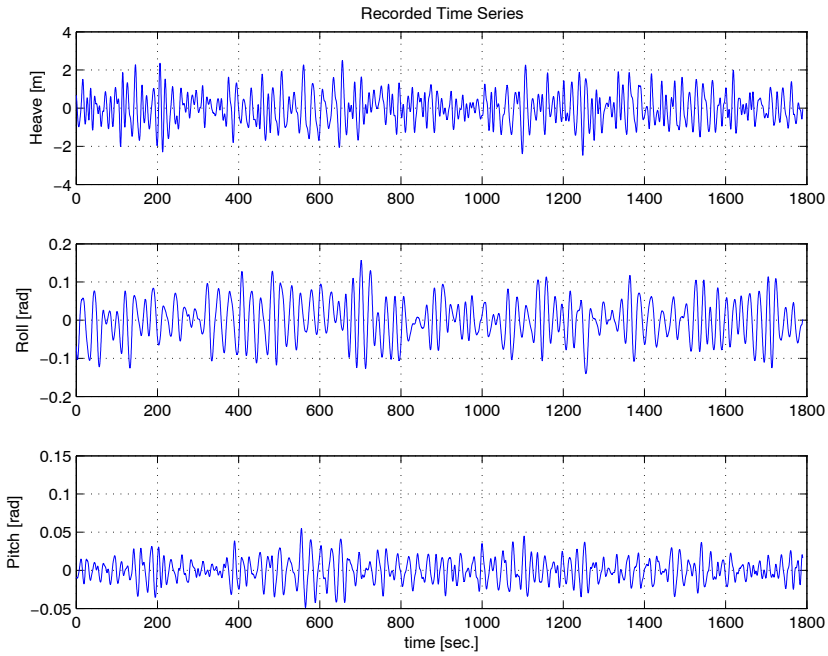

Figure B.13: *Time series for the responses of Data I.*

This page is intentionally left blank.

Appendix C

Preliminary Studies

C.1 Introduction

In the beginning of the present PhD research, work was also carried out in in the preliminary stage of the SeaSense project mentioned in Chapter 2. This appendix describes this work. In the appendix two parametric procedures for estimation of the wave spectrum are investigated. Fundamentally, the procedures are similar although the first procedure is based on a summation of so-called shape functions and leads to a linear optimisation problem in one vector, whereas the second procedure establishes a general optimisation function in several vectors. Both procedures and the relevant theory are described in the following.

As a general comment it should be noted that the present appendix is set up as a stand-alone chapter in the sense that it can be read with little knowledge of the information given previously. For this reason, repetitions will to some degree appear occasionally and, in other cases, the theory is given rather concisely.

C.2 Assumptions on the Wave Spectrum

The waves are assumed to be short-crested, and the introduction of directional spreading follows the traditional way by assuming a frequency-independent spreading function $f(\mu)$, so that the wave spectrum is written as

$$S(\omega, \mu) = S(\omega) f(\mu) \tag{C.1}$$

with

$$\int_{-\frac{\pi}{2}}^{\frac{\pi}{2}} f(\mu) \, d\mu = 1 \tag{C.2}$$

and ω being the wave frequency. It should be noted that the spreading is given relative to some fixed direction. In the calculations, this direction is taken to be the heading of the ship.

The spreading function is taken to be one of two options

$$f(\mu) = \begin{cases} \frac{2}{\pi}\cos^2\mu \\ \frac{8}{3\pi}\cos^4\mu \end{cases}, \quad |\mu| \leq \frac{\pi}{2} \tag{C.3}$$

C.3 Estimation by Use of Shape Functions

The method derived here has many similarities with the method given by Hua and Palmquist (1994), and for reference that work should be consulted.

It is important to note that in this method, the first of the parametric procedures, the encounter angle cannot be estimated, but must be given by the ship's officers (the user of the program). Moreover, the method can take only one response into account at a time. For this reason, the equation, from which the wave spectrum is to be found, is governed by the square of the amplitude of the transfer function for the considered response.

The main idea introduced by Hua and Palmquist (1994) is that the frequency-dependent part of the wave spectrum is composed of a summation of N shape functions

$$S(\omega) = \sum_{n=1}^{N} a_n \cdot f_n^S(\omega) \tag{C.4}$$

i.e. the spectrum is a linear combination of the shape functions $f_n^S(\omega)$.

The coefficients $a_1, a_2, ..., a_N$ are constant but until now unknown, whereas the shape functions are taken to be generalised JONSWAP spectra with $H_s = 1\text{m}$, while the peak magnifying factor γ and the zero-upcrossing period T_z must (somehow) be estimated or assumed from the on-site sea state. (The generalised JONSWAP spectrum is described in detail in (C.14).)

The unknown coefficients can be determined from the measured response spectrum $S_R(\omega_e)$, as the transfer function for the response $\Phi_R(\omega_e)$ yields the theoretical relationship between the response and the wave spectrum

$$S_R(\omega_e) = \int_{-\frac{\pi}{2}}^{\frac{\pi}{2}} S(\omega)\,\Phi_R^2(\omega, \beta - \mu)\,f(\mu)\left|\frac{d\omega}{d\omega_e}\right| d\mu \tag{C.5}$$

where ω_e is the encounter frequency and $|\cdot|$ denotes the absolute value. Here it must be remembered that the wave frequency is a function of the encounter frequency according to

the triple-valued function problem (e.g. Figure 3.3)

$$\omega \;=\; \begin{cases} \frac{1\pm\sqrt{1-4V/g\cos(\beta-\mu)\omega_e}}{2V/g\cos(\beta-\mu)} \\ \\ \frac{1+\sqrt{1+4V/g\cos(\beta-\mu)\omega_e}}{2V/g\cos(\beta-\mu)} \end{cases} \tag{C.6}$$

with V and β being the speed and the encounter angle, respectively, of the ship.

Thus, the integrand in (C.5) should be evaluated as

$$\sum_{j=1}^{q} S\left(\omega_j\right) \Phi_R^2\left(\omega_j, \beta-\mu\right) f\left(\mu\right) \left|\frac{d\omega}{d\omega_e}\right|_{\omega_j=\omega_j(\omega_e)} \quad , \quad q \;=\; 1 \text{ or } 3 \tag{C.7}$$

for each encounter frequency ω_e. q is determined on the basis of the number of real and positive values for the wave frequency, ω, from (C.6). This evaluation is to be done in all of the expressions below but for the sake of clarity the notation is left out.

By equalising the amount of energy, from integration of the left- and the right-hand side of (C.5), a kind of variational function, that is, a cost function, can be formulated in the least squares sense

$$F\left(a_1, a_2, ..., a_N\right) \equiv \int_0^{\infty} \left[\int_{-\frac{\pi}{2}}^{\frac{\pi}{2}} S\left(\omega\right) \Phi_R^2\left(\omega, \beta-\mu\right) f\left(\mu\right) \left|\frac{d\omega}{d\omega_e}\right| d\mu - S_R\left(\omega_e\right)\right]^2 d\omega_e \tag{C.8}$$

Hence, the coefficients $a_1, a_2, ..., a_N$ are determined by minimising F, i.e.

$$\frac{\partial F}{\partial a_n} = 0 \quad \text{for } n = 1, 2, ..., N \tag{C.9}$$

Insertion of (C.4) and (C.8) in (C.9) yields the following expression for the determination of the unknown coefficients

$$\begin{aligned} & \int_0^{\infty} \left[\int_{-\frac{\pi}{2}}^{\frac{\pi}{2}} \left(\sum_{n=1}^{N} a_n \cdot f_n^S\right) \Phi_R^2\left(\omega, \beta-\mu\right) f\left(\mu\right) \left|\frac{d\omega}{d\omega_e}\right| d\mu\right] \\ & \cdot \left[\int_{-\frac{\pi}{2}}^{\frac{\pi}{2}} f_n^S \Phi_R^2\left(\omega, \beta-\mu\right) f\left(\mu\right) \left|\frac{d\omega}{d\omega_e}\right| d\mu\right] d\omega_e \\ = \; & \int_0^{\infty} S_R\left(\omega_e\right) \left[\int_{-\frac{\pi}{2}}^{\frac{\pi}{2}} f_n^S \Phi_R^2\left(\omega_e, \beta-\mu\right) f\left(\mu\right) \left|\frac{d\omega}{d\omega_e}\right| d\mu\right] d\omega_e \quad \text{for } n = 1, 2, ..., N \end{aligned} \tag{C.10}$$

Thus, a set of N equations can be set up for the determination of the N unknown coefficients. In matrix notation the system reads

$$\mathbf{Fa} = \mathbf{b} \tag{C.11}$$

where

$$\begin{aligned} F_{mn} &= \int_0^\infty \left[\int_{-\frac{\pi}{2}}^{\frac{\pi}{2}} f_m^S \Phi_R^2 (\omega_e, \beta - \mu) f(\mu) \left| \frac{d\omega}{d\omega_e} \right| d\mu \right] \\ &\quad \cdot \left[\int_{-\frac{\pi}{2}}^{\frac{\pi}{2}} f_n^S \Phi_R^2 (\omega_e, \beta - \mu) f(\mu) \left| \frac{d\omega}{d\omega_e} \right| d\mu \right] d\omega_e \end{aligned} \tag{C.12}$$

$$b_m = \int_0^\infty \left[\int_{-\frac{\pi}{2}}^{\frac{\pi}{2}} f_m^S \Phi_R^2 (\omega_e, \beta - \mu) f(\mu) \left| \frac{d\omega}{d\omega_e} \right| d\mu \right] S_R(\omega_e) \, d\omega_e \tag{C.13}$$

Given the coefficients $a_1, a_2, ..., a_N$ and the shape functions, the estimated frequency-dependent wave spectrum simply follows from (C.4).

Basically, the major drawback or difficulty of the present method for estimation of the wave spectrum is how many shape functions (i.e. 'unit JONSWAP' spectra) to use and which parameters (zero- upcrossing period and peak magnifying factor) to choose. In the present work, four shape functions has been suggested, and with respect to the zero-upcrossing period this is based on the peak period determined from the global maximum of the measured response spectrum. In order to deal with both wind waves and swells, a zero-upcrossing period of $(T_z - 1\text{s})$ is also taken into account. Finally, for both these T_z-values, peak magnifying factors of $\gamma = 1$ and $\gamma = 3.3$, which correspond to a Pierson Moskowitz and a JONSWAP spectrum, are considered. Thus, the estimated spectrum is based on a linear combination of four shape functions with $H_s = 1\text{m}$ and parameters

$$\begin{aligned} (T_z, \gamma)_1 &= (T_z, 1) \\ (T_z, \gamma)_2 &= (T_z, 3.3) \\ (T_z, \gamma)_3 &= (T_z - 1, 1) \\ (T_z, \gamma)_4 &= (T_z - 1, 3.3) \end{aligned}$$

C.4 Optimisation of JONSWAP Spectra

For the procedure above to work, a priori knowledge of the peak magnifying factor, the zero-upcrossing period and of the encounter angle must be at hand, i.e. the parameters must

be estimated/assumed and then given manually. Obviously, this is not acceptable if a fully automated system is sought for. Instead, the method that will be dealt with below takes all of the parameters in the generalised JONSWAP spectrum to be unknowns, and then, from an optimisation, determines the values of these. Furthermore, the mean wave direction in the sense of an encounter angle is estimated. The method does, however, not differentiate between waves entering from the port side or the starboard side. For this reason the phase lag of the individual response is not considered, which means that the governing equations will be based on the square of the amplitudes of the frequency response functions.

In dimensional form the generalised JONSWAP spectrum reads, e.g. Jensen et al. (2004)

$$S\left(\omega;\gamma,T_s,H_s\right) \;=\; 173H_s^2T_s\left(\omega T_s\right)^{-5}e^{-\frac{692}{(\omega T_s)^4}}\frac{1}{F_1}\gamma^{\exp\left[-\frac{1}{2}\left(\frac{0.206F_2T_s\omega-1}{\sigma}\right)^2\right]} \tag{C.14}$$

where the coefficients F_1 and F_2 depend on γ as shown below

$$\begin{array}{rcll} 1 & \leq & \gamma \leq 2: & F_1 = 0.24\gamma + 0.76; \quad F_2 = -0.05\gamma + 1.05 \\ 2 & \leq & \gamma \leq 3: & F_1 = 0.22\gamma + 0.80; \quad F_2 = -0.02\gamma + 0.99 \\ 3 & \leq & \gamma \leq 4: & F_1 = 0.20\gamma + 0.86; \quad F_2 = -0.02\gamma + 0.99 \\ 4 & \leq & \gamma \leq 5: & F_1 = 0.20\gamma + 0.86; \quad F_2 = -0.01\gamma + 0.95 \\ 5 & \leq & \gamma \leq 6: & F_1 = 0.18\gamma + 0.96; \quad F_2 = -0.01\gamma + 0.95 \end{array} \tag{C.15}$$

and

$$\begin{array}{l} \sigma = 0.07 \;\; \text{for} \;\; 0.206F_2T_s\omega \leq 1 \\ \sigma = 0.09 \;\; \text{for} \;\; 0.206F_2T_s\omega > 1 \end{array} \tag{C.16}$$

In order to introduce the zero-upcrossing period the following relation is applied, e.g. Gran (1992)

$$T_s = T_z\frac{\sqrt{\left(10.89+\gamma\right)\left(5+\gamma\right)}}{6.774+\gamma} \tag{C.17}$$

As for the previous procedure based on shape functions, N spectra can be applied and, hence, the variational function to be optimised will be a function of $4N$ independent parameters, namely $H_{s,n}$, $T_{Z,n}$, γ_n and β_n.

Basically, the variational or cost function follows from (C.8)

$$F \equiv \sum_{i=1}^{K}\int_0^{\infty}\left[\int_{-\frac{\pi}{2}}^{\frac{\pi}{2}} S\left(\omega\right)\Phi_{R,i}^{\,2}\left(\omega,\beta-\mu\right)f\left(\mu\right)\left|\frac{d\omega}{d\omega_e}\right|d\mu - S_{R,i}\left(\omega_e\right)\right]^2 d\omega_e \tag{C.18}$$

and the wave spectra $S(\omega)$, i.e. the parameters in (C.14), are determined by minimising F. It should be noted that the first expression of the integrand of (C.18) is to be evaluated according to (C.7). Moreover, it is seen that K responses can be considered when the cost function is set up.

Obviously, constraints can be put on the parameters, and the following constraints seem reasonable

$$\begin{aligned} 0 \leq H_{s,n} \leq 15 \quad [\text{m}] \\ 5 \leq T_{z,n} \leq 18 \quad [\text{s}] \\ 1 \leq \gamma_n \leq 6 \\ 0 \leq \beta_n \leq \pi \end{aligned} \tag{C.19}$$

Furthermore, it must be taken into account that waves cannot be infinitely steep. This is assured by introducing the following constraint which relates the zero-upcrossing period with the significant wave height, Jensen (2001)

$$T_z > 8.1\sqrt{\frac{H_s}{g}} \tag{C.20}$$

where g is the acceleration of gravity.

The optimisation problem can be solved as a constrained non-linear minimisation to which - among others - a Sequential Quadratic Programming (SQP) method can be applied, e.g. the MatLab Help Tutorial MatLab (2005). (Here it is solved by a pre-developed method, `fmincon`, in MatLab.)

It should be noted that the results, which are shown below are based on either 1, or a summation of 2 generalised JONSWAP spectra.

C.5 Results

The present appendix describes the analysis of full-scale data when the estimations of wave spectra are based on the parametric estimation. The analysed data has been obtained in the joint Danish project SeaSense (2003), and the considered ship is a PanMax container ship. The main dimensions of this ship are given in Table C.1.

It is important to emphasise that the results presented in the following reflect preliminary results in terms of the status of the SeaSense project. At this stage it was of interest to see if some response was better than another when the wave spectrum should be estimated. Hence, the responses are dealt with individually, so that a wave spectrum is estimated for each of the considered responses. This contradicts what would be optimal, namely to integrate all the responses in one single estimation.

Table C.1: *Ship data.*

Main Data	
Length between perpendiculars, L_{pp}	284.7 m
Breadth, B	32.2 m
Draught, T	11.2 m
Block coefficient, C_{b}	0.627

Figure C.1: *Wave impact with major spray.*

The data originates from a trip when the North Atlantic was crossed in a severe storm.

In the analysis three different kinds of responses are considered: the acceleration at the centreline at FP, the relative motion approximately 10m behind FP and the strain amidships. Both of the latter signals are, in theory, constructed as the mean of two signals from port and starboard, respectively. However, problems arose for the strain signal at starboard, so that the 'mean' strain signal is only based on the signal at port. As regards the frequency response functions, the square root of the RAO of the three responses is plotted in Section C.10 for different encounter angles.

As a comment it is noted that the cross spectral analysis carried out for the measured responses is performed by FFT combined with appropriate smoothing.

On the following pages, plots of the estimated wave spectrum are seen for different periods of time, i.e. date of origin. Each page contains one figure which corresponds to a specific period of time and, as will be noted, three plots are seen. The upper plot shows the estimated wave spectrum with the estimation based on shape functions, whereas the middle plot depicts the estimated wave spectrum obtained from the optimisation. For both of these plots three

spectra are seen: 1) the spectrum derived from the strain signal, 2) the spectrum derived from the acceleration signal, and 3) the spectrum derived from the relative motion signal. The lower plot in the figure shows the estimated wave spectrum based on the extrapolated wave height derived from both the acceleration and the relative motion signals. In all the cases the spectra are plotted as function of the angular wave frequency.

The estimation based on optimisation is done with a sum of two spectra where among others the two headings β are optimised. In case of two different values for the headings it may therefore be argued that it is somehow physically incorrect to sum the two spectra to obtain one resulting spectrum. However, for the comparison by the other method based on shape functions, this has been done. As regards the overall parameters determined from the optimisation, these are seen in Table C.9. It should be emphasised that these numbers only relate to the optimisation method and, hence, represent the wave spectrum in a swell and a wave part.

The signals taken into account all have a duration of 1800 sec. and, in general, the signals have been recorded in the severest period of time with respect to sea states and wind speeds. The starting time for each period considered is seen from the first column in Table C.2. This column shows the UTC time and the number 'ddmmyytt' denotes the date *dd*, in month *mm*, in year *yy*, at time *tt* (in hours). In the table the speed of the ship is also given and, furthermore, the observed/guessed heading is shown. Due to darkness no visual observation could be made for the wave height, and for the same reason the values of the heading are connected with some uncertainty. However, from experience, the ship's officers have to some extent a feeling of the heading (behaviour of the rudder, major water sprays seen in the light from the mast in front of the 'wave breaker'). In the table, the T_z-values used in the estimation method based on shape functions are also shown. These values are approximated from the peak period of the measured response spectrum for the strain.

It should be noted that the response spectra for the strain, acceleration and relative motion are seen in Section C.11 at the very end of this appendix. Here both the non-smoothed spectrum as obtained from a direct FFT and the smoothed spectrum as obtained by performing data windowing (with a Parzen window) are shown. Moreover, the response spectrum is also calculated/predicted from the estimated wave spectrum and the transfer function, and results are depicted for both of the wave estimation procedures.

Table C.2: *UTC time and relevant data.*

UTC	Speed [kn]	Heading [deg.]	T_z [s]
02120200	16.5	185	9.7
02120202	13.0	195	10.6
02120204	11.7	205	10.8
02120206	12.0	195	9.9
02120208	12.5	210	9.5

As it will be seen, all of the figures in the following pages are 'summarised' in a table at

the bottom of each page. In the table, the significant wave height is calculated from the estimated wave spectrum according to

$$H_s = 4\left(\int_0^\infty S(\omega)\, d\omega\right)^{\frac{1}{2}} \tag{C.21}$$

In this connection, it should be remarked that the recorded data, related to the sea state parameters and given in Table C.3, has been obtained from different kinds of measurements such as meteorological bureaus, ship observations, satellites etc. Unfortunately, data for only two of the considered periods has been obtained. As regards the accuracy, which is found to one decimal, this seems questionable. However, for completeness, the numbers in the table have been copied as they were found in the recorded file!

Table C.3: *Recorded wave heights and periods.*

UTC	H_{s} (wave)	H_{s} (swell)	$\sqrt{H_{\mathrm{s,w}}^2 + H_{\mathrm{s,s}}^2}$	T_{p} (swell)	T_{p} (wave)
02120200	7.7m	3.1m	8.3m	16.4s	11.6s
02120206	7.8m	4.2m	8.9m	15.3s	11.2s

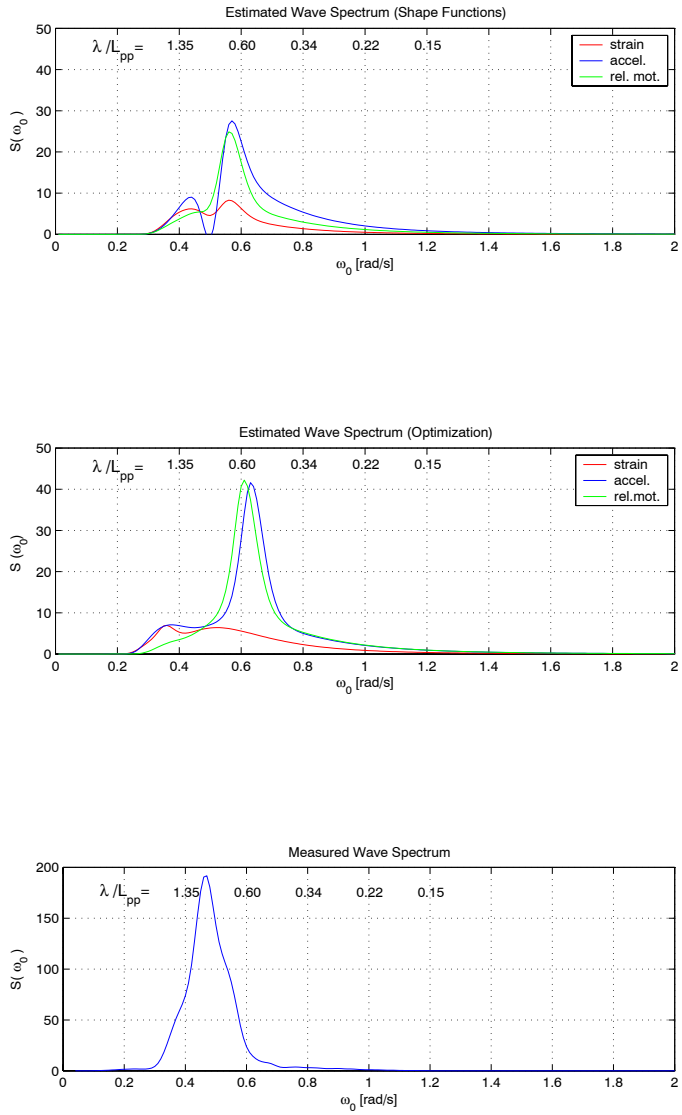

Figure C.2: *UTC: 02120200. Estimated wave spectra by use of shape functions (upper plot) and by optimisation (middle plot). The lower plot is based on the extrapolated wave height. (Note the difference in scale in the lower plot.) All spectra as function of the wave frequency.*

Table C.4: *Estimated significant wave heights and peak periods. The first number is from the method with shape functions, the second number from optimisation.*

	Strain	Acceleration	Rel. Motion	Wave Height
H_s [m]	6.2 / 7.0	9.7 / 11.2	8.5 / 10.9	21.5
T_p [s] (swell)	14.6 / 18.0	14.6 / 18.0	- / -	14.0
T_p [s] (wave)	11.4 / 12.6	11.3 / 10.0	11.2 / 10.5	-

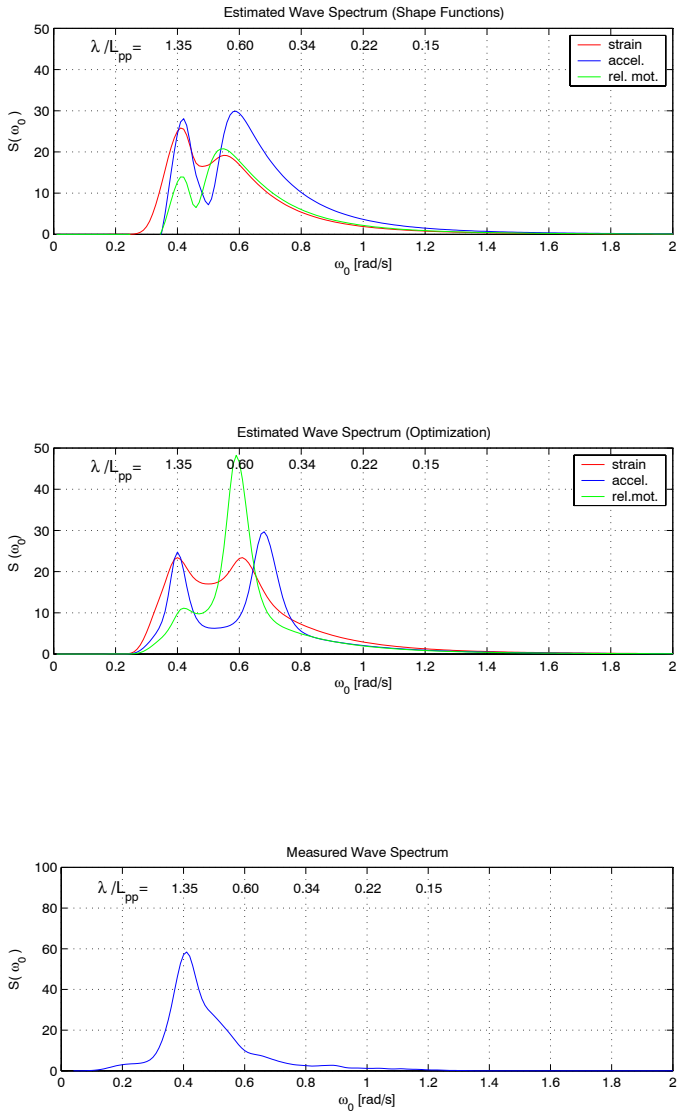

Figure C.3: *UTC: 02120202. Estimated wave spectra by use of shape functions (upper plot) and by optimisation (middle plot). The lower plot is based on the extrapolated wave height. (Note the difference in scale in the lower plot.) All spectra as function of the wave frequency.*

Table C.5: *Estimated significant wave heights and peak periods. The first number is from the method with shape functions, the second number from optimisation.*

	Strain	Acceleration	Rel. Motion	Wave Height
H_s [m]	11.6 / 12.7	12.8 / 11.1	10.4 / 11.7	13.4
T_p [s] (swell)	15.7 / 15.8	15.6 / 15.8	15.6 / 15.6	15.7
T_p [s] (wave)	11.9 / 10.5	10.8 / 9.2	11.9 / 11.0	-

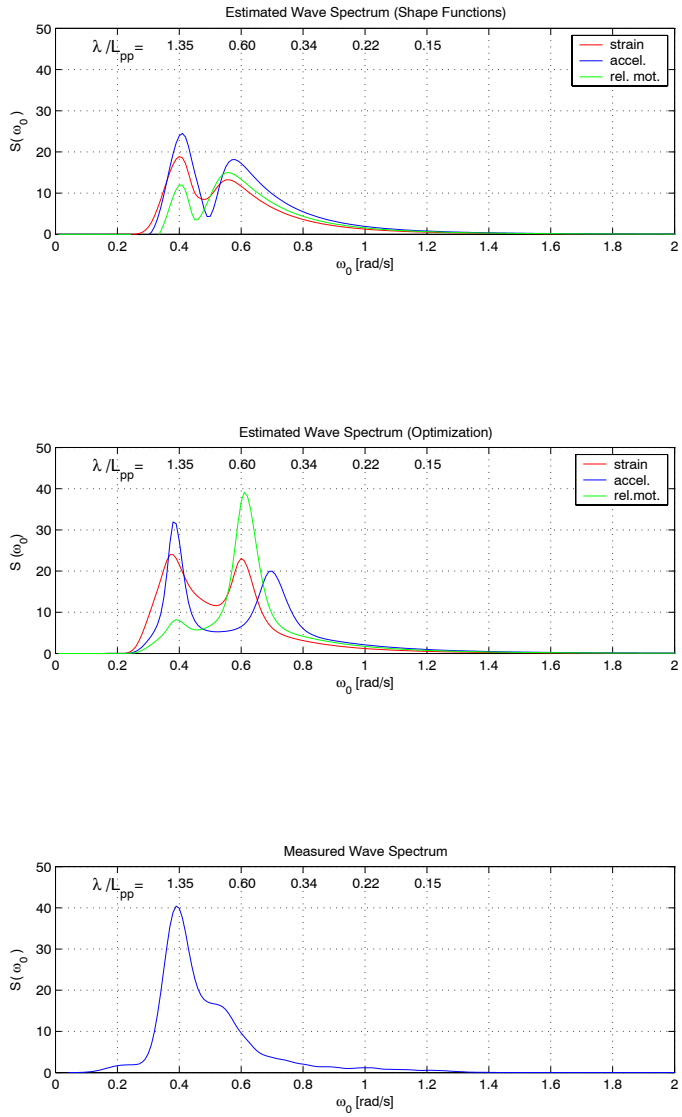

Figure C.4: *UTC: 02120204. Estimated wave spectra by use of shape functions (upper plot) and by optimisation (middle plot). The lower plot is based on the extrapolated wave height. All spectra as function of the wave frequency.*

Table C.6: *Estimated significant wave heights and peak periods. The first number is from the method with shape functions, the second number from optimisation.*

	Strain	Acceleration	Rel. Motion	Wave Height
H_s [m]	9.5 / 11.1	10.7 / 10.7	8.9 / 10.5	11.4
T_p [s] (swell)	15.7 / 16.1	15.7 / 16.0	15.7 / 15.9	15.9
T_p [s] (wave)	11.4 / 10.5	11.2 / 9.2	11.4 / 10.4	-

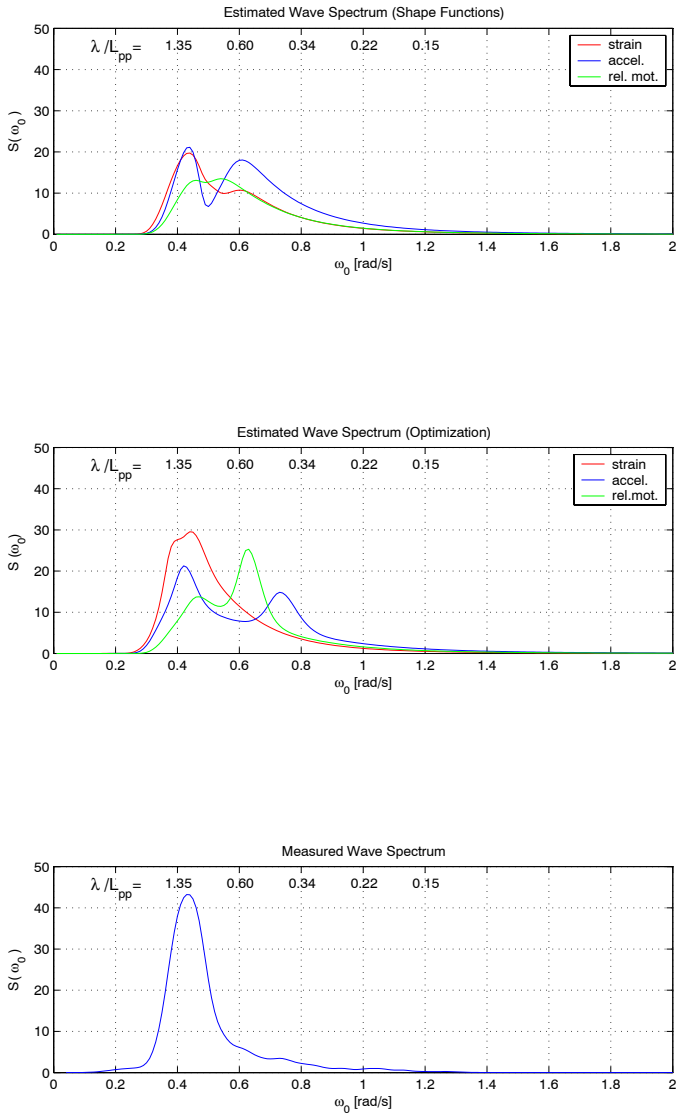

Figure C.5: *UTC: 02120206. Estimated wave spectra by use of shape functions (upper plot) and by optimisation (middle plot). The lower plot is based on the extrapolated wave height. All spectra as function of the wave frequency.*

Table C.7: *Estimated significant wave heights and peak periods. The first number is from the method with shape functions, the second number from optimisation.*

	Strain	Acceleration	Rel. Motion	Wave Height
H_s [m]	9.7 / 11.3	11.1 / 10.8	9.1 / 10.1	11.3
T_p [s] (swell)	14.6 / 15.5	14.6 / 15.6	14.4 / 13.7	14.6
T_p [s] (wave)	10.5 / -	10.5 / 8.7	12.1 / 10.1	-

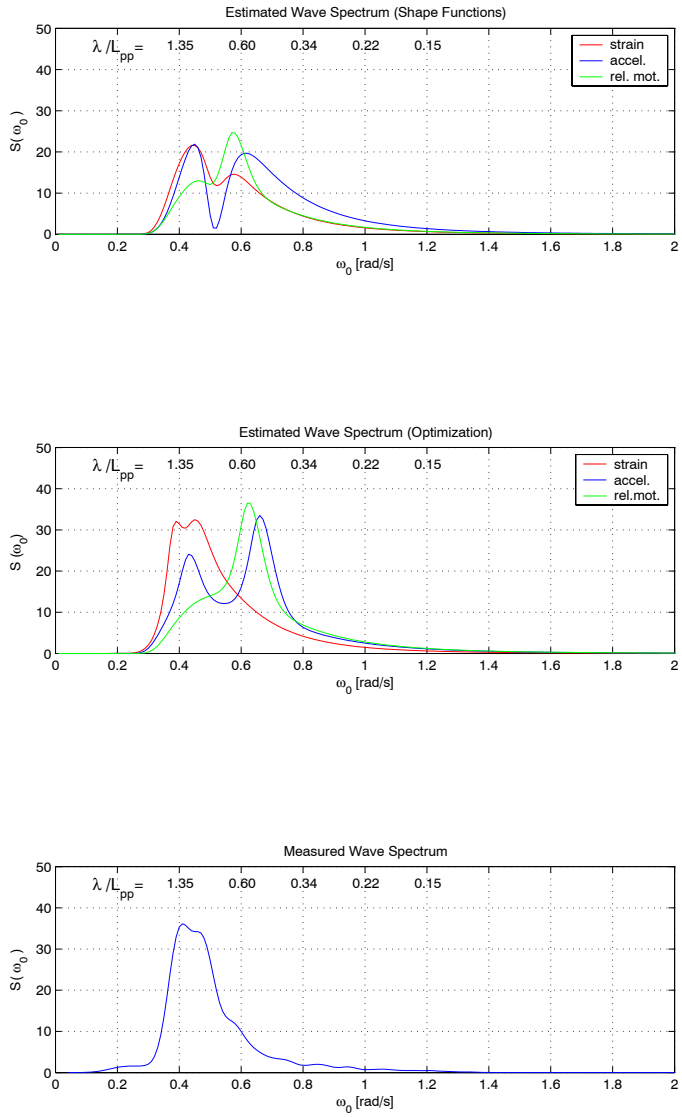

Figure C.6: *UTC: 02120208. Estimated wave spectra by use of shape functions (upper plot) and by optimisation (middle plot). The lower plot is based on the extrapolated wave height. All spectra as function of the wave frequency.*

Table C.8: *Estimated significant wave heights and peak periods. The first number is from the method with shape functions, the second number from optimisation.*

	Strain	Acceleration	Rel. Motion	Wave Height
H_s [m]	10.3 / 12.0	11.4 / 12.3	10.1 / 12.0	11.4
T_p [s] (swell)	14.0 / 16.0	14.0 / 14.4	13.9 / -	15.5
T_p [s] (wave)	11.1 / 14.9	10.5 / 9.5	11.1 / 10.1	-

Table C.9: *Wave parameters determined from the optimisation. The first number corresponds to the swell part, the second number to the wave part. Note β is given as a value between 180 and 270 deg. (and 0 and 90 deg.)*

UTC: 02120200	Strain	Acceleration	Rel. Motion
H_s [m]	4.3 / 5.6	5.4 / 9.8	3.9 / 10.2
T_z [s]	13.1 / 8.1	11.9 / 8.1	10.8 / 8.3
T_p [s]	18.0 / 12.6	18.0 / 10.0	- / 10.5
β [deg.]	182 / 206	180 / 180	180 / 196
γ	1.7 / 1.0	1.0 / 6.0	1.0 / 4.9

UTC: 02120202	Strain	Acceleration	Rel. Motion
H_s [m]	9.1 / 8.8	7.1 / 8.5	5.5 / 10.3
T_z [s]	11.4 / 7.7	12.2 / 7.5	11.3 / 8.6
T_p [s]	15.8 / 10.5	15.8 / 9.2	15.6 / 11.0
β [deg.]	180 / 215	180 / 259	180 / 187
γ	1.3 / 1.9	3.3 / 6.0	1.9 / 5.6

UTC: 02120204	Strain	Acceleration	Rel. Motion
H_s [m]	8.9 / 6.6	7.5 / 7.7	4.8 / 9.4
T_z [s]	12.1 / 8.4	13.0 / 7.2	12.0 / 8.4
T_p [s]	16.1 / 10.5	16.0 / 9.2	15.9 / 10.4
β [deg.]	223 / 228	180 / 259	182 / 206
γ	1.4 / 5.7	4.2 / 4.2	1.8 / 6.0

UTC: 02120206	Strain	Acceleration	Rel. Motion
H_s [m]	5.3 / 10.0	8.4 / 6.7	7.3 / 7.0
T_z [s]	12.7 / 10.1	11.0 / 6.7	9.9 / 8.1
T_p [s]	15.5 / -	15.6 / 8.7	13.7 / 10.1
β [deg.]	235 / 230	180 / 233	193 / 184
γ	2.8 / 1.4	1.6 / 3.6	1.4 / 6.0

UTC: 02120208	Strain	Acceleration	Rel. Motion
H_s [m]	4.9 / 11.0	8.6 / 8.8	7.4 / 9.5
T_z [s]	13.4 / 10.0	10.9 / 7.7	9.8 / 8.0
T_p [s]	16.0 / 14.9	14.4 / 9.5	- / 10.1
β [deg.]	247 / 235	233 / 187	194 / 184
γ	6.0 / 1.4	1.9 / 5.4	1.0 / 4.1

C.6 General Comments on the Estimations

As seen from the figures in the preceding, the visual agreement between the estimated wave spectra is reasonable, although (slight) discrepancies are present. Moreover, it should be noted that the amount of energy, measured by the significant wave height, does not vary significantly when the different estimations for each period are compared. However, the amount of energy seems to be too large when compared to the recorded values given in Table C.3.

A general feature of the estimations, both for the method of shape functions and the method based on optimisation, is the tendency towards a double-peaked wave spectrum. A double-peaked spectrum seems reasonable under the given circumstances, since both wind waves and swells were most likely present at the times considered. Although the locations of the peaks to some extent coincide for the different methods and signals, notable differences are observed in some cases. Especially, the high-frequency peak for the acceleration signal seems to deviate from the others when the optimisation method is considered. For the method based on shape functions the differences are not so pronounced, which is trivially explained by the fact that the zero-upcrossing periods are chosen in advance (deviations can, however, be present because of different peak enhancement factors). As regards the wave spectra estimated from the extrapolated wave height, the tendency towards a double-peaked spectrum is not seen. Similarly, the double-peaked spectrum is less notable when the relative motion signal is considered. In this context it should be remembered that the relative motion signal is to be judged relatively critically, since this signal in rather long periods can be 'saturated', cf. Figure 6.6 in Chapter 6.

From Figure C.2 and to some extent also Figure C.3 it is noted that the estimated spectra obtained from the extrapolated wave height contain much more energy than the other estimations. An explanation for this fact cannot be given but as seen from the time histories of the wave heights, cf. Figure C.15-C.19 in Section C.12 below, it is evident that the extrapolated wave heights around UTC: 02120200 (Figure C.15) are, indeed, greater than those in the other periods of time.

C.7 Estimation Based on Optimisation

From a detailed study of the estimated wave spectra based on the optimisation method, Table C.9 should be considered. Generally, a reasonable agreement is found between the spectra. Moreover, it is seen that, in all the cases, the estimated headings, to a certain degree, are in the range of the headings observed/felt on the ship, cf. Table C.2.

C.8 Estimation Based on Shape Functions

Apparently, the best agreement between the estimated wave spectra based on the individual signals is obtained by the method based on shape functions. However, some difficulties/problems of this method should be noted. Firstly, the method requires input of several of the wave parameters: T_z - and γ-values and the heading β must all be specified. Of these values, the former two can probably be given with the least certainty and, although the zero-upcrossing period to some extent can be approximated from the response spectra, the fact that the values must somehow be given by the user is seen as a major problem. Secondly, it may vary, from time to time, how many spectra are optimal to use and, thirdly, a closer inspection of the upper plots in Figures C.2, C.3 and C.4 reveals that in the low-frequency region, negative values of the wave spectrum can occur.

C.9 Conclusions

Overall, the estimations of the wave spectra from the measured ship responses have taken place with relatively fair consistency. However, it cannot from this study be concluded that any response is better to use than others, when wave spectra are to be estimated. Hence, it is optimal to integrate all responses in the estimation.

Two different parametric methods were studied. The method based on shape functions is very fast (computational time in the order of seconds) but requires input of wave parameters as well as of the heading. Moreover, problems arise sometimes with negative values of the wave spectrum. Conversely, the method based on an optimisation is rather slow with computational times in the order of several minutes due to the non-linear optimisation. Of course, this can be reduced by down-scaling the frequency resolution and the accuracy with which the optimisation should take place. On the contrary, no input of wave parameters or headings is required (except for an initial guess for the optimisation), which is an obvious advantage for the optimisation method compared to the method based on shape functions. In conclusion, the optimisation method is thus to be preferred of the two methods.

C.10 Transfer Functions

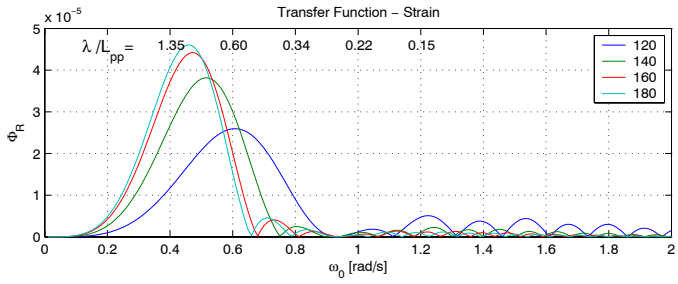

Figure C.7: *Transfer function for strain amidships. Depicted for different headings.*

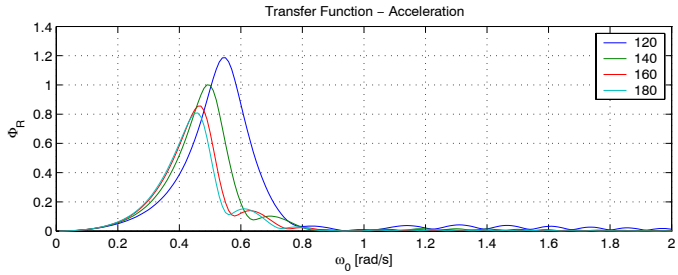

Figure C.8: *Transfer function for acceleration at FP. Depicted for different headings.*

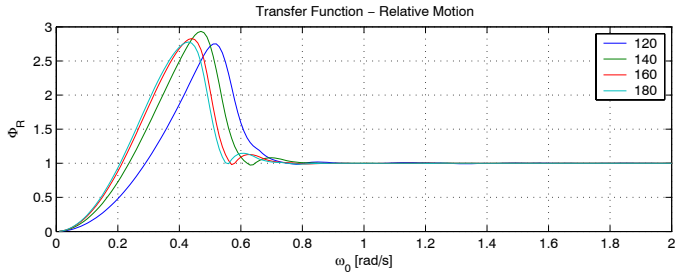

Figure C.9: *Transfer function for relative motion 10m behind FP. Depicted for different headings.*

C.11 Response Spectra

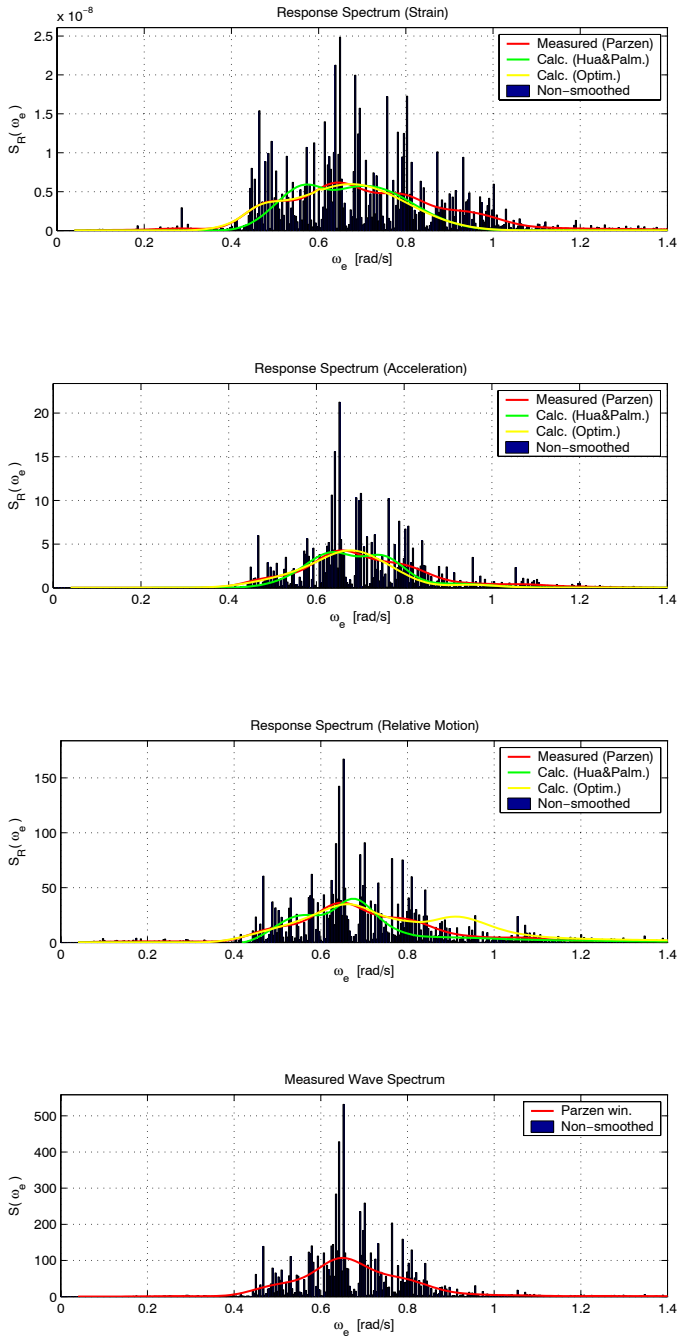

Figure C.10: *UTC: 02120200. Measured and calculated response spectra for strain, acceleration, relative motion and wave height. V = 16.5kn. β = 185 deg.*

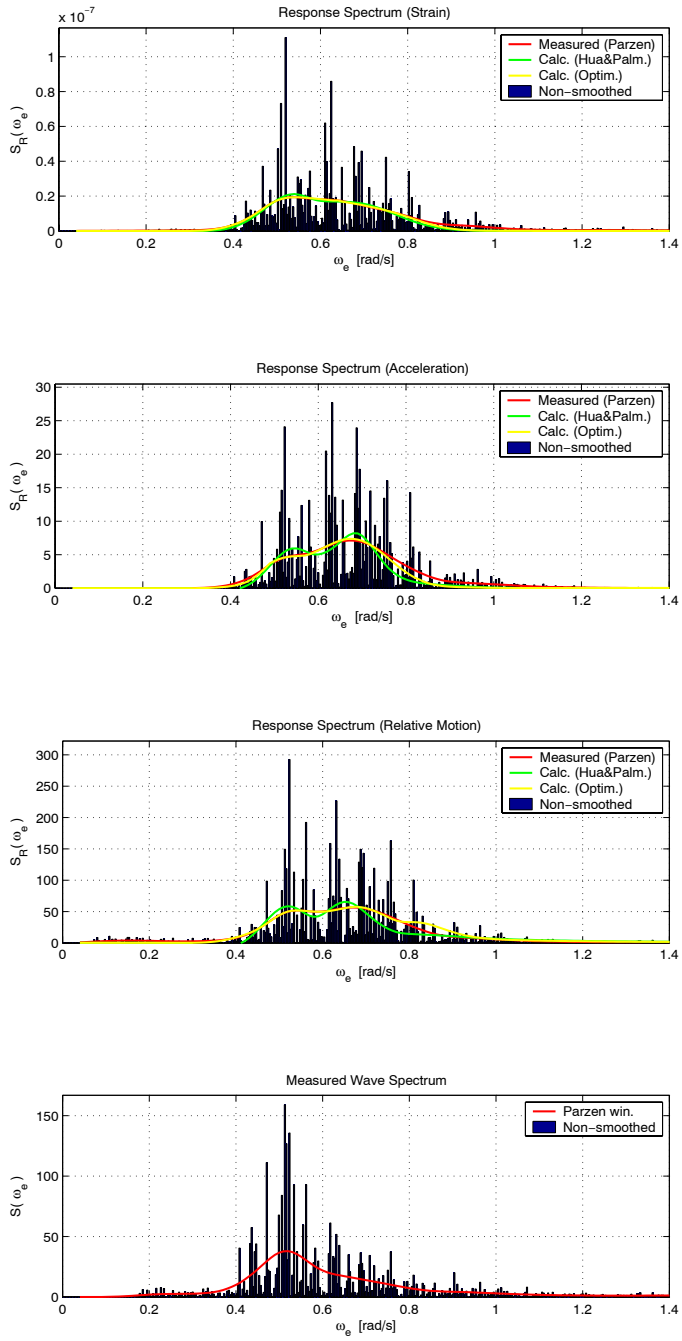

Figure C.11: *UTC: 02120202. Measured and calculated response spectra for strain, acceleration, relative motion and wave height. $V = 13.0$kn. $\beta = 195$ deg.*

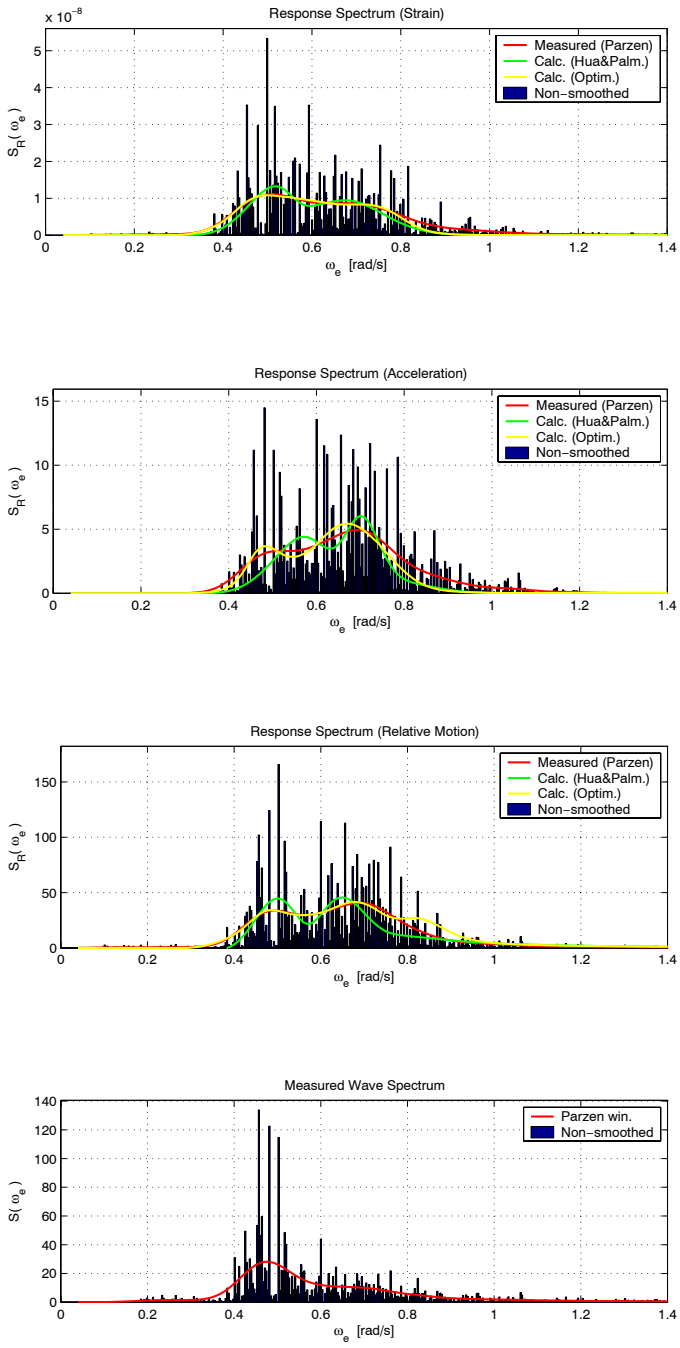

Figure C.12: *UTC: 02120204. Measured and calculated response spectra for strain, acceleration, relative motion and wave height. $V = 11.7$kn. $\beta = 205$ deg.*

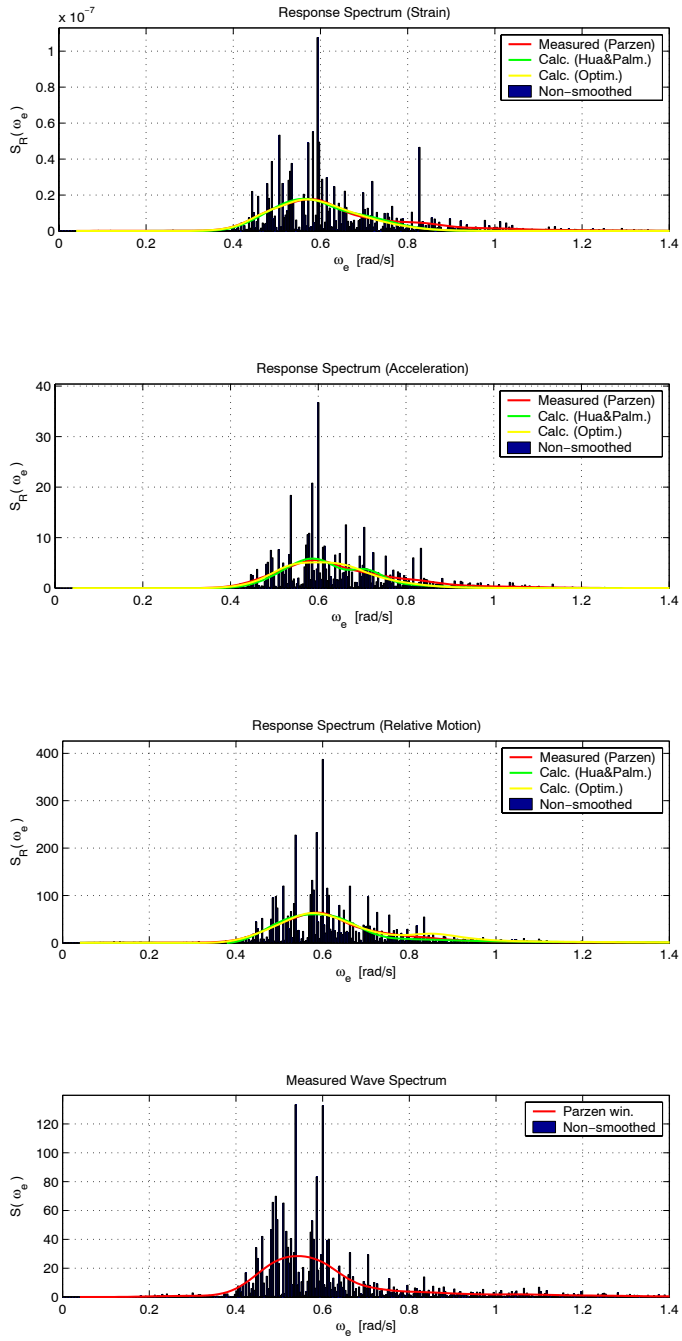

Figure C.13: *UTC: 02120206. Measured and calculated response spectra for strain, acceleration, relative motion and wave height. $V = 12.0$kn. $\beta = 195$ deg.*

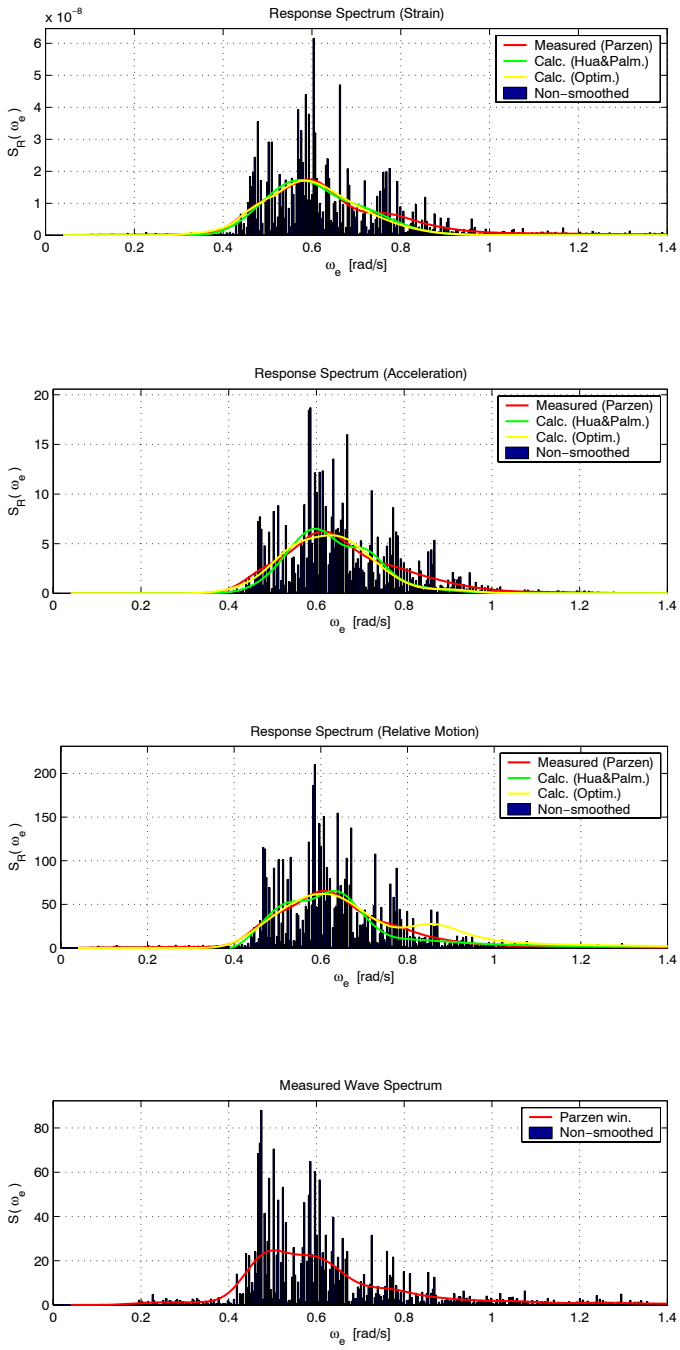

Figure C.14: *UTC: 02120208. Measured and calculated response spectra for strain, acceleration, relative motion and wave height. $V = 12.5$kn. $\beta = 210$ deg.*

C.12 Time History of Wave Height

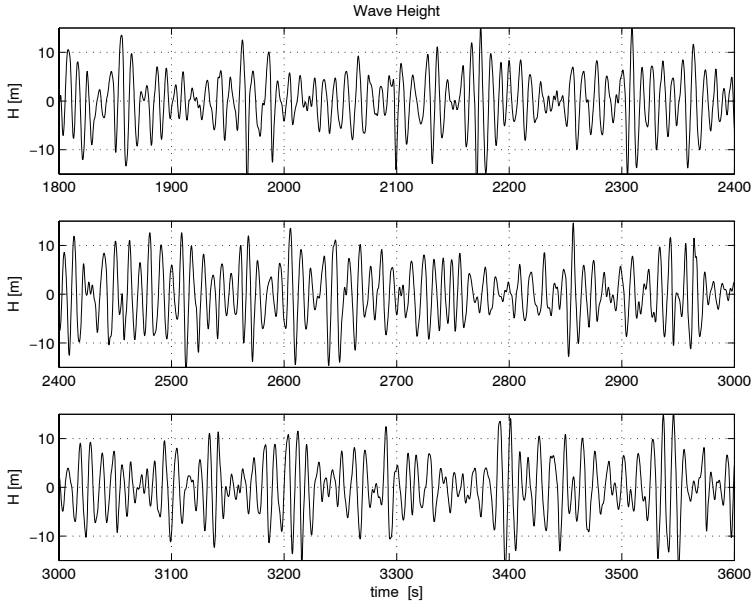

Figure C.15: *Time history of the extrapolated wave height. UTC: 02120200.*

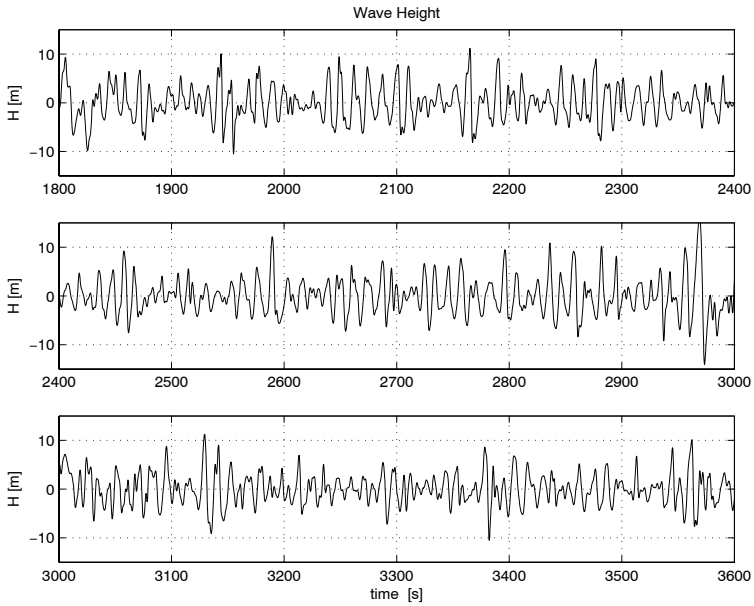

Figure C.16: *Time history of the extrapolated wave height. UTC: 02120202.*

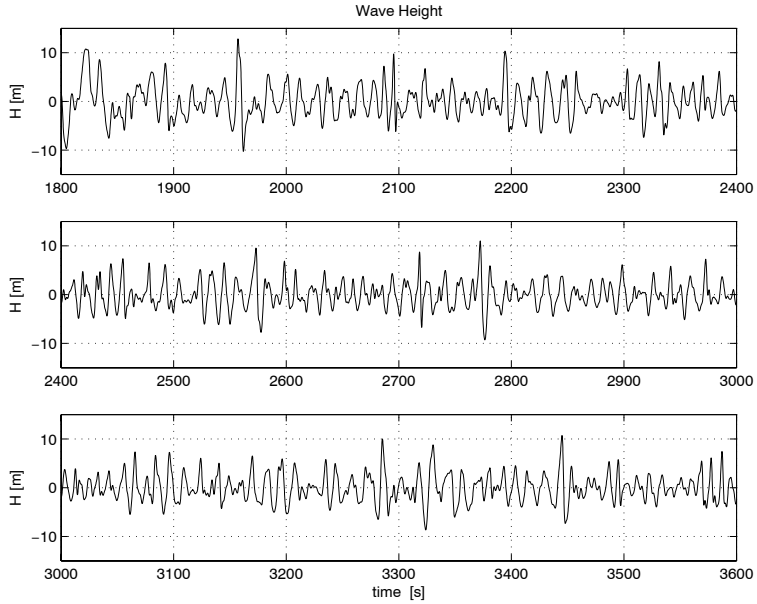

Figure C.17: *Time history of the extrapolated wave height. UTC: 02120204.*

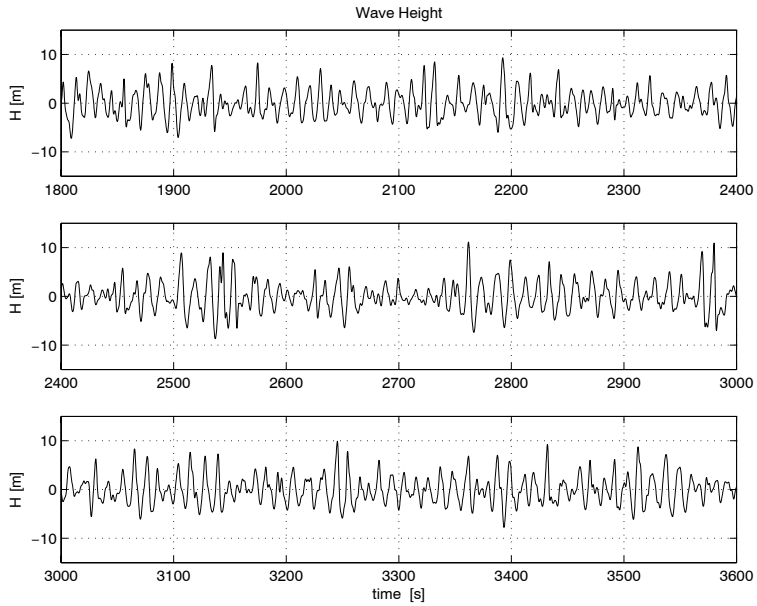

Figure C.18: *Time history of the extrapolated wave height. UTC: 02120206.*

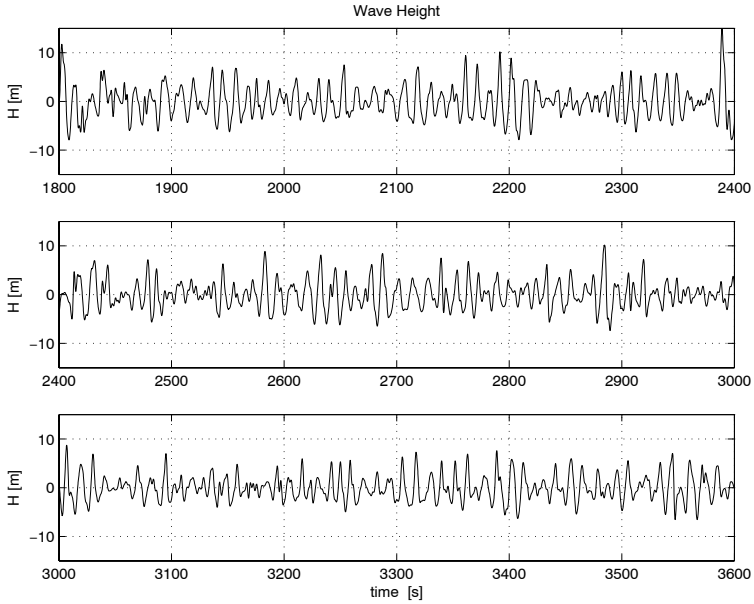

Figure C.19: *Time history of the extrapolated wave height. UTC: 02120208.*

Appendix D

Numerical Simulations

D.1 Introduction

In this appendix two numerical examples are studied. Basically, the examples are identical to the example in Chapter 7 and, thus, based on simulated ship responses, the wave spectrum is to be estimated. In both examples an encounter angle of 150 deg. is assumed, but in the first case a one-peaked wave spectrum is studied, whereas the second example deals with the estimation of a double-peaked wave spectrum.

D.2 One-peaked Spectrum

As foundation for the numerical simulation of the ship responses, a Pierson Moskowitz spectrum is assumed. The characteristic wave parameters are

$$\begin{aligned} H_s &= 2 \text{ m} \\ T_z &= 8 \text{ sec.} \end{aligned} \tag{D.1}$$

In Figures D.1 and D.2 the frequency response functions, i.e. $|\Phi_R(f_{e,i})|$ as the square root of the response amplitude operator (RAO), and the corresponding time series for heave, pitch, and roll are shown. As seen from Figure D.2 an hour of time has been simulated, and in the Bayesian estimation all the data of that period is to be used. It should be noted that the complex transfer functions, $\Phi_R(f_{e,i})$, are calculated by the New Strip Method, Strip-calculations (2004). For a detailed analysis of the frequency response functions reference is made to Appendix A, where the square root of the response amplitude operator (RAO) is depicted for a range of encounter angles and speeds.

As outlined previously, the optimal solution, as given by the Bayesian estimation, is obtained for the minimum value of ABIC. In Figure D.3 the ABIC values are plotted as function of

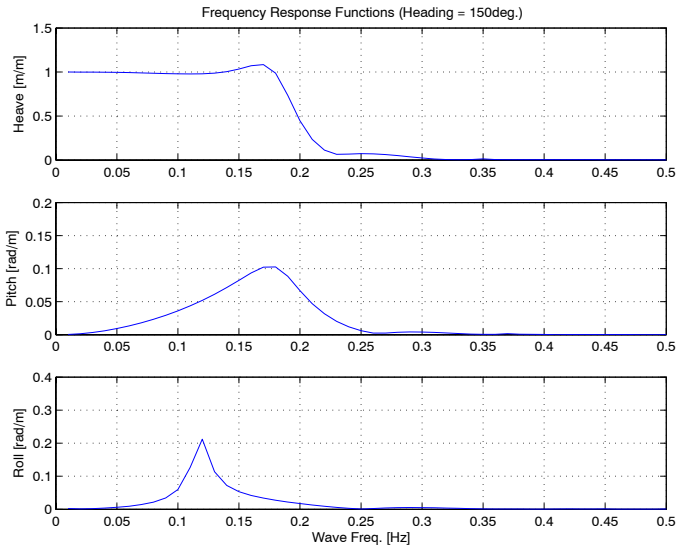

Figure D.1: *Frequency response functions calculated by the New Strip Method.*

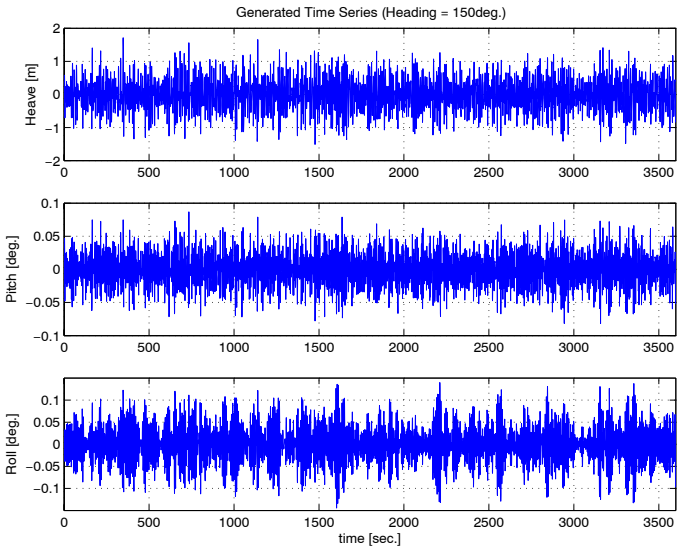

Figure D.2: *The 'measured', i.e. generated, time series.*

the natural logarithm of the hyperparameter u. From the figure it is seen that ABIC draws a downward convex curve, which attains a minimum of -1437 at $\ln u = -2.25$ corresponding to $u = 0.105$.

For this value of the hyperparameter, the estimation yields the wave spectrum shown in Figure D.4. In the figure two curves are depicted, the red one is the true Pierson Moskowitz spectrum and the other is the estimated wave spectrum as obtained from the Bayesian estimation. Note that the spectra are plotted as function of the true wave frequency f_0.

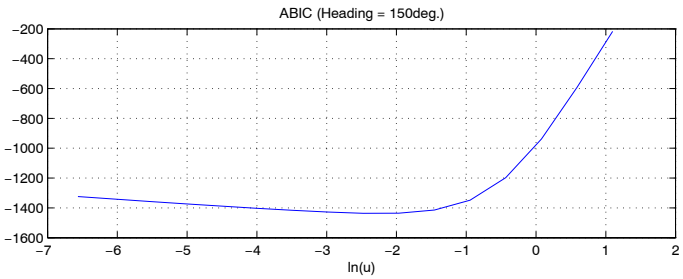

Figure D.3: *ABIC as function of the logarithm to the hyperparameter.*

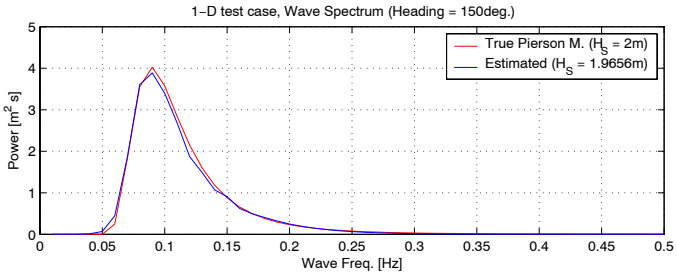

Figure D.4: *The true PM spectrum and the estimated wave spectrum.*

As seen from the comparison between the two graphs in Figure D.4, very good agreement exists. This is, indeed, reflected in the value of significant wave height that is found from the area under the spectrum, see e.g. Jensen (2001)

$$H_s = 4\left(\int E\left(f_0\right) df_0\right)^{\frac{1}{2}} \tag{D.2}$$

Thus, the relative deviation in the significant wave height for the two cases amounts to -1.7%.

To study the sensitivity of the solution to the hyperparameter, u, Figure D.5 should be considered. From this figure it seen that the solution, in the present one-dimensional example, is not particularly sensitive to the value of the hyperparameter. The legend 'optimal' corresponds to the minimum of ABIC for $u = 0.105$, and the three comparative cases are, in decreasing order, $u = 3.00$, $u = 1.08$, and $u = 0.0014$.

As a consequence of the very good estimation of the wave spectrum, the estimated response spectra are also very close to the 'measured', that is, the generated response spectra, which is seen from Figure D.6. Note that these spectra are shown as function of the encounter frequency f_e.

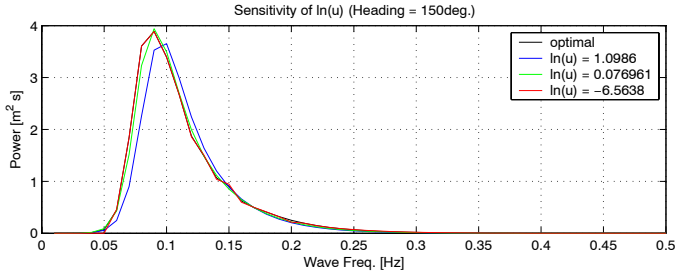

Figure D.5: *The estimated wave spectrum for different values of the hyperparameter.*

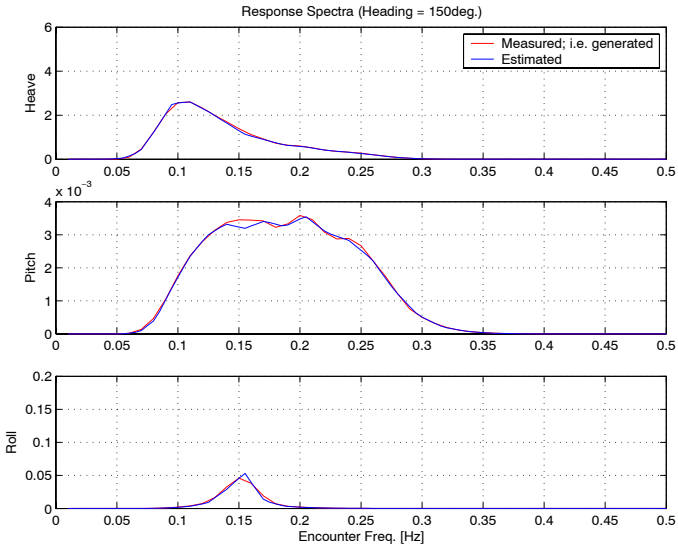

Figure D.6: *Comparisons of the response spectra.*

D.3 Double-Peaked Wave Spectrum

The last example shows the ability of the model to handle wave spectra with more peaks. Thus, the true wave spectrum used for the generation of the responses is taken as the sum of two individual PM spectra with the following data

$$\begin{aligned} H_s^{(1)} &= 1.5 \text{ m} & H_s^{(2)} &= 2 \text{ m} \\ T_z^{(1)} &= 10 \text{ sec.} & T_z^{(2)} &= 4 \text{ sec.} \end{aligned} \tag{D.3}$$

and the encounter angle equals 150 deg.

In Figure D.7 the estimated wave spectrum is compared with the true one, which is the red graph, and it is seen that good agreement exists. Furthermore, in Figure D.8 the estimated responses are seen to predict the generated responses very well.

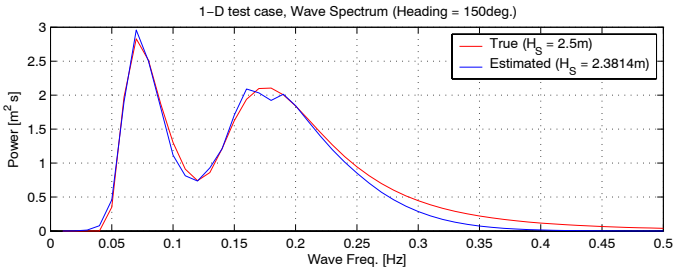

Figure D.7: *The true and the estimated wave spectra.*

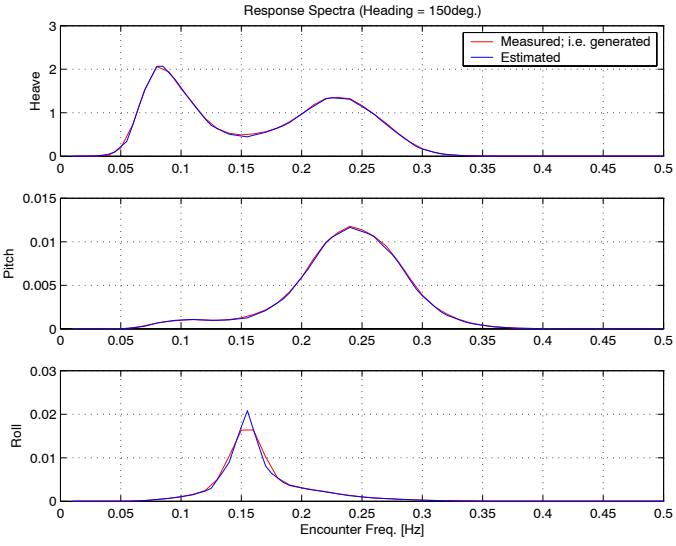

Figure D.8: *The generated and estimated response spectra.*

This page is intentionally left blank.

Appendix E

Additional Results for the Shioji-Maru

E.1 Introduction

The present appendix contains additional results for the research and training ship, the Shioji-Maru, the responses of which were studied in Chapter 8.

E.2 Normalised Response Spectra

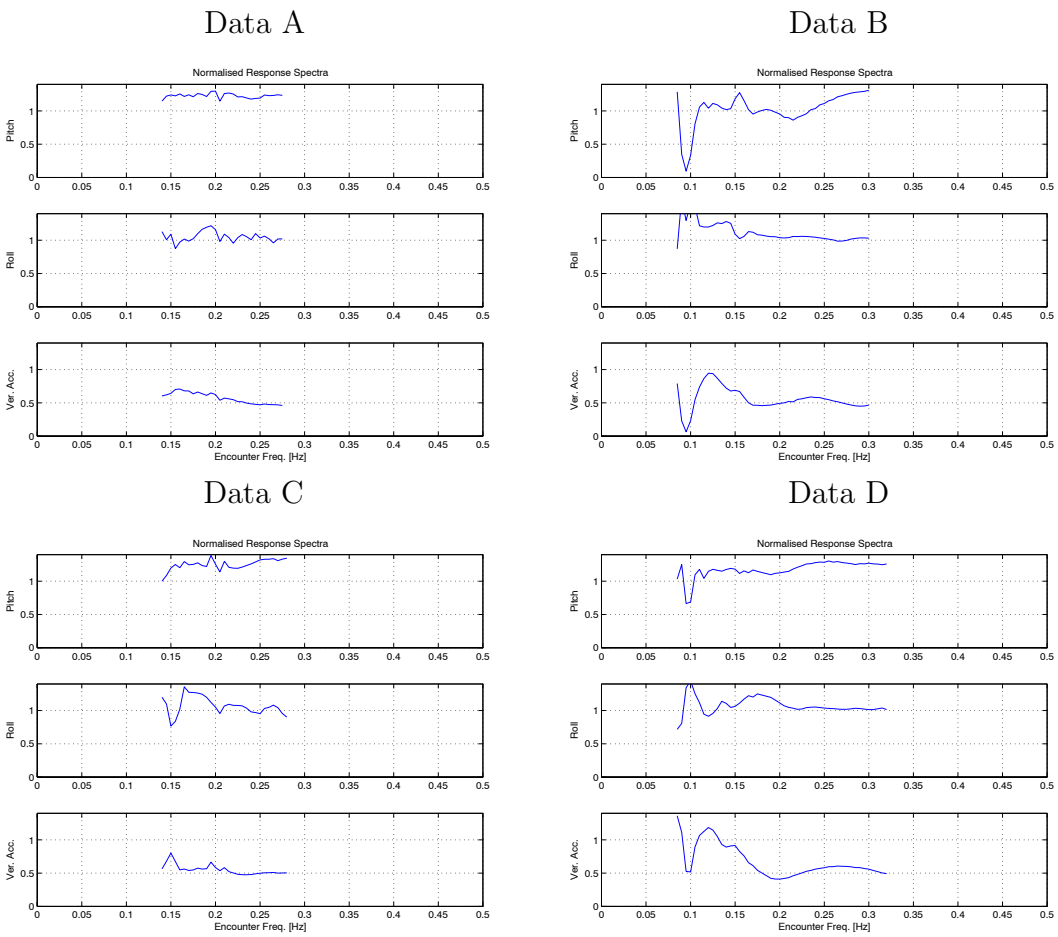

Figure E.1: *Comparisons of measured and estimated response spectra for the four data set; illustrated as function of the encounter frequency. Note the difference in scale.*

Appendix F

Additional Results for the Container Ship

F.1 Introduction

In the appendix, additional results can be found for the containership which was studied in Chapter 9.

F.2 Comparative Plots - Sway in place of Roll

Data A

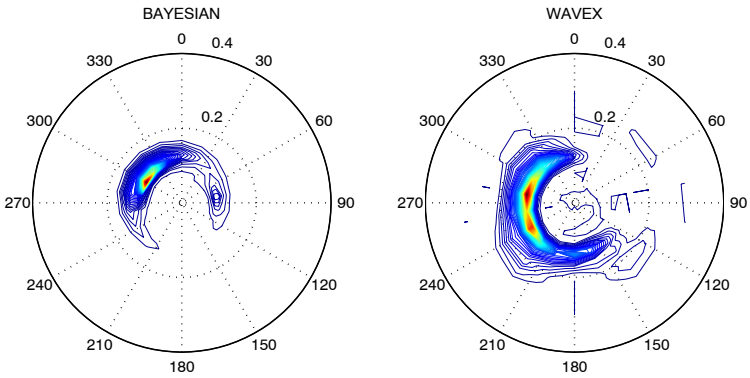

Figure F.1: *The estimated wave spectra for Data A. Relative ship course being 0 deg., and wave field depicted as approaching waves.*

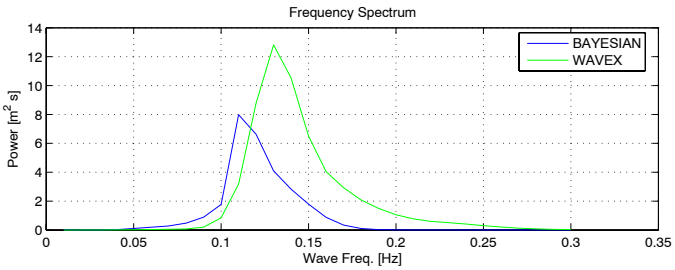

Figure F.2: *Integrated frequency spectra for Data A.*

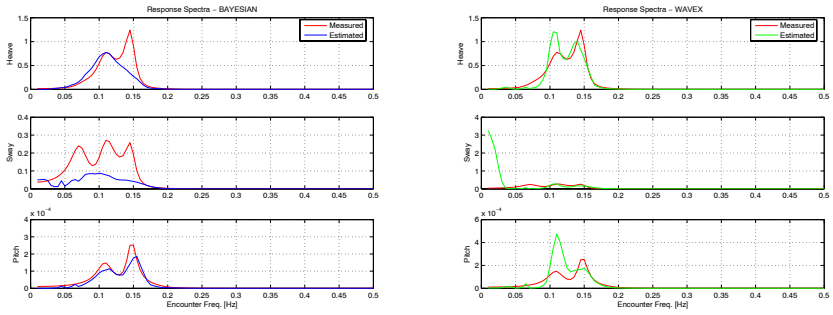

Figure F.3: *Response spectra for Data A; measured and 'estimated' with the latter based on the estimated wave spectra. Note the difference in scales. Units:* Heave [m^2s], Sway [m^2s], Pitch [rad^2s]

Data B

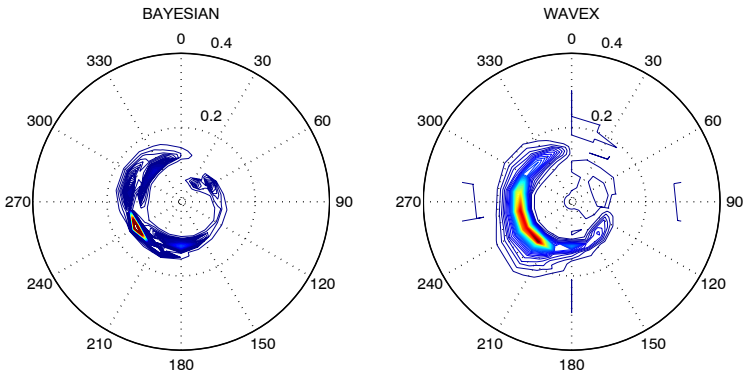

Figure F.4: *The estimated wave spectra for Data B. Relative ship course being 0 deg., and wave field depicted as approaching waves.*

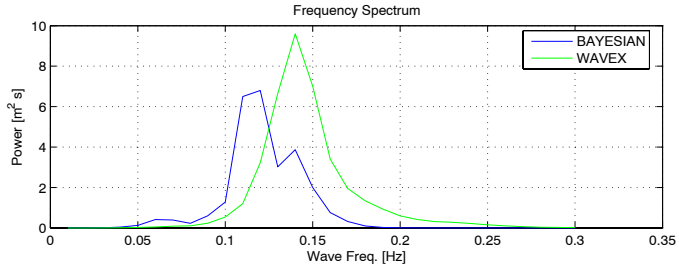

Figure F.5: *Integrated frequency spectra for Data B.*

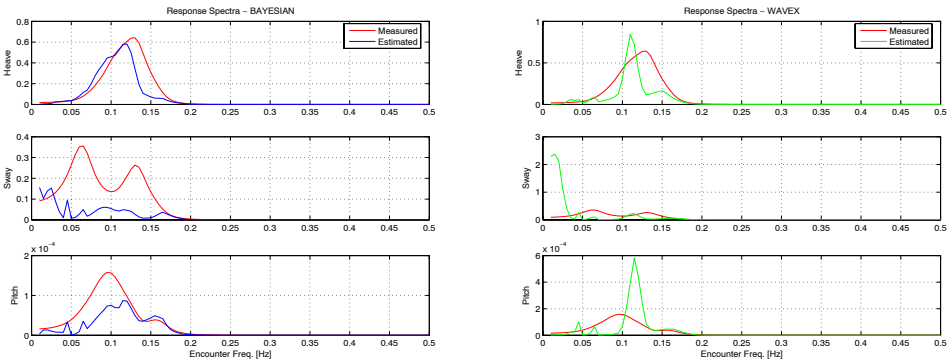

Figure F.6: *Response spectra for Data B; measured and 'estimated' with the latter based on the estimated wave spectra. Units:* Heave [m^2s], Sway [m^2s], Pitch [rad^2s]

Data C

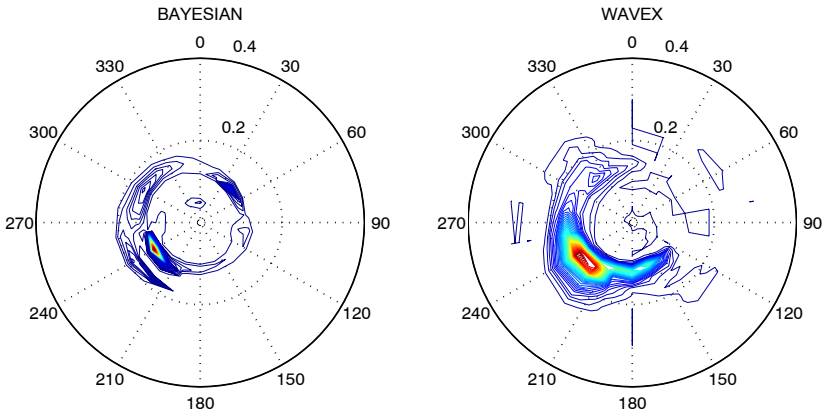

Figure F.7: *The estimated wave spectra for Data C. Relative ship course being 0 deg., and wave field depicted as approaching waves.*

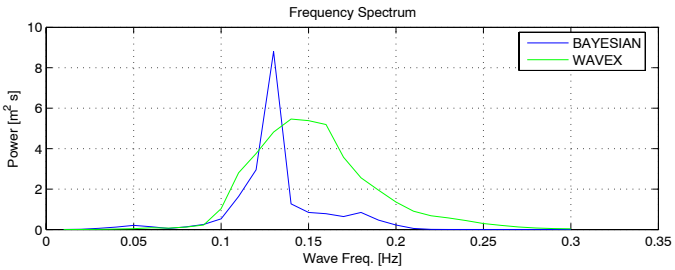

Figure F.8: *Integrated frequency spectra for Data C.*

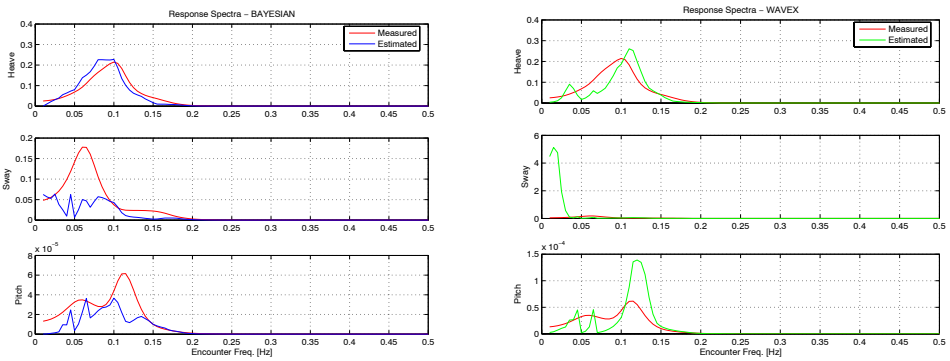

Figure F.9: *Response spectra for Data C; measured and 'estimated' with the latter based on the estimated wave spectra. Note the difference in scales. Units:* Heave [m^2s], Sway [m^2s], Pitch [rad^2s]

Data D

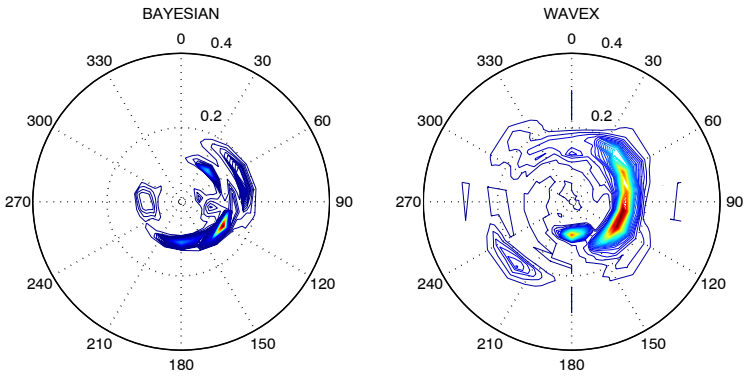

Figure F.10: *The estimated wave spectra for Data D. Relative ship course being 0 deg., and wave field depicted as approaching waves.*

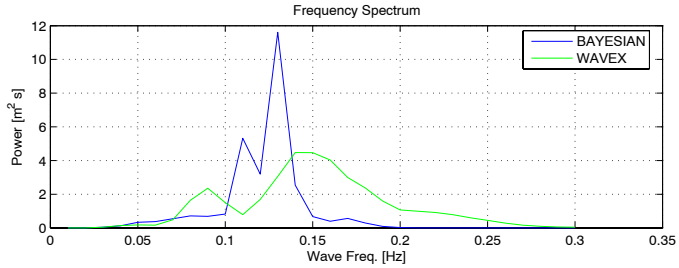

Figure F.11: *Integrated frequency spectra for Data D.*

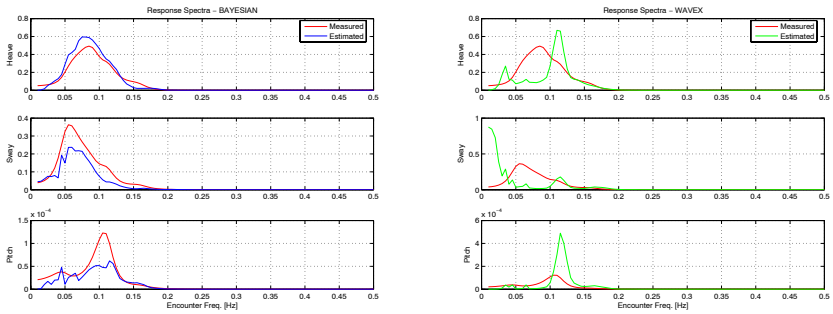

Figure F.12: *Response spectra for Data D; measured and 'estimated' with the latter based on the estimated wave spectra. Note the difference in scales. Units:* Heave [m^{2}s], Sway [m^{2}s], Pitch [rad^{2}s]

Data E

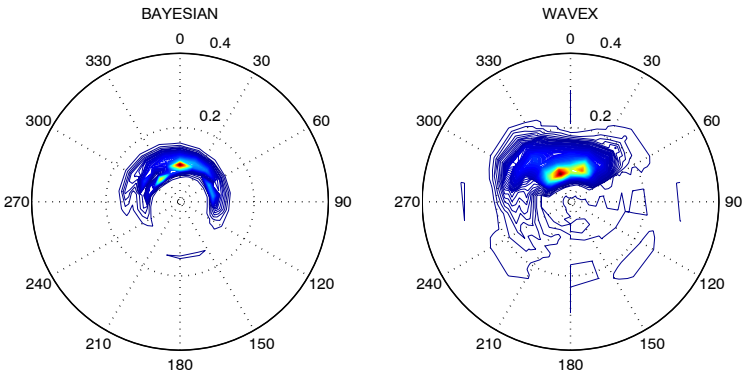

Figure F.13: *The estimated wave spectra for Data E. Relative ship course being 0 deg., and wave field depicted as approaching waves.*

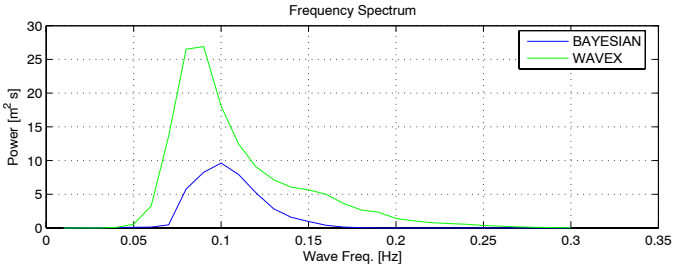

Figure F.14: *Integrated frequency spectra for Data E.*

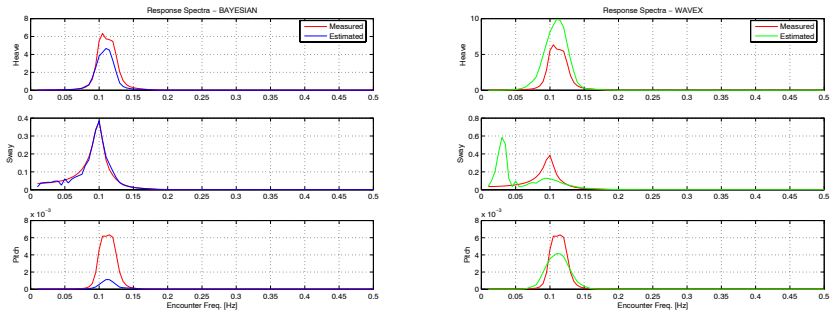

Figure F.15: *Response spectra for Data E; measured and 'estimated' with the latter based on the estimated wave spectra. Note the difference in scales. Units:* Heave [m^{2}s], Sway [m^{2}s], Pitch [rad^{2}s]

Data F

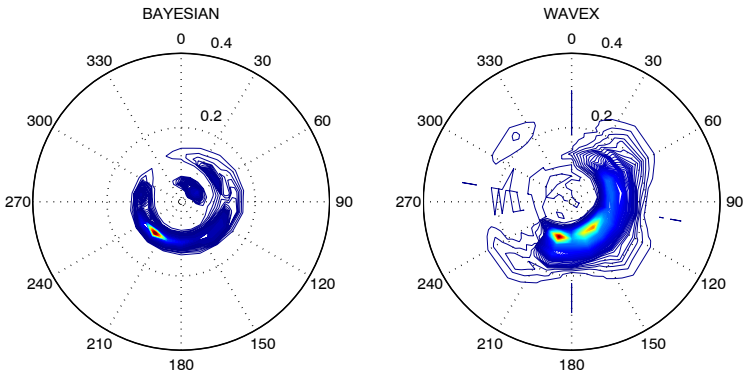

Figure F.16: *The estimated wave spectra for Data F. Relative ship course being 0 deg., and wave field depicted as approaching waves.*

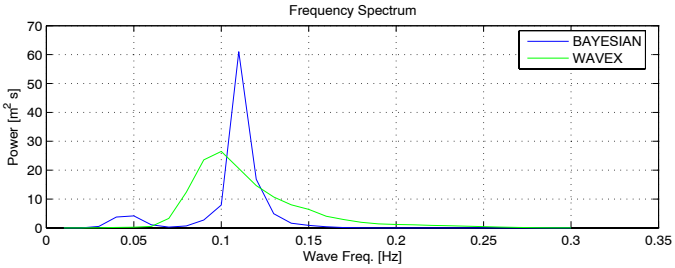

Figure F.17: *Integrated frequency spectra for Data F.*

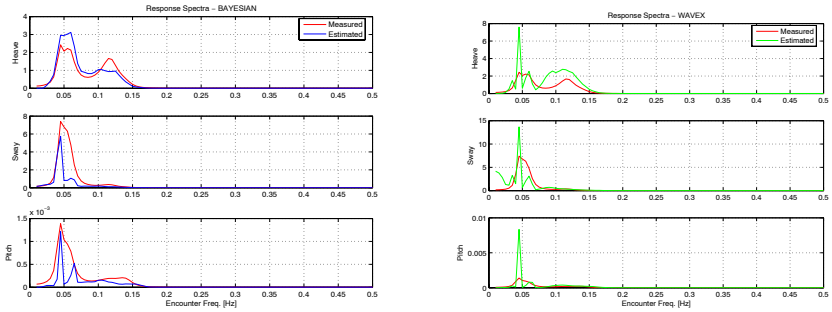

Figure F.18: *Response spectra for Data F; measured and 'estimated' with the latter based on the estimated wave spectra. Note the difference in scales. Units:* Heave [m^{2}s], Sway [m^{2}s], Pitch [rad^{2}s]

Data G

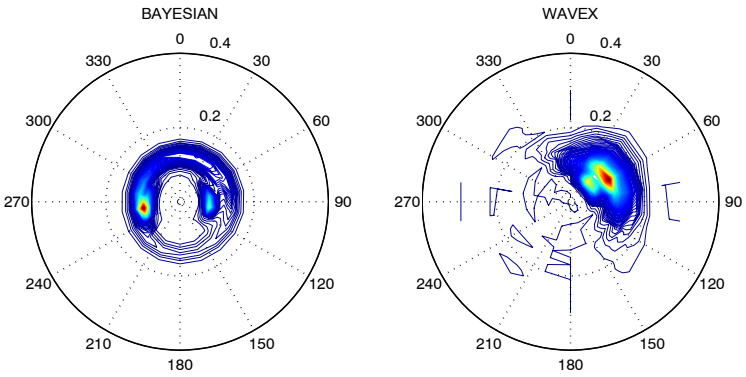

Figure F.19: *The estimated wave spectra for Data G. Relative ship course being 0 deg., and wave field depicted as approaching waves.*

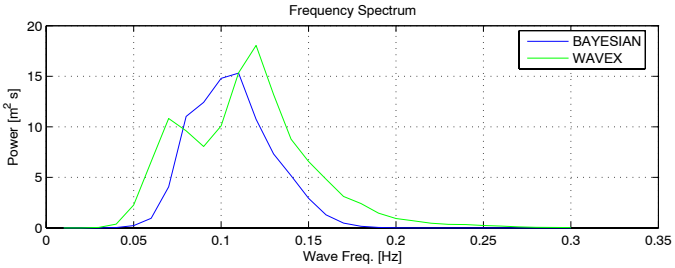

Figure F.20: *Integrated frequency spectra for Data G.*

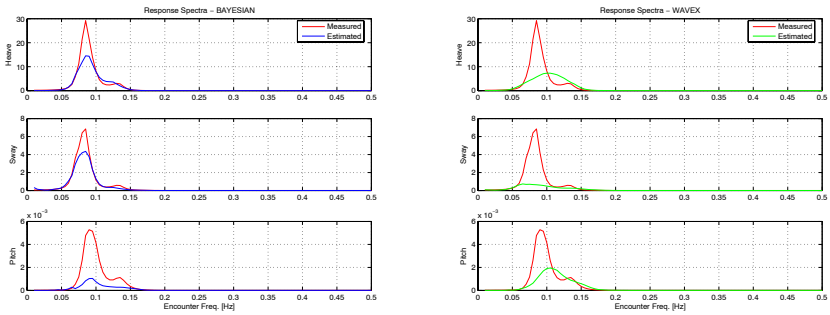

Figure F.21: *Response spectra for Data G; measured and 'estimated' with the latter based on the estimated wave spectra. Note the difference in scales. Units:* Heave [m^2s], Sway [m^2s], Pitch [rad^2s]

Data H

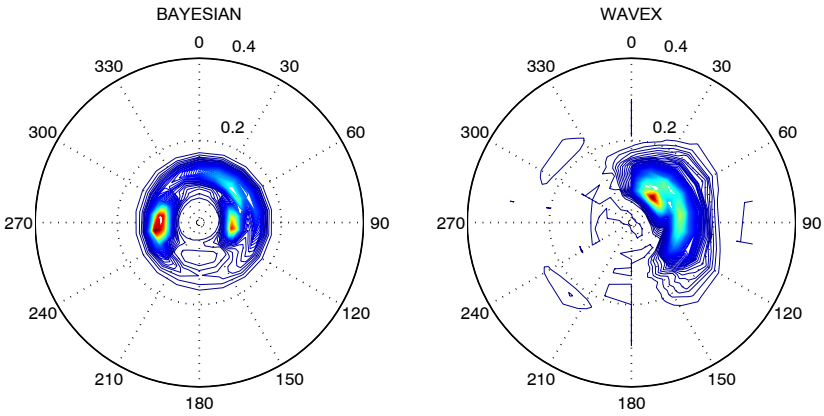

Figure F.22: *The estimated wave spectra for Data H. Relative ship course being 0 deg., and wave field depicted as approaching waves.*

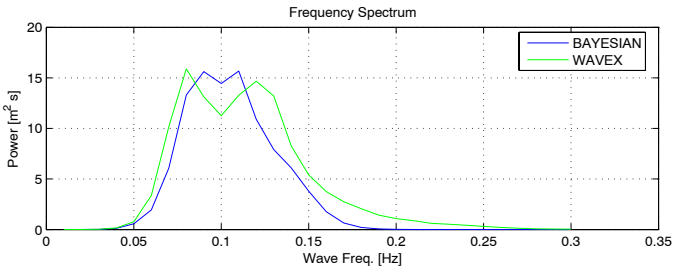

Figure F.23: *Integrated frequency spectra for Data H.*

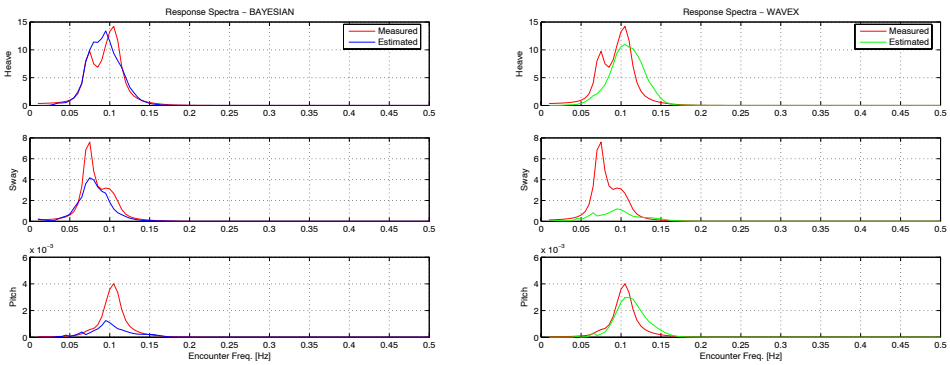

Figure F.24: *Response spectra for Data H; measured and 'estimated' with the latter based on the estimated wave spectra. Note the difference in scales. Units:* Heave [m^2s], Sway [m^2s], Pitch [rad^2s]

Data I

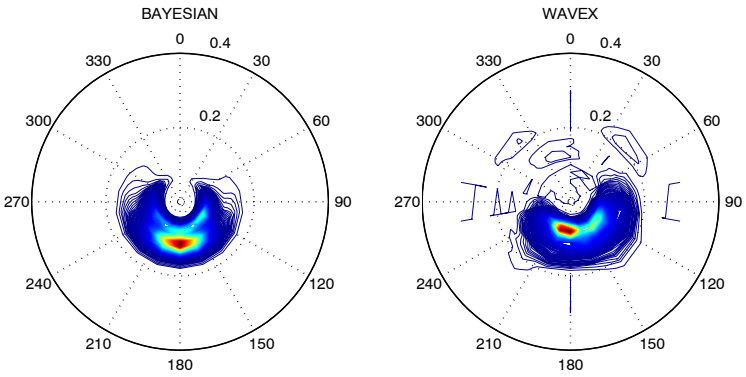

Figure F.25: *The estimated wave spectra for Data I. Relative ship course being 0 deg., and wave field depicted as approaching waves.*

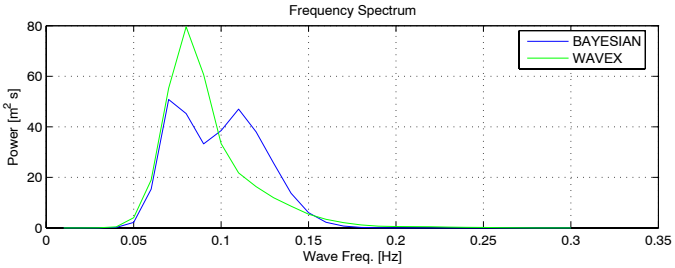

Figure F.26: *Integrated frequency spectra for Data I.*

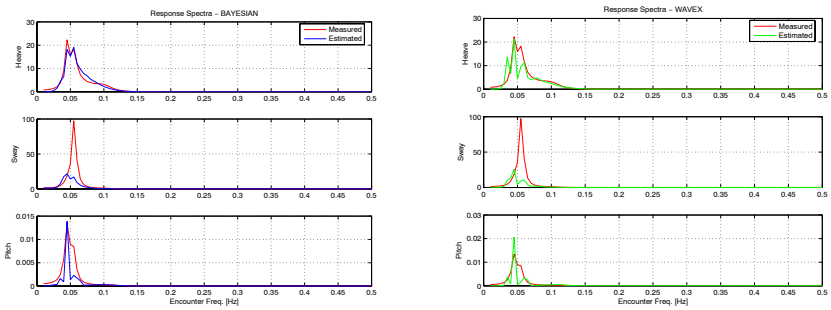

Figure F.27: *Response spectra for Data I; measured and 'estimated' with the latter based on the estimated wave spectra. Note the difference in scales. Units:* Heave [m^2s], Sway [m^2s], Pitch [rad^2s]

F.3 Directional Wave Spectra

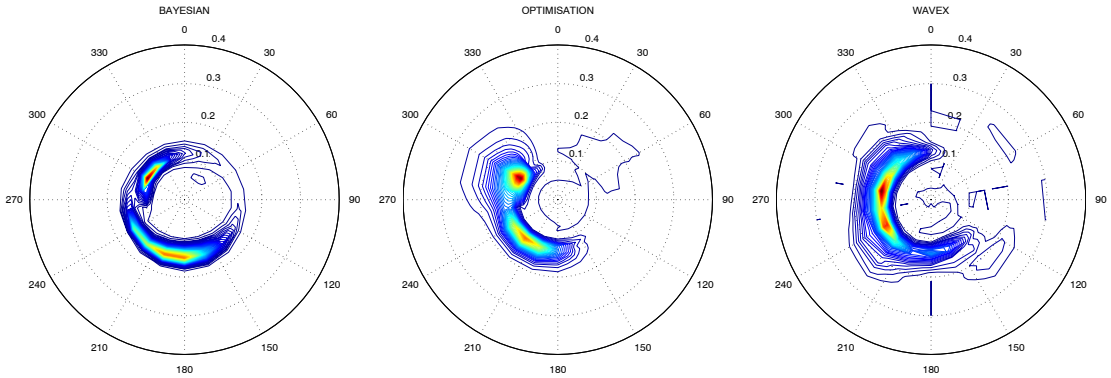

Figure F.28: *The estimated wave spectra of Data A. The ship course is 0 deg. and the waves are shown as approaching.*

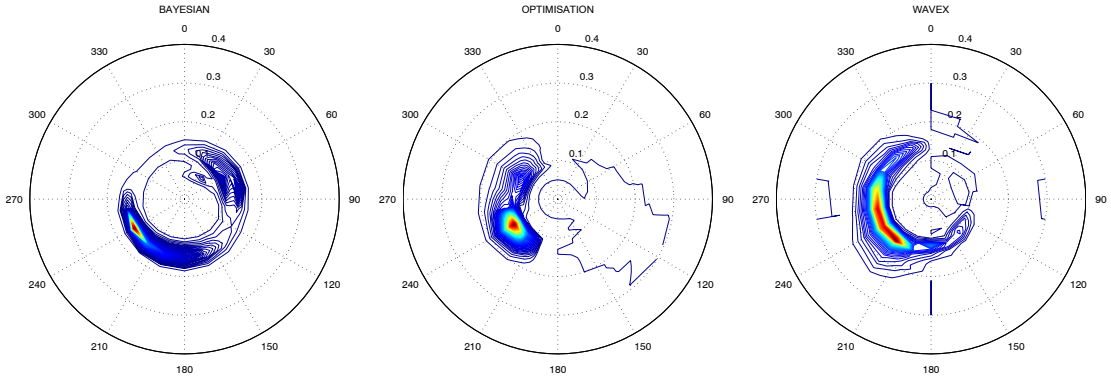

Figure F.29: *The estimated wave spectra of Data B. The ship course is 0 deg. and the waves are shown as approaching.*

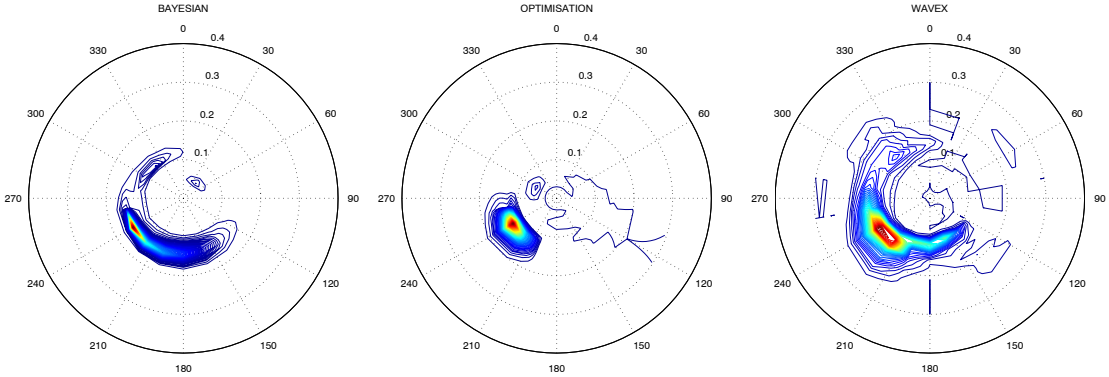

Figure F.30: *The estimated wave spectra of Data C. The ship course is 0 deg. and the waves are shown as approaching.*

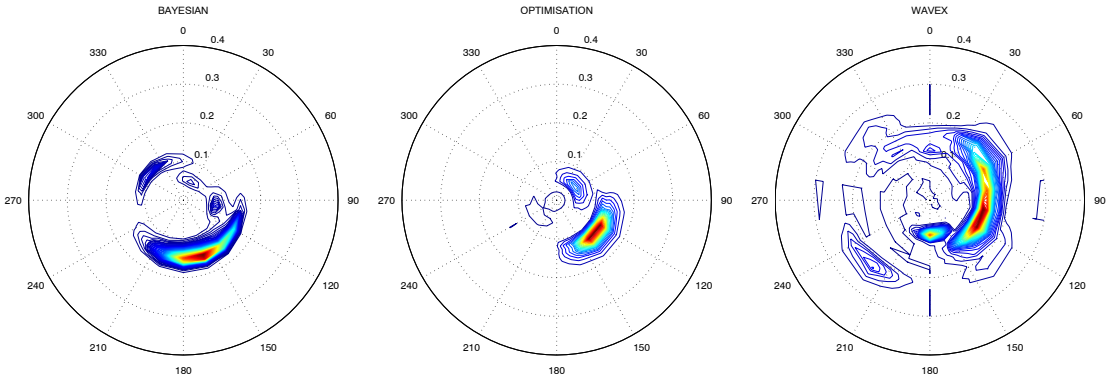

Figure F.31: *The estimated wave spectra of Data D. The ship course is 0 deg. and the waves are shown as approaching.*

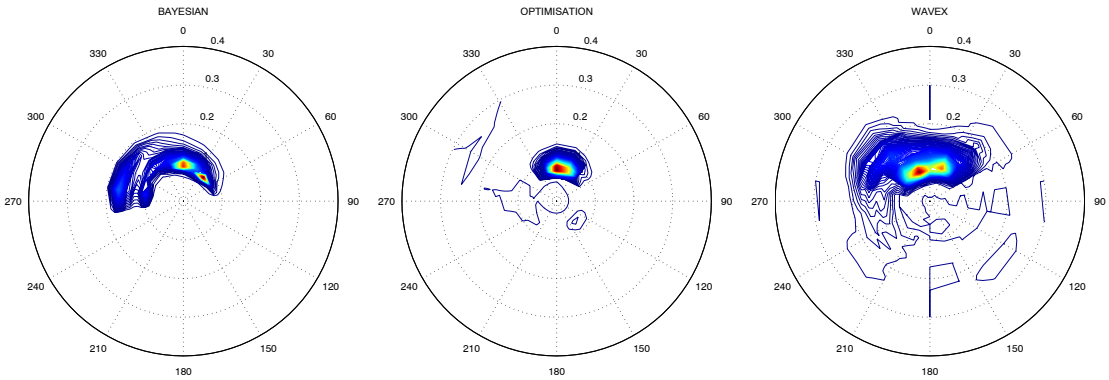

Figure F.32: *The estimated wave spectra of Data E. The ship course is 0 deg. and the waves are shown as approaching.*

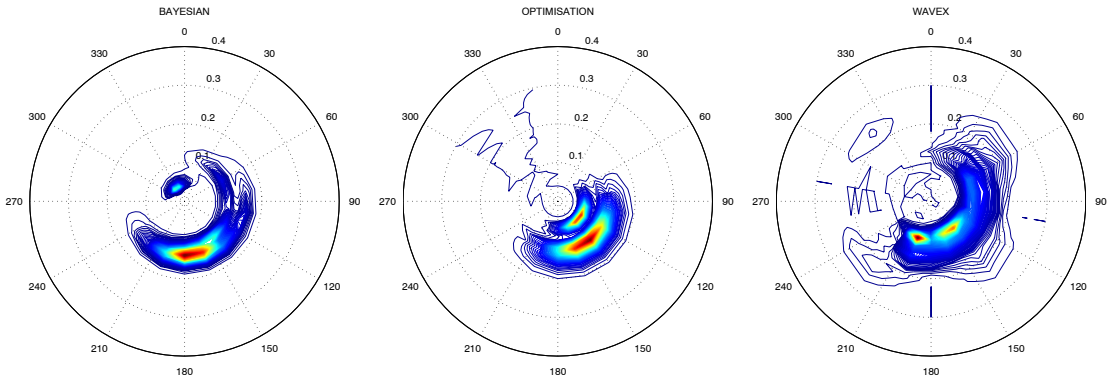

Figure F.33: *The estimated wave spectra of Data F. The ship course is 0 deg. and the waves are shown as approaching.*

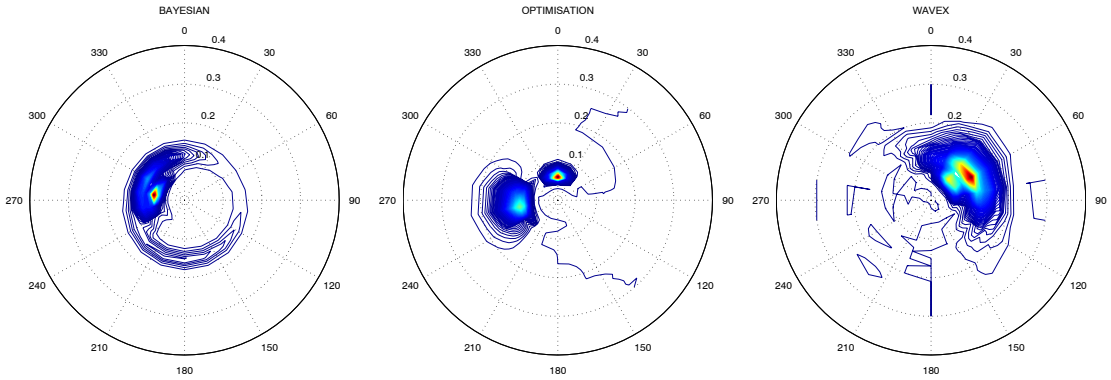

Figure F.34: *The estimated wave spectra of Data G. The ship course is 0 deg. and the waves are shown as approaching.*

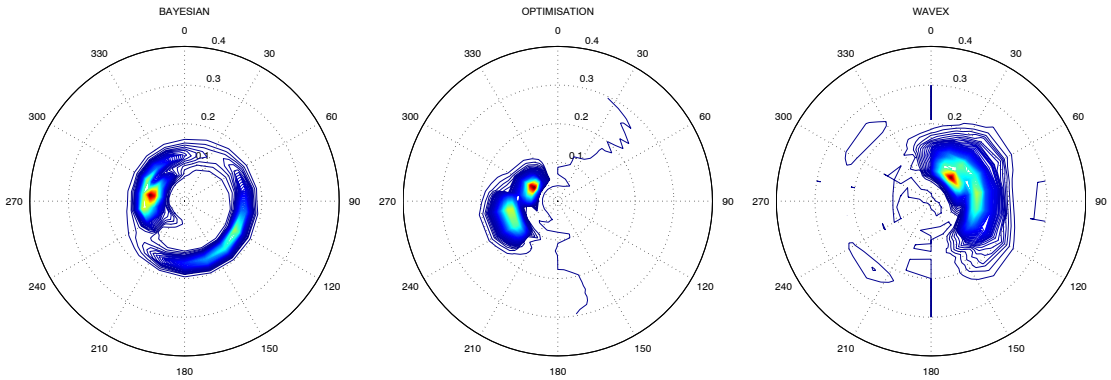

Figure F.35: *The estimated wave spectra of Data H. The ship course is 0 deg. and the waves are shown as approaching.*

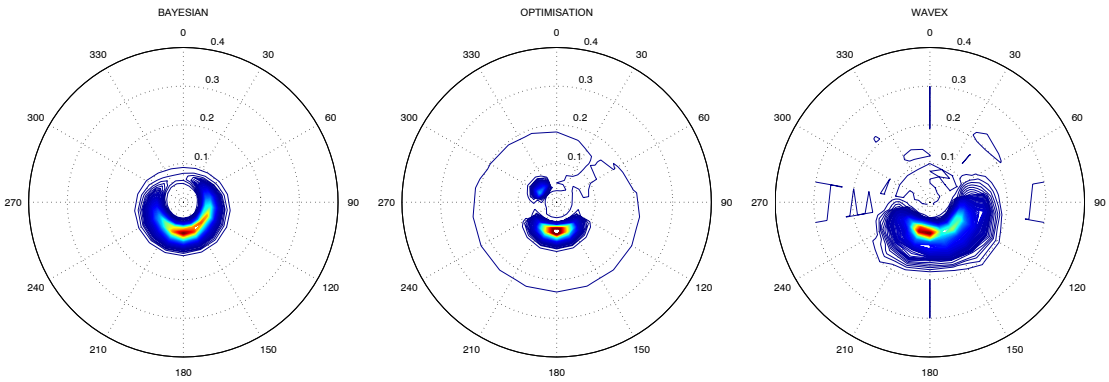

Figure F.36: *The estimated wave spectra of Data I. The ship course is 0 deg. and the waves are shown as approaching.*

F.4 Comparative Plots - Non-normalised Equation System

Data A

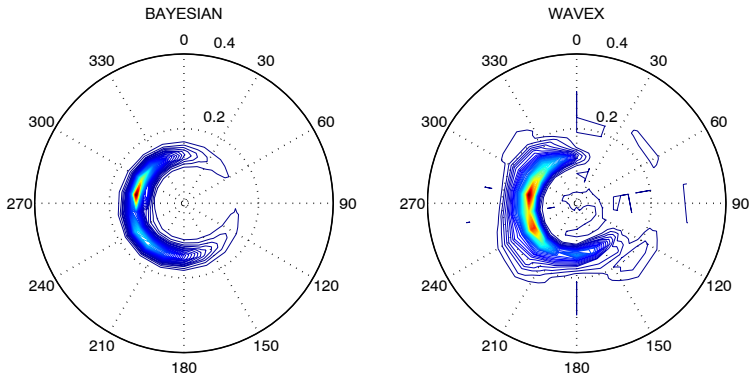

Figure F.37: *The estimated wave spectra for Data A. Relative ship course being 0 deg., and wave field depicted as approaching waves.*

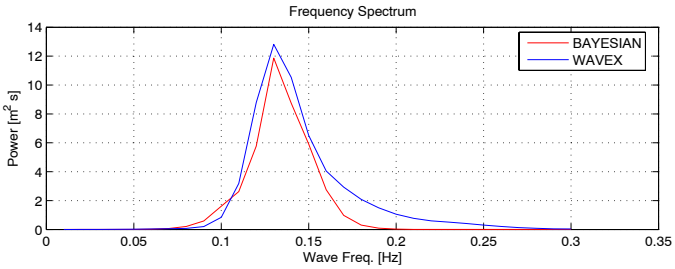

Figure F.38: *Integrated frequency spectra for Data A.*

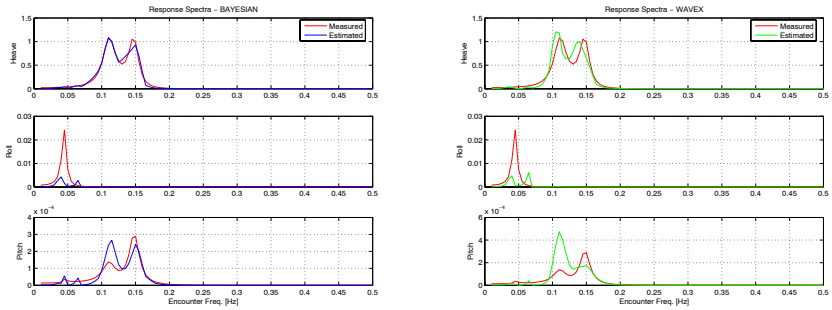

Figure F.39: *Response spectra for Data A; measured and 'estimated' with the latter based on the estimated wave spectra. Units:* Heave [m^2s], Roll [rad^2s], Pitch [rad^2s]

Data B

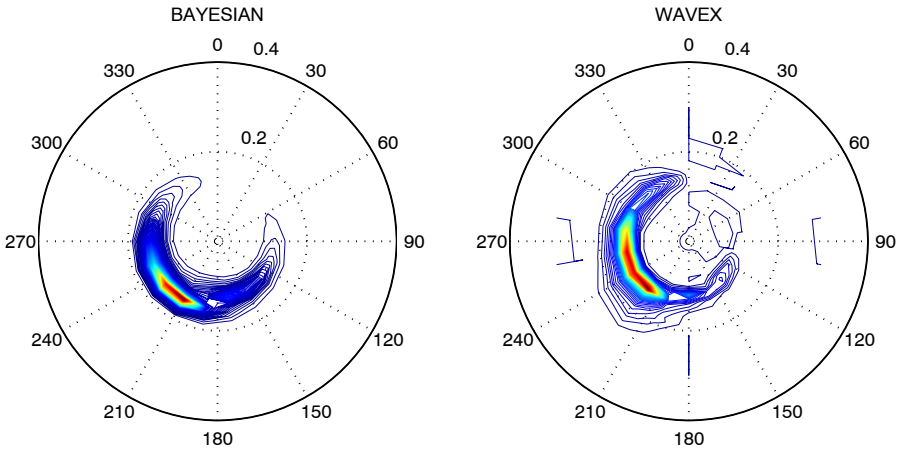

Figure F.40: *The estimated wave spectra for Data B. Relative ship course being 0 deg., and wave field depicted as approaching waves.*

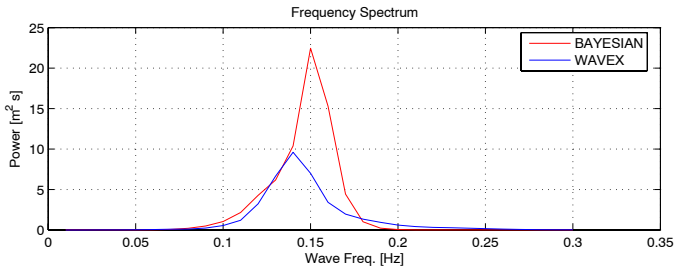

Figure F.41: *Integrated frequency spectra for Data B.*

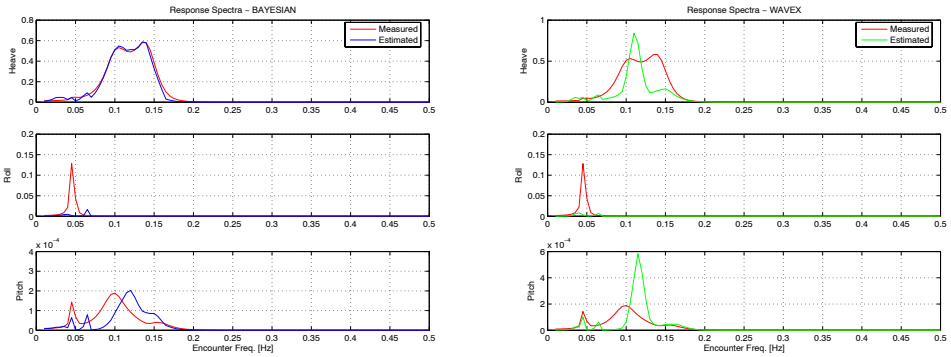

Figure F.42: *Response spectra for Data B; measured and 'estimated' with the latter based on the estimated wave spectra. Note the difference in scales. Units:* Heave [m^2s], Roll [rad^2s], Pitch [rad^2s]

Data C

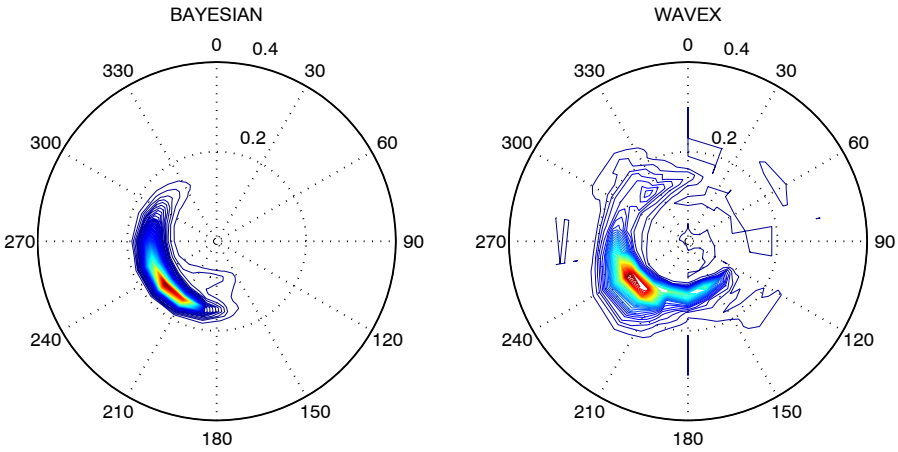

Figure F.43: *The estimated wave spectra for Data C. Relative ship course being 0 deg., and wave field depicted as approaching waves.*

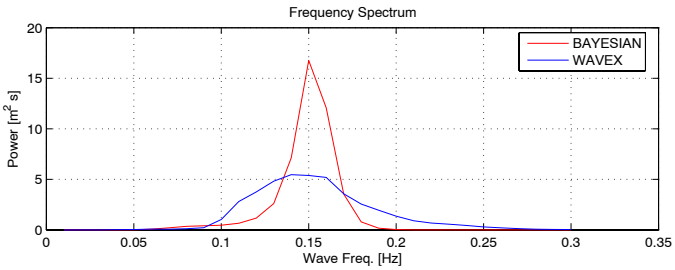

Figure F.44: *Integrated frequency spectra for Data C.*

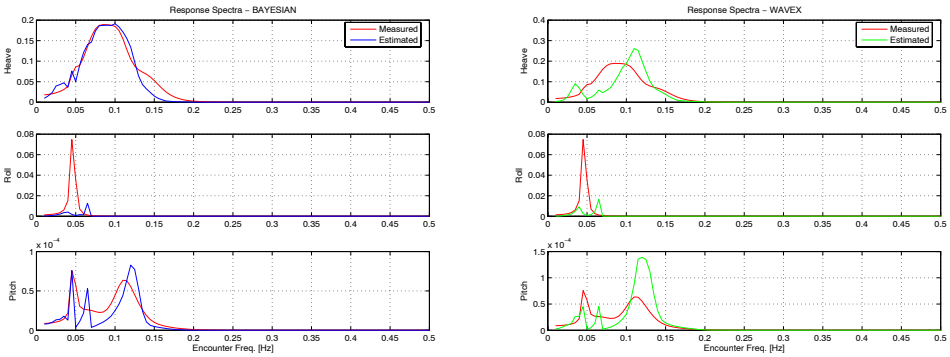

Figure F.45: *Response spectra for Data C; measured and 'estimated' with the latter based on the estimated wave spectra. Note the difference in scales. Units:* Heave [m^2s], Roll [rad^2s], Pitch [rad^2s]

Data D

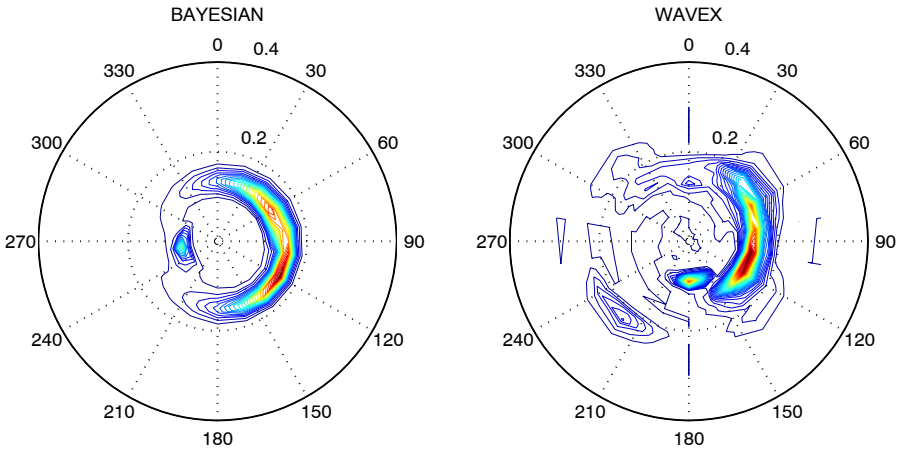

Figure F.46: *The estimated wave spectra for Data D. Relative ship course being 0 deg., and wave field depicted as approaching waves.*

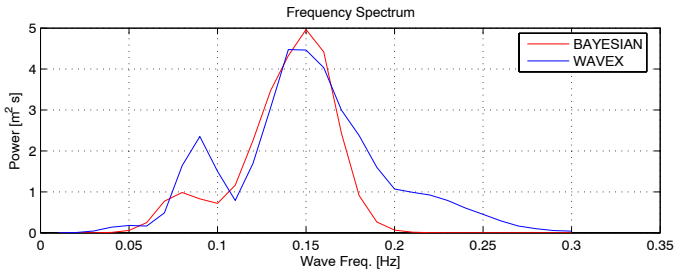

Figure F.47: *Integrated frequency spectra for Data D.*

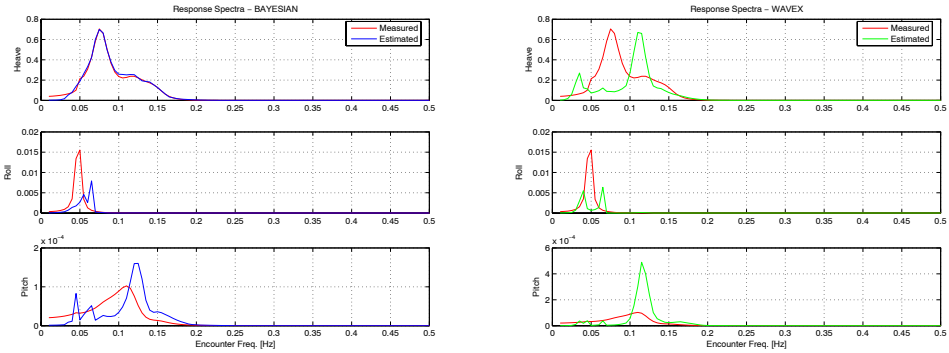

Figure F.48: *Response spectra for Data D; measured and 'estimated' with the latter based on the estimated wave spectra. Note the difference in scales. Units:* Heave [m^2s], Roll [rad^2s], Pitch [rad^2s]

Data E

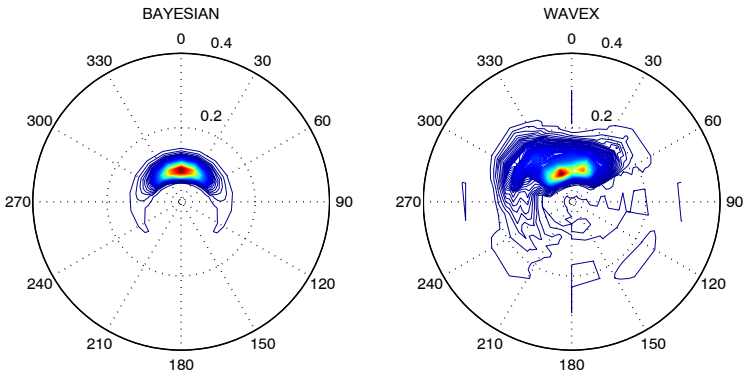

Figure F.49: *The estimated wave spectra for Data E. Relative ship course being 0 deg., and wave field depicted as approaching waves.*

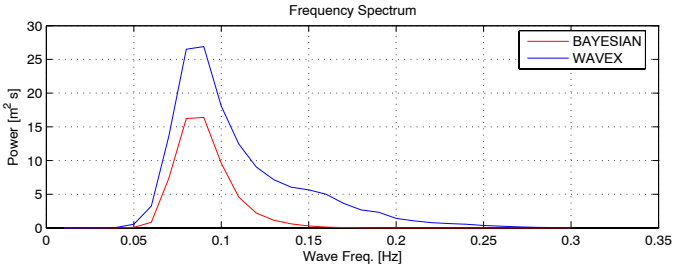

Figure F.50: *Integrated frequency spectra for Data E.*

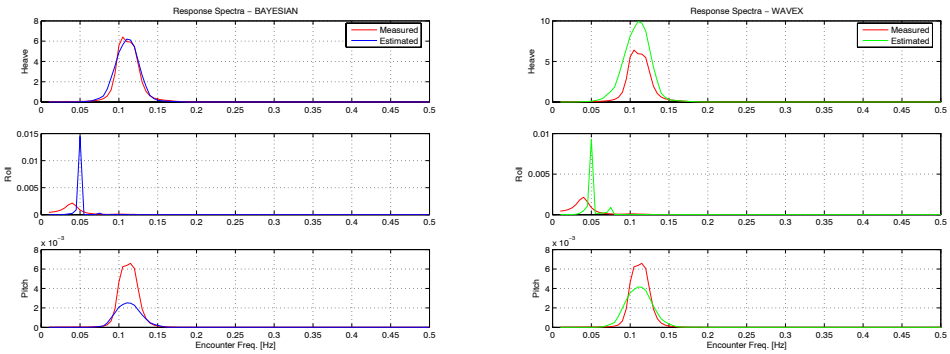

Figure F.51: *Response spectra for Data E; measured and 'estimated' with the latter based on the estimated wave spectra. Note the difference in scales. Units:* Heave [m^2s], Roll [rad^2s], Pitch [rad^2s]

Data F

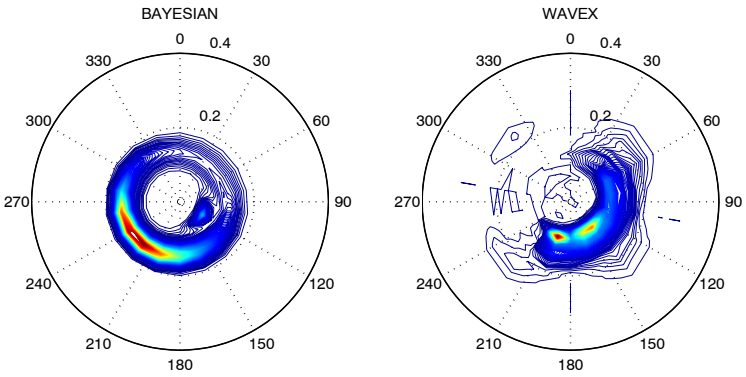

Figure F.52: *The estimated wave spectra for Data F. Relative ship course being 0 deg., and wave field depicted as approaching waves.*

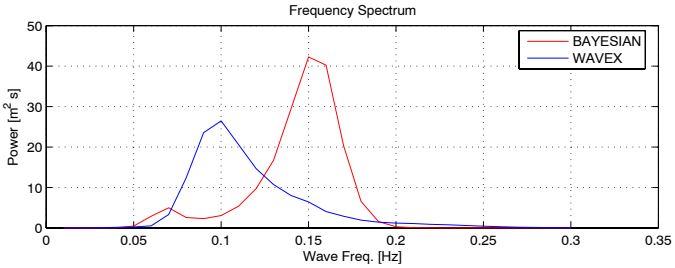

Figure F.53: *Integrated frequency spectra for Data F.*

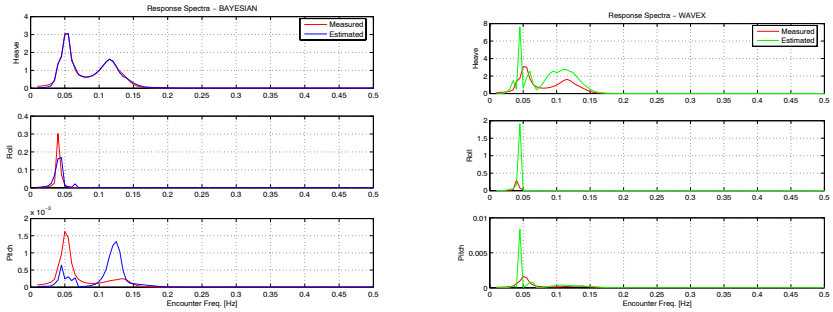

Figure F.54: *Response spectra for Data F; measured and 'estimated' with the latter based on the estimated wave spectra. Note the difference in scales. Units:* Heave [m^{2}s], Roll [rad^{2}s], Pitch [rad^{2}s]

Data G

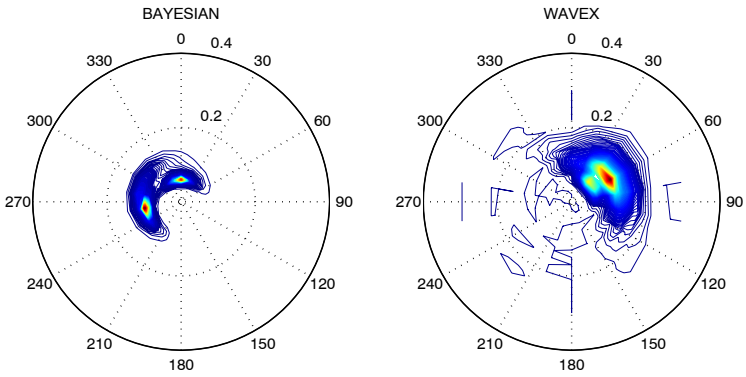

Figure F.55: *The estimated wave spectra for Data G. Relative ship course being 0 deg., and wave field depicted as approaching waves.*

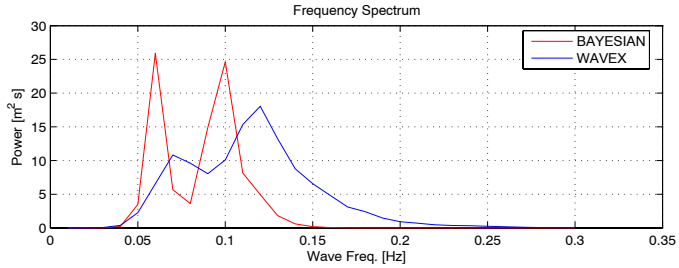

Figure F.56: *Integrated frequency spectra for Data G.*

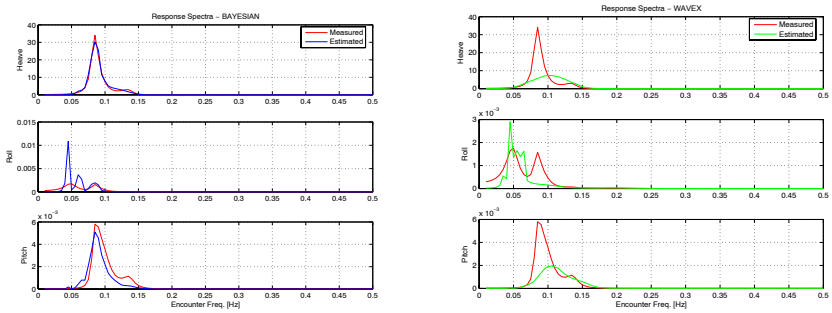

Figure F.57: *Response spectra for Data G; measured and 'estimated' with the latter based on the estimated wave spectra. Note the difference in scales. Units:* Heave [m^{2}s], Roll [rad^{2}s], Pitch [rad^{2}s]

Data H

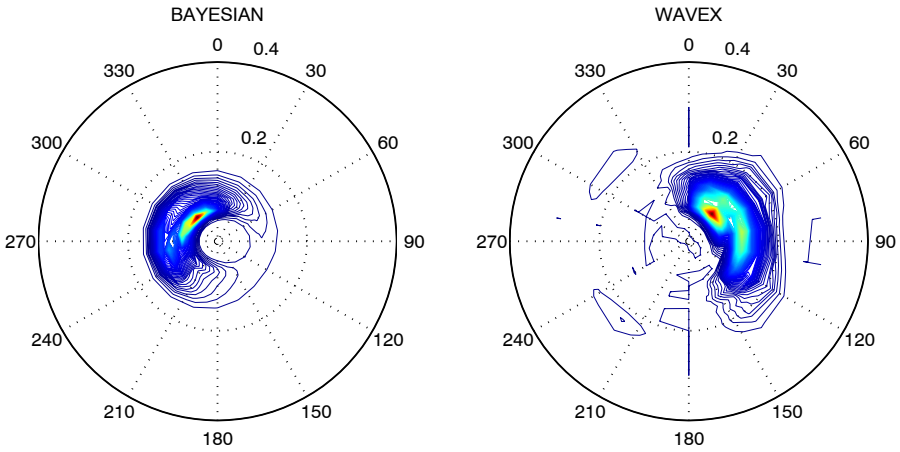

Figure F.58: *The estimated wave spectra for Data H. Relative ship course being 0 deg., and wave field depicted as approaching waves.*

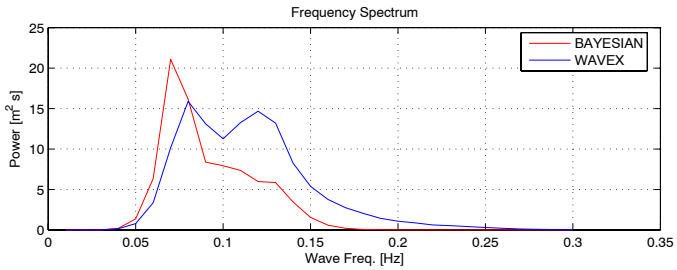

Figure F.59: *Integrated frequency spectra for Data H.*

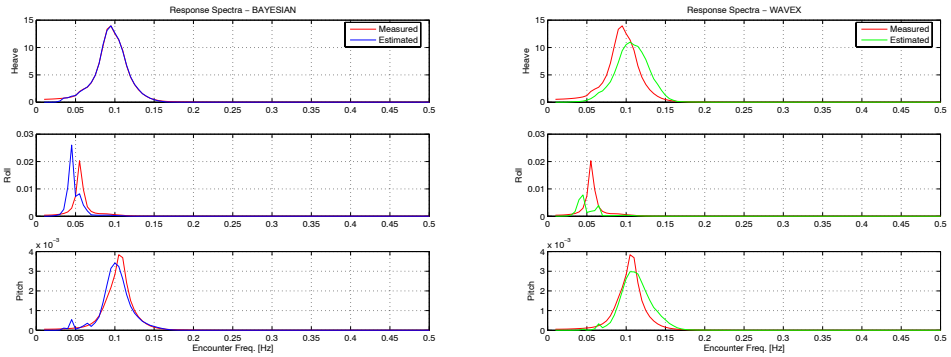

Figure F.60: *Response spectra for Data H; measured and 'estimated' with the latter based on the estimated wave spectra. Note the difference in scales. Units:* Heave [m^2s], Roll [rad^2s], Pitch [rad^2s]

Data I

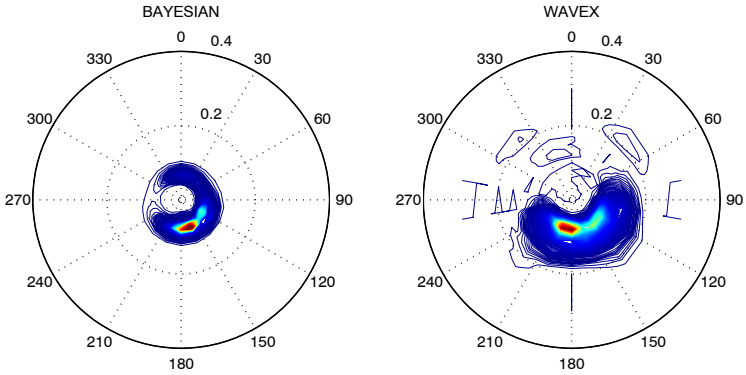

Figure F.61: *The estimated wave spectra for Data I. Relative ship course being 0 deg., and wave field depicted as approaching waves.*

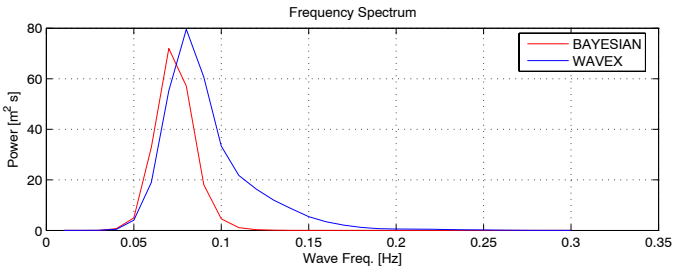

Figure F.62: *Integrated frequency spectra for Data I.*

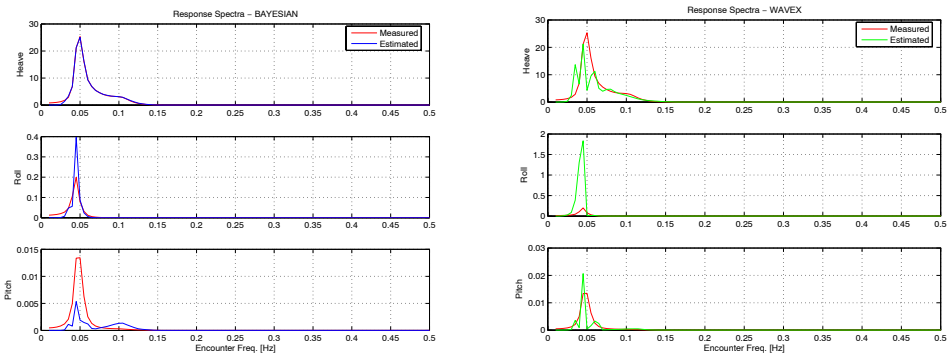

Figure F.63: *Response spectra for Data I; measured and 'estimated' with the latter based on the estimated wave spectra. Note the difference in scales. Units:* Heave [m^2s], Roll [rad^2s], Pitch [rad^2s]

PhD Theses
Department of Naval Architecture and Offshore Engineering
Technical University of Denmark · Kgs. Lyngby

1961 Strøm-Tejsen, J.
Damage Stability Calculations on the Computer DASK.

1963 Silovic, V.
A Five Hole Spherical Pilot Tube for three Dimensional Wake Measurements.

1964 Chomchuenchit, V.
Determination of the Weight Distribution of Ship Models.

1965 Chislett, M.S.
A Planar Motion Mechanism.

1965 Nicordhanon, P.
A Phase Changer in the HyA Planar Motion Mechanism and Calculation of Phase Angle.

1966 Jensen, B.
Anvendelse af statistiske metoder til kontrol af forskellige eksisterende tilnærmelsesformler og udarbejdelse af nye til bestemmelse af skibes tonnage og stabilitet.

1968 Aage, C.
Eksperimentel og beregningsmæssig bestemmelse af vindkræfter på skibe.

1972 Prytz, K.
Datamatorienterede studier af planende bådes fremdrivningsforhold.

1977 Hee, J.M.
Store sideportes indflydelse på langskibs styrke.

1977 Madsen, N.F.
Vibrations in Ships.

1978 Andersen, P.
Bølgeinducerede bevægelser og belastninger for skib på lægt vand.

1978 Römeling, J.U.
Buling af afstivede pladepaneler.

1978 Sørensen, H.H.
Sammenkobling af rotations-symmetriske og generelle tre-dimensionale konstruktioner i elementmetode-beregninger.

1980 Fabian, O.
Elastic-Plastic Collapse of Long Tubes under Combined Bending and Pressure Load.

1980 Petersen, M.J.
Ship Collisions.

1981 Gong, J.
A Rational Approach to Automatic Design of Ship Sections.

1982 Nielsen, K.
Bølgeenergimaskiner.

1984 Nielsen, N.J.R.
Structural Optimization of Ship Structures.

1984 Liebst, J.
Torsion of Container Ships.

1985 Gjersøe-Fog, N.
Mathematical Definition of Ship Hull Surfaces using B-splines.

1985 Jensen, P.S.
Stationære skibsbølger.

1986 Nedergaard, H.
Collapse of Offshore Platforms.

1986 Yan, J.-Q.
3-D Analysis of Pipelines during Laying.

1987 Holt-Madsen, A.
A Quadratic Theory for the Fatigue Life Estimation of Offshore Structures.

1989 Andersen, S.V.
Numerical Treatment of the Design-Analysis Problem of Ship Propellers using Vortex Lattice Methods.

1989 Rasmussen, J.
Structural Design of Sandwich Structures.

1990 Baatrup, J.
Structural Analysis of Marine Structures.

1990 Wedel-Heinen, J.
Vibration Analysis of Imperfect Elements in Marine Structures.

1991 Almlund, J.
Life Cycle Model for Offshore Installations for Use in Prospect Evaluation.

1991 Back-Pedersen, A.
Analysis of Slender Marine Structures.

1992 Bendiksen, E.
Hull Girder Collapse.

1992 Petersen, J.B.
Non-Linear Strip Theories for Ship Response in Waves.

1992 Schalck, S.
Ship Design Using B-spline Patches.

1993 Kierkegaard, H.
Ship Collisions with Icebergs.

1994 Pedersen, B.
A Free-Surface Analysis of a Two-Dimensional Moving Surface-Piercing Body.

1994 Hansen, P.F.
Reliability Analysis of a Midship Section.

1994 Michelsen, J.
A Free-Form Geometric Modelling Approach with Ship Design Applications.

1995 Hansen, A.M.
Reliability Methods for the Longitudinal Strength of Ships.

1995 Branner, K.
Capacity and Lifetime of Foam Core Sandwich Structures.

1995 Schack, C.
Skrogudvikling af hurtiggående færger med henblik på sødygtighed og lav modstand.

1997 Simonsen, B.C.
Mechanics of Ship Grounding.

1997 Olesen, N.A.
Turbulent Flow past Ship Hulls.

1997 Riber, H.J.
Response Analysis of Dynamically Loaded Composite Panels.

1998 Andersen, M.R.
Fatigue Crack Initiation and Growth in Ship Structures.

1998 Nielsen, L.P.
Structural Capacity of the Hull Girder.

1999 Zhang, S.
The Mechanics of Ship Collisions.

1999 Birk-Sørensen, M.
Simulation of Welding Distortions of Ship Sections.

1999 Jensen, K.
Analysis and Documentation of Ancient Ships.

2000 Wang, Z.
Hydroelastic Analysis of High-Speed Ships.

2000 Petersen, T.
Wave Load Prediction—a Design Tool.

2000 Banke, L.
Flexible Pipe End Fitting.

2000 Simonsen, C.D.
Rudder, Propeller and Hull Interaction by RANS.

2000 Clausen, H.B.
Plate Forming by Line Heating.

2000 Krishnaswamy, P.
Flow Modelling for Partially Cavitating Hydrofoils.

2000 Andersen, L.F.
Residual Stresses and Deformations in Steel Structures.

2000 Friis-Hansen, A.
Bayesian Networks as a Decision Support Tool in Marine Applications.

PhD Theses
Maritime Engineering · Department of Mechanical Engineering
Technical University of Denmark · Kgs. Lyngby

2001 Lützen, M.
Ship Collision Damage.

2001 Olsen, A.S.
Optimisation of Propellers Using the Vortex-Lattice Method.

2002 Rüdinger, F.
Modelling and Estimation of Damping in Non-linear Random Vibration.

2002 Bredmose, H.
Deterministic Modelling of Water Waves in the Frequency Domain.

2003 Urban, J.
Crushing and Fracture of Lightweight Structures.

2003 Lazarov, B.S.
Slepian Simulations of Plastic Displacement of Randomly Excited Hysteretic Structures.

2003 Ravn, E.S.
Probabilistic Damage Stability of Ro-Ro Ships.

2003 Törnqvist, R.
Design of Crashworthy Ship Structures.

2003 Nielsen, K.B.
Numerical Prediction of Green Water Loads on Ships.

2004 Folsø, R.
Comfort Monitoring of High Speed Passenger Ferries.

2004 Fuhrman, D.R.
Numerical Solutions of Boussinesq Equations for Fully Nonlinear and Extremely Dispersive Water Waves.

2004 Dietz, J.S.
Application of Conditional Waves as Critical Wave Episodes for Extreme Loads on Marine Structures.

2004 Berggreen, C.
Damage Tolerance of Debonded Sandwich Structures.

PhD Theses
Section of Coastal, Maritime and Structural Engineering · Department of Mechanical Engineering Technical University of Denmark · Kgs. Lyngby

2005 Berntsen, N.
Modelling Granular Media and Molecular Dynamics Simulations of Ellipses..

2005 Nielsen, U.D.
Estimation of Directional Wave Spectra from Measured Ship Responses.

Coastal, Maritime and Structural Engineering

Department of Mechanical Engineering

Technical University of Denmark

Nils Koppels Allé, Building 403
DK-2800 Kgs. Lyngby
Denmark
Phone + 45 4525 1360
Fax + 45 4588 4325
info.skk@mek.dtu.dk
www.mek.dtu.dk

ISBN 87-89502-51-5